

**Teleconnections between Decadal Rainfall Variability and
Global Sea Surface Temperatures and Simulation of future
Climate Scenarios over East Africa**

By

PHILIP OMONDI AMING'O
DEPARTMENT OF METEOROLOGY,
UNIVERSITY OF NAIROBI,
P.O. BOX 30197,
NAIROBI, KENYA




A THESIS SUBMITTED IN FULFILLMENT OF THE REQUIREMENT FOR THE
DEGREE OF DOCTOR OF PHILOSOPHY (PHD) IN METEOROLOGY,
UNIVERSITY OF NAIROBI,
KENYA.

AUGUST 2010

**UNIVERSITY OF NAIROBI
LIBRARY**

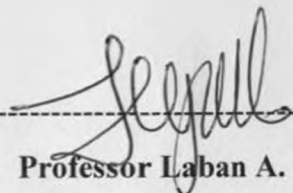
DECLARATION

This thesis is my original work and has not been presented for a degree at any other University.

Signature: -----

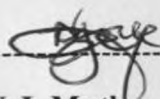
Date-----

Philip Omondi Aming'o
Department of Meteorology,
University of Nairobi

Signature: -----

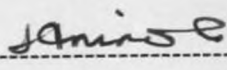
Date-----

Professor Laban A. Ogallo
Department of Meteorology,
University of Nairobi

Signature: -----

Date 25/08/10

Prof N.J. Muthama
Department of Meteorology,
University of Nairobi

Signature: -----

Date 27/08/2010

Dr Joseph Ininda
Department of Meteorology,
University of Nairobi

DEDICATION

I dedicate this dissertation to my Mother Helidah Achola who inculcated in me the spirit of hard work and determination necessary for any achievement in life.

ACKNOWLEDGEMENT

I wish to express my sincere appreciation Professor Laban Ogallo for the academic mentoring he inculcated in me as my supervisor. His astute approach to scientific questions and valuable discussions made working with him not only fulfilling academically, but also enriched my personality.

Many thanks to Prof J. N. Muthama and Dr J. Ininda for their tireless advice, valuable guidance, constructive criticisms, constant reading, making of corrections and offering of very valuable suggestions in the writing of the manuscripts that led to the successful and timely completion of this final work.

I am grateful to the IGAD Climate Prediction and Application Centre (ICPAC) through the Director Professor Laban A. Ogallo, for providing me with the scholarship and computer resources that made the pursuance of this study successful.

Thanks to the University of Nairobi, department of meteorology and teaching staff for the training. I would also like to sincerely appreciate the entire members of staff, ICPAC, for many useful discussions and support during the period of this study.

I wish to extend my special regards to the support I received from my family especially my wife Lucy Atieno Omondi, who continued to encourage me throughout the period of my study, and my children who missed my fatherly guidance during my study period.

TABLE OF CONTENTS

DECLARATION-----	i
DEDICATION-----	ii
ACKNOWLEDGEMENT-----	ii
TABLE OF CONTENTS-----	iv
LIST OF FIGURES-----	vii
LIST OF TABLES-----	xiii
LIST OF ACRONYMS-----	xiv
LIST OF ACRONYMS CONTINUED-----	xv
ABSTRACT-----	xvi
CHAPTER ONE: INTRODUCTION-----	1
1.2 OBJECTIVE OF THE STUDY-----	5
1.3 JUSTIFICATION OF THE STUDY-----	6
1.4 AREA OF STUDY AND ITS PHYSICAL FEATURES-----	8
CHAPTER TWO: LITERATURE REVIEW-----	11
2.1 RAINFALL CLIMATOLOGY OF EAST AFRICA-----	11
2.1.1 INTER TROPICAL CONVERGENCE ZONE (ITCZ)-----	14
2.1.2 SUBTROPICAL ANTICYCLONES-----	17
2.1.3 MONSOONS-----	18
2.1.4 EASTERLY AND WESTERLY WAVES-----	20
2.1.5 TROPICAL CYCLONES-----	21
2.1.6 QUASI-BIENNIAL OSCILLATION-----	23
2.1.7 MADDEN JULIEN OSCILLATION (MJO)-----	24
2.1.8 SEA SURFACE TEMPERATURE-----	25
2.2 DECADAL CLIMATE VARIABILITY-----	31
2.2.1 DECADAL RAINFALL PREDICTABILITY AND PROJECTION-----	34
2.3 APPLICATION OF GLOBAL CLIMATE MODELS (GCMs) AND REGIONAL CLIMATE MODELS (RCMs)-----	35
CHAPTER THREE: DATA AND METHODOLOGY-----	38
3.1 DATA-----	38
3.1.1 OBSERVED DATA-----	38
3.1.2 CLIMATE RESEARCH UNIT (CRU) DATA-----	39
3.2 MODEL OUTPUT DATA-----	44
3.2.1 FORCING DATA FOR THE REGIONAL CIRCULATION MODEL-----	44
3.2.2 ERA-40 RE-ANALYSIS-----	44
3.3 METHODOLOGY-----	45
3.3.1 DATA QUALITY CONTROL METHODOLOGY-----	46
3.3.2 SPECTRAL ANALYSIS METHODS-----	47
3.3.3 TREND ANALYSIS-----	49
3.3.4 PRINCIPAL COMPONENT ANALYSIS (PCA)-----	50

3.3.5	NUMBER OF SIGNIFICANT PRINCIPAL COMPONENTS-----	55
3.3.6	THE SCREE METHOD-----	55
3.3.7	KAISER'S CRITERION-----	56
3.3.8	LOGARITHM OF EIGENVALUES (LEV)-----	56
3.3.9	SAMPLING ERRORS OF EIGENVALUES-----	56
3.4	TELECONNECTION BETWEEN REGIONAL DECADAL RAINFALL VARIABILITY PATTERNS AND GLOBAL SEA SURFACE TEMPERATURES-----	57
3.4.1	CORRELATION METHOD-----	57
3.4.2	CANONICAL CORRELATION ANALYSIS (CCA)-----	58
3.4.3	SINGULAR VALUE DECOMPOSITION (SVD)-----	61
3.5	PREDICTION OF DECADAL RAINFALL PATTERNS-----	64
3.5.1	MULTIPLE REGRESSION MODELS (MRM)-----	64
3.5.2	ANOVA FOR MULTIPLE LINEAR REGRESSION-----	66
3.5.3	VERIFICATION OF THE FORECAST-----	67
3.6	PROJECTION OF FUTURE REGIONAL CLIMATE-----	68
3.6.1	MODEL DOMAIN-----	70
3.6.2	DESCRIPTION OF MODEL EXPERIMENTS-----	72
3.6.3	EVALUATION AND VALIDATION OF GCM OUTPUT AND PRECIS SIMULATIONS-----	73
3.6.4	PRECIS REGIONAL CLIMATE PROJECTIONS-----	74
	CHAPTER FOUR: RESULTS AND DISCUSSIONS-----	76
4.1	DATA QUALITY CONTROL RESULTS-----	76
4.2	DELINEATION OF EAST AFRICA CLIMATE ZONES BASED ON MODES OF DECADAL RAINFALL VARIABILITY-----	78
4.3	EXISTANCE OF DECADAL MODES IN THE INTERANNUAL RAINFALL RECORDS-----	84
4.3.1	TREND ANALYSIS-----	84
4.3.2	SPECTRAL ANALYSIS-----	90
4.4	TELECONNECTION BETWEEN REGIONAL DECADAL RAINFALL VARIABILITY PATTERNS AND GLOBAL SEA SURFACE TEMPERATURES-----	91
4.4.1	SINGULAR VALUE DECOMPOSITION (SVD) RESULTS FOR THE OCTOBER – DECEMBER SEASON-----	92
4.4.2	SINGULAR VALUE DECOMPOSITION (SVD) FOR THE JUNE – AUGUST SEASON-----	106
4.4.3	SVD RESULTS FOR THE MARCH – MAY SEASON-----	122
4.5	USING GLOBAL OCEANS SST MODES TO DERIVE FUTURE DECADAL RAINFALL VARIABILITY PATERNS-----	139
4.5.1	RESULTS FROM DECADAL RAINFALL NOW CAST FOR SEPTEMBER – DECEMBER SEASON-----	139
4.5.2	RESULTS FROM DECADAL RAINFALL NOW CASTS FOR MARCH – MAY SEASON-----	142

4.5.3	RESULTS FROM DECADAL RAINFALL NOWCASTS FOR JUNE – AUGUST (JJA) SEASON-----	143
4.6	DECADAL PREDICTIONS AND REGIONAL CLIMATE SCENARIOS DERIVED FROM PRECIS SIMULATIONS-----	146
4.6.1	SURFACE AIR TEMPERATURE-----	148
4.6.2	PRECIPITATION-----	149
4.6.3	PRECIS SIMULATED PRECIPITATION AND TEMPERATURE CLIMATOLOGY-----	152
4.6.4	TEMPERATURE CLIMATOLOGY-----	152
4.6.5	RAINFALL CLIMATOLOGY-----	155
4.6.6	FURTHER PRECIS MODEL VALIDATION-----	159
4.6.7	PROJECTION OF CLIMATE FOR THE REGION-----	164
	CHAPTER FIVE: SUMMARY, CONCLUSIONS AND RECOMMENDATIONS-----	170
5.1	SUMMARY-----	170
5.2	CONCLUSIONS-----	177
5.3	RECOMMENDATIONS-----	177
5.3.1	RECOMMENDATIONS FOR FURTHER RESEARCH WORK-----	177
5.3.2	RECOMMENDATIONS TO POLICY MAKERS-----	179
5.3.3	RECOMMENDATIONS TO USERS OF CLIMATE INFORMATION AND PREDICTION PRODUCTS-----	180
5.3.4	RECOMMENDATIONS TO NATIONAL METEOROLOGICAL AND HYDROLOGICAL SERVICES-----	180
	REFERENCES -----	181

LIST OF FIGURES

Figure 1:	Topographical features of the outer domain, with areas higher than 1000m shaded (Adopted from Anyah, R., 2005).....	9
Figure 2:	Mean annual rainfall cycles for (a) Mbeya (b) Lodwar and (c) Mbarara stations over east Africa (Omondi, 2005).....	12
Figure 3a:	Schematic of the general patterns of winds, pressure and convergence over Africa during January (adapted from Nicholson et al., 1988). Dotted lines indicate the Intertropical Convergence Zone, dashed lines, other convergence zones.....	14
Figure 3b:	Schematic of the general patterns of winds, pressure and convergence over Africa during July/August season (adapted from Nicholson et al., 1988). Dotted lines indicate the Intertropical Convergence Zone, dashed lines, other convergence zones.....	15
Figure 4:	The schematic of east-west Walker global circulation (Adapted from Indeje, 2000)	17
Figure 5:	Schematic representation of the global thermohaline circulation. Warm currents are drawn in red while blue depicts the deep cold	26
Figure 6:	The distribution of the stations representing homogeneous rainfall zones over the study region	40
Figure 7:	Homogeneous climatic zones for March-May season used in the study.....	42
Figure 8:	Homogeneous climatic zones for October-December season used in the study	42
Figure 9:	Homogeneous climatic zones for June - August season used in the study.....	43
Figure 10:	Region of study in relation to the model domain.....	72
Figure 11:	Cumulative March – May (MAM) seasonal rainfall totals over Zone 1.....	77
Figure 12:	Single mass curve for Zones 2 as represented by (Kigoma).....	78
Figure 13:	Selection of the dominant PCA for March-May decadal rainfall modes with points above the dotted lines significant at the 5% level.....	79
Figure 14:	Homogeneous climatic zones over East Africa obtained from combined PCA and simple correlation analyses using the Decadal rainfall variability (March-May).	81

Figure 15:	Selection of the dominant PCA for October - December decadal rainfall modes with points above the dotted lines significant at the 5% level.....	82
Figure 16:	Homogeneous climatic zones over East Africa obtained from combined PCA and simple correlation analyses using the October-December Decadal rainfall variability.....	83
Figure 17a:	Unsmoothed Interannual rainfall patterns for March-May for zone 10	86
Figure 17b:	Unsmoothed Interannual rainfall patterns for October-December for zone 4.....	86
Figure 18:	Smoothed inter-annual March – May rainfall anomalies for zone 3 as represented by Voi.....	87
Figure 19:	Graphical plots of March -May decadal rainfall variability for the representative stations over eastern Africa region.....	88
Figure 20:	Graphical plots of October - December decadal rainfall variability for the representative stations over eastern Africa region.....	89
Figure 21:	Spectral analysis of the smoothed March – May seasonal rainfall for zone 8 as represented by Mbarara.....	90
Figure 22:	Spectral analysis of the smoothed October – December seasonal rainfall for zone 6 as represented by Gulu.....	91
Figure 23:	Spatial patterns (S1) of the first SVD mode for (a) October-December rainfall (b) Indian Ocean SST presented as homogeneous correlation maps...	94
Figure 23c:	Time series of expansion coefficients (s1) of the first SVD mode for October - December rainfall and Indian Ocean SST anomalies.....	95
Figure 24:	Spatial patterns (S2) of the second SVD mode for (a) October-December rainfall (b) Indian Ocean SST presented as homogeneous correlation maps...	96
Figure 24c:	Time series of expansion coefficients (s2) of the second SVD mode for October - December rainfall and Indian Ocean SST anomalies.....	97
Figure 25:	Spatial patterns (S1) of the first SVD mode for (a) October-December rainfall (b) Atlantic SST presented as homogeneous correlation maps.....	98
Figure 25c:	Time series of expansion coefficients (s1) of the first SVD mode for October - December rainfall (bold lines) and Atlantic Ocean SST (dotted lines).....	99
Figure 26:	Spatial patterns (S2) of the second SVD mode for (a) October-December	

	rainfall (b) Atlantic SST presented as homogeneous correlation maps.....	100
Figure 26c:	Time series of expansion coefficients (s_2) of the second SVD mode for October - December rainfall (bold lines) and Atlantic Ocean SST.....	101
Figure 27:	Spatial patterns (S_1) of the first SVD mode for (a) October – December rainfall (b) Pacific SST presented as homogeneous correlation maps.....	103
Figure 27c:	Time series of expansion coefficients (s_1) of the first SVD mode for OND rainfall and Pacific Ocean SST anomalies.....	104
Figure 28:	Spatial patterns (S_2) of the second SVD mode for (a) October – December rainfall (b) Pacific SST presented as homogeneous correlation maps.....	105
Figure 28c:	Time series of expansion coefficients (s_2) of the second SVD mode for OND rainfall and Pacific Ocean SST anomalies.....	106
Figure 29:	Spatial patterns (S_1) of the first SVD mode for (a) JJA rainfall season (b) Indian SST presented as homogeneous correlation maps.....	108
Figure 29c:	Time series of expansion coefficients (s_1) of the first SVD mode for JJA rainfall (continuous lines) and Indian Ocean SST (dotted lines) anomalies....	109
Figure 30:	Spatial patterns (S_2) of the second SVD mode for (a) JJA rainfall season (b) Indian SST presented as homogeneous correlation maps.....	110
Figure 30c:	Time series of expansion coefficients (s_2) of the second SVD mode for JJA rainfall (continuous lines) and Indian Ocean SST (dotted lines) anomalies	111
Figure 31:	Spatial patterns of the third SVD mode for (a) JJA rainfall and (b) Indian Ocean SST presented as homogeneous correlation maps.....	112
Figure 31c:	Time series of expansion coefficients (s_3) of the third SVD mode for JJA rainfall (continuous lines) and Indian Ocean SST (dotted lines) anomalies....	113
Figure 32:	Spatial patterns (S_1) of the first SVD mode for (a) June - August rainfall (b) Atlantic SST presented as homogeneous correlation maps.....	114
Figure 32c:	Time series of expansion coefficients (s_1) of the first SVD mode for June - August rainfall and Atlantic Ocean SST anomalies.....	115
Figure 33:	Spatial patterns (S_3) of the third SVD mode for (a) June - August rainfall (b) Atlantic SST presented as homogeneous correlation maps.....	116
Figure 33c:	Time series of expansion coefficients (s_3) of the third SVD mode for June - August rainfall (full lines) and Atlantic Ocean SST anomalies (dotted lines)...	117
Figure 34:	Spatial patterns (S_2) of the second SVD mode for (a) JJA rainfall season (b)	

	Pacific SST presented as homogeneous correlation maps.....	118
Figure 34c:	Time series of expansion coefficients (s_2) of the second SVD mode for June - August rainfall (full lines) and Pacific Ocean SST anomalies (dotted lines).	119
Figure 35:	Spatial patterns (S_3) of the third SVD mode for (a) June - July rainfall (b) Pacific SST presented as homogeneous correlation maps.....	121
Figure 35c:	Time series of expansion coefficients (s_3) of the third SVD mode for JJA rainfall and Pacific Ocean SST anomalies.....	122
Figure 36:	Spatial patterns of the first SVD mode for (a) MAM rainfall and (b) Indian Ocean SST presented as homogeneous correlation maps.....	124
Figure 36c:	Time series of expansion coefficients (s_1) of the first SVD mode for March - May rainfall and Indian Ocean SST anomalies.....	125
Figure 37:	Spatial patterns of the second SVD mode for (a) MAM rainfall and (b) Indian Ocean SST presented as homogeneous correlation maps.....	126
Figure 37c:	Time series of expansion coefficients (s_2) of the second SVD mode for March - May rainfall and Indian Ocean SST anomalies.....	127
Figure38:	Spatial patterns of the third SVD mode for (a) MAM rainfall and (b) Indian Ocean SST presented as homogeneous correlation maps.....	128
Figure 38c:	Time series of expansion coefficients (s_3) of the third SVD mode for March - May rainfall and Indian Ocean SST anomalies.....	129
Figure 39:	Spatial patterns of the second SVD mode (S_2) for (a) MAM rainfall and (b) Atlantic Ocean SST presented as homogeneous correlation maps.....	130
Figure 39c:	Time series of expansion coefficients (s_2) of the second SVD mode for March - May rainfall and Atlantic Ocean SST anomalies.....	131
Figure 40:	Spatial patterns of the third SVD mode (S_3) for (a) MAM rainfall and (b) Atlantic Ocean SST presented as homogeneous correlation maps.....	132
Figure 40c:	Time series of expansion coefficients (s_3) of the third SVD mode for March - May rainfall and Atlantic Ocean SST anomalies.....	133
Figure 41:	Spatial patterns (S_2) of the second SVD mode for (a) March - May rainfall (b) Pacific SST presented as homogeneous correlation maps.....	135
Figure 41c:	Time series of expansion coefficients (s_2) of the second SVD mode for MAM rainfall and Pacific Ocean SST anomalies.....	136
Figure 42:	Spatial patterns (S_3) of the third SVD mode for (a) March - May rainfall (b)	

	Pacific SST presented as homogeneous correlation maps.....	137
Figure 42c:	Time series of expansion coefficients (s3) of the third SVD mode for MAM rainfall and Pacific Ocean SST anomalies.....	138
Figure 43a:	Time series plot of the observed and model estimates of the October – December decadal rainfall for zone 1 as represented by DIA.....	141
Figure 43b:	Time series plot of the observed and model estimates of the October – December decadal rainfall for zone 3 as represented by Dodoma.....	141
Figure 44a:	Time series plot of the observed and model estimates of the March – May decadal rainfall for zone 8 as represented by Masindi.....	142
Figure 44b:	Time series plot of the observed and model estimates of the March – May decadal rainfall for zone 5 as represented by Lodwar.....	143
Figure 45a:	Time series plot of the observed and model estimates of the June – August decadal rainfall for Kisumu.....	144
Figure 45b:	Time series plot of the observed and model estimates of the June – August decadal rainfall for Mbarara.....	144
Figure 46:	Mean surface temperature 1961-1990 (a) RCM (b) CRU (c) differences between CRU and RCM aggregated to the grid of the RCM.....	149
Figure 47:	March-May (1961-1990) Mean Rainfall climatology for (a) GCM (b) RCM and (c) Observed CRU Rainfall aggregated to RCM grid.....	151
Figure 48:	Observed and simulated annual cycle of RCM mean (a) maximum (b) minimum temperature patterns using CRU, HadAM3P, ECHAM4 and ERA 40 forcing data.....	153
Figure 49:	Mean spatial seasonal temperature climatology during all the seasons.....	154
Figure 50:	Mean spatial seasonal rainfall climatology aggregated to RCM grid for all seasons.....	155
Figure 51:	Simulated and observed mean annual rainfall cycles for stations in the region.....	157
Figure 52:	East Africa topography showing values of altitude in meters (m) as is represented in PRECIS RCM model.....	159
Figure 53a:	Scatter plot for semi-observed CRU plotted against ECHAM4 model out put	160

Figure 53b:	Scatter plot for semi-observed CRU plotted against HadAM3P model model out put	160
Figure 53c:	Scatter plot for semi-observed CRU plotted against ERA40 model out put	161
Figure 53d:	Scatter plot for semi-observed CRU plotted against Ensemble Mean RCM output.....	161
Figure 54:	Seasonal cycles of the various RCM models together with mean ensemble output after calibration	162
Figure 55:	Future temperature for 2020 using Mean Ensemble projection SRES A2.....	163
Figure 56:	Projection of future mean surface temperature (°C) for the period 2100 with reference to the baseline of 1961-1990 for the mean ensemble RCM under A2 scenario for December-February season	165
Figure 57:	Spatial patterns of the changes in seasonal mean surface air temperature (°C) for the period 2071-2100 with reference to the baseline of 1961-1990 under the Mean Ensemble A2 scenario for (a) December-February (b) March-May (c) June-August and (d) September-December.....	166
Figure 58:	The future change in March to May (MAM) seasonal precipitation for the period 2010-2020 in mm/day and also as a percentage of the present day with reference to the baseline of 1961-1990.	167
Figure 59:	Graphical plot for projected MAM seasonal rainfall for North-eastern sub-region as represented by Lodwar using smoothed and unsmoothed.....	168

LIST OF TABLES

Table 1a:	List and locations of stations used in the study.....	41
Table 1b:	Rainfall stations used to represent March-May (MAM) climatic zones.....	41
Table 2:	Rainfall stations used to represent October-December (OND) climatic zones	43
Table 3:	Rainfall stations used to represent June-August (JJA) climatic zones	44
Table 4:	ANOVA table for Multiple Linear Regression	67
Table 5:	Contingency table for observed and forecasted model.....	68
Table 6:	Eigenvalues, variance and accumulated variance extracted by each mode of the decadal MAM rainfall.....	79
Table 7:	Eigenvalues, variance and accumulated variance extracted by each mode of the decadal OND rainfall.....	82
Table 8:	Summary of some statistics from SVD analysis for specific Ocean SSTs and decadal OND rainfall.....	92
Table 9:	Summary of some statistics from SVD analysis for decadal JJA rainfall seasons for and specific Ocean SSTs.....	107
Table 10:	Summary of some statistics from SVD analysis for decadal MAM rainfall seasons for the specific Ocean SSTs.....	123
Table 11:	Assessment of the skill of the September -December regression models	140
Table 12:	Mean 1.5 m surface air temperature statistics for RCM and GCM for land points only over the region.	147
Table 13:	Seasonal land precipitation (mm/day) statistics for land points only aggregated to the RCM domain	150
Table 14:	Computed percentage absolute mean error (AME) between PRECIS RCM outputs and Observed rainfall records	158
Table 15:	Statistical results from the calibration of the model for the period 1961-1990	162
Table 16:	Average changes of precipitation under SRES A2 and B2 scenarios over east Africa region from PRECIS simulation relative to baseline (1961-1990)	164
Table 17:	Average changes of mean precipitation under SRES A2 and B2 scenarios over east Africa region from PRECIS simulation (1961-1990)	167
Table 18:	2071-2100 changes of mean seasonal rainfall and temperature under SRES A2 scenario from PRECIS relative to 1961-1990.....	168

LIST OF ACRONYMS

1	ACIA	Arctic Climate Impact Assessment
2	AMO	Atlantic Multidecadal Oscillation
3	ANOVA	Analysis of variance
4	AOGCM	Atmosphere Ocean Global Circulation Model
5	ASALs	Arid and Semi Arid Lands
6	CLIVAR	CLImate VARIability
7	CLIMDEV	Climate for Development in Africa
8	CRU	Climatic Research Unit of the University of East Anglia
9	DRC	Democratic Republic of Congo
10	ECHAM4	European Community Hamburg Model version 4
11	ENSO	El Nino-Southern Oscillation
12	EOF	Empirical Orthogonal Function
13	ERA40	European Centre for Medium-range Weather Forecasts (ECMWF) Re-Analysis 40
14	EROS	Earth Resources Observation and Science
15	FA	Factor Analysis
16	GCM	General Circulation Model
17	GDP	Gross Domestic Product
18	GHA	Greater Horn of Africa
19	GRVS	Great Rift Valley System
20	HadAM3P	Hadley Center Atmosphere-only global Model
21	HadCM3	Hadley Center Coupled Model version 3
22	ICPAC	IGAD Climate Prediction and Applications Centre
23	ICSU	International Council for Science
24	IGAD	Intergovernmental Authority on Development
25	IOD	Indian Ocean Dipole
26	IPCC	Intergovernmental Panel on Climate Change
27	ISDR	International Strategy for Disaster Reduction
28	ITCZ	Inter-Tropical Convergence Zone
29	JJA	June July August
30	KMD	Kenya Meteorological Department
31	LEV	Natural Logarithm Method
32	LDA	Linear Discriminant Analysis
33	MAM	March April May
34	MDGs	Millennium Development Goals
35	MLR	Multiple Linear Regression
36	MOC	Meridional Overturning Currents
37	NAO	North Atlantic Oscillation
38	NCAR	National Center for Atmospheric Research
39	NCEP	National Centers for Environmental Prediction
40	NIDIS	National Integrated Drought Information System
41	NMHS	National Meteorological/Hydrological Service
42	NMS	National Meteorological Service
43	NOAA	National Oceanic and Atmospheric Administration
44	OND	October – December

LIST OF ACRONYMS CONTINUED

45	PCA	Principal Component Analysis
46	PDO	Pacific Decadal Oscillation
47	PRECIS	P roviding R EGional C limates for I mpact S tudies
48	QBO	Quasi-Biennial Oscillation
49	RCM	Regional Climate Model
50	RegCM3	Regional Climate Model version 3
51	SLRM	Simple Linear Regression Model
52	SO	Southern Oscillation
53	SOI	Southern Oscillation Index
54	SRES	Special Report on Emissions Scenarios
55	SST	Sea Surface Temperature
56	THC	Thermohaline Circulation
57	TMA	Tanzania Meteorological Agency
58	TAV	Tropical Atlantic Variability
59	UK	United Kingdom
60	UMD	Uganda Meteorological Department
61	UNEP	United Nations Environment Programme
62	USGS	United States Geological Survey
63	WCRP	World Climate Research Programme
64	WMO	World Meteorological Organization

ABSTRACT

The overall objective of this study is to investigate the dominant spatial and temporal decadal rainfall variability modes and their teleconnection with decadal variability modes of the specific global oceans. Knowledge derived from the teleconnection is used to examine the predictability potentials of the modes of decadal variability of East African rainfall. Specific objectives that were undertaken to achieve the overall objective of the study include delineation of the region into homogenous zones with similar decadal variability modes; investigation of the teleconnection of the regional decadal rainfall variability patterns with global Sea Surface Temperatures modes; examination of the predictability potentials of the regional decadal rainfall variability patterns together with probable future regional climate scenarios and compare near-term projections with predicted decadal rainfall using Regional Climate Model (RCM).

The data sets used in the study include monthly observed rainfall over East Africa and global sea surface temperature covering the period 1950 to 2008. Other data sets used include gridded data of the University of East Anglia's Climate Research Unit (CRU) for the period 1961 to 1990; the European Centre for Medium-range Weather Forecasts (ECMWF) 40-year Re-Analysis (ERA40) and European Community Hamburg Model version 4 (ECHAM4) model output. The observed rainfall and sea surface temperature data used in the study were smoothed using a nine point binomial coefficient filter to remove all fluctuations equal to and less than 9 years.

The methods used to investigate the specific objectives included mass curve analysis to assess the quality of data used, trend and spectral analyses to investigate the dominant patterns of the existing decadal rainfall variability. Principal Component Analysis (PCA) was used to delineate the region into homogenous decadal rainfall zones while Canonical Correlation Analysis (CCA) and Singular Value Decomposition (SVD) techniques were used to investigate teleconnection amongst decadal rainfall with Sea Surface Temperature (SST) modes over various parts of the global oceans. The predictability potentials of the regional decadal rainfall variability patterns were assessed using correlation and Multiple Linear Regression (MLR) methods. A high resolution

Regional Climate Model (RCM), PRECIS (Providing Regional Climates for Impacts Studies), was applied to generate regional climate scenarios. Besides, PRECIS model was applied to produce hindcasts, that were compared with observed rainfall, and near-term future projections that were compared with predicted decadal rainfall.

The patterns of decadal variability showed that although wet and dry decades were recurrent, and sometimes extend over large areas, there were very few decades when floods or drought covered the whole of East Africa region except for the wet decade of 1961-1970 during the short rains (October-December) season. Results from spectral density analysis of rainfall time series smoothed with a 9-point binomial coefficients filter showed dominance of ten years period that were significant at 95% confidence level when both white and red noise hypotheses were used. The Principal Component Analysis results for decadal rainfall records yielded seven and nine homogeneous decadal rainfall zones for October-December (OND) and March-May (MAM) seasons respectively. Thus for the first time this study has provided detailed analysis and characterization of decadal rainfall modes for East Africa and delineated the region into homogenous zones, based on modes of decadal variability. This can be of great use in the long-term planning and management of all rainfall dependent activities in the region.

The results obtained from analyses of teleconnection between the regional decadal rainfall variability patterns and the global sea surface temperatures using Singular Value Decomposition (SVD) analysis showed high values of Square Covariance Fractions (SCF) explained by the first three modes of the global oceans. The results for the first SVD modes for Indian, Atlantic and Pacific oceans, respectively, contributed to 50%, 43% and 38% of the total square covariance for March – May, 65%, 48% and 40% for September - December rainfall seasons. During June- August season however, the first SVD modes accounted for 61%, 39% and 42% respectively for the same oceans. It was very evident that the El Niño modes were prominent over the Pacific Ocean, while Indian Ocean dipole was a key feature over the Indian Ocean basin. An inter-hemispheric dipole mode that is common during ENSO was a prominent feature in the Atlantic Ocean. In general, the results from the SVD highlighted the significant roles of all the global oceans in the observed decadal rainfall variability modes over the region. Based on previous studies conducted on the rainfall variability over the region, this study is the first

one to clearly demonstrate strong covariance between decadal rainfall variability and specific global oceans SSTs over parts of East Africa.

Results from Multiple Linear Regression (MLR) method showed substantial variation of the model prediction skill of the decadal rainfall variability modes within various homogenous zones and seasons. The Heidke Skill Score (HSS) values derived from model simulations were ≥ 0.30 at all locations indicating that the models could provide forecasts with useful skills. The percentage of correct forecast in all categories was found to be between 38% and 64% for all zones. Thus, the study has for the first time demonstrated that SST decadal variability modes can provide useful insight of decadal rainfall variability over East Africa region.

The regional model (PRECIS) simulations reproduced realistic annual cycles and inter annual variability patterns characteristic of the regional climate. PRECIS model also captured the general trend of the interannual rainfall anomalies for the training period of the model. The amplitudes of the individual extreme rainfall events were however not well resolved in most years and seasons. However, the downscaled global climate scenarios using PRECIS model were in general agreement with projected decadal variations using Multiple Linear Regression (MLR) models in most locations of the region.

The results of this study, therefore, have provided some very useful insights, tools, methods and products that can be broadly used to inform short to long term planning and management of all rainfall dependent activities in the region. In particular, the outcomes of this study will be useful milestone in mainstreaming decadal climate variability information into the regional economic development strategies. The results can be integrated in the development of new climate risk management tools to aid in coping with current climate variability and adaptation to future climate changes in East Africa.

CHAPTER ONE: INTRODUCTION

Most of socio-economic activities in East Africa region are rain dependent. The occurrences of both too little rainfall (droughts) and too much rainfall (floods) often lead to devastation of most economic, social and environment systems in East Africa. Many past studies of the region have concentrated in the investigation of extreme climate events on daily, seasonal and inter annual time scales despite evidences for recurrences of floods and droughts at decadal time scales. The knowledge of decadal rainfall variability patterns both in time and space is critical in climate risk management for medium to long term planning and sustainable development of all rainfall dependent activities in the region. The term East Africa is used in this study to refer to the three countries namely Kenya, Uganda and Tanzania.

East Africa is one of the regions with very high degree of rainfall variability both in space and time. Most of the hazards resulting into disasters in the region are climate related. Over 70% of the region is classified as Arid and Semi Arid Lands (ASALs). Agriculture is the mainstay of the economies of the region with over 78% of the total population dependent on rain-fed agriculture. The most dominant economic activity is small-scale subsistence farming in spite of low and erratic rainfall with recurrent droughts in most parts of the region. Therefore, efforts to improve understanding of rainfall variability and changes at different time and space scales forms an important research focus for the entire region.

Over 90% of natural disasters in the region are related to extreme climate events such as floods, droughts, cyclones, among others (ISDR, 2005). The percentage of climate related disasters is higher in the region with the poor being most vulnerable to current hazards and to the expected climate change impacts. These climate related disasters are often associated with severe socio-economic impacts such as lack of food, water, energy, and many other basic needs; famine; mass migration of animals and people; loss of life and property; and damage to infrastructure, among many other socio-economic miseries. The region undergoes regular devastating droughts and floods, that often lead to near collapse of agro-based economies and livelihoods, spread of diseases

and other socio-economic disasters. These impacts can result into limited progress and/or stagnation of socio-economic growth of the region.

Environmental degradation brought about by extreme climate events remains a major concern. The vulnerability of the communities is exacerbated by high rate of unemployment among the youths, constituting 60% of the population. The unemployment rate often rise during the years of climate extremes when raw materials are wiped out; low water levels in dams leading to power shortages and rationing, disease epidemics, among many other challenges. The recent climate risks including potential impacts of climate change calls for immediate attention and actions that can jeopardize sustainable economic development program of the region.

Some recent studies have noted significant changes in the frequency and intensity of severe weather events, onset and ceasession of rainfall season and climate extremes (IPCC 2007, Gitau 2005, Hastenrath and Polzin, 2004). At times some of the extreme events have persisted for months or years exacerbating the ever growing socio-economic problems of the region. Changes are also being observed in the patterns of many socio-economic variables. For example, the highlands that were previously free of malaria epidemics have now become malaria high-risk areas (Zhou et al., 2004; van Lieshout et al., 2004; IPCC, 2007).

Many studies have shown that Atlantic Ocean have strong influence on the climate of the regions neighbouring it and beyond (Hastenrath and Heller, 1977; Moura and Shukla, 1981; Parker et al., 1988; Hu and Huang, 2006; Chang et al., 1998; Wang, 2002; Sutton and Hodson, 2007). Significant teleconnection have been observed between the Great Ocean Conveyor (GOC) and the associated currents that influence the global climate patterns through ocean-atmosphere interactions (Hashizume et al., 2003; Jochum et al., 2007; Qiao et al., 2004; Marmorino et al., 2004; Valsala and Ikeda, 2007; Zang and Gottschalk, 2002). The amount of heat transported around by atmospheric and oceanic currents plays an important role in determining the mean climate of any region (Shukla, 1991; Wunsch and Heimbach, 2006) and the ocean waves have significant influence on Sea Surface Temperatures (SSTs). The GOC transports warm and low salinity water from

the tropical Pacific and Indian oceans round South Africa to north Atlantic near Iceland (Burroughs, 1999).

Some recent studies have noted that heavy rains and the associated floods affecting parts of the region are observed after an average of five to ten years followed by another five to ten years of depressed rains and associated drought (Omondi 2005; Schreck and Semazzi, 2004). The Intergovernmental Panel on Climate Change (IPCC 2007) assessment indicates that both droughts and floods have increased in frequency and severity in the recent years, and are projected to increase in the future at many locations world wide, with far reaching implication on the demand and availability of quality fresh water resources. There are also large year to year variations in precipitation received at various locations of Africa (Ogallo, 1979; Nicholson, 2000b). In some years extreme floods / droughts are observed leading to too much / too little water on the surface with far reaching physical, environmental and socio-economic impacts. Over the region, a single drought or flood can draw back many years of national socio-economic development growth. Climate extremes are also linked to many regional conflicts and insecurity when societies compete over limited water, food and graze lands. The impacts of climate variability including changes in the patterns of the extreme events have potential to destabilize livelihood systems and future development activities.

Timely availability of climate information through prediction and early warning can provide useful tools for forward planning to reduce the vulnerability and risks of the hydro-meteorological hazards. Lead time of the early warning system is important for the general planning and management of the disaster systems. Most of the recent prediction and early warning systems have been based on El Niño and the associated SSTs (Indeje, 2000; Mutemi, 2003, Mwale et al., 2004, Gitau, 2005, Nyakwada, 2009). These have been done for periods of days to seasons.

The development of policies useful in addressing challenges posed by climate variability requires adequate knowledge of climate extremes on longer time scale. The knowledge of decadal rainfall variability over the region is therefore essential for economic planning in all rainfall dependent activities. This calls for quantification of

how much change or variability the climate of a particular region has taken place and future likely changes. Although prediction of climate variability beyond three months remains a challenge in the sub-region particularly among climate research scientists, there is need to attempt to project future climate variability beyond seasonal timescale using global and regional circulation models.

One of the key challenges of the global scientific community is proper understanding and forecasting of decadal climate variability. This is an issue and challenge that has also been recongnized by the World Climate Research Programme (WCRP) of the World Meteorological Organization (WMO) and International Council for Science (ICSU). Recent studies have shown that it is now possible to do seamless prediction of the climate system from weekly weather to seasonal, interannual, decadal and centennial climate variations (WCRP, 2005). Reliable decadal predictions have application in many sectors such as health, agriculture, water management, tourism, forestry, fisheries, electrical power generation, shipping and offshore construction (Crawford et al, 2006). These applications would all be irrelevant without the additional knowledge of Anthropogenic Climate Change (ACC). However, in the light of ACC, many public and private sectors are now facing the problem of assessing what infrastructure investment is needed to adapt to climate change. Whilst mitigation policy is relevant for controlling carbon concentrations a hundred or more years ahead, infrastructure investment decisions in climate-sensitive areas are most relevant on the decadal timescale. Hence, developing a reliable decadal prediction system will be a key contribution to developing appropriate strategies for climate adaptation.

Whereas there has been reasonable and relevant capacity building to generate skilfull weather and seasonal prediction in the region, limited (or none) attempt has been made to develop similar capacity and skills for decadal predictions. But, at the same time information of extreme climate variations at decadal timescales is becoming extremely useful for decision makers in diverse arenas, from water managers to public health experts, medium and long term national development plans; among many other sectors that are sensitive to climate variability and changes. Information about decadal climate variability and change are necessary in the development of climate risk planning tools

that are critical for development, food security, water resources, fisheries, public health among many other sectors.

Therefore, the primary goal of this dissertation research is to investigate characterize and improve our understanding of spatial and temporal decadal climate variability and near-term (decadal) future climate projections over East Africa region. It also examines the potential use of the derived characteristics and modes of present and future decadal predictability and predictions in the improvement of regional climate risk reduction strategies, including coping with the current climate extremes and development of realistic climate change adaptation tools and strategies.

The overall and specific objectives of this study are described in the subsequent section.

1.2 OBJECTIVE OF THE STUDY

The overall objective of this study is to investigate the dominant spatial and temporal decadal rainfall variability modes and their teleconnection with global sea surface temperatures modes. To achieve this primary goal, the specific objectives were developed as:-

- i) Delineate the East African region into zones with similar decadal variability modes
- ii) Determine the significance of existing decadal modes in the observed interannual rainfall records.
- iii) Investigate the teleconnection of the regional decadal rainfall variability patterns to global Sea Surface Temperatures
- iv) Examine the predictability potentials of the regional decadal rainfall variability patterns
- v) Examine probable future regional climate scenarios and compare near-term projections with predicted decadal rainfall using Regional Climate Model (RCM).

1.3 JUSTIFICATION OF THE STUDY

The decadal time scale is widely recognized as a key planning horizon for governments, businesses and other societal entities (Vera et al., 2009). Decadal climate variability is closely related to health, mainly applied to the possible changes in temperature and rainfall, and the estimation of propagation of disease vectors. Diseases carried by insects expand in geographical range as temperatures rise and fall. Warmer weather enables tropical insects to carry diseases toward higher latitudes. Wetter weather allows malaria to spread to new regions, and increase in severity in already-infected areas. Decadal predictions will enable societies and agencies to enhance their response strategies to spread of diseases in new territories and also developing mitigation measures to combat spread of diseases under changing climates

Extreme climatic events have often wiped out decades of national development investments, and infrastructures as many nations are forced to redirect most of their scarce resources planned for national development activities to disaster response and recovery, including emergency relief activities. The rapid accumulation of climate-related risks in recent decades and the associated patterns of losses indicate ineffectiveness and even breakdown in spontaneous adaptation and coping (UNDP 2002). Strategy to reduce losses of lives, socio-economic setbacks and environment degradation by the various climate related hazards requires an effective Integrated Disaster management strategy that takes into consideration risks that the various hazards pose on various poverty reduction and sustainable development systems driven by the socio-economic and livelihood systems of the specific locations of the region.

Within East Africa region, rainfall variability is strongly influenced by El Nino-Southern Oscillation (ENSO) on interannual time scales (Ogallo 1988, Indeje et al., 2000, Mutemi 2003). ENSO which is associated with the cycle of warm and cold sea surface temperature (SST) anomalies in the central and eastern equatorial Pacific, has impacts that affect global climate on interannual and interdecadal time scales (e.g., Karoly et al., 1996). Only a few climate phenomena have been studied in depth, the most prominent being the interannual variations associated with ENSO and global sea surface temperature (Ogallo et al., 1988; Indeje et al., 2000; Mutemi, 2003; Owiti, 2005). Much

attention has been devoted to how and why precipitation varies in association with the ENSO (Ogallo 1988, Indeje, 2000; Mutemi 2003; Owiti 2005) and Sea Surface temperature gradients (Nyakwada 2009), but very little has been done, in terms of comprehensive studies, to consider variability on longer time scales and what might possibly be forcing such variability.

Studies based on observed rainfall records over the region have shown strong evidence of decadal variability with teleconnection to modes of variabilities over parts of the global oceans (Omondi, 2005; Schreck and Semazzi, 2004; Muthama et al., 2008). There is therefore need to improve forecasting of decadal climate variability. Such forecasts would provide vital information to policy-makers for making long-term decisions to prepare the communities for the anticipated impacts of near-term (decadal) climactic changes.

The increased persistence and severity of extreme climatic events and the high potential for their occurrences in the region need long lead-time, but also skilful forecasts and/or knowledge on probable future climate scenarios to enable planners formulate decisions on the appropriate way to prepare the communities for the anticipated impacts of climate extremes, including climate change. Furthermore, the attainment of the strategic development plans of the three countries in the region as stipulated in (Kenya's Vision 2030, Uganda's Vision 2035 and Tanzania's Vision 2025) would largely depend on how well the predictability and prediction of these extreme climate events are understood and thus mainstreamed into these developmental plans and visions.

Sustainable socioeconomic development of the region requires integration of climate knowledge if the diversified livelihoods of the various communities are to be sustained and poverty alleviated; and also if the international community's strategy for global sustainable development and poverty reduction targets under Agenda 21 in the Millennium Development Goals (MDGs) is to be attained.

The importance of decadal climate variability has also been recognized by the Intergovernmental Panel on Climate Change (IPCC), which will include results from experiments specifically designed to provide decadal climate projections in its next, Fifth,

Assessment report (Taylor et al., 2008). That importance is also recognized through a number of national initiatives aimed at providing future climate information for decadal and longer time scales (Meehl et al., 2009).

In a previous study using eighty-year record of observed rainfall from the region, Omondi (2005) showed pronounced decadal rainfall fluctuations). Based on some of the identified as outstanding issues and subsequent recommendations from this earlier study, this work employed modeling technique to project into the future with particular interest of examining likely changes in rainfall pattern from the present to late 21st centuries (i.e. the 2010–2100) with focused interest on decadal projections. With the vulnerable local communities and high spatial variation of rainfall in the region, this study probes into simulated precipitation changes at temporal scales longer than the commonly used interannual variations. This research is devoted to improving the knowledge on decadal scale climate variability and assesses how the derived modes and patterns of regional decadal rainfall variability could be used to improve regional climate risk reduction strategies that incorporate coping with the current climate extremes as well as developing realistic climate adaptation strategies.

The prospect of decadal prediction and its recognized importance has led, in part, to the initiation, in several countries, of climate services intended to bridge the gap between the seasonal-to-interannual (SI) climate information provided by the National Meteorological and Hydrological Services and the broad scale, longer time horizon information considered by the IPCC assessments.

1.4 AREA OF STUDY AND ITS PHYSICAL FEATURES

The area covered in this study is East Africa. The term East Africa is used in this study to refer to three countries namely Kenya, Tanzania and Uganda located within latitudes 5°N to 12°S and longitudes 29°E to 42°E.

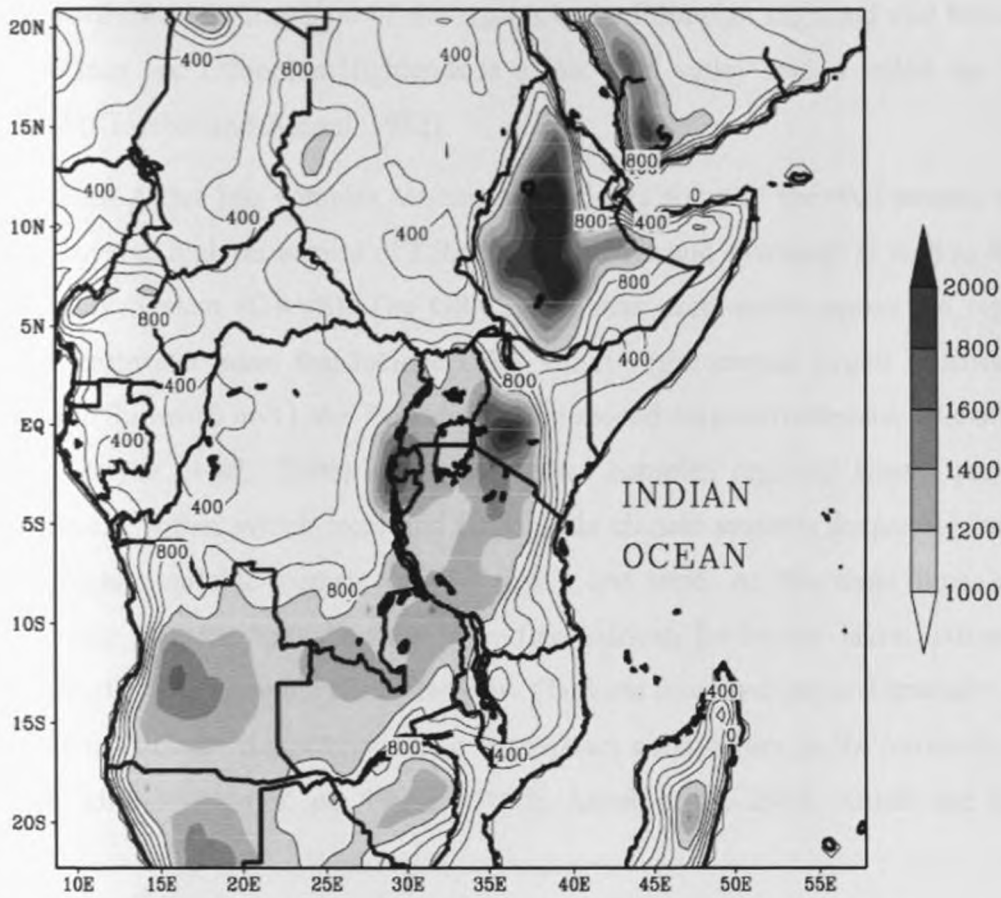


Figure 1: Topographical features of the outer domain, with areas higher than 1000m shaded (Adopted from Anyah, R., 2005)

Figure 1 shows the topographical features of East Africa region. Most parts of the region lie above 1000 metres above sea level. The land rises gradually from the eastern coastline on the Indian Ocean through the remnants of the rain forests to the dry bush country of the Nyika plateau and to the forest covered East Africa highlands. The highest mountains in Africa are located in this region with Mt. Kilimanjaro (5895m) and Kipengere Ranges in south-western Tanzania, Mt. Kenya (5199m), and Mt. Elgon (4321m) in Kenya together with Mt. Ruwenzori (5109) in Uganda. From the central highlands the land drops gradually a way to the west to Lake Victoria at 1132m above mean sea level. To the west of the domain the land drops to the Democratic Republic of Congo basin (400 to 1000m AMSL). The central highlands make up the eastern and western escarpments of the Great Rift Valley, which enters the region from the north, passes southwards through Kenya into Tanzania and runs into the South Africa countries.

In the northeast neighborhood of the region is the Ethiopian highland and between the East African and Ethiopian Highlands is a low level valley region called the Turkana Channel (Kinuthia and Asnani, 1982).

East Africa has complex terrain that includes some of the well-known, tropical, glacier covered high mountains of Kilimanjaro, Kenya and Rwenzori as well as the Great Rift Valley System (GRVS). The GRVS that runs north-south across the region has several freshwater lakes that include Lake Victoria (the second largest freshwater lake after Lake Superior) and Lake Tanganyika, the second deepest freshwater lake after Lake Baikal (Anyah *et al.*, 2006). As a whole the complex regional terrain presents an environment within which local and large scale climate systems frequently interact to create highly variable climate in both space and time. At the same time, complex topographic features, including the large East African freshwater lakes, extensive and high mountains, orographic channeled flow (Turkana low-level jet) and spatially variable land use/land cover characteristics, are significant contributors to the variability of the regional climate (Sun *et al.*, 1999a, 1999b; Anyah *et al.*, 2006; Anyah and Semazzi, 2006).

The largest water body over East Africa is Lake Victoria. Others are lakes Turkana and Tanganyika found within the floor of the Great Rift Valley. The large water bodies and complex terrains have profound effects on the rainfall climatology over the region. There are large spatial and temporal variations in the rainfall characteristics over the region due to the complex topographical patterns, the existence of many large inland lakes, together with several other regional factors (Asnani and Kinuthia 1979; Ogallo 1982; Anyah 2005; Njau 2006). The diversity in orography has profound effects on the overall climate dynamics and the spatial distribution of key meteorological parameters like wind, surface temperatures and rainfall (Ininda 1994, 1995). Indeje *et al.*, (2000) have stated the dominant roles of orography in climate dynamics. In the region, orography determines the positions of the semi-permanent upper tropospheric troughs and ridges in the westerlies, the orographic convective precipitation systems, the development and maintenance of mesoscale circulations, and the blocking and channeling effects on the low-level jet streams.

CHAPTER TWO: LITERATURE REVIEW

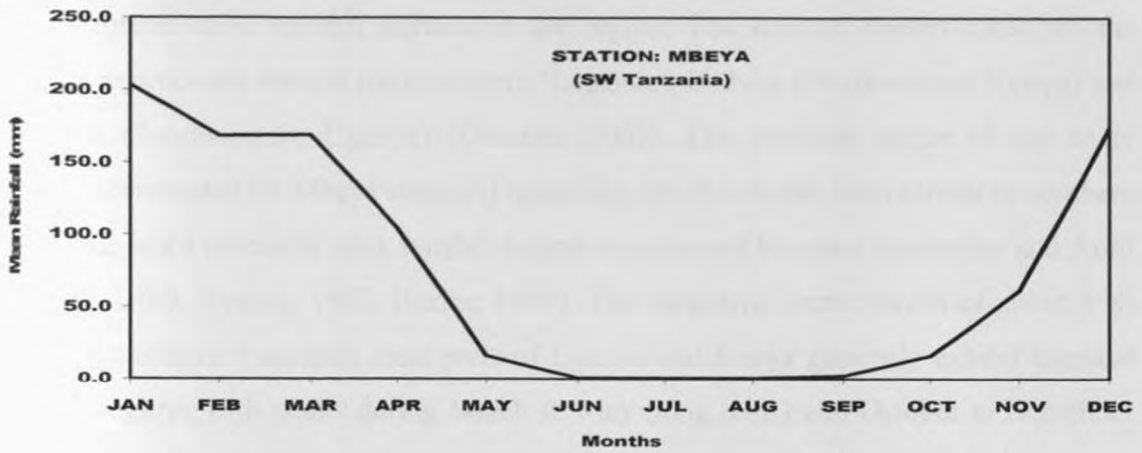
In this chapter, the literature relevant to this study is reviewed. Some literature from past studies on spatial and temporal rainfall variability over the region that has been undertaken is also reviewed. Some relevant literature from other regions is also included in this section. The literature reviewed includes past studies associated with the systems that control the space-time variability of rainfall in East Africa. The next section gives review on the climatology of rainfall over East Africa region.

2.1 RAINFALL CLIMATOLOGY OF EAST AFRICA

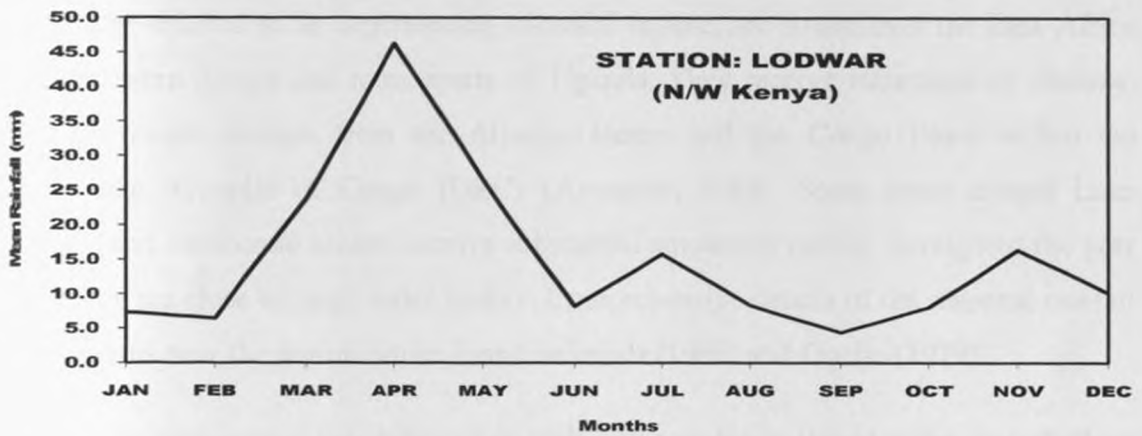
Unique regional features such as the Rift Valley and mountains interact with both the synoptic and the large-scale systems to produce the observed rainfall distribution (Mukabana, 1992; Asnani, 1993). Seasonal rainfall patterns over East Africa are very complex due to the existence of complex topography (Figure 1) such as the Rift Valley system, mountains, plateaus and large inland water bodies (Asnani and Kinuthia, 1979; Ogallo 1979, 1980; Asnani, 1993, 2005; Ininda, 1995; Okoola, 1996; Mukabana and Pielke, 1996). The temporal variations of rainfall over East Africa occurs on various time scales, which include diurnal (Johnson, 1962; Asnani and Kinuthia, 1979; Asnani, 1993; Barring, 1987), quasi-biweekly (Okoola, 1989), intraseasonal/monthly (Tomsett, 1969), seasonal (Ogallo, 1988), annual (Ogallo, 1980) and decadal (Omondi, 2005; Shreck and Semazzi, 2004). The quasi-periodic fluctuations of time-scales greater than a year have also been observed (Rodhe and Virji, 1976; Nyenzi, 1992; Ogallo, 1989).

There are two major rainfall seasons experienced over East Africa, these are locally referred to as the “long rains” (March-May) and the “short rains” (October-December). The long rainfall season is concentrated within March to May (MAM) while the short rainfall season occurs about late September to November/early December

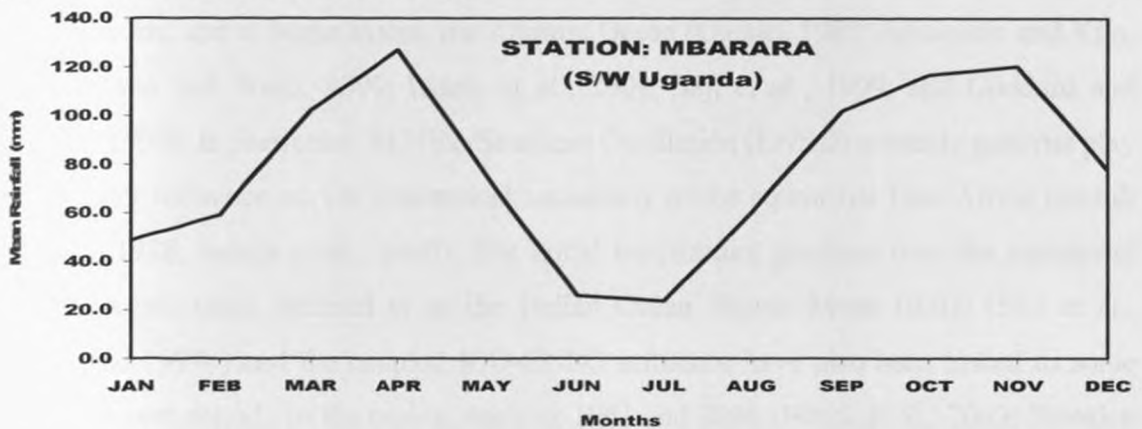
(SOND).



(a) Mbeya in Southwest Tanzania



(b) Lodwar in Northwestern Kenya



(c) Mbarara in Southwestern Uganda

Figure 2: Mean annual rainfall cycles for (a) Mbeya (b) Lodwar and (c) Mbarara stations over East Africa (Omondi, 2005).

Figures 2a, 2b and 2c show some examples of seasonal rainfall variations from some representative rainfall stations in the region. The stations chosen based on the rainfall regimes are Mbeya (southwestern Tanzania), Lodwar (Northwestern Kenya) and Mbarara (Southwestern Uganda) (Omondi, 2005). The southern sector of the study region, represented by Mbeya station (Figure 2a), which extends from central to southern Tanzania, has a unimodal peak rainfall regime experienced between September and April (Ogallo, 1980; Nyenzi, 1992; Bazira, 1997). The equatorial sector (north of about 5°S) covering northern Tanzania, most parts of Uganda and Kenya generally exhibit bimodal rainfall regime, with peaks during March to May (long rains) and October to December (short rains). During northern hemisphere summer, some areas receive substantial amount of rainfall besides the two long and short rainfall seasons. The regions that are, commonly referred to as experiencing trimodal regime, are found over the East Africa coast, western Kenya and most parts of Uganda. They receive incursions of shallow, westerly, moist airmass from the Atlantic Ocean and the Congo Basin within the Democratic Republic of Congo (DRC) (Anyamba, 1984). Some areas around Lake Victoria and the coastal sectors receive substantial amount of rainfall throughout the year since they are close to large water bodies. Comprehensive details of the seasonal rainfall distributions over the region can be found in Ininda (1995) and Ogallo (1979).

The inter-annual variability of rainfall in the region is linked to the perturbations in the global sea surface temperature, especially over the equatorial Pacific and Indian Ocean basins, and to some extent, the Atlantic Ocean (Ogallo, 1988; Nicholson and Kim, 1997; Mutai and Ward, 2000; Indeje et al., 2000; Saji et al., 1999; and Goddard and Graham 1999). In particular, El Niño/Southern Oscillation (ENSO) anomaly patterns play a dominant influence on the interannual variability of the equatorial East Africa rainfall (Ogallo, 1988; Indeje et al., 2000). The zonal temperature gradient over the equatorial Indian Ocean, often referred to as the Indian Ocean Dipole Mode (IOD) (Saji et al., 1999a and 1999b) and the coupled IOD-ENSO influence have also been linked to some of the wettest periods in the region, such as 1961 and 2006 (Black et al., 2003; Bowden and Semazzi, 2007).

The SST anomalies occurring over the Pacific, Atlantic and Indian Oceans either all at the same time or each at different times, intriguingly influence the interannual variability of the regional rainfall. At the same time, complex topographic features including the large East African freshwater lakes, extensive and high mountains, orographic channeled flow (Turkana low-level jet) and spatially variable land use/land cover characteristics are significant contributors to the variability of rainfall (Sun et. al., 1999; Anyah et al., 2006; Anyah and Semazzi, 2006a, 2006b) in the region. It is noteworthy that high rainfall areas are concentrated over the highlands and near the large water bodies. Arid and semi-arid areas of the region including Eastern and Northern Kenya, Northeastern Uganda, and Central Tanzania receive very low rainfall annually.

The sub-section that follows gives a brief discussion on some of the systems that influence weather patterns in the study region.

2.1.1 INTER TROPICAL CONVERGENCE ZONE (ITCZ)

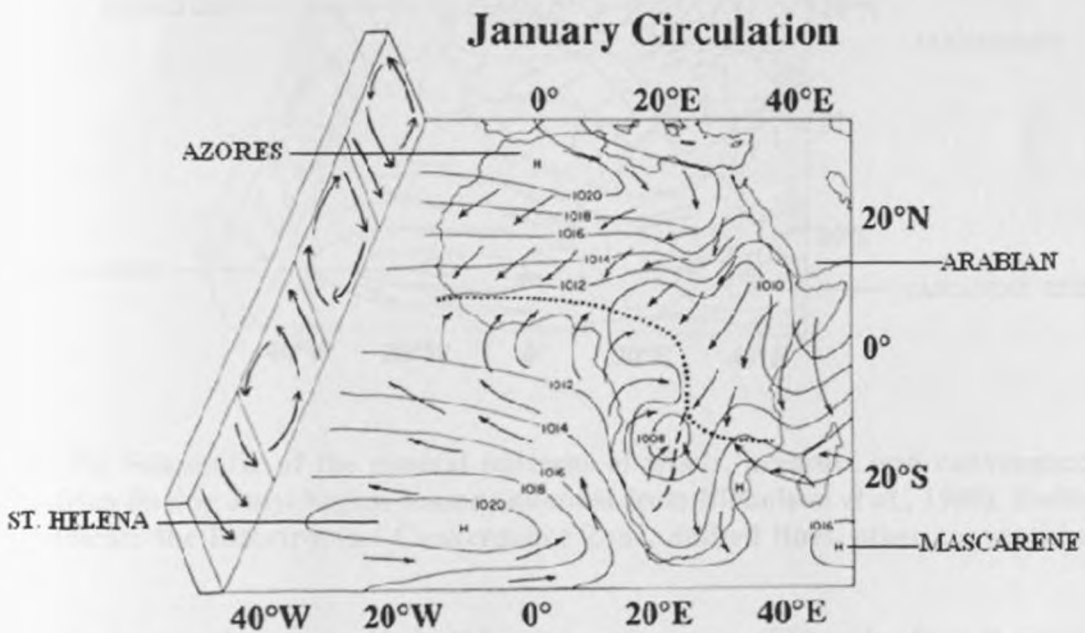


Figure 3a: Schematic of the general patterns of winds, pressure and convergence over Africa during January (adapted from Nicholson *et al.*, 1988). Dotted lines indicate the Intertropical Convergence Zone, dashed lines, other convergence zones.

The ITCZ is the main synoptic scale system that controls the intensity and migration of the seasonal rainfall over the eastern Africa. It is a boundary of confluence of hemispheric winds near the surface as a result of inter-hemispheric monsoon wind systems over the region. Due to the complex effects of topographical diversity on low-level synoptic circulation, the convergence zone is difficult to locate at low levels over East Africa. The ITCZ is however detectable in the wind field near 700mb (Kiangi et al., 1981). Over East Africa, and during the southern hemisphere summer, during the months of November to March, the ITCZ has two unique components i.e. the normal east-west orientation called the zonal component and the north-south oriented component (Figure 3a) referred to as meridional component (Nicholson et al.,1988, Ininda 1994, Okoola 1999).

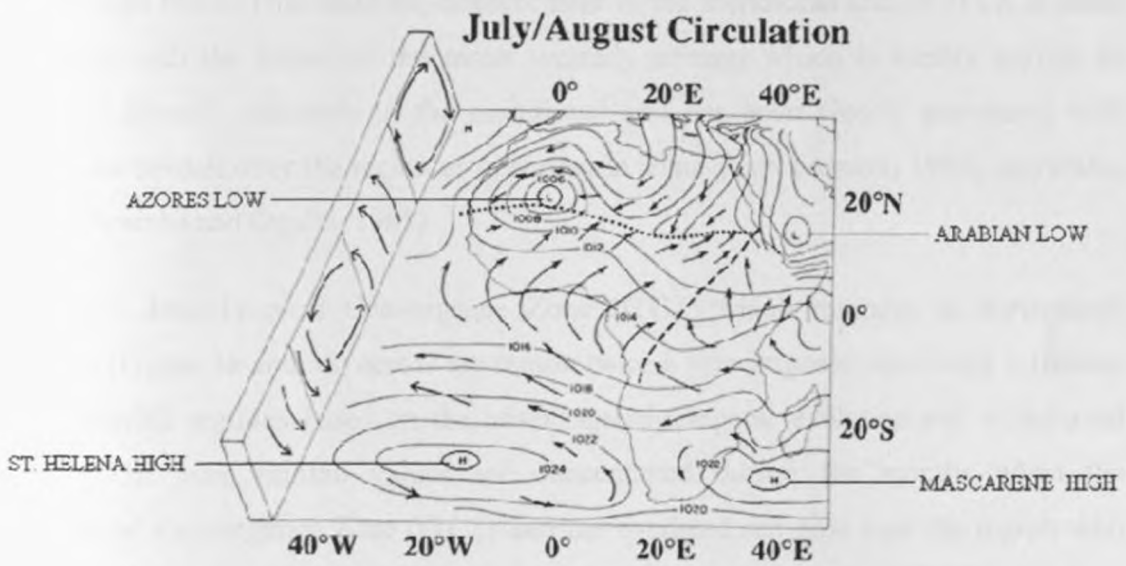


Figure 3b: Schematic of the general patterns of winds, pressure and convergence over Africa during July/August season (adapted from Nicholson et al., 1988). Dotted lines indicate the Intertropical Convergence Zone, dashed lines, other convergence zones.

The converging northeasterly (NE) and southeasterly (SE) trades form the zonal component. The north-south oscillation of the zonal component is primarily responsible for both the long and the short rainfall seasons over East Africa. The strength of ITCZ depends on the intensity of the NE and SE trade winds, which in turn are driven by the subtropical anticyclones. This weak surface ITCZ is attributed to presence of complex

topography which includes the Great Rift Valley and chains of high mountains like Mt. Kenya and Mt. Kilimanjaro which are over 5000m AMSL (Mukabana, 1992). This weakness is thus specifically due to the effects of the thermally-induced mesoscale circulations associated with the complex orography and the presence of large water bodies. The meridional component is formed by the convergence between the easterly winds from the Indian Ocean and the moist westerlies from the Atlantic Ocean and the Congo basin. It oscillates roughly between longitudes 25°E and 36°E. Sometimes it couples with the quasi-permanent Lake Victoria Trough to give active weather over much of western Kenya throughout the year (Asnani, 1993, 2005). The meridional branch of the ITCZ (Figure 3b) is shifted furthest east during June/July which causes large parts of the region to be under a moist westerly monsoonal current from Atlantic Ocean and the moist Congo basin. This eastward displacement of the meridional arm of ITCZ is often associated with the influx of the moist westerly airmass which is locally known as “Congo Airmass”. Anomaly in the meridional arm has been closely associated with anomalous rainfall over the region as observed in some years (Asnani, 1993; Anyamba, 1983; Anyamba and Ogallo, 1985).

The Inter-Tropical Convergence Zone (ITCZ) which migrates in north-south direction (Figure 3a and 3b) across the region twice a year imposes significant influence on the rainfall regimes based on the onset, spatial-temporal evolution and withdrawal pattern. The peak rainfall values are concentrated during the months when the Intertropical Convergence Zone (ITCZ) and the overhead sun pass over the region with the former lagging behind the later by 3-4 weeks (Okoola 1998). Since ITCZ is the main rain-producing system in East Africa, interannual fluctuations in rainfall amount and distribution have in the past been generally attributed to anomalies in the large-scale factors that influence the characteristics of the ITCZ in the region. For instance, the 1984 drought was associated with the non-establishment of the zonal arm of the ITCZ as a result of a series of tropical cyclones in the Indian Ocean that rendered the low level flow over the region diffluent as it was diverted to the low pressure systems over the ocean (Anyamba, 1984). Moreover the meridional arm of the ITCZ was weak as a result of anomalous warming of the Atlantic waters off the African Coast (Okoola, 1998). The 1972 drought on the other hand was attributed to anomalous easterly flow (Minja, 1984).

The 1961/62 floods, the worst experienced in the region this century, were associated with a very strong low-level westerly wind anomaly (Anyamba, 1984; Anyah and Semazzi, 2006).

2.1.2 SUBTROPICAL ANTICYCLONES

These are synoptic-scale quasi-permanent high-pressure belts due to descending arms of the Hadley circulation (Figure 4). They are characterised by anticyclonic circulation which gives rise to subsidence and low level horizontal velocity divergence of airmasses. These anticyclones create pressure difference between the equatorial regions and the sub-tropics necessary for driving the tropical trade winds. The anticyclones affecting the flow over East Africa are the Arabian, Mascarene, the Azores and the St. Helena high (Figure 3a and 3b). The Azores and the Arabian anticyclones control the flow of the northeasterlies from the Northern Hemisphere, while the flow of the southeast monsoons from the Southern Hemisphere is controlled by the Mascarene and the St. Helena anticyclones. These systems are most intense during the winter seasons of each hemisphere and weaker during summer.

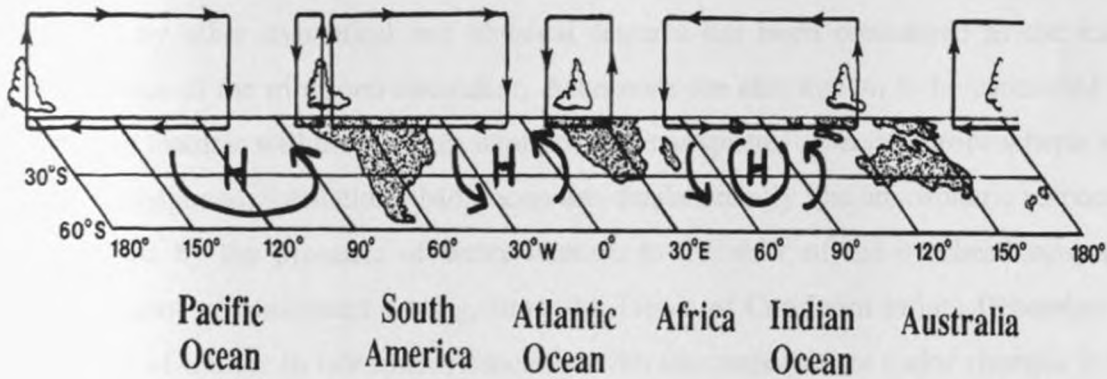


Figure 4: The schematic of east-west Walker global circulation (Adapted from Indeje, 2000)

The Arabian high generates stronger North Easterlies (NE) during the short rainfall period than the South Easterlies (SE) from the relatively weaker Mascarene high. However, since the North Easterlies do not have long trajectory over the ocean, as compared to South Easterlies which have a longer trajectory over south West Indian Ocean, ITCZ yields lesser rainfall during the September-November period. During the

March-May season, the Mascarene high drives stronger and moister SE into East Africa. Convergence of SE with the NE, both of which have stronger easterly component results into Long rainfall season. Intensification in the strength of the St. Helena high implies stronger moist westerlies and therefore a stronger meridional arm of the ITCZ.

The characteristics of these anticyclones together with the other weather systems over the Indian Ocean and the Congo/DRC basin (like the easterly waves, equatorial westerlies and tropical storms) are the major sources of moisture transport into the region. For example, the intensification of the St. Helena anticyclones over the southern Atlantic reactivates the Congo Air Boundary pushing it eastwards to couple with Lake Victoria Trough and initiate active convection over western parts of the region (Trewartha, 1981). This incursion of the Congo airmass causes the third peak in rainfall within a year over the western parts of the region centred on July/August.

2.1.3 MONSOONS

Monsoons are defined as the seasonal reversal of the cross-equatorial winds that follow the overhead sun and the ITCZ. The differential heating of the land and sea enhanced by other dynamical and physical features has been considered as the main driving force of the monsoon circulation. Monsoons are also known to be controlled by circulation features within the whole depth of the atmosphere, especially tropospheric and lower stratospheric circulations. Monsoons are, fundamentally, the atmospheric response, complicated by the presence of water vapour, to the shift of the overhead sun, and therefore zone of maximum heating, from the Tropic of Capricorn in late December to the Tropic of Cancer in late June. Associated with this response are major changes in jet stream movements and a meridional shift of the rain-bringing ITCZ. Monsoons are characterised by major wind systems that seasonally reverse direction (e.g., one that blows for six months from the northeast and six months from the southeast). The primary cause of monsoons is the difference between annual temperature trends over land and sea. Seasonal changes in temperature are large over land but small over oceans. Monsoons blow from cold towards warm regions from sea toward land in summer and from land toward sea in winter. Most summer monsoons produce large amounts of rain while winter monsoons tend to cause drought.

The climate of East Africa region is influenced by the northeast and southeast monsoons, which are experienced during southern and northern summer respectively (Trewartha 1981, Anyamba 1983, 1993; Findlater 1971). The northeast monsoons are generally continental, dry, shallow and diffluent. During the intermediate equatorial seasons (March-May and September-November) both monsoonal wind currents are present with one withdrawing while the other advancing. The monsoonal winds, which occur during the transitional seasons, have a strong zonal component and bring equatorial warm and moist air into the Equatorial East Africa region from the Indian Ocean. Sadler *et al.*, (1987) have shown warm surface waters (SST) over equatorial Indian Ocean during the transition months of April and November. This moist equatorial air has a conditionally unstable lapse rate and responds rapidly to low-level convergence with widespread cloudiness, showers and thunderstorms.

Many extreme rainfall anomalies in East Africa during the major rainy seasons have been associated with anomalies in the monsoonal wind systems, since they are the major transport mechanism of moisture into the region. Both monsoon currents are generally diffluent in the low levels and flow parallel to the coast so that they do not advect much moisture inland. They are relatively shallow extending up to about 600hPa; and are capped aloft by an easterly flow. The southeast monsoon is cool and moist and the warm easterly current aloft results in a persistent inversion near 600hPa, which inhibits cloud development. This inversion is occasionally broken by incursions of westerlies. The convergence of these winds determines the location of ITCZ. The characteristics of these winds over the region are controlled by the location, intensity and orientation of the major semi-permanent anticyclones of Africa, together with other related general circulation parameters (Njau 2006). The southeast monsoon from Mascarene high is relatively moister compared to the northeast monsoon with land trajectory originating from the Arabian ridge.

In the next section, the easterly and westerly waves are discussed.

2.1.4 EASTERLY AND WESTERLY WAVES

The easterly waves are westward propagating wavelike perturbations within the easterly current. They are observed equator-ward of the subtropical high-pressure belts in the neighbourhood of the ITCZ and are associated with the origin of tropical cyclones. Their conditions at a specific location will depend on whether it is the location of origin, enhancement or decay. Easterly waves forming in the Pacific have been observed to cross the Indian Subcontinent into the Arabian Sea and weaken towards the Western Arabian Sea (Asnani 1993). The arrival of an easterly wave is recognized by the disturbance of the weather condition and changes in the surface pressure.

Asnani (1993) gives a detailed discussion of tropical easterly waves. The easterly waves are known to influence the weather of the region. Fremming (1970) observed rain associated with an easterly wave disturbance that affected the coast and mainland areas of East Africa region during south east monsoon in September, 1967. Cadet and Olory-Togbe 1977, Cadet 1978 studied time longitude sections of cloudiness over the Indian Ocean during the northern summer, between 25 June and 10 August, 1975. They found the existence of westward propagating disturbances in the Indian Ocean to the south of the equator (7.5° S and 12.5° S) and eastward propagating ones to the north of the equator. According to their findings the perturbations to the south of the equator displayed wavelength of 7,500 km, periodicity of about two weeks, and phase speed of about 5° - 6° longitude per day. The development of deep westerlies usually presages imminent widespread of rains over East Africa. The westerlies are accompanied by deep stratified cloud with embedded cumulonimbus. The seasonal characteristics of the ITCZ occasionally induce westerly winds over the equator, particularly when the monsoon winds change direction after crossing the equator through the influence of the Coriolis force.

In their study of easterly and westerly waves, Kabanda and Jury (1999), found that the convection is enhanced by an increase of upper westerlies in the equatorial band which assists overturning and convective outflow. During July and August the phenomena mostly affects Uganda and western Kenya while in January through March it affects mainly central and southern Tanzania. These westerlies are relatively moist and

unstable and give widespread rains over equatorial eastern Africa (Trewartha, 1981). An increase in the westerlies often leads to widespread heavy rains during the major rainfall seasons of April-May and October-November when winds are predominantly easterly, Beresford (1982).

Nakamura (1968) distinguished two regimes of westerlies over East Africa, those occurring in January–March over the southern Tanzania and the May - October westerlies. The latter were observed to affect a wider area of the eastern parts of the region, extending from 10° S, across the equator into the northern hemisphere at 700–500 hPa embedded in easterly currents. Studies show the occurrence of equatorial westerlies over the West Indian Ocean during normal years, maximum intensity of westerlies are generally observed at 700 hPa level, while easterlies were dominant at the upper levels during the long-rains season (Murakami and Sumathipala, 1989; Okoola 1989, 1999). The 1961/62 floods, one of the worst floods experienced in the East Africa region were associated with a very strong low level westerly anomaly (Anyamba, 1993).

The next sub-section discusses tropical cyclones, which are amongst the synoptic features with significant influence on the rainfall of the region.

2.1.5 TROPICAL CYCLONES

The tropical cyclones that influence weather over East Africa form in the West Indian Ocean region, equator ward of 20° latitude. North of the equator, they form in northern spring and late fall and move northward into the Arabian Sea. They are cyclonic vortices whose origins are almost invariably in the low latitudes between 50 and 200 North or South of the equator. In these latitudes, the deflecting force of the earth's rotation (Coriolis force) is sufficiently large to produce cyclonic circulation. According to World Meteorological Organization (WMO) tropical storm is a low pressure system whose sustained wind speeds is 34-63 knots and becomes a tropical cyclone when the sustained wind speed is equal to or in excess of 64 knots (Reiter, 1961). Intense depressions occur in several tropical southern/western Indian Ocean regions during certain periods of the year and these are popularly known as cyclones in the southwest Indian Ocean and Arabian Sea, and as Willy-Willy in Australia. There are other regional

names given to similar weather systems appearing in different parts of the world (Asnani, 1993).

Tropical cyclones usually reach their maximum frequency in August-September in the Northern Hemisphere and January-February in Southern Hemisphere. They cause severe weather that is destructive to both life and property (Asnani, 1993). These systems rarely reach the East Africa coast, however, there have been few occasions like in October 1972 and 1984 when they reached the coast and caused increased rainfall as far as Somalia and northern Kenya. Their effects are felt and can cause heavy precipitation for one or two days, as far as 200 km away from the East Africa coast. On the other hand, if a tropical cyclone passes further south and settles over Madagascar, it causes deviation of moisture laden south easterlies towards this low-pressure vortex thereby causing a dry spell over East Africa. In 1984 for example, high frequency of tropical cyclones in the Mozambique Channel contributed to the failure of the rains in many countries in eastern Africa (Anyamba and Ogallo, 1985). The monsoon winds accelerated into the channel and resulted into the non-establishment of the ITCZ in the region.

Jury *et al.*, 1999 showed that tropical cyclone days over Indian Ocean contains prominent decadal cycles, higher frequencies linked to QBO and have positive relationships with SSTs over the entire south west Indian Ocean from September to March. The presence of the cyclone near East Africa coast increases the pressure gradients between northern Africa and the Atlantic and the southwest Indian Ocean, causing moist westerlies to converge into eastern Africa. Such was the case during the floods of 1961/62 (Anyamba, 1983). According to Jury (1993), and Rocha and Simmonds (1996) a warm Indian Ocean is frequently associated with an increased frequency of tropical cyclones and strengthened equatorial surface westerlies. However, high frequency of occurrence of tropical cyclones in the South West Indian Ocean (SWIO) during the rainfall season leads to widespread rainfall deficits and drought in the East Africa region. The 1984, March-May, drought was associated with the non-establishment of the zonal arm of the ITCZ as a result of a series of tropical cyclones in the Indian Ocean which rendered the low level flow over eastern African diffluent as it was diverted to the low pressure systems over the ocean (Anyamba and Ogallo 1985).

It can, therefore, be concluded that the influence of the tropical cyclones on rainfall of the region depends on the season, track and location of the cyclones. The tropical cyclones can either enhance or reduce rainfall depending on the above characteristics.

2.1.6 QUASI-BIENNIAL OSCILLATION

The Quasi-Biennial Oscillation (QBO) is the alternation in phase of the zonal winds in the lower stratosphere with period of 26-30 months. There is vertical propagation in the phases of the zonal winds leading to changes in vertical wind shear and the associated stability. Several studies have reported the presence of the QBO in various atmospheric parameters and at different regions of the globe. Some of the atmospheric variables that have exhibited QBO include temperature (Rasmusson *et al.*, 1981), ozone (Funk and Garnham, 1962; Hasebe, 1980), Indian monsoon (Mukherjee *et al.*, 1979) and African rainfall (Rodhe and Virji, 1976; Ogallo, 1982; Nicholson and Entekhabi, 1986; Indeje and Semazzi, 2000).

Indeje *et al.*, (2000) found a statistical association between rainfall over East Africa and QBO to be strongest during the boreal summer season (June-August) and weakest in boreal winter (December-February). The strongest correlations were found over western parts of East Africa. Their results further indicated a significant relationship between QBO and the Indian Ocean Dipole Mode Index (DMI). Ogallo *et al.*, (1994) have investigated the characteristics of QBO over tropical eastern Africa using zonal wind composites from Nairobi, Kenya for the period 1966-1987. Their results, based on spectral analysis indicated the dominance of a 28 months period in the zonal wind component. Their results also indicated significant association (at 5% level) between rainfall and QBO signal based on the reversal in zonal winds.

Distinct QBO spectral peaks in East Africa have been reported in several studies [e.g. Rodhe and Virji (1976); Ogallo (1982); Nicholson and Entekhabi (1986)]. Nicholson and Entekhabi (1986) presented evidence of several quasi-periodicities common to African rainfall, especially over southern and equatorial regions of the continent. In the low latitudes, spectral peaks in the ranges of 2.2 to 2.4 and 5.0 to 6.3

years are common. Recurrences of QBO mode has been reported by several authors Indeje and Semazzi (2000); Claud and Terry (2007) among others.

Studies have demonstrated that the QBO plays an important role in linking the different layers of the atmosphere by descent from middle stratosphere after a few months affecting several tropospheric and surface parameters such as rainfall (Njau 2006). This suggests that the global wind circulation in the lower stratosphere can after a few months produce some effects on the major weather events that occur over the globe. The lower stratospheric QBO plays a role in modulating rainfall over South Africa (Mason and Tyson, 1992) and East Africa (Jury et al., 1994; Kabanda and Jury, 1999 and Indeje et al., 2000). The Walker circulation cell connecting Africa and the Indian Ocean (Figure 4) interacts with the QBO, and during its westerly phase rising tropospheric motion occurs over Africa. During the QBO easterly phase tropical cyclones are more frequent in the Indian Ocean and convection increases significantly over Madagascar (Jury et.al., 1995). A study by Kabanda and Jury (1999) found a positive correlation of 0.32 between the long-rains season and QBO with a 6-month lag over northern Tanzania region.

2.1.7 MADDEN JULIEN OSCILLATION (MJO)

Another westerly wave with significant influence on rainfall over East Africa region is the Madden-Julian Oscillation (MJO). The Madden-Julian Oscillation (MJO) is a coupled ocean-atmosphere phenomenon characterized by eastward progression of tropical convection over the Indian and western Pacific Oceans (Wheeler and Hendon, 2004; Omeny, 2006). The MJO, which consists of pulses of strong winds and pressure surges, has a strong influence on regional rainfall (Burroughs 1999; Matthews, 2008; Omeny, 2006). The MJO is at its strongest during the months of December and May (Burroughs, 1999). Enhanced MJO activity in Western Pacific Ocean in spring is associated with an eastward-expanded warm pool and low frequency westerly surface zonal wind anomalies, which favour the development of El Niño (Hendon *et al.*, 2007). The most favoured location for formation of primary MJO is the Indian and maritime continent of western Pacific oceans (Matthews, 2008).

MJO accounts for most of the weather variabilities that occur in the tropics (Madden and Julian, 1972, 1994; Omeny, 2006) at intraseasonal time scales (10-90 days). Anyamba, (1990), Camberlin and Okoola (2003) demonstrated associations between the extreme rainfall events that occur over East Africa at intraseasonal time scales and the MJO. Pohl and Camberlin (2006) attributed the interannual variability in March-May rainfall over East Africa to fluctuations in the amplitude of the MJO. Results of MJO study by Omeny (2007) revealed strong association between East Africa rainfall and the MJO to the west of the region especially around the Lake Victoria. The rainfall is also shown to depend on the configuration of the winds at low and upper levels. Based on composite analysis, extreme rainfall events are shown to occur during preferential phases of the MJO (Omeny, 2006). Phase 2 coincides with enhanced rainfall, high negative Outgoing Longwave Radiation (OLR) values as well as westerly and easterly winds configuration at 700hpa and 200hpa while phase 5 and 6 are associated with depressed rainfall.

2.1.8 SEA SURFACE TEMPERATURE

The amount of heat transported around by atmospheric and oceanic currents plays an important role in determining the mean climate of any region on earth (Wunsch and Heimbach, 2006) and the ocean waves have significant influence on Sea Surface Temperatures (SSTs) (Zang and Gottschalk, 2002; Hashizume et al., 2003; Marmorino et al., 2004; Qiao et al., 2004; Jochum et al., 2007; Valsala and Ikeda, 2007). Figure 5 shows an illustration that describes the flow pattern of the major subsurface ocean currents. This system is continuously moving water from the surface to deep within the oceans and back to the top of the ocean. The thermohaline circulation, involving high latitude sinking and distributed upwelling and mixing at lower latitudes is believed to be responsible for the longer time scales of climate variability (Deser et al., 2004; Lee et al., 2006; Boer and Lambert, 2008; Keenlyside et al., 2008 and Meehl et al., 2009).

The term thermohaline circulation (THC) refers to the part of the large-scale ocean circulation that is driven by global density gradients created by surface heat and freshwater fluxes. The thermohaline circulation is sometimes called the ocean conveyor

belt, the great ocean conveyor, or the global conveyor belt (Figure 5). It is also used in some occasions to refer to the Meridional Overturning Circulation (MOC). The thermohaline circulation plays an important role in supplying and redistribution of heat to the various regions, and thus in regulating the amount of heat regions. Changes in the thermohaline circulation have significant impacts on the earth's radiation budget. As the thermohaline circulation governs the rate at which deep waters are exposed to the surface, it at the same time play important role in determining the concentration of carbon dioxide in the atmosphere.

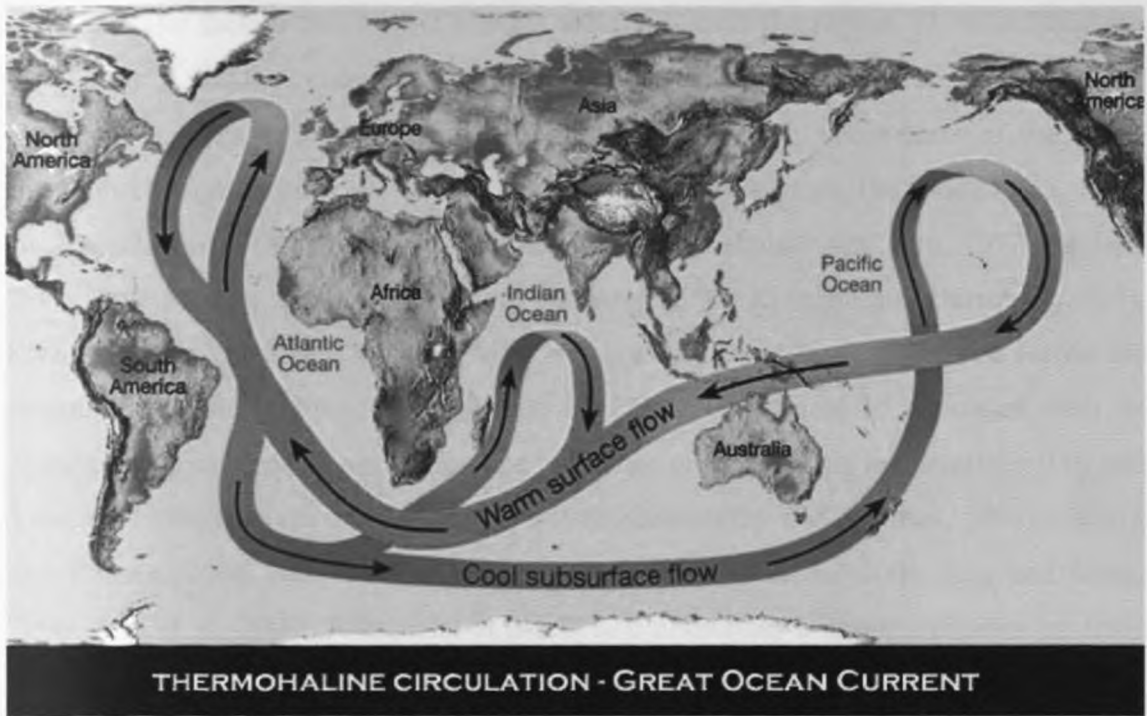


Figure 5: Schematic representation of the global thermohaline circulation. Warm currents are drawn in red while blue depicts the deep cold (Source: Gross 1972)

East Africa rainfall is influenced by SST over the Atlantic, Indian and Pacific Oceans (Frederiksen et al., 2001; Goddard and Graham, 1999; Ogallo et al., 1988; Okoola, 1996; Omondi, 2005; Owiti, 2005; Nyakwada, 2009). Ogallo *et al.*, (1988) and Ogallo (1988) have shown that rainfall in the coastal and western parts of East Africa has significant correlation with the Southern Oscillation Index (SOI) and SST over parts of the Pacific and Indian Oceans. The study by Nicholson and Entekhabi (1987) indicated a strong relationship between East Africa rainfall and sea surface temperatures along the

Benguela coast. In his investigation of interannual variability of surface fields over the Indian Ocean, Cadet and Beltrando (1987), and Cadet and Diehl (1984) indicated that Indian Ocean parameters have significant influence on East Africa weather. Although the land surface processes could be playing an important role in modifying the climate conditions globally, a large body of results based on numerical and statistical modeling has firmly established that SST anomaly forcing, is the major climate forcing factor due to its high memory (Hastenrath, 1990; Repelli and Nobre, 2004).

The large-scale ocean-atmosphere ENSO phenomenon and SST related indices are two major factors that control climate variability over the region. El Niño /Southern Oscillation (ENSO) occur as a result of instabilities in air-sea interaction in the Pacific Ocean and it has impacts on regional climate extremes in many parts of the globe (Ropelewski and Halpert, 1987, 1996; Ogallo, 1988; Ogallo et al., 1988; Beltrando, 1990; Hastenrath et al., 1993; Nicholson and Kim, 1997a; Nicholson and Kim, 1997b; Indeje, 2000; Indeje et al., 2000; Schreck and Semazzi, 2004; Korecha and Barnston, 2007). ENSO is an event when SSTs are high and sea surface pressure difference across the equatorial Pacific is low. The influence of ENSO on climate is associated with its disruption of the general circulation and influence on sea surface temperatures (Ort and Yienger, 1996; Chevrin and Druyan, 1984; Krishnamurthy and Kirtman, 2003; Colberg and Reason, 2004; Schreck and Semazzi, 2004; Tanaka et al., 2004; Kug and Kang, 2006; Rao et al., 2007; Annamalai et al., 2007). ENSO has a strong influence on trade winds (Colberg and Reason, 2004) and climate of the region (Ogallo and Suleiman, 1987; Ropelewski and Halpert, 1987; Wassila et al., 1999; Wang and Eltahir, 1999). El Nino has been observed to weaken the Hadley circulation (Colberg and Reason, 2004; Rao et al., 2007). The ENSO phenomenon has been studied largely in the context of the Pacific Ocean and adjacent regions; although research has long established that it is a global scale phenomenon (Wallace et al., 1998). Major ENSO episodes lead to massive displacements of rainfall regions of the tropics, bringing drought to vast areas and torrential rains to other regions.

Many studies have investigated the relationship between East Africa rainfall and ENSO (Ropelewski and Halpert, 1987; Ogallo et al., 1988; Indeje, 2000; Mutemi, 2003;

among others). ENSO has been observed to play dominant role of interannual climate variability pattern over eastern Africa (Ogallo and Suleiman 1987, Mason *et al* 1999, Ropelewski and Halpert, 1987, 1996; Ogallo et al., 1988; Beltrando, 1990; Hastenrath *et al.*, 1993; Nicholson and Kim, 1997a; Indeje, 2000; Indeje et al., 2000; Schreck and Semazzi, 2004; Korecha and Barnston, 2007; Mutemi, 2003, Indeje, 2000, Nyakwada, 2009). Interannual variability in rainfall over East Africa during the October to December season correlates strongly with the Sea Surface Temperature (SST) changes in the tropical Pacific associated with the ENSO phenomenon (Ogallo et al., 1988; Indeje, 2000; Indeje et al., 2000; Schreck and Semmazzi, 2004). Mutemi (2003) for example, found a strong relationship between rainfall over East Africa and evolutionary phases of ENSO. The results showed that ENSO plays a significant role in determining the monthly and seasonal rainfall patterns in East Africa region. Mutemi (2003) also observed shifts in the onset / cessation of rainfall patterns over some regions while in others a significant reduction in the seasonal peak was evident. Nicholson and Kim (1997a) found that ENSO has little influence on long rainfall season (MAM) but significantly modulates the short rains (OND). Ogallo (1988) found significant instantaneous and time lagged correlation between East Africa seasonal rainfall and the Southern Oscillation Index (SOI). Ogallo *et al.*, (1988) suggested that about 36% of the short rainfall variation in East Africa could be explained by SST variations in western Pacific and most of Indian Ocean where correlation values are near 0.6.

Indian Ocean Dipole Mode (IOD) is the variability in Indian Ocean SST that is characterized by a perturbed zonal gradient in SST and anomalous low-level winds (Saji et al., 1999; Black, 2004; Owiti, 2005). The strength of the dipole is measured by the Dipole Mode Index (DMI), which is defined as the difference in SST anomaly between the Western and Eastern Indian Ocean (Saji et al., 1999; Black, 2004; Owiti, 2005). The DMI varies between -1 and 1.5°C with a standard deviation of 0.3. Rainfall in the region has been shown to be above average during the September–December season, when the DMI is greater than one standard deviation above the mean. This implies that the Indian Ocean Dipole exerts some control on rainfall in East Africa (Black et al., 2003; Black, 2004).

Most important findings from the recent studies on the Tropical Indian Ocean variability modes are the existence of an ocean-atmosphere coupled mode, typified by the dipole structure in SST anomalies (Beltrando and Cadet, 1990; Beltrando and Camberlin, 1993; Reason et al., 2000; Saji et al., 1999; Webster et al., 1999; Behera et al., 2005, 2006; Murtugudde et al., 2000; Hastenrath, 2000, 2002; Hastenrath and Polzin 2003; Owiti, 2005). Detailed description of the Indian Ocean Dipole (IOD) mode has been presented by Saji et al., 1999; Black, 2004 and Owiti, 2005.

The warm western and cool eastern Indian Ocean is associated with enhanced October - December seasonal rainfall over the region (Behera et al., 2005; Black et al., 2003; Black, 2004; Clark et al., 2003; Owiti, 2005; Saji and Yamagata, 2003a). Anomalous latent heat flux and vertical heat convergence associated with the modified Walker circulation contribute to the alteration of western anomalies. The heavy rains of 1961 which covered the entire region were due to the strong positive phase of Indian Ocean Dipole (Anyamba, 1983). Owiti (2005) showed that the extreme rainfall conditions over East Africa during the short rainfall season are associated with positive IOD phases.

There is good evidence that the observed teleconnection between East Africa rainfall and ENSO is a manifestation of a link between ENSO and the Indian Ocean Dipole. Each of the previous four, strongest ENSO warm phases associated with high rainfall in East Africa (1963, 1972, 1982 and 1997) coincided with a dipole event (Black, 2004; Owiti, 2005). Moreover, there is a significant correlation ($R = 0.57$) between the Dipole Mode Index and Niño 3.0 SST (Black, 2004; Owiti, 2005). The relationship between the IOD and El Niño is however, very complex (Black, 2004). Some studies have indicated that IOD is not related to ENSO (Saji and Yamagata, 2003b; Song *et al.*, 2007) while some have indicated some relationships (Huang and Shukla, 2007; Tozuka *et al.*, 2006, 2007) and some have indicated that some events are independent from ENSO but some co-occur with ENSO (Ihara *et al.*, 2008). IOD events that occur at the same time with ENSO events are stronger than those that occur independently (Saji and Yamagata, 2003a, 2003b; Song et al., 2007). An example is the 1997/98 El Niño and positive phase IOD related floods that created havoc and destruction of properties worth

billions of dollars in the region. In some IOD years, such as 1961, there was no El Niño; in other years, such as 1986, there was an El Niño but no IOD. Closer analysis, however, reveals that an IOD only ensues if the El Niño is strong during autumn (Black, 2004). For example, in 1986–1987 (the strongest El Niño not associated with an IOD), the event peaked in the summer of 1986 and was weak during the autumns of both 1986 and 1987. The occurrence of IOD events when there is no El Niño (most notably during 1961) suggests that the IOD can be triggered by factors other than ENSO (Saji et al., 2005).

The north-south movement of the sun causes seasonal variations in the strengths of meridional Sea Surface Temperature gradients, and the intensity and position of southeast trade winds (Yu and Rienecker 2000; Nyakwada 2009). The intensity and location of the ITZC is highly dependent on temperature gradients through their influence on pressure gradients (Vidyunmala *et al.* 2007). Zonal Sea Surface Temperature gradients that influence climate of the region and beyond include the SST gradients in the Indian Ocean associated with the IOD (Behera et al., 2005; Clark et al., 2003; Owiti, 2005; Saji et al., 1999; Singhrattna et al., 2005; Webster et al., 1999; Yu and Rienecker, 2000; Nyakwada 2009). SST gradients together with the associated pressure gradients have significant influence on the winds and precipitation patterns in the tropical region (Moura and Shukla, 1981; Lindzen and Nigam, 1987; Clark et al., 2003; Nyakwada, 2009).

There has been improvement in the skills of seasonal rainfall prediction over East Africa region through the use of sea surface temperature gradient modes within March-May and September-December months (Nyakwada 2009). These meridional and zonal gradients that have significant influence on regional rainfall have been mainly concentrated in both the Atlantic and Indian Oceans.

Quite a lot of research has been undertaken linking some of variability of east African rainfall with ENSO and IOD variability modes (Ropelewski and Halpert, 1987; Ogallo and Suleiman, 1987; Ogallo, 1988; Wallace et al., 1998; Camberlin et al., 2004; Yamaguchi and Noda, 2005; Owiti, 2005; Wang and Eltahir, 1999). Several studies have noted some increase in ENSO recurrences in the recent years (IPCC, 2007b;

Krishnamurthy and Kirtman, 2003; Colberg and Reason, 2004; England and Huang, 2005; Kug and Kang, 2006; Nagura et al., 2008). A few other studies have associated some of the recent changes in global, regional and local climate variability patterns to climate change (Krishnamurthy and Kirtman, 2003; IPCC 2007b; Nagura et al., 2008).

2.2 DECADAL CLIMATE VARIABILITY

Several studies have demonstrated evidence of strong decadal pattern of climate variability (Latif and Barnett, 1994; Trenberth and Hurrell, 1994; Zhang et al., 1997; Bader and Latif, 2003; Deser et al., 2004; Omondi, 2005; Lee et al., 2006; Boer and Lambert, 2008; Keenlyside et al., 2008 and Meehl et al., 2009). Other studies suggests that decadal variability in the Pacific may be either linked to changes in the El Niño / La Niña signal in the equatorial Pacific (Trenberth and Hurrell, 1994; Deser et al., 2004) or to midlatitude air-sea instabilities (Latif and Barnett, 1994). As a whole, tropical SST changes display decadal trends and strong correlations with long-term rain and drought cycles as well as tropical storm frequency (Tyson et al., 1975; Nicholson, 2000b; Tyson et al., 2002).

A number of studies have examined decadal tropical and midlatitude Atlantic climate variability. Some of these studies (Rajagopalan *et al.*, 1998; Robertson *et al.*, 2000; Tourre *et al.*, 1999; Bader and Latif, 2003; Deser et al., 2004) suggest that tropical ocean-atmosphere interaction can perturb the North Atlantic. This tropics-midlatitude connection is mostly identified through inspection of spatial patterns from modeling experiments (Robertson *et al.*, 2000; Latif et al. 2006) and empirical analyses (Tourre *et al.*, 1999; Rajagopalan *et al.*, 1998). Mehta (1998a, 1998b) suggested the existence of a relationship between tropical and extra tropical annual SST anomalies, but concluded that there was no dynamical-thermodynamical dipole mode of SST variations. Modeling and empirical studies show that extratropical forcing of the Tropics at decadal timescale, excited by the North Atlantic Oscillation (NAO), can force a dipole pattern linking the two hemispheres (Xie and Tanimoto 1998; Tanimoto and Xie 1999). Power *et al.* (1999) linked decadal filtered SST in the Tasman Sea to the eastern Australia annual rainfall. They showed that when SSTs in the Tasman Sea were above average, then Australian rainfall was also above average.

Perhaps the most striking finding is the linkage of decadal drought frequency in the Sahel to sea surface temperature (Hulme, 1992; Lamb and Pepler, 1992; Nicholson et al., 2000a; L'Hôte et al., 2002; Zhang and Delworth, 2006). Other droughts on decadal-timescale, such as the “dust-bowl” in the Southern U.S.A in the 1930s have been linked to variations in SST (Worster, 1979; Woodhouse and Overpeck, 1998; Bark, 1978). Nicholson (2000b) showed rainfall time series for 1901-1994 of three African regions displaying decadal rainfall variations. In South Africa, and some neighbouring areas, an austral summer rainfall signal at near bi-decadal scales has been known for some time (Tyson et al., 1975; Tyson and Preston-Whyte, 2000). In the Pacific/Indian Ocean basins, there are strong signals of decadal variability associated with the Pacific Decadal Oscillation (PDO) with statistical links to the climate of the surrounding regions. For example, during the 20th century, El Niño- like phases of the PDO coincided with decades in which ENSOs impact on Australia was weak, whereas La Niña- like phases of the PDO coincided with decades in which ENSOs impact on Australia was strong (Power et al, 1999).

There is clear evidence, however, of decadal variability in the heat and freshwater content of the Atlantic Ocean (e.g., Lozier et al. 2008), as well as evidence of ocean circulation changes in recent decades (e.g., Hakkinen and Rhines 2004; Curry and Mauritzen 2005). These have likely played an important role in the evolution of the Atlantic SSTs. The slow changes in Atlantic SSTs have affected regional climate trends over parts of North America and Europe (e.g., Enfield et al. 2001; Sutton and Hodson 2005) and hemispheric temperature anomalies (Zhang et al., 2007). Sea ice concentration in the Greenland Sea (Venegas and Mysak 2000), and hurricane activity in the tropical Atlantic and Caribbean (e.g., Goldenberg et al., 2001; Webster et al., 2005; Zhang and Delworth 2006; Trenberth and Shea 2006) have also been affected. In addition, tropical Atlantic SST anomalies have contributed to rainfall anomalies over the Caribbean and the Northern region of Brazil, and have also been associated with persistent and severe multi-year droughts over parts of Africa, including the Sahel (Bader and Latif 2003, Giannini et al., 2003, Lu and Delworth 2005; Hoerling et al., 2006). Tropical Atlantic SST variations are also linked to drought conditions over portions of North America, although tropical

Pacific SST variations appear to play a more dominant role (Schubert et al., 2004; Seager et al., 2005, 2008; Seager, 2007).

Over East Africa region, there is substantial evidence for decadal climate variability in the observed climate system (Nicholson 2000b; Schreck and Semazzi, 2004; Bowden et al., 2004, Omondi, 2005, Muthama et al., 2008). Decadal rainfall signals in East Africa are linked with the Pacific Decadal Oscillation (PDO) (CLIVAR VACS 2007). Several parts of the region experience strong decadal signal during the short rainy season of October – December (Schreck and Semazzi, 2004; Bowden et al., 2004; Omondi, 2005; CLIVAR VACS, 2007; Muthama et al., 2008). Previous studies (Omondi, 2005; Schreck and Semazzi, 2004; Muthama et al., 2008) have examined modes of decadal signal in the rainfall patterns over equatorial eastern Africa. Muthama et al., 2008, found that amongst the numerous mathematical functions considered, the fourth degree polynomial fitted best for prediction purposes of both the short (October-December) and the long (March-May) decadal rains over Nairobi. They used the fourth degree polynomial function to generate ten-year periodicity of rainfall variations, corresponding to the sunspots cycle of approximately 11.3 years.

Analysis of October - December rainfall index over Lake Victoria region reveals insignificant variability at decadal timescales (Mistry and Conway, 2003). Other parts of the region have also experienced decadal signals in the impacts of ENSO and the Indian Ocean Zonal Mode (Clark et al., 2003) on rainfall during the 'short rains' season. Schreck and Semazzi (2004) in their study isolated a mode linked to decadal trend during the past two decades using the EOF method. They suggested that the northern sector of GHA is getting wetter while the southern sector is becoming drier. Their analysis explored the possible association of the trend with global warming and found similar trend to the global warming index constructed by globally averaging surface temperature data from the CRU archive. A similar and consistent trend was found by Dai et al., 1997. Omondi (2005) also indicated decadal signals in filtered observed rainfall record varying after every 10 years during the major rainfall season of March – May and second season of October – December. However, the third minor rainfall season of June – August, displayed 20-year signal in their time series patterns.

2.2.1 DECADAL RAINFALL PREDICTABILITY AND PROJECTION

A new field of study, “decadal prediction”, is emerging in climate science (CLIVAR 2007; Meehl et al., 2007; Seager et al., 2007; Knutson and Tuleya, 2004; Meehl et al., 2009). Decadal prediction lies between seasonal/interannual forecasting and longer term climate change projections, and focuses on time-evolving regional climate conditions over the next 10-30 years. Numerous assessments of climate information user needs have identified this timescale as being important to infrastructure planners, water resource managers, and many others.

Extreme events such as frequent droughts, floods, heat wave, e.t.c as well as the need to adapt to time-evolving climate change and increasing temperatures have raised concern among policy and decision makers about climate change in the near term, i.e., out to 10 to 30 years (Meehl, 2009; Reason et al.,2006), referred to as the “decadal” timescale. Impacts due to these conditions have significant social, economic and environmental implications and are consistent with the climate change projections of some models (Seager et al., 2007; Knutson and Tuleya, 2004; Meehl et al., 2007).

Some studies suggest that much of the observed inherent decadal variability, particularly that in the Atlantic, arises from slow variations in the ocean circulation, and that this variability may be predictable if the ocean state could be properly initialized (e.g. Collins et al, 2006). Predictability of decadal oceanic modes could lead to regional prediction skill in some areas over and above that arising from commitment and forcing (Meehl et al., 2009). Previous research has demonstrated that modes of climate variability influence mean and extreme climate over large parts of the globe through teleconnections (Mantua et al., 1997; Knight et al., 2006; and Hegerl Seager et al., 2005).

If the initial state of the coupled climate system could be captured, especially the decadal mechanisms that reside primarily in the oceans, and if their time evolution could be predicted by models started from that state, then decadal variations in regional climate, including the behavior of extremes, could be better predicted.

2.3 APPLICATION OF GLOBAL CLIMATE MODELS (GCMs) AND REGIONAL CLIMATE MODELS (RCMs)

The General Circulation Models (GCMs) are used to simulate the evolution of the atmosphere through time from some initial state. The importance of the GCMs for climate studies is their ability to model the evolution of the atmosphere in response to external forcing mechanisms such as doubling of carbon dioxide, increase in soil moisture, and increase in sea surface temperatures. Global Climate Models (GCMs) are currently the most appropriate and widely used tools to generate future climate change scenarios. For example Shongwe et al., (2008), demonstrated a positive shift in rainfall distribution in East Africa during the wet seasons using GCM projections of future climate of the region. However, in order to formulate adaptation policies in response to climate change impacts, reliable climate change information is usually required at finer spatial scales than that of a typical GCM grid-cell which is usually in the order of 300 x 300 km.

Though GCMs can satisfactorily simulate the atmospheric general circulation at the continental scale, they are not necessarily capable of capturing the detailed processes associated with regional/local climate variability and changes that are required for regional and national climate change assessments. This is particularly true for heterogeneous regions, where sub-GCM grid-scale variations in topography, vegetation, soils and coastlines have a significant effect on the climate. In addition, at coarse grid resolutions, the magnitude and intensity of extreme events such as cyclones or heavy rainfall (floods) are often not captured, nor realistically reproduced. GCMs also have difficulties with the regional climate, which is influenced by local factors such as, steep orography that may not be represented by the relative coarse resolution. Therefore, one possible solution to this model deficiency has been to combine a GCM with a high-resolution Regional Climate Model (RCM), a technique commonly referred to as “Nested” or Regional climate modeling which provides finer spatial and temporal details than the GCM. “Nested” Regional Climate Modeling is thus a strategy to locally increase the model resolution. In this way, the GCM simulates the response of the general

circulation to the large scale forcings while the RCM simulates the effect of sub-GCM-grid scale forcings and provides fine scale regional information.

A regional climate model (RCM) is a comprehensive physical model representing all of the important components of the climate system. In a review by Wang et al., (2004), several studies have demonstrated the use of high spatial resolution to resolve complex lower boundary conditions and meso-scale weather systems that makes RCMs ideal investigative tools for studying regional climate processes and variability. It has a higher resolution than a GCM and covers a limited area of the globe. Such numerical climate models have also been employed in climate studies over parts of Africa with encouraging results (Folland et al., 1991; Rocha and Simmonds, 1996; Kida et al. 1991; Indeje, 2000; Anyah and Semazzi, 2006; 2007). The initial conditions (IC) and lateral boundary conditions (LBC) for the RCM are obtained from the GCM or analyses of observations (“one-way nesting”). Whereas the initial conditions in RCMs become less important with time though still relevant and the simulated climate is largely determined by the internal dynamics of the region of interest. The regional climate modeling approach is however very dependent on lateral boundary forcing, which is either supplied by the GCMs or observational data.

The GCM-RCM nesting approach has been implemented in short-range weather and climate forecasts as well (Giorgi and Marinucci 1996; Giorgi and Mearns 1999; Giorgi et al., 1993a, 1993b; Sun et al., 1999a, 1999b; Anyah et al., 2006). The one way nesting technique that has been used in many previous studies consists of using the output of GCM global climate simulations to provide driving initial and time-dependent lateral boundary conditions for high-resolution regional climate model simulations over areas of interest. With this methodology the regional climatic effects of the sub-GCM grid-scale forcings, (e.g. effects of complex topographical features, coastlines, and large lakes, etc) are represented in a physically based way (Giorgi and Mearns 1991). Schreck and Semazzi (2004) demonstrated how a high-resolution RCM could be used to resolve the detailed regional features associated with the East Africa climate variability.

Several RCM-based studies have been carried out over East Africa (Sun et al., 1999a, 1999b; Indeje et al., 2000; Anyah et al., 2006; Anyah and Semazzi, 2006, 2007; Sabiti, 2008). Sun et al. (1999a, 1999b) used a 60 km resolution RCM (RegCM2 from NCAR, USA) to investigate rainfall over eastern Africa. Anyah et al., 2006 used an enhanced version of the RegCM3 modified at North Carolina State University for multi-year simulations of the East Africa climate. Indeje (2000) study focused on prediction of equatorial eastern Africa climate using NCAR Regional Climate Model (RegCM2) simulations. He demonstrated the added value of the nesting approach in improving regional climate simulations. The model realistically reproduced the observed characteristics of the Turkana low-level jet. Preliminary application of the RegCM2 in the prognostic mode successfully produced 3-months projection of the extreme seasonal anomalies associated with the 1997 ENSO event.

HadRM3P RCM is a high resolution model that can be applied easily to any area of the globe to generate detailed climate change projections (Islam et al., 2007). Examples of climate change scenarios using Hadley Centre RCMs (HadRM3P) over other parts of the globe have been documented. A single 30-year climate change simulation, using the A2 SRES emission scenario, was performed with the RCM (HadRM3P) over South Africa (Hudson and Jones, 2002). It has been applied in China (Yinlong et al., 2006), Eritrea (Beraki, 2005), South Africa (Hudson and R.G. Jones, 2002), Bangladesh (Islam et al., 2007), India (Kolli et al., 2006), over Lake Victoria basin (Sabiti 2008) among others. In this study, the Hadley Center's current version of the Regional Climate Model (HadRM3P) has been used. The full model description is provided in the next section 3.6.1.

CHAPTER THREE: DATA AND METHODOLOGY

This chapter discusses details of the data used and methodology employed to address the specific objectives of this study.

3.1 DATA

This section outlines the data sets that were adopted to achieve the objectives of the study. The data used in this study include rainfall, mean surface temperature, Sea Surface Temperature (SST) that include station observations, global and regional climate model output and reanalyzed data. Detailed descriptions of the datasets are presented in the next sub-sections.

3.1.1 OBSERVED DATA

The rain gauge observations network over East Africa is quite sparse. Furthermore, the available data are also riddled with numerous gaps in both space and time. These limitations in the quantity and quality of *insitu* observations impose substantial constraints on diagnostic studies of the regional climate (rainfall) variability. Monthly rainfall data covering the period 1920 to 2008 was used. The data was obtained from IGAD Climate Prediction and Applications Centre (ICPAC), the Kenya Meteorological Department (KMD), Tanzania Meteorological Agency (TMA) and Uganda Meteorological Department (UMD). The observed monthly rainfall data used are from 37 stations (Figure 6) unevenly distributed over East Africa. These together with Tables 1, 2 and 3 are those that had the highest loadings with the Principal Component (PC) modes dominant in specific zones and also had high correlation with most stations within the respective zones.

The rainfall data used for the comparison and validation of the model output were the observed daily station and the University of East Anglia's Climate Research Unit (CRU) gridded rainfall data. Daily rainfall data covering the period 1961 to 1990 for some selected stations in the southern, central and northern sectors of East Africa were used for evaluating the model simulations. These stations were selected based on

their long record of data with less than 2% missing and their unique rainfall regimes i.e unimodal, bimodal and trimodal. The daily data was obtained from the Meteorological Services of the three East Africa countries where the daily climate data archives are kept and not ICPAC as with other observed monthly data.

3.1.2 CLIMATE RESEARCH UNIT (CRU) DATA

The University of East Anglia's Climate Research Unit (CRU) TS 2.0 dataset used in this study comprises of 1200 station observed monthly data for the period 1901-2000 covering the global land surface and have been interpolated onto regular $0.5^{\circ} \times 0.5^{\circ}$ grid spacing (Mitchel et al., 2005). The dataset contains five climatic variables; precipitation, surface temperature, diurnal temperature range (DTR), cloud cover and vapor pressure. It is a revised and extended version of similar data constructed by New et al., (1999). In this study only the surface temperature and precipitation variables have been used for model evaluation.

Figures 7, 8 and 9 show the delineated homogeneous rainfall regions over East Africa for the March – May, October – December and June - August rainfall seasons respectively. The homogeneous climate zones delineated through principal component analysis (PCA) used in this study are adopted from ICPAC (1999) and are being used for operational work. Similar climate zones are normally adopted for use during annual capacity building workshops at ICPAC (ICPAC, 1999). Many recent studies including Owiti (2005); Omondi (2005); Komutunga (2006); Njau (2006); Omeny (2007) and Nyakwada (2009) used the same homogenous zones in order to reduce the number of rainfall stations used in their studies.

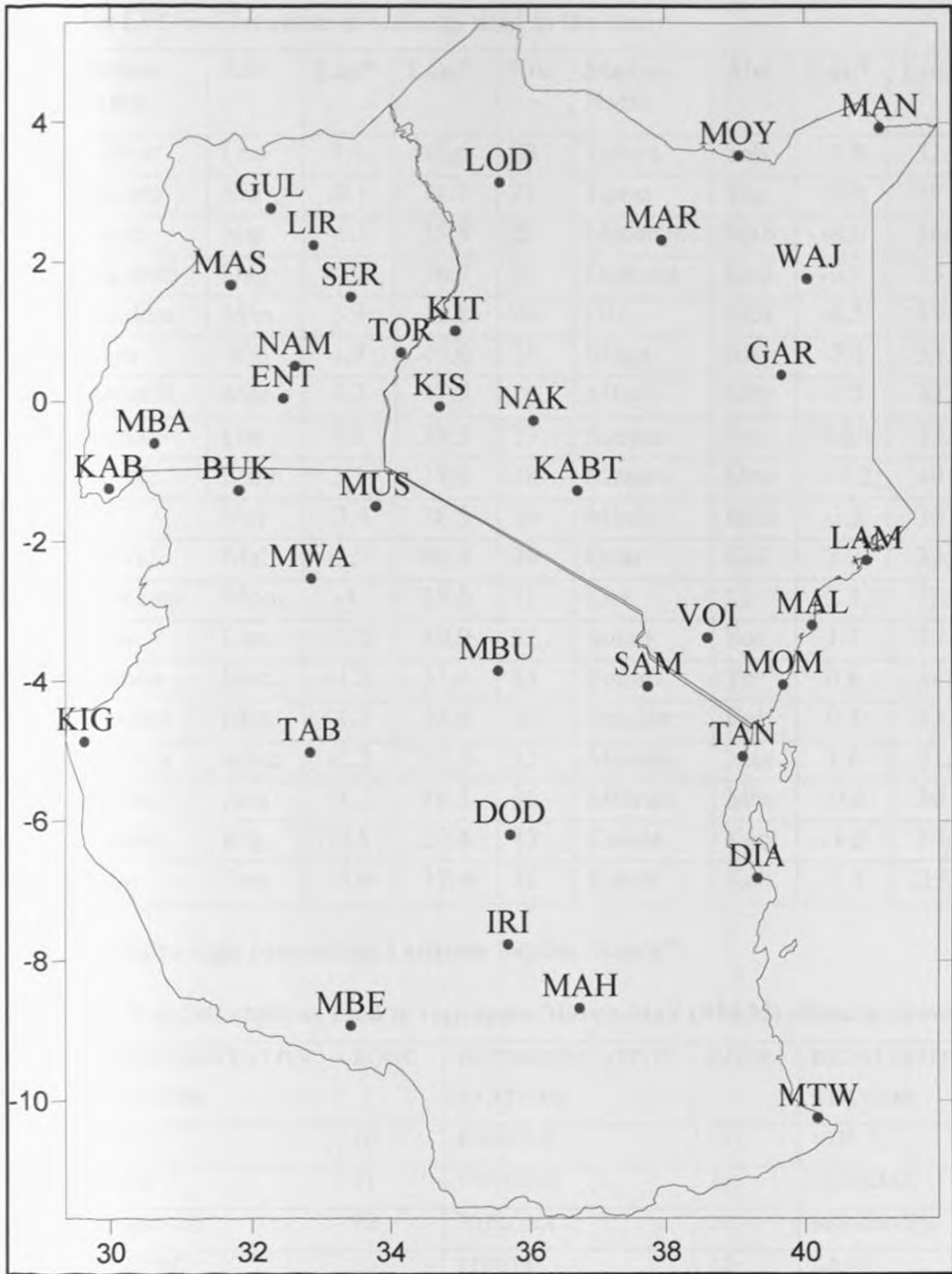


Figure 6: The distribution of the stations representing homogeneous rainfall zones over the study region

Table 1a: List and locations of stations used in the study

No.	Station Name	Abr	Lat/°	Lon/°	No.	Station Name	Abr	Lat/°	Lon/°
1	Lodwar	Lod	3.1	35.6	20	Tabora	Tab	-5.0	32.5
2	Kisumu	Kis	-0.1	34.7	21	Tanga	Tan	-5.0	39.0
3	Narok	Nar	-1.1	35.8	22	Mahenge	Mah	-8.6	36.7
4	Dagoretti	Dag	-1.3	36.7	23	Dodoma	Dod	-6.1	35.4
5	Mandera	Man	3.9	41.8	24	DIA	DIA	-6.5	39.1
6	Wajir	Waj	1.7	40.0	25	Iringa	Iri	-7.3	35.4
7	Marsabit	Mar	2.3	37.9	26	Mbeya	Mbe	-8.5	33.2
8	Garissa	Gar	0.5	38.5	27	Songea	Son	-10.4	35.3
9	Moyale	Moy	3.5	39.0	28	Mtwara	Mtw	-10.2	40.1
10	Voi	Voi	-3.4	38.5	29	Mbulu	Mbu	-3.8	35.5
11	Malindi	Mal	-3.2	40.1	30	Gulu	Gul	2.7	32.2
12	Mombasa	Mom	-4.	39.6	31	Lira	Lir	2.3	32.9
13	Lamu	Lam	-2.2	40.9	32	Soroti	Sor	1.7	33.6
14	Bukoba	Buk	-1.2	31.4	33	Tororo	Tor	0.6	34.1
15	Musoma	Mus	-1.3	33.4	34	Entebbe	Ent	0.1	32.4
16	Mwanza	Mwa	-2.2	32.5	35	Masindi	Mas	1.6	31.7
17	Arusha	Aru	-3.2	36.3	36	Mbarara	Mba	-0.6	30.6
18	Kigoma	Kig	-4.5	29.4	37	Kabete	Kabt	-1.2	36.7
19	Same	Sam	-4.0	37.4	38	Kabale	Kab	-1.4	29.2

KEY: Negative sign preceding Latitude implies ‘South’

Table 1b: Rainfall stations used to represent March-May (MAM) climatic zones

ZONE	REPRESENTATIVE STATION	ZONE	REPRESENTATIVE STATION	ZONE	REPRESENTATIVE STATION
1	GULU	10	KABALE	19	VOI
2	LIRA	11	ENTEBBE	20	DODOMA
3	MASINDI	12	BUKOBA	21	MOMBASA
4	SERERE	13	MBULU	22	LAMU
5	KITALE	14	KABETE	23	IRINGA
6	LODWAR	15	MOYALE	24	MAHENGE
7	MANDERA	16	GARISSA	25	MTWARA
8	MARSABIT	17	KIGOMA	26	KISUMU
9	MBARARA	18	TABORA	27	MWANZA

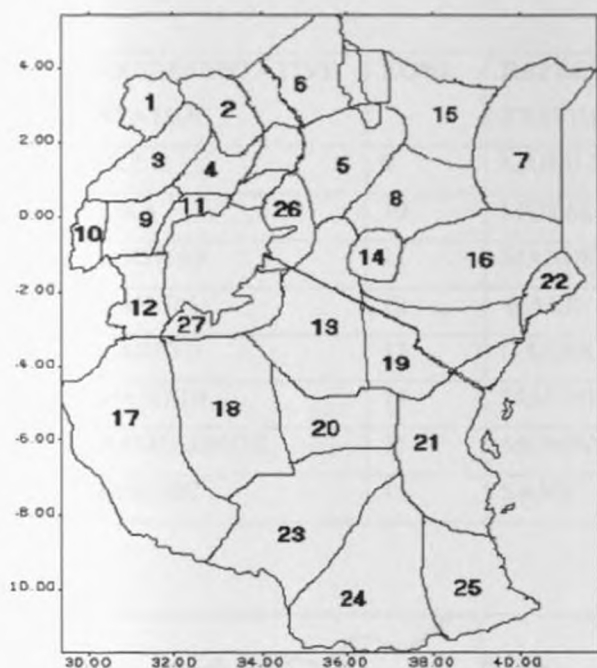


Figure 7: Homogeneous climatic zones for March-May season used in the study (source: ICPAC 1999)

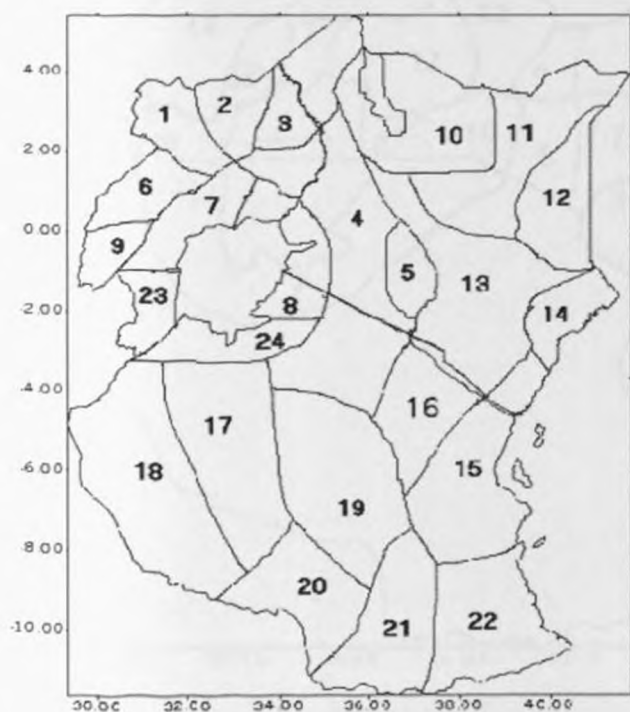


Figure 8: Homogeneous climatic zones for October-December season used in the study (source: ICPAC, 1999)

Table 2: Rainfall stations used to represent October-December (OND) climatic zones

ZONE	REPRESENTATIVE STATION	ZONE	REPRESENTATIVE STATION	ZONE	REPRESENTATIVE STATION
1	GULU	9	KABALE	17	TABORA
2	LIRA	10	MOYALE	18	KIGOMA
3	LODWAR	11	MANDERA	19	DODOMA
4	NAKURU	12	WAJIR	20	MBEYA
5	KABETE	13	GARISSA	21	MAHENGE
6	MASINDI	14	MALINDI	22	MTWARA
7	NAMULONGE	15	MOMBASA	23	BUKOBA
8	KISUMU	16	SAME	24	MWANZA

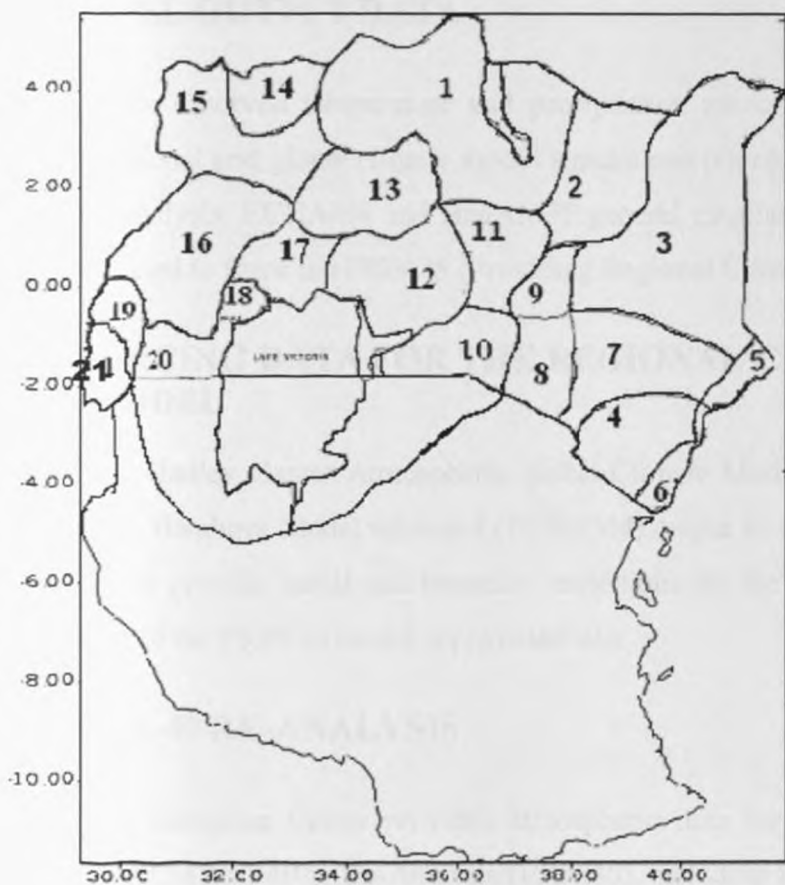


Figure 9: Homogeneous climatic zones for June - August season used in the study (source: ICPAC 1999)

Table 3: Rainfall stations used to represent June-August (JJA) climatic zones

ZONE	REPRESENTATIVE STATION	ZONE	REPRESENTATIVE STATION	ZONE	REPRESENTATIVE STATION
1	LODWAR	9	NAKURU	17	NAMULONGE
2	MARSABIT	10	NAROK	18	ENTEBBE
3	WAJIR	11	MARALAL	19	KABALE
4	VOI	12	TORORO	20	MBARARA
5	LAMU	13	SOROTI	21	BUSENYI
6	MOMBASA	14	GULU		
7	MAKINDU	15	LIRA		
8	KABETE	16	MASINDI		

3.2 MODEL OUTPUT DATA

Often observed temperature and precipitation are often used to evaluate and validate regional and global climate model simulations (Gordon et al., 2000). However, ERA-40 reanalysis, ECHAM4 and HadAM3P general circulation model (GCM) output have been used to force the PRECIS (Providing Regional Climate for Impact Studies).

3.2.1 FORCING DATA FOR THE REGIONAL CIRCULATION MODEL

The Hadley Center Atmospheric global Climate Model (HadAM3P), European Community Hamburg Model version 4 (ECHAM4) output as well as ERA-40 reanalysis were used to provide initial and boundary conditions for the PRECIS model. Detailed description of the PRECIS model is provided later.

3.2.2 ERA-40 RE-ANALYSIS

The European Centre provides atmospheric data for Medium-Range Weather Forecasts (ECMWF) 40-yr Re-Analysis (ERA-40), including mean monthly rainfall and temperature. These data are available on 2.5° x 2.5° latitude-longitude regular grid globally for the period 1979 to 2001. The data were obtained from the ECMWF Web site (<http://data.ecmwf.int/data/>) taken in 2008. It has been shown that ERA-40 re-

analysis does have many shortcomings in high southern latitudes (Bromwich and Fogt 2004) that limit its applicability before 1979. However, the dataset was preferred in this study due to its superior performance over East Africa, in particular during the modern satellite era over the National Centers for Environmental Prediction–National Center for Atmospheric Research (NCEP–NCAR) reanalysis (Bromwich and Fogt, 2004) but, in this still, the NCEP–NCAR reanalysis was used occasionally to independently validate the ERA-40 results and in most cases showed similar results.

The SST data used in this study was obtained from the National Center for Environmental Prediction/Climate Prediction Center (NCEP/CPC). The global SST data used is the NOAA / CDC Optimum Interpolation (OI) Sea Surface Temperature (SST) Version 2 (OISSTv.2). The data are on $1.0^{\circ} \times 1.0^{\circ}$ grid point resolution and is often known as optimal interpolation (OI) SST in literature following Reynolds and Smith (1994). The data set is a blend of insitu and satellite SSTs, but also includes those simulated by sea-ice cover (Reynolds and Marsico, 1993; Reynolds and Smith, 1994; Reynolds et al., 2002; Smith and Reynold, 2002). The SST data, used by ICPAC in seasonal rainfall forecast over the region, extended within the period 1950 – 2008. SSTs have long memory and therefore have wide usage in most climate prediction models (Kirtman et al., 1997; Mutemi, 2003; Owiti, 2005; Omondi, 2005; Smith et al., 2007; Smith et al., 2008; Nyakwada, 2009). Several efforts have been made to improve the quality of SST records due to their value in climate prediction (Smith and Reynolds, 2004; Smith et al., 2008). Kanamitsu et al., 2002; McPhaden et al., 1998; Smith and Reynolds, 2002, 2004; Smith et al., 2008 among other authors, have discussed the details of these data. It is important to note that quality of SST data to the south of 30°S may not be of good quality for a study (Weare 1977).

The next section is devoted to the various methods that were used to achieve both the over all and specific objectives of the study.

3.3 METHODOLOGY

As highlighted in section 1.2, the overall objective of this study is to investigate dominant spatial and temporal decadal climate variability patterns over East Africa, and

examine the potential use of the derived characteristics in the prediction of decadal climate variability modes. The specific objectives addressed in this study include examining statistically significant decadal modes in the observed interannual rainfall records with the view to delineating the region into zones with similar decadal variability modes; determine the reality of the decadal modes observed from the available records through climate modeling simulations; investigate the teleconnection of the regional decadal rainfall variability patterns with global Sea Surface Temperatures; examine the predictability potentials of the regional decadal rainfall variability patterns; examine probable future regional climate scenarios and compare near-term projections with predicted decadal rainfall using Regional Climate Model (RCM).

The methods adopted included the methods used to organize the data to meet the needs of the study such as estimating missing records, generating areal rainfall estimates, data standardization, empirical orthogonal function (EOF), singular value decomposition (SVD) and canonical correlation analysis (CCA).

3.3.1 DATA QUALITY CONTROL METHODOLOGY

Stations with missing rainfall data were filled using cross-station correlation matrix which enables identification of best station (source station) at which rainfall is significantly correlated with the target station. Only stations with a maximum of 10% of the total data missing were estimated at any location in order to minimize erroneous results which may be due to the chance that the estimated data can be a poor representation of reality. In practise, the source station must have a rainfall value (Z) at that point on the time series and the equation estimating the missing value is:

$$Z_{target} = \frac{\bar{Z}_{target}}{\bar{Z}_{source}} \times Z_{source} \dots\dots\dots (1)$$

It should be noted that the two pairs of stations must have high value of correlation coefficient.

The quality of the estimated data was examined using cumulative single and double mass curves. These involve the plotting of the cumulative rainfall totals against

time for a particular location. A linear relationship was indicative of homogeneous data and hence good estimation of missing data. For heterogeneous data, more than one line was common.

3.3.2 SPECTRAL ANALYSIS METHODS

A time series provides useful information about the physical, biological, or socioeconomic system that it represents. The purpose of time series analysis is to determine some of the system's key properties by quantifying certain features of the time series (Ghil, et. al., 2002). These properties can then help understand and predict the system's future behaviour.

Spectral analysis method on the other hand is a technique employed to detect periodic or quasi-periodic fluctuations in time series by transforming the data into a frequency domain. Various methods have been developed to estimate the spectrum from an observed time series. Details of spectral analysis are given in standard statistical textbooks such as Jenkins and Watts (1968), Chatfield (1975), Bloomfield (1976), Wilks (1995), Ogallo (1977, 1981, 1982), Omondi (2005) among others.

Statistically significant peaks in decadal rainfall modes are determined using Spectral analysis technique (Ghil, et. al., 2002, Muthama et al., 2008). This analysis is useful in identifying significant frequency bands that are shared by most decadal rainfall records. Muthama et al., 2008 used stepwise regression technique and selected the fourth degree polynomial function to determine significant peaks and the general pattern of March-May and October - December seasonal rainfall over Nairobi with minimal acceptable error values. Some attempts have been made by Schreck and Semazzi, 2004, Omondi, 2005) among others to delineate the major decadal modes of rainfall variability of the region. These studies, however, did not examine the statistical significance and confidence level of the delineated decadal modes.

In this study, the focus is on time series in discrete time and consider therefore first the simple case of a scalar, linear ordinary differential equation with random forcing,

$$X(t+1) = \sum_{j=1}^M a_j X(t-M+j) + \sigma \xi(t) \dots\dots\dots (2)$$

Its constant coefficients a_j determine the solutions $X(t)$ at discrete times $t= 0, 1, \dots, n...$

In equation 2, the random forcing $\xi(t)$ is assumed to be white in time, i.e., uncorrelated from t to $t + 1$, and Gaussian at each t , with constant variance equal to unity. In the *Yule* (1927) and *Walker* (1931) method for the time domain approach, one computes the coefficients a_j and the variance σ^2 from a realization of X having length

$N, \{X(t):1 \leq t \leq N\}$.

Both deterministic (Eckmann and Ruelle, 1985) and stochastic (Hannan, 1960) processes can, in principal, be characterized by a function of frequency f (instead of time t). This function $S(f)$ is called the power spectrum in the engineering literature or the spectral density in the mathematics. Thus a very irregular motion possesses a smooth and continuous spectrum, which indicates that all frequencies in a given band are excited by such a process. On the other hand, a purely periodic or quasi-periodic process is described by a single line or a (finite) number of lines in the frequency domain. Between these two extremes, nonlinear deterministic but “chaotic” processes can have spectral peaks superimposed on a continuous and wiggly background (Ghil and Childress, 1987, Ghil and Jiang, 1998).

The most commonly used methods are the analysis of variance (ANOVA) techniques, the use of polynomial functions and methods based on rank statistics such as Mann-Kendall and the Spearman rank tests (Kendall, 1938, 1945, 1948; Kendall and Stuart, 1961; Siegel, 1956; WMO, 1966). The statistical significance of the spectral peaks centered around ten years (decadal modes) is tested using standard white and red noise hypotheses (Kendall 1938, Ogallo 1980, 1981).

The next sub-section presents methodology on statistical tests used in determining statistical significance trends in the peaks delineated.

3.3.3. TREND ANALYSIS

Trend presents the long term movement of the time series. The most common methods of computations include autocorrelation transform, Fast Fourier Transform (FTT), and Maximum Entropy method. Trend patterns can be derived from visual patterns derived from graphs or various statistical techniques (Ogallo, 1980, 1981; Omondi, 2005; Muthama et al., 2008). The visual methods of determining modes of decadal trend from smoothed graphs are very subjective. The most commonly used methods are the analysis of variance (ANOVA) techniques, the use of polynomial functions (Ogallo, 1980, 1981; Muthama et al., 2008) and non-parametric methods based on rank statistics such as Mann-Kendall and the Spearman rank tests. Details on these methods can be found in Omondi (2005). Other details can be obtained from Kendall (1938, 1945, and 1948), Kendall and Stuart (1961), Siegel (1956), WMO (1966). Climatological data are usually not normally distributed but skewed and sometimes have extreme values (outliers).

Non-parametric, or distribution free, tests are superior for hypothesis testing of this type of data, because they do not assume that the data follows a particular distribution. Information is extracted from the data by comparing each value with all others (ranking the data) instead of computing parameters (such as mean and standard deviation). Some parametric tests require data to be normally distributed and may produce erroneous conclusions when applied to non-normally distributed data depending on the degree of non-normality of the data series. Blackman-Tukey, Monte Carlo SSA (MC-SSA) spectrum, maximum entropy, and multitaper can provide confidence intervals for the estimates it produces (Ghil and Taricco, 1997; Ghil and Vautard, 1991; Ghil, M., and P. Yiou, 1996; Ghil et al., 2002).

Methods for delineation of the spatial patterns of decadal modes are presented in the next section

3.3.4 PRINCIPAL COMPONENT ANALYSIS (PCA)

Seasonal rainfall patterns over East Africa are complex partly due to local forcing as a result of complex terrain and other surface features that include large inland lakes, valleys and mountains. This has resulted into variations of seasonal rainfall and ENSO-related impacts over East Africa (Ogallo, 1988; Indeje, 2000) over relatively short distances. Hence, there is need to combine both empirical and numerical modelling approaches to study mechanisms associated with decadal rainfall variability over different parts of the region.

The use of normalized regionally averaged series reduce two problems inherent in the analysis of rainfall in sub-humid, tropical areas namely; the highly diverse means and variabilities and the randomness of the convective process reflected in individual station totals (Ogallo, 1988; Indeje, 2000). Spatial averages are more representatives of the large-scale conditions than are data for individual stations (Nicholson, 1986). Reduction of regional data and delineation of homogeneous climate zones is critical in studying mechanisms associated with these modes of variability. Regionalization and averaging of rainfall over large but homogeneous regions have the advantages of reducing meteorological noise in the data as well as minimizing the number of variables which describe the regional climate variability (Ogallo, 1988; Indeje, 2000; Mutemi, 2003; Nyakwada, 2009).

Principal Component Analysis (PCA), derived from Factor Analysis (FA), is a statistical technique used in identifying a relatively small number of factors that can be used to represent relationships among sets of many interrelated variables. The basic assumption of Factor Analysis is that underlying dimensions, or factors, can be used to explain complex climatological variables. This method has been widely used in determining regional homogeneous rainfall zones over Kenya and East Africa (Ogallo, 1988, 1989; Oludhe, 1987; Basalirwa, 1979, 1991; Ininda, 1994; Okoola, 1996; Indeje, 2000; Omondi, 2005; Komutunga, 2006; Nyakwada, 2009). Castell 1966 or Herman 1967 also presents detailed discussions on this method. Essentially, PCA method consists of a transformation of a greater number of un-orthogonal variables into a

smaller number of orthogonal variables, which present common causes of manifest variable changes.

If the parameter under study such as rainfall is fixed, then it is possible to generate the correlation data matrix between various locations (S-Mode) over a set of periods, or between periods (T-Mode) over a set of locations. The S-mode yield groupings of locations in terms of the change over time while the T-mode can yield groupings of periods with similar spatial patterns. In an S-mode analysis, the variables are stations and the observations are the values at each time. The principal component loading matrix contains the correlation of each station with each component. These can be plotted on a map to depict the spatial pattern of each component.

Many fundamental principals of the empirical orthogonal analysis are derived from the concept of variance. The first step of the empirical orthogonal analysis involves the calculation of the appropriate measures of association for the set of variable, followed by a construction of a set of orthogonal functions that represent the measured variables. In Factor Analysis, the orthogonal functions are defined as exact mathematical linear transformation of the original data. It therefore considers the unique variance, which is not accounted for by the common linear set of orthogonal functions (factors).

The fact that the solutions are mathematically orthogonal does not always imply that the underlying physical processes must be orthogonal. Adjustments to the frames of reference of the orthogonal vectors may be used to reduce the ambiguities, which often accompany the direct solutions, and this is often referred to as 'rotation'. The rotation does not affect the total variance explained by the eigenvalues. The two common methods of rotation are the 'orthogonal' and 'oblique' rotations. In the orthogonal rotation the reference axes are maintained at 90° , while in oblique case the components are partially correlated.

The type of orthogonal rotation includes the Varimax, Quantimax and Equimax methods (Gregory 1975, Ogallo 1988, Basalirwa 1991). The oblique types of rotation include the oblimax, oblimin, promax, and many others. The spatial patterns of the dominant PCA modes may then be used to group together stations with common

characteristics into homogeneous regions. The PCA statistics (Community) at each individual region is used to identify a representative station in each region for further analysis, Gregory (1975), Ogallo (1988), and Basalirwa (1991).

Factor loadings are usually similar to correlation coefficients and they can therefore be treated in the same way as correlation coefficients during tests for acceptable level of significance. It has however been noted that as one progress from one factor to another in ascending order, the acceptable level of significance for a particular loading becomes harder to attain (Ogallo 1988, Basalirwa 1991, Indeje 2000). As a rule of thumb, factor loadings having values ± 0.3 or greater are taken as significant for sample size greater than 100. Because of the uncertainty surrounding the assessment of error in small samples and also the gradual intrusion of the unique variance into higher factors, it is necessary to adjust the level of significance.

In this study, the decadal rainfall data from the 37 stations spread all over the region were anomalized with 1961-1990 climatological mean before subjected to principal component analysis. Stations were then annotated on the map according to the eigenvectors to which they were most strongly related. Stations retained through this process in each sub-region were re-subjected to PCA analysis and the important PC time series were correlated with the stations within that region. The stations with correlation coefficients less than 0.5 with the dominant PC were rejected in this iterative process.

The basic principles of PCA are derived from the concept of variance. The first step usually involves the computation of some measures of association between the set of variables used. This is usually followed by construction of a linear set of orthogonal vectors (eigenvectors), which are finally used to represent the various variables. Under PCA, the eigenvectors are scaled by the square root of the corresponding eigenvalue. The PCA model for any variable j may take the form:

$$z_j = a_{j1}F_1 + a_{j2}F_2 + \dots + a_{jm}F_m \quad (j = 1, 2 \dots m) \dots\dots\dots (3)$$

and

F_1, F_2, \dots, F_m represent the principal components, z_j the normalized rainfall records, a_{jm} the regression weight (loading) on the m^{th} principal component.

Principal components (PCs) are linear combinations from all predetermined variables. This means that they are abstract constructions, which can not be directly interpreted as being physically meaningful. Its simplicity lies in its restriction to linear functions of the original variables, and while this is a good approximation of the underlying variability in some datasets, it has been demonstrated that physical processes can highly be non-linear (Wilks 2006). The first PCA is that linear function which has the maximum possible variance, the second PCA is the linear function with maximum possible variance subject to being uncorrelated with the first PCA, and the third PCA is the linear function which maximises variance subject to being uncorrelated with the first and second PCA and so on. Each mode or PCA explains successively less of the total variability in the original dataset. In climatological studies the term PCA is often referred to as Empirical Orthogonal Function (EOF). Thus, this method finds the spatial patterns of variability (loadings or EOFs), their time variation (scores or PCA), and gives a measure of the importance of each pattern (Jolliffe 2002).

The PCA analysis is based on the covariance matrix of a space and time dependent field with zero temporal mean. The covariance matrix of the field is constructed and diagonalised, resulting in a set of eigenvalues and to each eigenvalue is a corresponding eigenvector. Each eigenvector is referred to as an EOF and represents a space pattern of the field variable and can be literally regarded as a map. The number of maps equals the number of eigenvalues and in general, these maps are very useful in meteorological analysis. To see how a given spatial pattern evolves in time, the eigenvector is projected onto the original field to obtain a time series. Mathematically, the temporal amplitudes (u_m) are given by:

$$u_m = e_m^T z' = \sum_{k=1}^K e_{km} z_k', m = 1, 2, \dots, M \dots \dots \dots (4)$$

where M is the number of the first eigenvectors (PCA) taken from the whole eigenvector (e) set of the variance-covariance matrix of the normalized rainfall field (Z').

Just as the PCA are orthogonal in space, the associated time series are orthogonal in time. The fraction of the total variance in the original data, which is accounted by a given PCA, is proportional to the associated eigenvalue. Together, an eigenvalue with its corresponding PCA and temporal amplitude define a mode of variability. The leading mode is related to the largest eigenvalue and extracts the largest fraction of total variance; the second mode extracts the largest fraction of the remaining variance, and so on (Richman, 1981; Ogallo, 1981, 1986, 1988 and 1989; Basalirwa 1999; Basalirwa et al., 1999; Indeje 2000).

In T-mode analysis of PCA, the standardized data matrix is transposed so that each of the individual time periods is changed to a variable while the station names become observations. This analysis produces components with loadings on the individual times and amplitudes or scores on the observations (stations) give the spatial pattern. The factor loadings in T-mode analysis are also time coefficients, which can be used as weights in areal averaging. While S-mode can be used to classify locations with similar temporal anomalies, T-mode can be used to classify years during which the specific sub-regions experienced similar spatial anomalies.

To effectively provide a better understanding of the physical processes responsible for decadal climate variability over the region, the study involved performance of cluster analysis on the rainfall stations network to group them into homogeneous decadal rainfall zones. The delineation of homogeneous zones was thereafter followed by identifying the stations with the largest correlation with the Principal Component (PC) time series associated with the first eigenvector of the decadal rainfall anomaly. The PCA concept was used in this study to establish the dominant modes in the observed decadal rainfall and SST data. The spatial patterns of the dominant modes observed in the SST fields were useful in selection of SSTs modes from the major global basins for the model developed. The use of PCA, however, requires the identification of the number of factors, which must be included in the solutions.

Some methods useful in determining the number of the PC's to include in the solutions are discussed in the next section.

3.3.5 NUMBER OF SIGNIFICANT PRINCIPAL COMPONENTS

Some of the basic steps in PCA include the choice of the number of factor solutions, rotation of components and the determination of the stability of the principal components. Most methods used in deciding the number of factor solutions to be retained try to ensure that only the components extracting substantial amount of the total variance that may not be considered as noise are retained in the final solutions. The PCA technique reduces the dimensionality of a given data set by describing it fully using new variables (principal components) that have two fundamental properties namely; (i) any two different components are uncorrelated, and (ii) that each component is derived from an empirical orthogonal variable accounting for a maximum in residual total variance of the original data set (Ehrendorfer, 1987). The use of PCA, however, requires the identification of the number of factors, which must be included in the solutions (Ogallo, 1981, 1989; Indeje, 2000; Nyakwada, 2009).

Each of the new variables explains a certain percentage of the variance in the original data and they all, cumulatively, explain the total variance. The number of factors considered would normally affect the configuration of the type maps achieved. It is, therefore, critical to identify only those modes that produce patterns that may be physically interpretable as opposed to those that emerge only due to random processes (noise). Several tests exist for the determination of the appropriate number of components to retain.

3.3.6 THE SCREE METHOD

This method plots each raw eigenvalue against each mode producing an exponential curve that decreases as the number of modes increase. The point where the curve of the graph breaks becomes nearly linear is the determining number of significant principal components. The principal components after this point, which have nearly equal eigenvalues, theoretically represent random noise and may be discarded (Cattel,

1966). Cohen (1983) gives a variation of this test where the data is rotated before graphing. This gives a more distinct break in the curve.

The Scree test of Catell (Catell, 1966), where the eigenvalues are plotted against the factor numbers, the highest eigenvalue corresponds to the first ordinate point where the graph develops to a linear relationship, suggests that the Kaiser's Criterion might be more reliable only when the numbers of variables are between 20 and 50.

3.3.7 KAISER'S CRITERION

This method, developed by Kaiser (1959), is one of the simplest methods of determining the significant principal components (PCs). This method assumes that all PCs whose corresponding eigenvalues are greater than or equal to one are significant. It retains only those PCs that extract variance at least as much as the equivalent of one original variable. Thus in Kaiser's Criterion (Kaiser, 1958), only the latent roots (eigenvalues) greater than unity are considered.

3.3.8 LOGARITHM OF EIGENVALUES (LEV)

An adaptation of the scree graph is the log-eigenvalue diagram, where $\log(\lambda_k)$ is plotted against k . It is based on the conjecture that eigenvalues corresponding to 'noise' should decay geometrically; therefore, those eigenvalues should appear linear (Craddock, 1973). Farmer (1971) investigated the procedure by studying LEV diagrams from different groupings of 6000 random numbers. He contends that the LEV diagram is useful in determining the dimension of the data.

3.3.9 SAMPLING ERRORS OF EIGENVALUES

North *et al.*, (1982) uses the sampling errors of the associated eigenvalues in determining significant principal components. The aim of the method is to determine whether a sample component faithfully represents a real eigenvalue. The method assumes that the sampling errors are of the order $(2/N)^{1/2}$, where N is the total number of observations. Dealing with first order, the shift in the eigenvectors can be shown to

depend strongly on the spacing of the eigenvalues whereas the shift of the eigenvalues does not.

If the sampling error of a particular eigenvalue, λ_a , given by $\delta\lambda_a \approx \lambda_a(2/N)^{1/2}$, is comparable to or larger than the spacing between λ_a and λ_b , a neighbouring eigenvalue, then the component associated with λ_a will be comparable to the size of the neighbouring component associated with λ_b . The above results in the rule of thumb that tests for degeneracy by examining if $\lambda_a - \lambda_b > (2/N)^{1/2}$ and retains only the principal components that satisfy the condition. The Kaiser's criterion, Scree test and North *et al.*, sampling errors test were used to ascertain significant number of principal components to retain for rotation.

The next section gives brief description of the method adopted to study teleconnection between regional decadal rainfall variability patterns and global SSTs.

3.4 TELECONNECTION BETWEEN REGIONAL DECADAL RAINFALL VARIABILITY PATTERNS AND GLOBAL SEA SURFACE TEMPERATURES

Three methods are adopted to investigate the teleconnection between the regional decadal rainfall variability patterns and global SSTs. These include simple correlation method, Canonical Correlation Analysis (CCA) and Singular Value Decomposition (SVD).

3.4.1 CORRELATION METHOD

Correlation analysis examines the relationship between pairs of variables namely the dependent variable (Y) and the independent variable (X). The degree of relationships between the pair of variables Y and X is often quantified using correlation coefficient (Equation 5). This simple correlation coefficient (r_{xy}) between two variables may be expressed as:-

$$r_{xy} = \frac{\frac{1}{n} \sum_{i=1}^n (x_i - \bar{x})(y_i - \bar{y})}{\left[\frac{1}{n} \sum_{i=1}^n (x_i - \bar{x})^2 \frac{1}{n} \sum_{i=1}^n (y_i - \bar{y})^2 \right]^{1/2}} \dots\dots\dots (5)$$

Where X_i and Y_i are sea surface temperature and decadal rainfall for the specific regions at times t , and, \bar{x} and \bar{y} arithmetic means of X_i and Y_i at time t , respectively. N is the length of records. The value of r_{xy} lies between -1 and +1, if it is equals +1, then X and Y are perfectly correlated, while it is zero when there is no relationship between the variables. Negative and positive values of r_{xy} reflect negative (one increases as the other decreases) and positive (both increase and decrease simultaneously) relationships between X and Y.

Correlation analysis alone is not sufficient to delineate linkages between multiple dependent / independent variables. It is also weak in identifying linkages that are not temporally symmetrical, for example, high linkages with maximum Sea Surface temperatures (SST) values but no linkages with minimum SST values. The statistical significance of r_{xy} may be estimated, using the standard t - test (Equation 6).

$$t_{N-2} = r \sqrt{\frac{N-2}{1-r^2}} \dots\dots\dots (6)$$

t_{N-2} is the student t - distribution value with $N-2$ degrees of freedom and N is the length of records. The details of t - test can be obtained in many standard references (WMO, 1966; Wannacott and Wannacott, 1985; Wilks, 2006).

In this study, correlation method is adopted to investigate if the main modes of variation in the decadal rainfall fields are related to the same frequencies of variation in several SST indexes chosen in key-areas (e.g. Nyakwada, 2009).

3.4.2 CANONICAL CORRELATION ANALYSIS (CCA)

Unlike PCA, Canonical Correlation Analysis (CCA) is a statistical technique that identifies a sequence of pairs of patterns in two multivariate data sets and constructs sets of transformed variables by projecting the original data onto these patterns. The patterns are chosen such that new variables defined by projection of the two data sets onto these patterns exhibit maximum correlation but are uncorrelated with the projections of the data onto any of the other identified patterns. CCA is a multivariate statistical technique

that calculates linear combinations of a set of predictors that maximizes relationships in a least square sense to the similarly calculated linear combinations of a set of predictand. The superiority of CCA over other several techniques is its ability to operate on full fields of information and to objectively define the most highly related patterns of predictor and predictand (Barnett and Preisendorfer 1987; Indenje 2000; Mutemi 2003; Omondi 2005; Nyakwada 2009).

Canonical Correlation Analysis (CCA) goes beyond the limitation of the simple correlation analysis by taking into consideration the full space and time dimensions of the fields analyzed and this is an exceptional skill capability of the technique. CCA also gives an extensive set of diagnostics that offer some insight into the physical base of the relationships used to form the predictions. The advantages of CCA include ability to operate on full fields of information and to objectively define the most highly related pattern of predictors and predictands. Its capability to define both the space and time evolution of the predictor dataset that best predicts an associated pattern of a predictand is powerful. The disadvantages of CCA include the estimation of the reverse matrices needed in CCA, which may be impossible for highly inter-correlated data fields since the matrices may be degenerative. The transformation of the variables into orthogonal variates helps reduce the problems associated with inter-relationship in the data sets (Repelli and Nobre 2004). CCA can also be unstable if the records are not long enough or if there is noise in the data.

The CCA selects pairs of spatial patterns of two space / time dependent variable sets such that the (time dependent) pattern amplitudes are optimally correlated. The strength and the sign of the corresponding patterns are described by the canonical correlation coordinates. Since the canonical series are normalized to unit variance, the canonical correlation patterns are expressed in the units of the variable they represent and indicate the "typical" strength of the mode of co-variation described by the patterns. The correlation between the canonical coordinates measures the degree of association between the canonical patterns of predictor and predictand variables (Cheery, 1997; von Storch and Zwiers 1999, Xoplaki et al., 2003).

Prior to the CCA, the original data are projected onto their PCA. An advantage of using the PCA in the CCA is that the input data are independent, since the PCA are uncorrelated. The selection procedure for the number of PCA from the predictand and the predictor field for the subsequent CCA is of great importance. On the one hand, too few PCA will omit part of the significant signal, thus resulting in a poorer prediction of the overall CCA models. On the other hand, using too many PCA will fit the statistical models too strongly to particular data sets considered, and most likely resulting in missing an adequate description of the underlying process.

A CCA transform pairs of original centred data vectors x' and y' into sets of new variables, called *canonical variates*, v_m and w_m , defined by the dot products

$$v_m = a_m^T x' = \sum_{i=1}^I a_{m,i} x'_i, m=1, \dots, \min(I, J); \dots\dots\dots (7a)$$

and

$$w_m = b_m^T y' = \sum_{j=1}^J b_{m,j} y'_j, m=1, \dots, \min(I, J); \dots\dots\dots (7b)$$

This construction of canonical variates is similar to that of the principal components u_m (Equation 4), in that each is a linear combination of (a sort of weighted average) of elements of the respective data vectors x' and y' . These vectors of weights, a_m and b_m , are called the canonical vectors. One data- and canonical-vector pair need not have the same dimension as the other. The vectors x' and a_m each have I elements, and the vectors y' and b_m each have J elements. The number of pairs, M , of canonical variates that can be extracted from the two data sets is equal to the smaller of the dimensions of x and y ; that is, $M = \min(I, J)$.

The canonical vectors a_m and b_m are the unique choices that result in the canonical variates having the properties

$$corr[v_1, w_1] \geq corr[v_2, w_2] \geq \dots \geq corr[v_M, w_M] \geq 0; \dots\dots\dots (8a)$$

$$\text{corr}[v_k, w_m] = \begin{cases} r_{cm}, & k=m \\ 0, & k \neq m \end{cases}; \dots\dots\dots (8b)$$

and

$$\text{Var}[v_m] = a_m^T [S_{x,x}] a_m = \text{Var}[w_m] = b_m^T [S_{y,y}] b_m = 1, \dots\dots\dots (8c)$$

Equation 8a shows that each of the M successive pairs of canonical variates exhibits no greater correlation than the previous pair. These correlations between the pairs of canonical are called the *canonical correlations*, r_c . Equation 8b states that each canonical variate is uncorrelated with all of the other canonical variates except its specific counterpart in the m^{th} pair. Finally, Equation 8c states that each canonical variate has unit variance.

In this study the CCA was computed for the SST (predictor) and the station rainfall (predictand) to extract the dominant patterns of linear covariability while Singular Value Decomposition (SVD) was performed on the correlation matrix of the truncated PCs of the two data sets. The results formed the foundation for the development of empirical relationships between decadal rainfall and SST modes.

3.4.3 SINGULAR VALUE DECOMPOSITION (SVD)

Singular Value Decomposition (SVD) analysis is a technique employed in geophysical science to identify pairs of spatial patterns whose time series are characterized by maximum temporal covariance. It tends to compress complicated temporal covariance between two fields into a relatively few pairs of spatial patterns by maximizing temporal covariance explained by each pair of spatial patterns while constraining them to be spatially orthogonal to the preceding ones of the same field.

In general, SVD technique is a basic matrix operation in linear algebra that isolates pairs of spatial patterns between two data fields through decomposition of their temporal covariance matrix and their associated time series. Both CCA and SVD are generalization of PCA analysis, designed for a single data field, to two data fields and

identify linear combinations of variables (or spatial patterns) in two fields that are most strongly related to each other (Bretherton et al., 1992; Wallace et al., 1992; Xinhua and Timothy, 1995). The difference between CCA and SVD is that CCA identifies spatial patterns by maximizing the temporal correlation between two data fields, whereas SVD maximizes the temporal covariance between two data fields.

The SVD method has been used in this study to further examine the detailed patterns of the dominant modes of decadal variations in rainfall and their teleconnection to the global SST changes. Detailed descriptions of SVD analysis can be found in Bretherton et al., (1992) and von Storch and Navarra (1995). Exploiting the spatial coherence of climate signals in data series with low signal to noise ratios facilitates their identification (Mann and Park, 1996) while preserving spatial information and allowing the isolation of signals that might largely cancel in coarse spatial averaging (e.g., signals which largely involve dipole and quadrupole patterns). A brief outline of the SVD process in atmospheric science applications is given below, following Cherry (1997).

Let x and y be $n_t \times p$ and $n_t \times q$ data matrices, where the means of the columns of x and y are all equal to zero. Let $c_{xy} = (1/n_t)XY^T$ be the $p \times q$ matrix whose elements are the covariances between the time series in the two fields. SVD finds linear combinations of the data X_{a_i} and Y_{b_i} [$i = 1, 2, \dots, r; r = \min(p, q)$], with the maximum covariance, subject to the $p \times 1$ vectors a_i and $q \times 1$ vectors b_i satisfying the orthogonality constraints:

$$a_i^T a_j = b_i^T b_j = \delta_{ij} \dots \dots \dots (9)$$

Where $\delta_{ij} = 1$ if $i = j$ else $\delta_{ij} = 0$ if $i \neq j$.

The solution: $c_{xy} = ADB^T$ defines the singular value decomposition, and A is a $p \times r$ semiorthogonal matrix, D is an $r \times r$ diagonal matrix, and B is a

$q \times r$ semiorthogonal matrix. The i th columns of A and B contain the left and right weight (singular) vectors a_i and b_i , and the i^{th} element of D (the i^{th} singular value) is the covariance of X_{ai} and Y_{bi} . The vectors X_{ai} and Y_{bi} are referred to as the i^{th} pair of SVD expansion coefficients. The two sets of expansion coefficients (which are time series) will tend to be correlated with one another because:

$$Cov(X_{ai}, Y_{bi}) = cor(X_{ai}, Y_{bi}) \sqrt{[var(X_{ai})var(Y_{bi})]} \dots \dots \dots (10)$$

Thus finding a_i and b_i to maximize the covariance of the expansion coefficients will tend to produce pairs of expansion coefficients that are correlated. In practical application, it is desirable to find the directions in “ p space” and “ q space” so that when the variables in the two sets of data are projected onto these two axes, they are as similar as possible. The next step is to find a second set of directions, orthogonal to the first, with similar properties, and so on up to “ r ” such pairs of directions.

In CCA formulation, the SVD is used to solve explicitly the weights x and y by applying it on the triple product matrix:

$$c = S_{yy}^{-1/2} S_{yz} S_{zz}^{-1/2} \dots \dots \dots (11)$$

Obtaining the solutions x and y with the SSTs at concurrent season with rainfall would give the CCA specification skill while letting the SSTs lags rainfall give the CCA model prediction skills.

The Square Covariance Fractions (SCF) explained by each mode and the correlation coefficient (r) between the expansion coefficient of both ocean SSTs and OND rainfall are presented as indicators of the strength of the coupling between the two variables. In this study, the covariability between the atmosphere and ocean was explored by performing SVD analysis of rainfall and SST anomalies at decadal time scale.

3.5 PREDICTION OF DECADAL RAINFALL PATTERNS

This section highlights the methodology used to predict decadal rainfall over the region. Interest in knowledge of climate information beyond seasonal timescale has constantly been shown by policy makers and planners and had also become a compelling issue that emerged from IPCC Fourth Assessment Report (AR4) (IPCC 2007). This is a time frame of interest for many activities that support decision-making regarding impacts of climate variability and change, yet it has not been emphasized in the current climate change projections and associated studies. The techniques adopted in this study include Multiple Linear Regression (MLR) and verification procedures to test the skills of the forecasts developed. Regression and correlation analyses which are standard linear methods that only extract the linear structures of the data (Hsieh, 2004) were also used as discussed in Omondi 2005.

The SVD and PCA analyses are employed first, to reduce the large dimensionality of the SST and rainfall data and the leading eigenmodes of SST retained as predictors of decadal rainfall variability in the delineated homogeneous climate zones. The longitude and latitudes of the ocean areas expressed as boxes greater or equal to 10° and with correlation greater or equal to ± 0.3 (North et al., 1982) were selected as predictors for rainfall in the specific homogeneous zones delineated over East Africa.

Skilful decadal forecasts would be useful in reducing and managing the risks associated with rainfall extremes. They would further provide useful inputs to the improvement of early warnings of extreme rainfall events and also offer valuable contribution towards disaster risk reduction and sustainable socio-economic development in the region.

3.5.1 MULTIPLE REGRESSION MODELS (MRM)

Multiple Linear Regression (MLR) analysis aims to produce predictand values of a dependent variable from a linear set of principal predictors that efficiently describe the collective variability of independent variable. MLR models the relationship between two or more explanatory variables and a response variable by fitting a linear equation to observed data. Every value of the independent variable, x , is associated with a value of

the dependent variable, y . The regression equations are usually derived using stepwise MLR, in which each potential predictor variable is evaluated for its individual significance level before being included in the equation and, with each addition; each variable within the equation is then evaluated for its significance as part of the model.

Fitting a Multiple Regression Model (MRM) is similar to that of a Simple Linear Regression Model (SLRM) which is usually done through the least squares method. In a multiple regression model, a single predictand, Y , has more than one predictor variable, X . Let k denote the number of predictor variables, then the prediction equation is

$$Y = b_0 + b_1x_1 + b_2x_2 + b_3x_3 + \dots + b_kx_k + \varepsilon \dots\dots\dots (12a)$$

or

$$Y = b_0 + \sum_{i=1}^n b_i x_i + \varepsilon_i \dots\dots\dots (12b)$$

where b_0 and b_i are the intercept and regression coefficients for the predictors, x_i . The same steps are followed for determining the prediction equation as for the case of SLRM. However, in this case, the variance of the error term is

$$S^2 = \frac{SSE}{n - (k + 1)} \dots\dots\dots (12c)$$

A test of the adequacy of the model is done by computing R^2 which is the multiple coefficient of determination given by

$$R^2 = 1 - \frac{SSE}{\sum_{i=1}^n (Y - \bar{Y})^2} \dots\dots\dots (12d)$$

For $R^2 = 0$, it implies lack of fit, while $R^2 = 1$ implies perfect fit.

To test the utility of this model, a Null hypothesis is define as:-

$$\begin{aligned}
 H_0: & \quad b_1 = b_2 = b_3 \dots = b_k = 0 \\
 & \text{against} \dots\dots\dots (13) \\
 H_1: & \quad \text{At least one of the } b_i \neq 0
 \end{aligned}$$

The test statistic is:

$$F_c = \frac{R^2/k}{(1-R^2)/[n-(k+1)]} \dots\dots\dots (14a)$$

the rejection region is if $F_{tabulated} > F_{c(n-k-1)}^k(\alpha) \dots\dots\dots (14b)$

Inference about a particular value would be made as follows:

$$H_0: b_2 = 0 \text{ (No relationship with SST of South Pacific)}$$

$$\text{against } H_1: b_2 \neq 0, \text{ i.e. } b_2 > 0 \text{ or } b_2 < 0 \dots\dots\dots (14c)$$

The test statistic is

$$t = \frac{b_2}{S} \sqrt{\sum_{i=1}^n (x_i - \bar{x})^2} \text{ with } \nu = n - 2 \dots\dots\dots (14d)$$

Choose $\alpha = 0.05$ and reject the null hypothesis if $t < -2.306$ or $t > 2.306$. An example of ANOVA table for Multiple Linear Regression Model is discussed in the next subsection.

3.5.2 ANOVA FOR MULTIPLE LINEAR REGRESSION

The ANOVA calculations for multiple regression are nearly identical to the calculations for simple linear regression, except that the degrees of freedom are adjusted to reflect the number of explanatory variables included in the model. For k explanatory variables, the model degrees of freedom (DFM) are equal to k , the error degrees of freedom (DFE) are equal to $(n - k - 1)$, and the total degrees of freedom (DFT) are equal to $(n - 1)$, the sum of DFM and DFE. An example of ANOVA table for a multiple linear regression is given in Table 4.

Table 4: ANOVA table for Multiple Linear Regression

Source	df	SS	MS	F
Regression	k	SSR	MSR = SSR/k	F = MSR/MSE
Residual	n - k - 1	SSE	MSE = SSE/n - k - 1	Larger values of F imply a stronger relationship while smaller values of F indicate weaker relationship
Total	n - 1	SST	MST = SST/(n-1)	

SS implies Sum of Squares while MS are Mean Square.

In multiple regression, the test statistic MSR/MSE has an F (k, n - k - 1) distribution. The ratio SSM/SST = R² is known as the squared multiple correlation coefficient. This value is the proportion of the variation in the response variable that is explained by the response variables.

3.5.3 VERIFICATION OF THE FORECAST

To assess the true skill of a forecast system, it is vital to minimize the risk of artificial skill that arises because the system has information that would not be available in real-time application. The safest solution is to define a period for model development and a completely independent period for model testing. It is desirable that the development period be as long as possible to increase the reliability of the statistical analysis. Over-fitting the model results from the use of too many predictors while under-fitting the model results from use of too few predictors. It is desirable to use average number of predictors giving average model efficiency (R²).

Statistics used to assess the forecast skill from a regression equation include the standard correlation between the forecast (*f*) and observed (*v*) variable (equation 5), F-ratio and the p-values. Summaries of the model forecasts and observed scores are presented in the form of contingency tables for each station. Table 5 shows a sample of a contingency table with arbitrary scores for both forecasts and the observations.

Table 5: Contingency table for observed and forecasted model

		Forecast			
		Dry	Normal	Wet	Total
Observation	Dry	a	b	c	J
	Normal	d	e	f	K
	Wet	g	h	i	L
	Total	M	N	O	T

$$\text{Percent Correct} = \frac{a + e + i}{T} \times 100\%$$

$$\text{Post Agreement} = \frac{a}{M}, \frac{e}{N}, \frac{i}{O} \text{ for Dry, Normal and Wet categories.}$$

The False Alarm Ratio, (FAR) = $1 - \frac{a}{M}$ or $1 - \frac{i}{O}$ for extreme dry or wet cases respectively. Other statistics that may be used include the root-mean-square error (RMSE), the absolute error (ABSE), and the bias (BIAS):

$$RMSE = \left[\frac{1}{N} \sum_{i=1}^N (f - v)^2 \right]^{1/2} \dots\dots\dots (15)$$

$$BIAS = \frac{1}{N} \sum_{i=1}^N (f - v) \dots\dots\dots (16)$$

$$ABSE = \frac{1}{N} \sum_{i=1}^N |f - v| \dots\dots\dots (17)$$

where the summation extends over the N forecast years. It is worth mentioning that RMSE and BIAS do not measure skill relative to reference score.

3.6 PROJECTION OF FUTURE REGIONAL CLIMATE

An attempt is also made in this study to generate (downscale) future climate projections (scenarios) of the East Africa using dynamical downscaling (regional climate modelling) technique. The Regional Climate Model (RCM) used in this study is the

PRECIS (Providing REgional Climates for Impacts Studies). This is the Hadley Center's version of the Regional Climate Model (HadRM3P) based on HadAM3P, which is an improved version of the atmospheric component of the latest Hadley Centre coupled Atmosphere Ocean Global Circulation Model (AOGCM), HadCM3, (Gordon et al., 2000).

The PRECIS model uses the same formulation of the climate system as in the mother GCM, HadAM3P that ensures the RCM provides high-resolution regional climate change projections generally consistent with the continental scale climate change projected by the GCM. The PRECIS climate model is thus an atmospheric and land surface model of limited area and high resolution. PRECIS is a hydrostatic, primitive equation gridpoint model containing 19 levels described by a hybrid vertical coordinate (Simmons and Burridge, 1981; Simon et al., 2004). In this study PRECIS has been used with horizontal resolutions of 50 km with 19 levels in the atmosphere (with the model top at about 30 km in the stratosphere) and four soil layers. The model has been applied in downscaling to 25 km horizontal resolution to capture finer details of climate impacts. However, for a bigger region like the whole of Greater Horn of Africa, the high computational costs and storage implications limited its use at 50km spatial resolution.

The model runs were performed for the present climate (1961–1990) using different base-line lateral boundary conditions (LBCs) and for future scenarios (2010–2100) using the special report on emissions scenarios (SRES) of the Intergovernmental Panel on Climate Change (IPCC). The model is driven at its lateral boundaries by relaxing surface pressure (p^*), the horizontal wind components (u and v available on the 19 model levels) and cloud-conserved temperature and moisture variables (θ and q_t on the 19 model levels) towards values interpolated in time from data saved every 6 hours from the GCM integration.

Dynamical flow, the atmospheric sulphur cycle, clouds and precipitation, radiative processes, the land surface and the deep soil are all described and information from every aspect is diagnosed from within the model (Simon et al., 2004). The PRECIS model, like all other RCMs requires prescribed surface and lateral boundary conditions.

Surface boundary conditions are only required over water, where the model needs time series of surface temperatures and ice extents. Lateral boundary conditions provide dynamical atmospheric information at the latitudinal and longitudinal edges of the model domain. There is no prescribed constraint at the upper boundary of the model. The lateral boundary conditions comprise the standard atmospheric variables of surface pressure, horizontal wind components and measures of atmospheric temperature and humidity. These lateral boundary conditions are updated every 6 hours, while the surface boundary conditions are updated every day. The details of this model description can be obtained from the UK Met Office PRECIS training Handbook Manual (Richard et al., 2003).

3.6.1 MODEL DOMAIN

The issue of optimum domain size has received significant attention in regional climate modeling (Denis *et al.*, 2002). In the choice of an RCM domain, it is desirable to select a domain that is both large enough that the regional model can develop its own internal regional-scale circulations, but not too large that the climate of the RCM deviates significantly from the GCM in the centre of the domain (Denis et al., 2002, Jones et al., 1995, Seth and Giorgi 1998; Kumar et al., 2006). Often the choice of model domain size is a compromise between requirement for a higher resolution and computational costs. However, other aspects such as the appropriate model physics parameterizations and/or local climate features/systems also count significantly.

Jones *et al.* (1995) investigated the influence of lateral boundary forcing on one-way nested RCM simulations using domains of four different sizes and showed that the largest domain produced significant deviations of RCM from GCM solutions. On the other hand, the smallest domain exhibited too strong large-scale control on the RCM solutions and thus showed very limited added value to the GCM output. Seth and Giorgi (1998) used analysis of observations (ECMWF reanalysis) as lateral boundary driving fields for RegCM2 and demonstrated that with a smaller domain the simulated precipitation was closer to observation compared to simulations with a larger domain. However, the climate sensitivity to the internal forcing was better captured with larger domain. This means that the optimum domain size should be one where large-scale

circulation in RCM is constrained to follow the driving GCM fields, but the finer mesoscale systems also have enough space to fully develop.

Sun et al.,(1999a) performed a suite of simulations with different domain sizes over eastern Africa during the initial customization of RegCM2 to simulate the climate of the region and showed that the domain which covered the main regional and large scale features i.e. East Africa and Ethiopian Highlands, western Indian Ocean, Tropical(Congo) rainforest, large inland lakes (Victoria, Tanganyika and Malawi) produced more realistic distribution of simulated precipitation and other meteorological fields.

In this study, the PRECIS RCM for the eastern Africa region was configured for a domain extending from about 13°S to 16°N and 24°E to 52°E (Figure 10) based on Sun et al., 1999a criteria. Sensitivity simulations were performed in order to determine an appropriate domain size. Two domains were tested, both extending from about 13°S to 5°N and 29°E to 44°E, but with one having a 0.44° resolution (~50 km) and the other a 0.22° resolution (~25 km), as well as a large domain (13°S to 16°N and 24°E to 52°E) at 0.44° resolution.

The model domain (13°S to 16°N and 24°E to 52°E) selected was sufficiently large so that synoptic and mesoscale circulations generated within the RCM were not undesirably damped and at the same time, reasonably small so that the deviation of the large-scale seasonally averaged RCM circulation from the driving AOGCM is not overwhelmingly large to imply a significant perturbation to the planetary-scale divergent circulation. These conditions are necessary to ensure physical consistency between the RCM solution and the pre-determined AOGCM solution external to the RCM domain (Seth and Giorgi 1998; Jones et al., 1995 and Denis et al., 2002). The control simulation of PRECIS model was investigated for December – February (DJF), March – May (MAM), June – August (JJA) and October – December (OND) seasons.

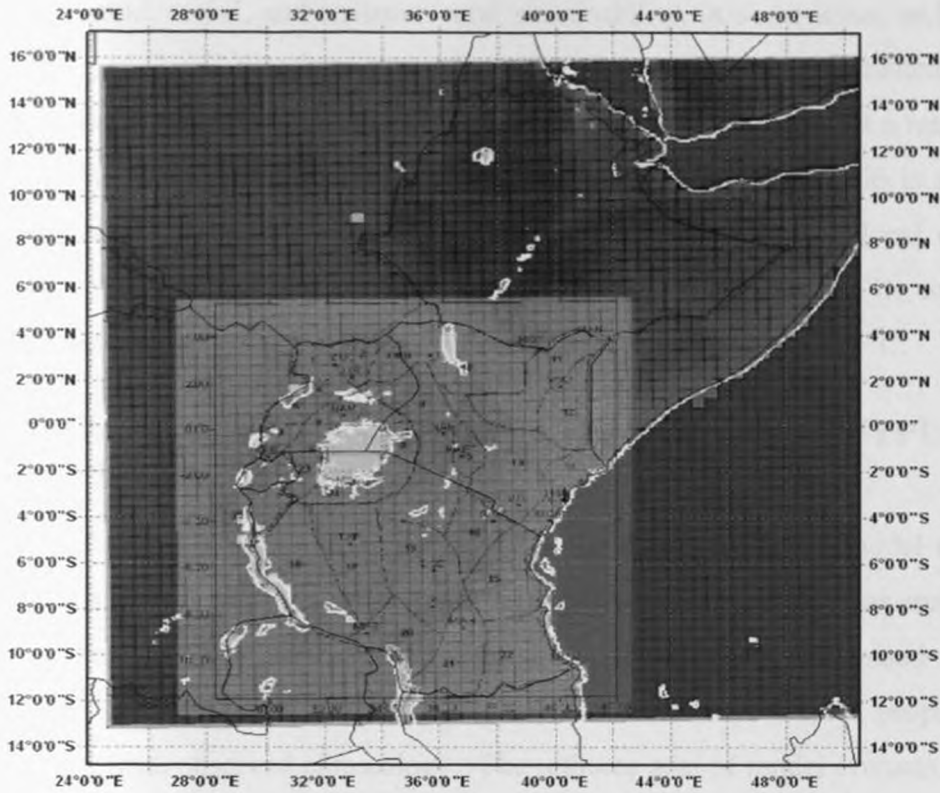


Figure 10: Region of study in relation to the model domain

3.6.2 DESCRIPTION OF MODEL EXPERIMENTS

The RCM was set up for the eastern Africa domain (Figure 10) and run to simulate the climate for the present (1961-1990) and a future period 2010-2100 using ERA-40 reanalysis, HadAM3P and ECHAM4 GCM output as initial and boundary forcing. The RCM model projections for 2010-2020 decade were compared with the predicted regional decadal rainfall variability patterns outlined in section 3.5. The A2 and B2 GCM future scenarios or storylines were used. Note that, A2 scenario is based on heterogeneous world with a large gap between the rich and the poor, high rates of population growth, and slower economic development. In the A2 scenario the distribution of new technology is assumed to be slow, and energy needs are largely met through fossil resources. This scheme results in medium to high emissions, with atmospheric CO₂ concentrations reaching 715ppm and global temperatures expected to increase by around 3.3°C by the 2080s (IPCC 2007). On the other hand, the B2 storyline describes technologically imbalanced world, a world with emphasis on local solutions

for economic, social, and environmental sustainability. In some areas, technology will develop rapidly, while other areas will be forced to make do with outdated technology. It describes a world with continuously increasing global population at a rate lower than A2, intermediate levels of economic development. While the scenario is also oriented towards environmental protection and social equity, it focuses on local and regional levels. The accompanying emissions scenario is medium low, with CO₂ concentrations at 562ppm and global temperatures expected to increase by around 2.3°C.

3.6.3 EVALUATION AND VALIDATION OF GCM OUTPUT AND PRECIS SIMULATIONS

Model evaluation and validation are essential parts of the model development process if models are to provide useful information to support decision-making. Model evaluation is done to ensure that the model is satisfactorily customised for different regions and the physics parameterizations have been implemented properly and are consistent with observed climatology. The ultimate goal of model evaluation/validation is to make the model useful for application to specific regions and that it provides reasonably accurate information about the regional climate systems being modelled.

A measure of the confidence in the projections of climate change from a particular climate model is based on the model's capability in simulating contemporary climate. Therefore, the regional climate model (PRECIS) was first run for a baseline period and results compared with the observed climatology over the same period (i.e. 1961-1990). Comparison is done for daily, monthly and seasonal means and frequency distribution over specific grid boxes or points.

The PRECIS simulations were also compared with the GCM output and observations at scales resolved by the GCM. This helps to to evaluate the biases between the RCM and the parent GCM and also an indication of the value added by using RCM. To achieve this model evaluation strategy, the PRECIS (RCM) and CRU data have been divided into large-scale (LS) and mesoscale (MS) components as suggested in some studies (Jones et al., 1995; Noguer et al., 1998 and Denis et al., 2002). The LS component is obtained through aggregation of the data to the scale of the GCM, by

averaging all land points lying within each GCM grid box, and the mesoscale component is obtained by calculating the difference between the large-scale component and the original data. The ensemble mean PRECIS output was obtained when ensemble members of ECHAM4 and HadAM3P were averaged and used as a forcing.

The PRECIS simulated temperature and precipitation have biases typical of many other GCMs or RCMs used in several studies cited here. But, the GCM biases are corrected before simulated temperature and precipitation are compared to observations. A simple bias correction approach as used by Durman et al., (2001) was applied. In this approach a monthly factor based on the ratio of present day simulated values to CRU observed values on a grid box basis is applied to the modelled climatic variables. Recently, Fowler et al., (2007) also used this approach to study the impact of climate change on the water resources in north-west England.

3.6.4 PRECIS REGIONAL CLIMATE PROJECTIONS

To generate climate change projections, two time-slice periods were used to drive the RCM. The first period is usually when there are no increases in emissions (i.e. to represent pre-industrial climate) or can be for a recent climate period. 1961-1990 is often chosen as it is the current WMO 30-year averaging period. The second period can be any period in the future, although will often be taken at the end of the century (for example, 2071-2100) when the climate change signal will be clearest against the noise of climate variability. The projected regional climate model in this study are based on the difference of two 30-year simulated climate regimes; the future climate (average for 2071 to 2100) minus the present day climate (average for 1961 to 1990).

The model simulations were performed with and without including sulphur cycle, to understand the role of regional patterns of sulphate aerosols in climate change. However, the effect of black carbon (soot) was not included in the simulation experiments. Using the model output from these experiments, high-resolution climate change scenarios have been developed for various surface and upper air parameters of critical importance to the impact assessments for East Africa region.

An effective way of exploring a model's internal variability is to use ensembles, effectively increasing simulation length while minimising the effect of the change in external forcing due to atmospheric composition. To increase the range of climate states captured, a set of realizations of a particular climate can be produced, each using the same evolution of atmospheric composition (recent or future). The individual members of the driving model ensemble are initialized with different (but equally plausible) states. The deterministic nature of the model produces a different (but again equally plausible) representation of the subsequent climate for each initial state.

In this study, the regional climate projections were computed by weighting output of ensemble members of the two GCMs, ECHAM4 and HadAM3P, used as forcings to PRECIS RCM for a high emissions scenario (SRES A2) and also low emission scenario (SRES B2).

ANALYSIS OF MODEL RESULTS

CHAPTER FOUR: RESULTS AND DISCUSSIONS

This chapter presents and discusses the results that were obtained from the various methods that were used to address the objectives of this study. These include results from (a) Correlation analysis and Principal Component Analysis (PCA) used for delineating zones with similar decadal variability modes; (b) spectral and trend analyses together with the associated statistical tests used to present some differences in decadal modes of variability for the specific delineated zones; (c) Singular Value Decomposition Analysis (SVDA) used for investigating the teleconnection of the regional decadal rainfall variability patterns with global sea surface temperatures, and (d) Multiple Linear Regression methods that were used to examine the predictability of the decadal variability modes in East Africa. The last section of the chapter presents the results from examination of probable future regional climate scenarios and compared the near-term projections with predicted decadal rainfall using Regional Climate Model. The results from various methods are presented separately and compared in the following sections. The quality of the rainfall records used is however presented first in the following subsection.

4.1 DATA QUALITY CONTROL RESULTS

The quality control of the few missing data is presented in this section. It was indicated in sections 3.3.1 that both correlation and regression were the key methods used to examine the quality of data used in this study. Less than 10% of the total records were estimated at all locations.

Examples of the results from the mass curves analysis are given in figures 11 and 12. Figure 11 shows an example of the mass curves that were obtained at most locations. The mass curves showed that in general only straight single line could be fitted to cumulative rainfall records, which is indicative of homogeneity of the records used in the study. Examples of the derived mass curves for heterogeneous records that were observed at few locations are shown in Figure 12. In this case more than one line could be fitted to the cumulative rainfall records. The non homogenous records that were included in the study were adjusted using double mass curve analyses. Some description of the single

mass and double mass curve methods were presented in section 3.3.1. Details of the methods are available in many standard climatological references including WMO (1966, 1986, Ogallo 1987).

In general the quality control analyses declared most of the records being used to be of good quality. These data formed the foundation of most the analyses that were undertaken to investigate various specific objectives in this study. The results from delineation of the spatial patterns of the decadal modes over the region are presented in the next section.

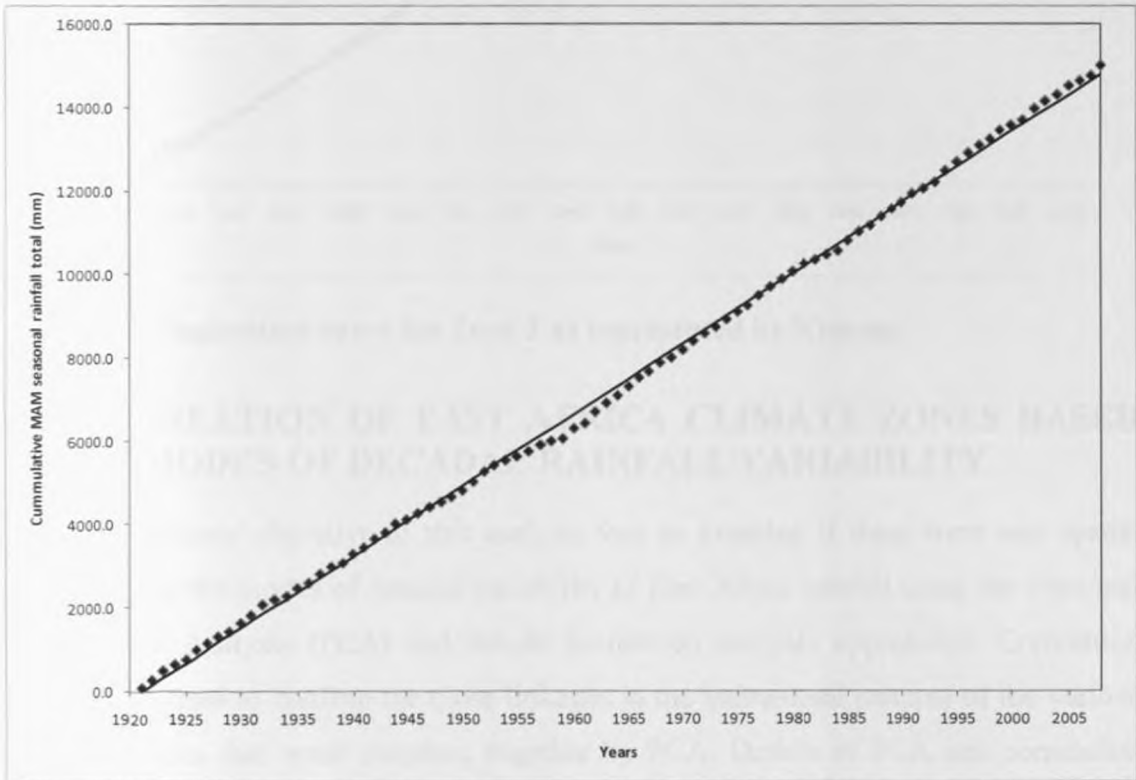


Figure 11: Cumulative March – May (MAM) seasonal rainfall totals over Zone 1

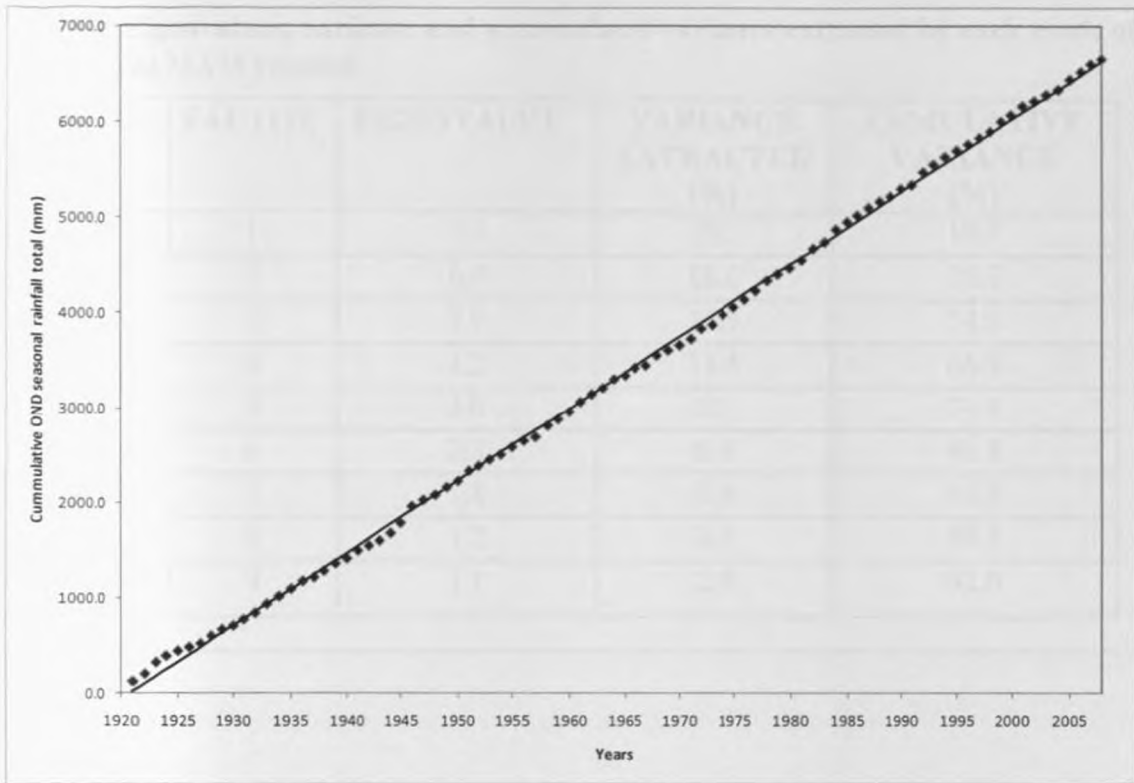


Figure 12: Single mass curve for Zone 2 as represented by Kigoma.

4.2 DELINEATION OF EAST AFRICA CLIMATE ZONES BASED ON MODES OF DECADEAL RAINFALL VARIABILITY

The primary objective of this analysis was to examine if there were any spatial differences in the modes of decadal variability of East Africa rainfall using the Principal Components Analysis (PCA) and simple correlation analysis approaches. Correlation method was used to confirm the close linkages in the interannual patterns of the various rainfall stations that were clustered together by PCA. Details of PCA and correlation methods were presented earlier in sections 3.3.4 and 3.4.1 respectively. It should be noted that the time series data used in various analyses in this study are rainfall records from specific locations that have been filtered with a nine point binomial co-efficient filter to remove all fluctuations less than 9 years. Thus only fluctuations with periods equal to or greater than 10 years are retained for all analyses.

The discussion of the results for the March-May (MAM) rainfall season is however, presented first.

Table 6: Eigenvalues, variance and accumulated variance extracted by each mode of the decadal MAM rainfall

PERIOD	FACTOR	EIGENVALUE	VARIANCE EXTRACTED (%)	CUMULATIVE VARIANCE (%)
MAM	1	7.3	19.7	19.7
	2	6.9	18.6	38.7
	3	5.9	15.9	54.8
	4	4.2	11.4	66.3
	5	3.0	8.1	74.4
	6	2.3	6.4	80.8
	7	1.8	5.0	85.8
	8	1.2	3.3	89.1
	9	1.1	2.9	92.0

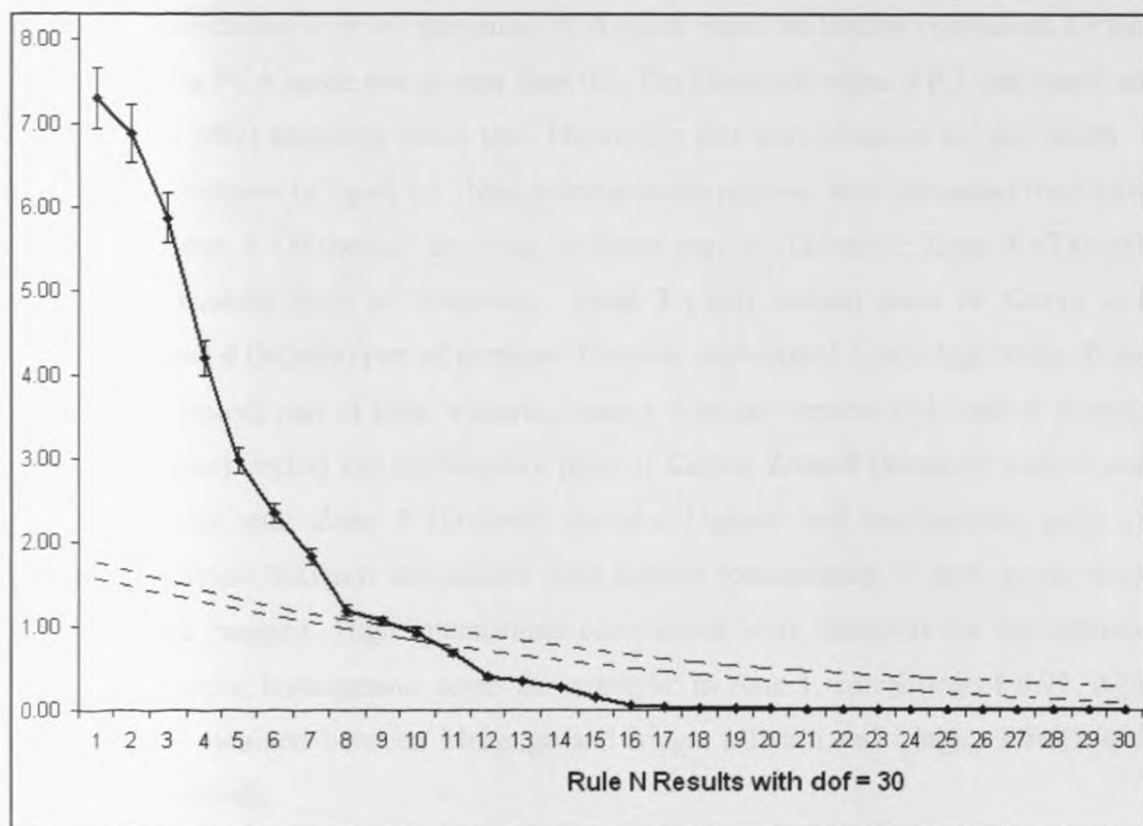


Figure 13: Selection of the dominant PCA for March-May decadal rainfall modes with points above the dotted lines significant at 5% level

Table 6 and Figure 13 give some examples of the results that were obtained from PCA analysis. The results include Scree test; Kaiser's criterion and North et al., (1982)

sampling errors test. All the results indicated that nine PCA modes were significant. These accounted for 92% of total MAM season decadal rainfall variance. The nine PCA modes were subjected to further analyses including orthogonal varimax rotation. The results indicated that the variance accounted for by each of the first four PCA modes were relatively low, each of them accounted for less than 20%. The first four PCA modes accounted for namely 19.7, 18.6, 15.9, and 11.4 % respectively. This may be due to the smoothing of fluctuations less than 9 years using binomial coefficient filter as highlighted under data analysis methodology.

The locations that had high degree of associations with one or a combination of PCA modes 1,2,3,4, etc were clustered together as homogenous locations with similar temporal variability with periods greater than 9 years. A location was considered to have significant association with any particular PCA mode when the loading coefficient for the station onto the PCA mode was greater than 0.3. The threshold value of 0.3 was based on North et al., (1982) sampling errors test. The results that were obtained for the March – May season is shown in figure 14. Nine homogeneous regions were delineated over East Africa i.e. **Zone 1** (Mahenge) covering southern part of Tanzania; **Zone 2** (Tabora) central and western parts of Tanzania; **Zone 3** (Voi) coastal areas of Kenya and Tanzania; **Zone 4** (Mbulu) part of northern Tanzania and central Kenya highlands; **Zone 5** (Musoma) eastern part of Lake Victoria; **Zone 6** (Garissa) eastern highlands of Kenya; **Zone 7** (Moyale) central and northeastern parts of Kenya; **Zone 8** (Mbarara) central and western Uganda and; **Zone 9** (Lodwar) northern Uganda and northwestern parts of Kenya. Correlation between the stations with highest communality in each group were computed and mapped. High interstations correlations were observed for the stations within the specific homogenous zones for example; in zone 1, correlation of 0.91, 0.74 and 0.54 was obtained between Mahenge and Iringa, Mtwara and Iringa, Mbeya and Mtwara respectively.

Twenty two (22) groupings were obtained when homogeneous zones derived for the MAM season using unsmoothed rainfall records for the three countries of the study region were merged (ICPAC, 1999; ICPAC, 2006; Owiti, 2005). Delineation of East Africa region using interannual rainfall records by Ogallo (1981a, 1989) and Indeje

(2000) yielded 12 and 9 zones respectively. The effect of smoothing rainfall records is observed to merge some groupings with similar decadal rainfall characteristics into same zones and therefore zones in the current study are significantly different from the patterns that have been obtained from past studies by Ogallo (1989); Mutua et al., (1999); ICPAC (1999); Indeje (2000) and ICPAC (2006) among others. When all records are used, the first few PCA modes explain very high percentages of variance. This may be associated with existence of dominant recurrences of variability modes of about 2 years (QBO modes), 3-7 years (IOD and ENSO modes), among others (Rasmusson *et al.*, 1981; Ogallo, 1977; 1994; Indeje, 2000; and Mutemi, 2003). High frequency of variability is associated with regional factors (systems) that are also varied (Ogallo, 1977, 1994; Indeje, 2000).

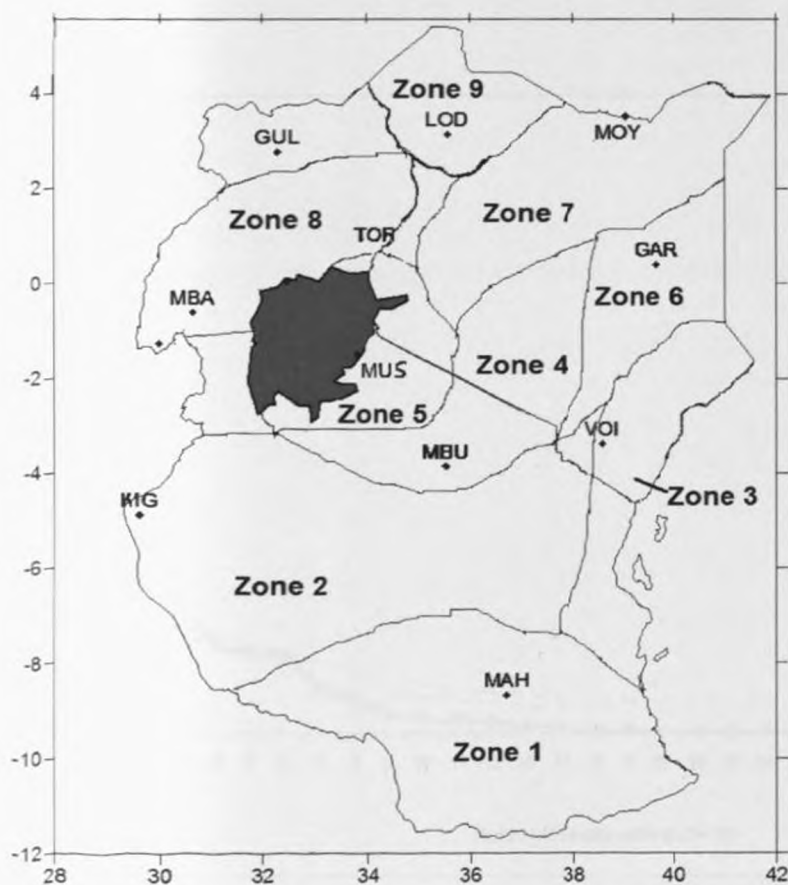


Figure 14: Homogeneous climatic zones over East Africa obtained from combined PCA and simple correlation analyses using the Decadal rainfall variability (March-May).

Table 7: Eigenvalues, variance and accumulated variance extracted by each mode of the decadal OND rainfall

PERIOD	FACTORS	EIGENVALUE	VARIANCE EXTRACTED (%)	CUMULATIVE VARIANCE (%)
OND	1	15.87	42.9	42.9
	2	5.25	14.2	57.1
	3	3.87	10.5	67.6
	4	2.67	7.2	74.8
	5	2.40	6.5	81.3
	6	2.32	6.3	87.6
	7	1.38	3.7	91.3

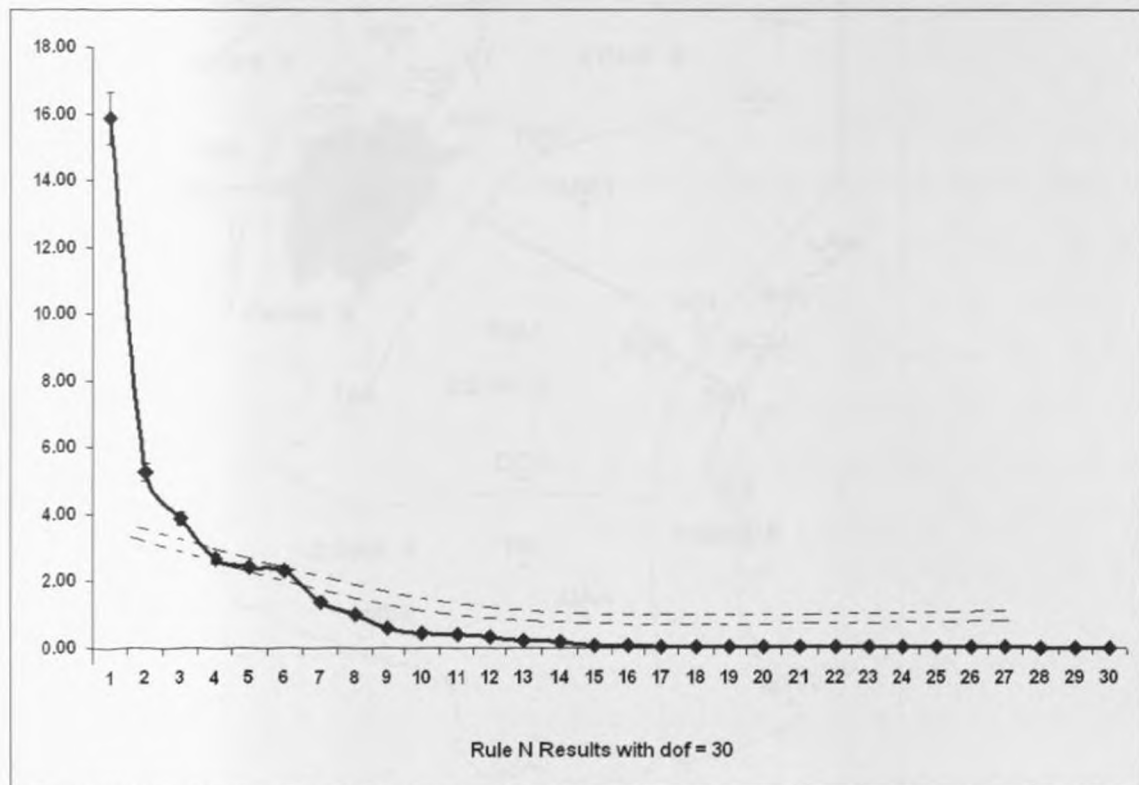


Figure 15: Selection of the dominant PCA for October - December decadal rainfall modes with points above the dotted lines significant at the 5% level

The results for the October-December (OND) season are presented in table 7 and figure 15. Table 7 and Figure 15 show eigenvalues, variance and accumulated variance

extracted by each PCA mode of decadal variability for the OND rainfall season. The results indicate that seven PCA modes, accounting for 91.3% of the total OND smoothed rainfall variance were significant. Unlike the MAM season, the first PCA mode for rainfall variability with fluctuation greater than or equal to 9 years accounted for very large percentage of variance (42.9 %). The second and third PCA modes accounted for 14.2 and 10.5% respectively. The spatial coherence of OND rainfall has been presented by many authors (Agumba, 1985; Ogallo, 1989; Hastenrath et al., 1993; Indeje, 2000; Indeje et al., 2000; Black et al., 2003; Clark et al., 2003; Mutemi, 2003; Schreck and Semazzi, 2004; Behera et al., 2005; Anyah et al., 2006).

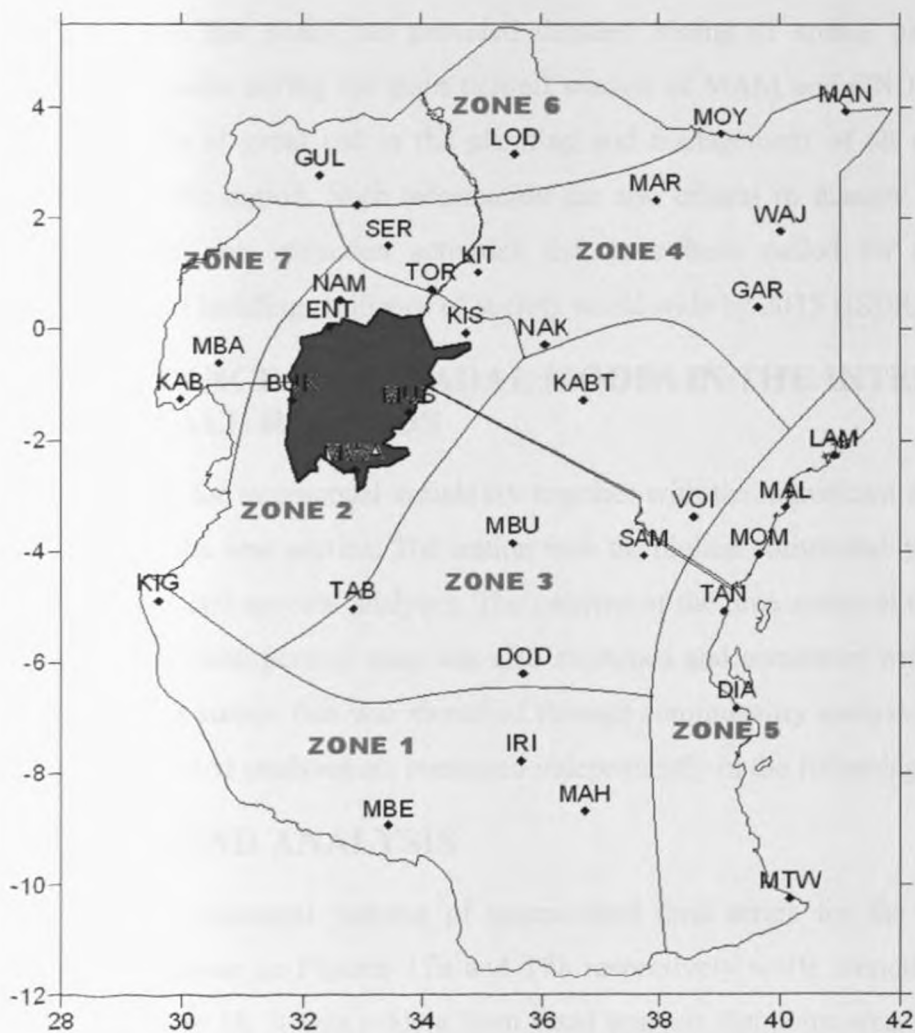


Figure 16: Homogeneous climatic zones over East Africa obtained from combined PCA and simple correlation analyses using the October-December Decadal rainfall variability

The spatial patterns of the dominant PCA modes were used to group together stations with common characteristics into homogeneous regions. The PCA statistics (Communality) at each individual region was therefore used to identify a representative station in each region for further detailed analyses (Gregory, 1975; Ogallo, 1988, 1989; Basalirwa, 1991; Indeje, 2000; Okoola, 1996; ICPAC, 1999; among many others). For example correlation between the stations with highest communality in every cluster was computed and this helped in the mapping of stations into zones. Correlation coefficients values as high as 0.94 were observed between Dares Salaam International Airport (DIA) and stations within zone 5.

Overall, this study has provided detailed zoning of spatial patterns of decadal variability modes during the main rainfall seasons of MAM and OND over East Africa, which can be of great use in the planning and management of all rainfall dependent activities in the region. Such information are also critical in disaster management, and other climate risk reduction activities that have been called for under the Hyogo Framework of building resilience of society world wide by 2015 (ISDR, 2005).

4.3 EXISTANCE OF DECADAL MODES IN THE INTERANNUAL RAINFALL RECORDS

Results for interannual variability together with the significant decadal modes are presented in the next section. The station with the highest communality in each zone was used in trend and spectral analyses. The patterns of the time series of the dominant PCA mode for the homogenous zone was also examined and compared with results from the representative station that was identified through communality analysis. The results from trend and spectral analyses are presented independently in the following two sections.

4.3.1 TREND ANALYSIS

The interannual patterns of unsmoothed time series for the MAM and OND seasons are given in Figures 17a and 17b respectively while smoothed time series is given in Figure 18. It was evident from trend analysis that some trends were discernible in some of the smoothed and unsmoothed times series. Trends analyses of unsmoothed rainfall have been presented by many authors (Landsberg, 1975; Bunting et al., 1975;

Tyson et al., 1975, 2002; Ogallo, 1977, 1980b, 1981b; Nicholson, 2000b and Omondi, 2005).

The unsmoothed records show high recurrences of floods and droughts with periods less than 9 years (Figure 17a and 17b). The unsmoothed records show that too much / too little rainfall received in one or two years determines the general trend of the decadal mean rainfall. Examples are the 1997 / 1998 El Niño related heavy rains and 1961 strong positive phase of Indian Ocean Dipole (IOD) related heavy rains that made 1990s and 1960s wet decades while the 1999 / 2000 La Niña related droughts made 2000 be a dry decade in most locations. Many recent studies have shown that within timescales of less than 9 years, the most common recurrences are of periods 2-3 years, and 3-7 years. These have been associated with Quasi Biannual Oscillation, Indian Ocean Dipole mode and El Niño Southern Oscillations systems (Ogallo, 1982, 1988; Nicholson and Entekhabi, 1986; Indeje and Semazzi, 2000; Collimore, 2003; Claud and Terry 2007; Ropelewski and Halpert, 1987; Ogallo and Suleiman, 1987; Wallace et al., 1998; Camberlin et al., 2004, Yamaguchi and Noda, 2005; Owiti, 2007).

This study, however, focused on decadal variability and thus, the long term trends brought about by waves less than ten years have been removed before subjecting the smoothed time series to trend and spectral analyses. Figure 18 shows some patterns of the decadal variability modes as were discernible from the smoothed time series but with trends for MAM season. It has been noted that after the removal of the long term trends and the observed rainfall records passed through a low-pass filter using a 9-point binomial coefficient filter in all seasons, decadal modes were clearly discernible. Various statistical tests were applied in order to test the statistical significance of the observed modes of decadal variability. Therefore to isolate decadal trend mode in interannual rainfall record, it is important to filter out noise in the data. Examples of decadal rainfall variations for selected regions are shown in Figures 19 and 20 for zones 1 to 4 for smoothed data where trends have been removed and data smoothed by a nine-point binomial coefficient filter to remove all fluctuations with less than 9 years.

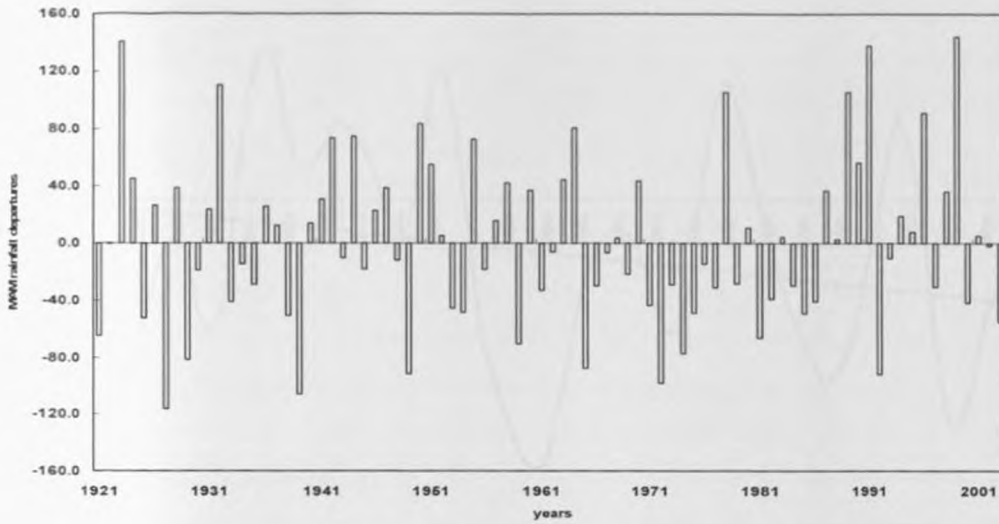


Figure 17a: Unsmoothed Interannual rainfall patterns for March-May for zone 10

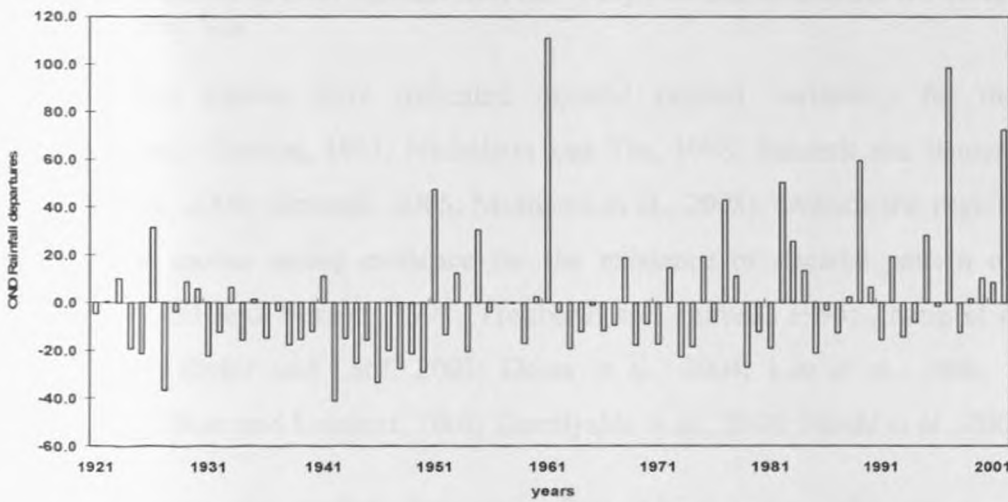


Figure 17b: Unsmoothed Interannual rainfall patterns for October-December for zone 4

It is evident that although wet and dry decades were recurrent, and sometimes extend over large areas, there were very few decades when floods or drought covered the whole of East Africa region except for the wet decade of 1961-70 during the OND season. This is due to the modification of climate by the regional systems that include the existence of the large inland lakes and complex topographical features that significantly modify large scale circulations over the region (e.g Mukabana and Peilke, 1996; Anyah et al., 2006, among others).

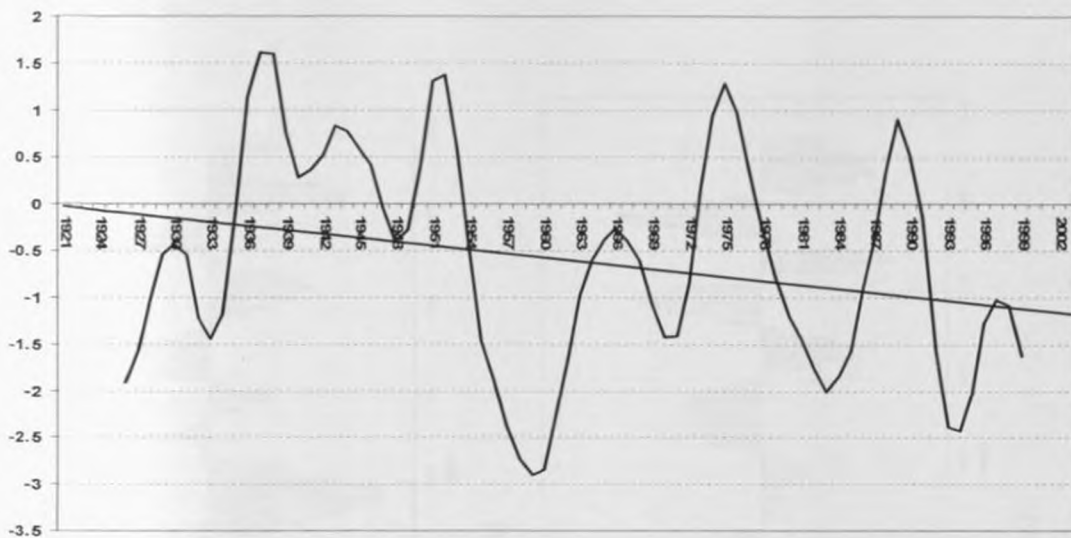
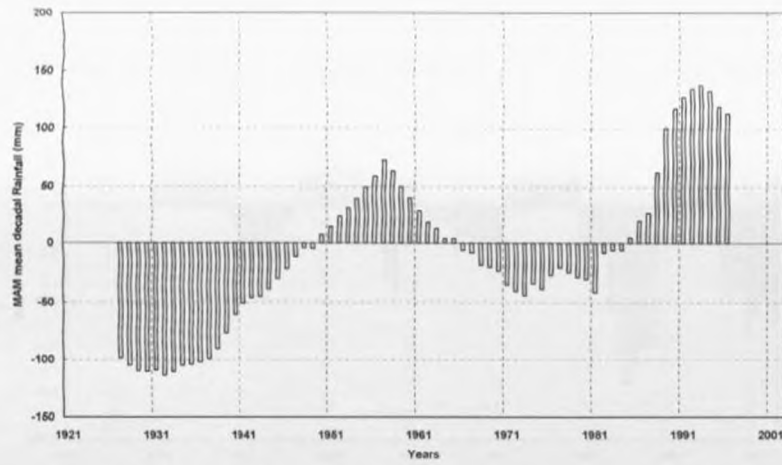


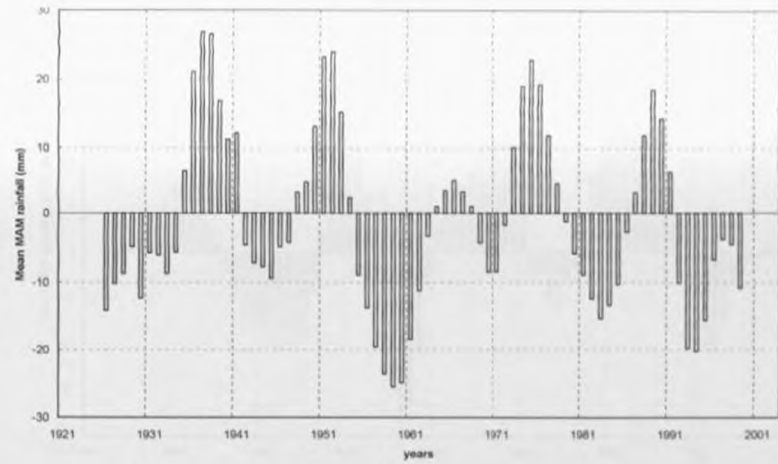
Figure 18: Smoothed inter-annual March – May rainfall anomalies for zone 3 as represented by Voi

Several studies have indicated decadal rainfall variability for the region (Nicholson and Chervin, 1983; Nicholson and Yin, 1998; Schreck and Semazzi, 2004; Bowden et al., 2004; Omondi, 2005; Muthama et al., 2008). Outside the region, various studies have shown strong evidence for the existence of decadal pattern of climate variability (Latif and Barnett, 1994; Trenberth and Hurrell, 1994; Zhang et al., 1997; Mehta, 1995; Bader and Latif, 2003; Deser et al., 2004; Lee et al., 2006; CLIVAR VACS, 2007; Boer and Lambert, 2008; Keenlyside et al., 2008; Meehl et al., 2009).

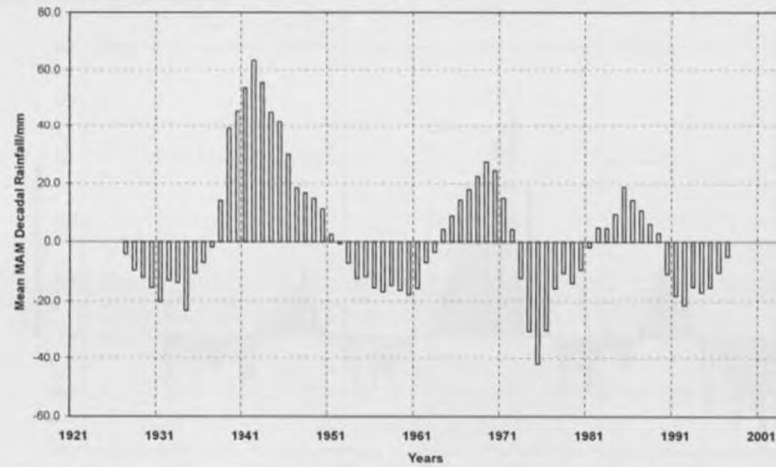
However, the studies done over East Africa region, did not examine the complexity of decadal variability within years and seasons. This study, therefore, has for the first time provided detailed empirical and dynamical investigation of climate factors and variability at time and space scales that can contribute not only to climate change adaptation studies, but also for medium and long-term development plans for the region. Some differences in the impacts of the decadal variability at various locations over East Africa reflect strong influence of the complex regional climate systems/forcing on fluctuations of the background global circulation systems. This has been shown in the observed teleconnection between regional climate extremes and global circulations induced by IOD, ENSO, QBO and MJO (Ogallo, 1988; Hastenrath, 1990; Indeje *et al.*, 2000; Mutemi, 2003; Repelli and Nobre, 2004; Owiti, 2005; Omeny et al., 2009).



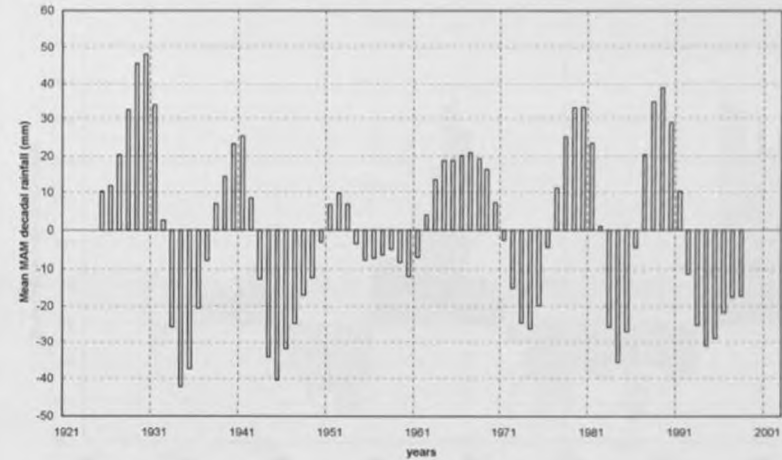
(i) Zone 1 (Mahenge)



(ii) Zone 2 (Tabora)

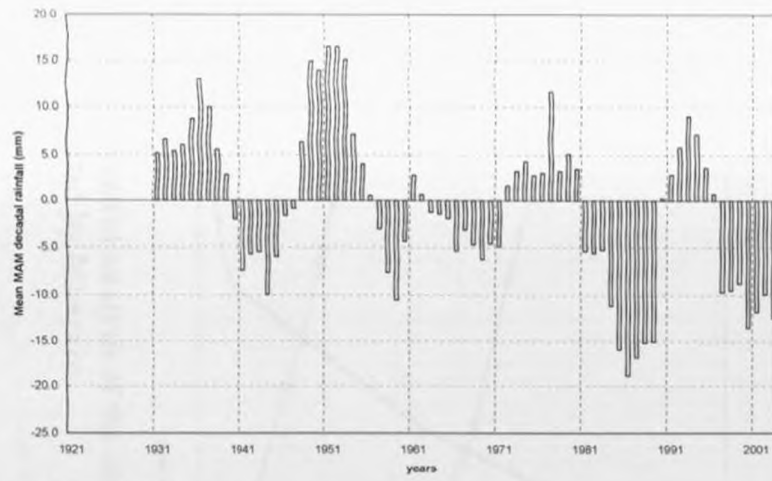


(iii) Zone 3 (Mombasa)

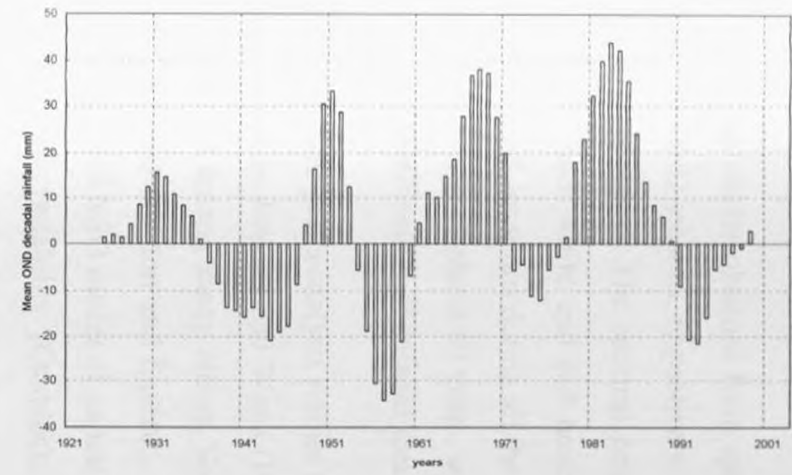


(iv) Zone 4 (Kabete)

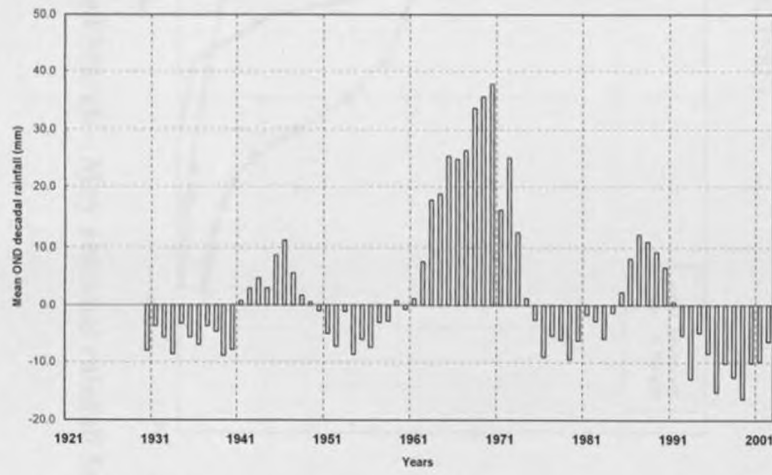
Figure 19: Graphical plots of March -May decadal rainfall variability for the representative stations over East Africa region



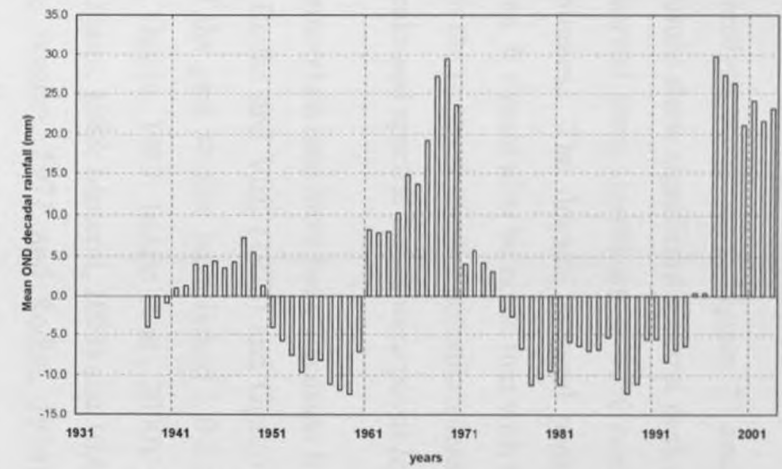
(i) Zone 1 (Iringa)



(ii) Zone 2 (Bukoba)



(iii) Zone 3 (Mbulu)



(iv) Zone 4 (Wajir)

Figure 20: Graphical plots of October - December decadal rainfall variability for the representative stations over East Africa region

4.3.2 SPECTRAL ANALYSIS

Some results obtained from spectral analysis are given in Figures 21 and 22 for MAM and OND seasons, respectively. The results show significant spectral peaks within decadal time scales. The spectral peaks observed were significant at 95% confidence level using both white and red noise hypotheses. The decadal spectral peaks were dominant at all locations during all the seasons. It should also be noted that with average length of records of about 80 years, and with the removal of all fluctuations less than 9 years, the identification of decadal spectral peaks and spectral bands were possible.

Spectral peaks analysis studies for unsmoothed data have been discussed by many authors such as Jenkins and Watts (1968); Rodhe and Virji (1976) and Ogallo (1977, 1980b, 1982) among many others. Some of the past studies have linked 2.0-3.3 years cycles to QBO (Holton and Lindzen, 1972; Ogallo, 1982; Indeje et al., 2000), 5.0-7.5 years cycles to ENSO modes of variability (Ogallo, 1988; Mutemi, 2003) and 10.0 – 11.0 years to solar variability (Craddock, 1968; Wagner, 1971 and Rodhe, 1974). Such fluctuations have also been indicated in the rainfall records from other parts of Africa (Tyson et al., 1975; Nicholson and Entekhabi, 1986).

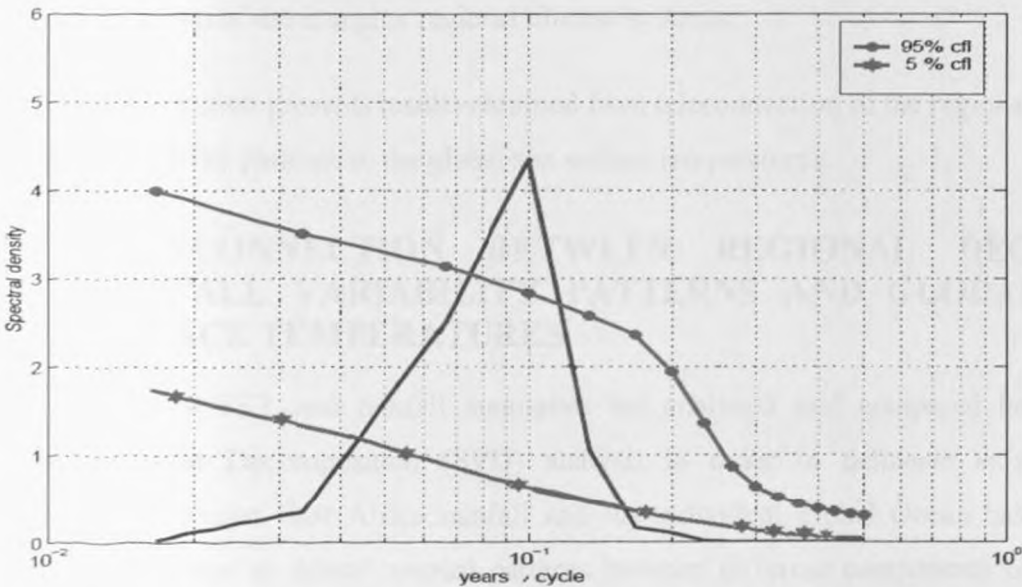


Figure 21: Spectral analysis of the smoothed March – May seasonal rainfall for zone 8 as represented by Mbarara

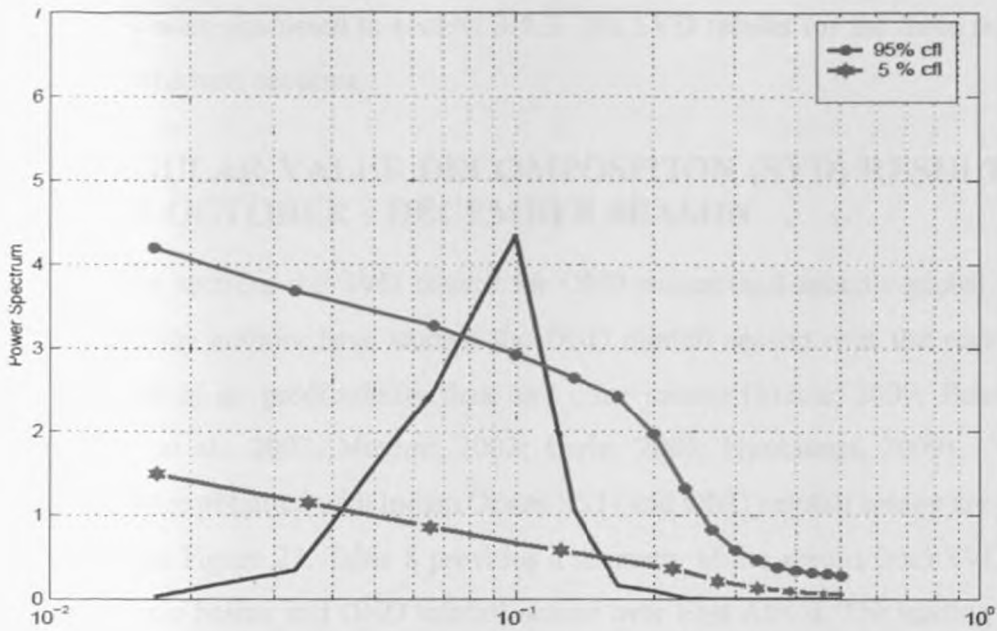


Figure 22: Spectral analysis of the smoothed October – December seasonal rainfall for zone 6 as represented by Gulu

The study has thus demonstrated the dominance of decadal variability in rainfall patterns over East Africa. There are, however, significant differences in the amplitudes and spectral bands of the spectral peaks from the various regions, which signified some differences in the impacts of the decadal variability of various parts of East Africa due to the modification of the complex regional climate systems.

Next section presents results obtained from teleconnection of the regional decadal rainfall variability patterns to the global sea surface temperatures.

4.4 TELECONNECTION BETWEEN REGIONAL DECADAL RAINFALL VARIABILITY PATTERNS AND GLOBAL SEA SURFACE TEMPERATURES

Decadal SST and rainfall anomalies are analyzed and compared here using Singular Value Decomposition (SVD) analysis in order to delineate existence of covariance amongst East Africa rainfall and the individual global Ocean basin SSTs. SVD can be used to detect coupled patterns between different components of climate systems. In this section, results for coupled patterns between modes of decadal rainfall variability and specific oceans are discussed. Details of SVD analysis method employed

in this study were discussed in section 3.4.3. The SVD results for the three seasons are presented in the next sections.

4.4.1 SINGULAR VALUE DECOMPOSITION (SVD) RESULTS FOR THE OCTOBER – DECEMBER SEASON

In this section, the SVD results for OND season and specific global SSTs are discussed. Many authors have studied the OND rainfall season over the region due to high potential of its predictability than any other season (Indeje, 2000; Behera et al., 2005; Black et al., 2003; Mutemi, 2003; Owiti, 2005; Nyakwada, 2009). The SVD results that were obtained with Indian Ocean SSTs and OND rainfall season are presented in Table 8 and Figure 23. Table 8 provides a summary of the results from SVD analysis for all the three basins and OND rainfall season over East Africa. The leading modes in each case were chosen for discussion in this section.

Table 8: Summary of some statistics from SVD analysis for specific Ocean SSTs and decadal OND rainfall

Oceans	OND Mode	Square Covariance fraction (SCF)	% of total mode covariance	Cumulative % covariance	Correlation coefficient (r)
INDIAN	1	26.7	65.2	65.2	0.99
	2	6.8	16.5	81.7	0.98
	3	3.6	8.8	90.5	0.94
ATLANTIC	1	18.7	47.8	47.8	0.97
	2	9.0	23.1	71.0	0.94
	3	4.9	12.5	83.5	0.76
PACIFIC	1	40.0	39.2	39.2	0.99
	2	28.0	27.5	66.7	0.96
	3	13.8	13.6	80.3	0.94

r is the correlation coefficient between the expansion coefficient of SSTs and OND rainfall modes

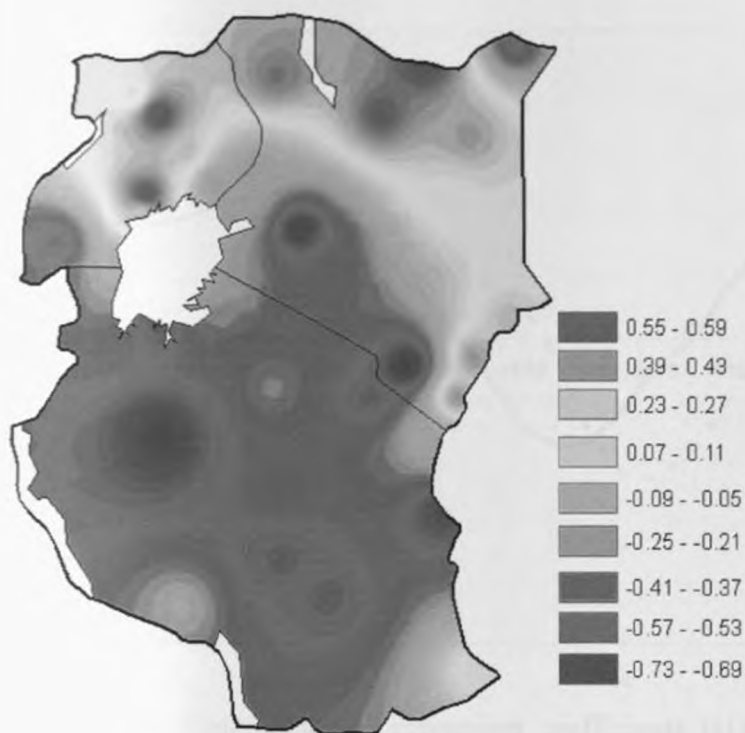
Indian Ocean is the nearest ocean to East Africa and the eastern coast of the region is bounded by the ocean. The ocean is therefore the major source of the moisture

for inland rainfall. Previous studies indicated that the SSTs over the Indian Ocean reach peak relationships with rainfall in this period (Mutai, 2003).

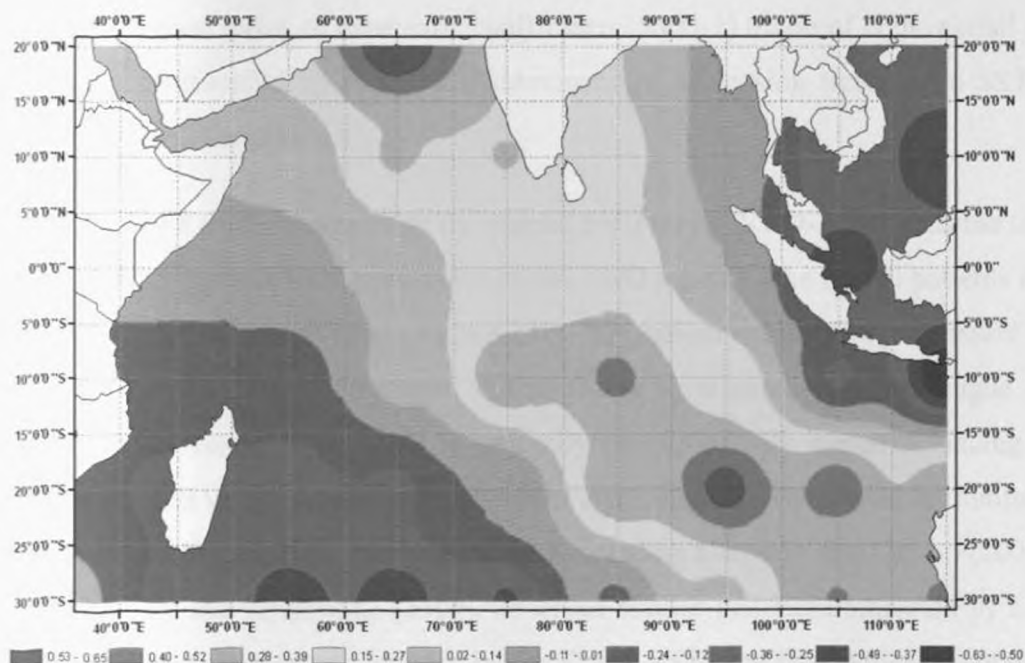
Indian Ocean SST and OND seasonal rainfall SVD modes accounted for 90.5% of the total square covariance. The first, second and third SVD modes accounted for 65.2, 16.5, and 8.8 % of the total square covariance of OND decadal rainfall variability. The first and second modes together explained most of the ocean-rainfall covariance (82%) and therefore the covariance of remaining SVD modes are not subject of discussion in this section.

The first SVD mode (SVD-1) between OND rainfall and Indian Ocean SST fields is characterized by negative loading patterns of rainfall over the southern sector and positive loading over the northern sector of the region (Figure 23a). The corresponding pattern in the Indian Ocean basin shows a dipole-like pattern with positive loading centred around eastern Indian Ocean (25°S-10°S, 80°E -110°E) and negative loadings over the western Indian Ocean (20°S-30°S, 50°E-70°E) (Figure 23b). This mode explains 65% of the total coupling covariance between Indian Ocean SST and OND rainfall (Table 9).

This mode seems to represent the mean seasonal patterns of SST over the ocean (Behera et al. 2005; Schreck and Semazzi 2004; Terray and Dominiak 2005; Tozuka et al. 2007). Such patterns over the Indian Ocean depicted by SVD mode 1, have been observed in some previous studies but using PCA and correlation analyses between Indian Ocean SST and the short rainfall season over East Africa (Behera *et al.*, 2005, 2006; Beltrando and Cadet, 1990; Nyakwada, 2009).



(a) OND rainfall Mode 1



(b) Indian Ocean SST Mode 1

Figure 23: Spatial patterns (S1) of the first SVD mode for (a) October-December rainfall (b) Indian Ocean SST presented as homogeneous correlation maps.

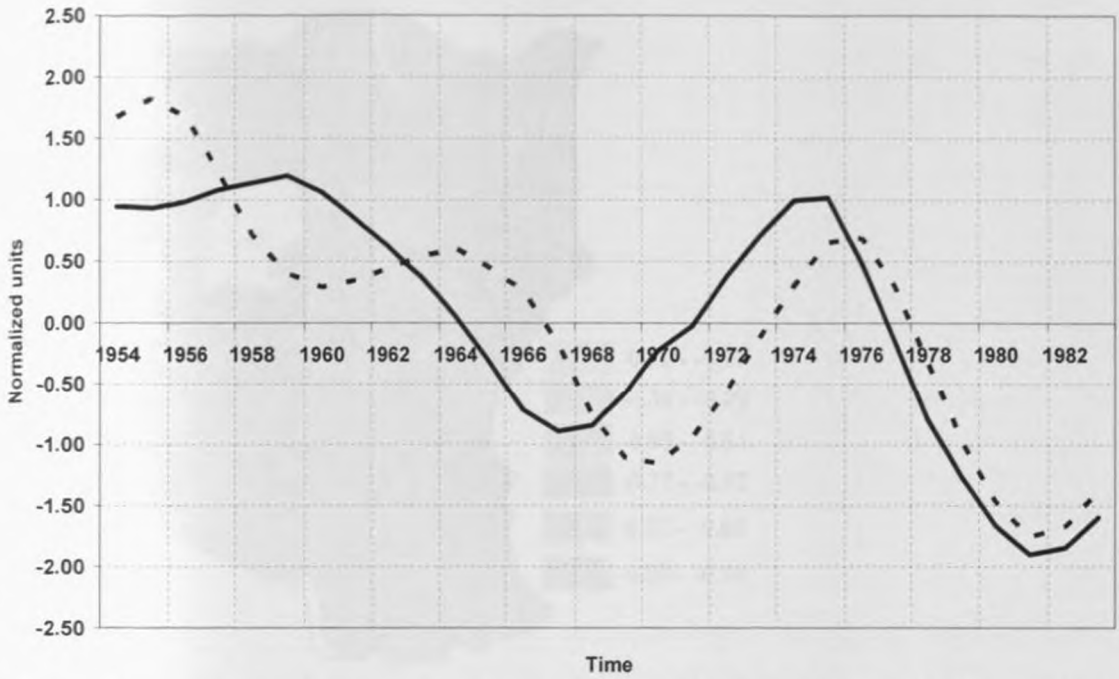
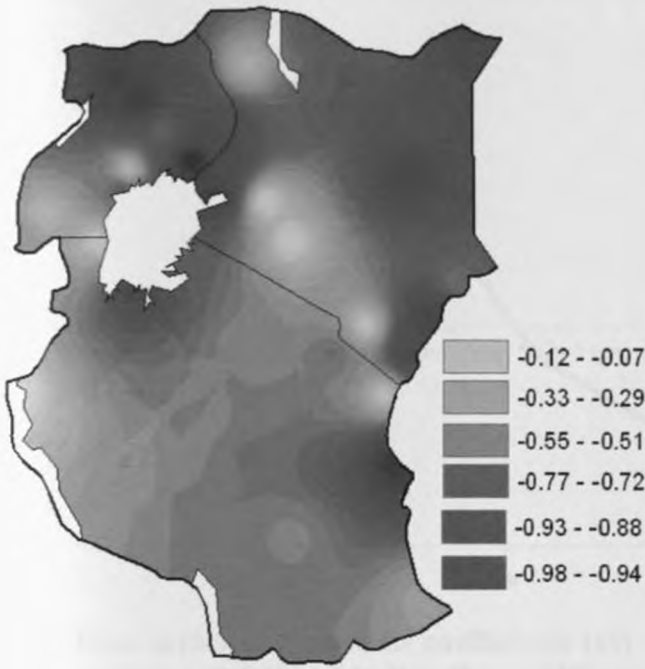


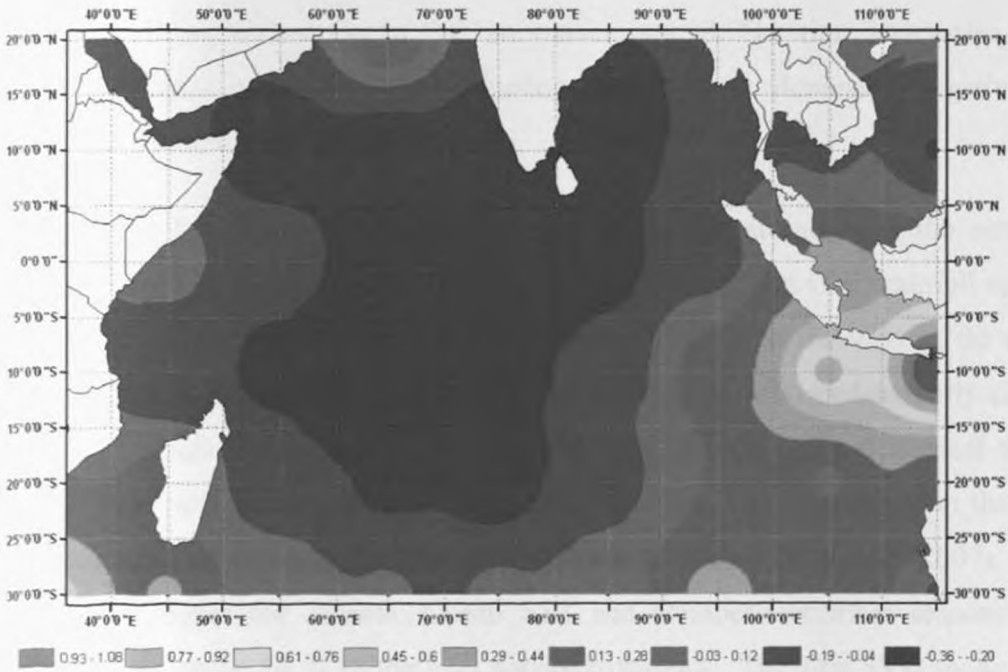
Figure 23c: Time series of expansion coefficients (s1) of the first SVD mode for October - December rainfall (bold lines) and Indian Ocean SST (dotted lines) anomalies.

The time series of expansion coefficients (SVD-1) mode of both rainfall and SST anomalies represented by Figure 23c demonstrates decreasing trends with SST leading decadal rainfall variations.

Table 8 further shows that the second SVD mode (SVD-2) between the two fields explains 16.5% of the total covariance of the OND rainfall. The spatial patterns of Indian Ocean SVD mode 2 is shown in Figure 24b. This pattern exhibits large coherent negative loading over the central equatorial Indian Ocean with small positive tongue over the Indo-Pacific Oceans. This signal is generally associated with negative loading patterns over most parts of the region especially over areas that receive substantial rainfall during OND season (Figure 24a). Previous authors including Harrison and Carson (2007); Ihara *et al.*, (2008); and Nyakwada (2009), observed similar patterns dominated by SVD-2 in their studies on correlations between Indian Ocean SSTs and East African rainfall.



(a) OND rainfall Mode 2



(b) SST Mode 2

Figure 24: Spatial patterns (S2) of the second SVD mode for (a) October-December rainfall (b) Indian Ocean SST presented as homogeneous correlation maps.

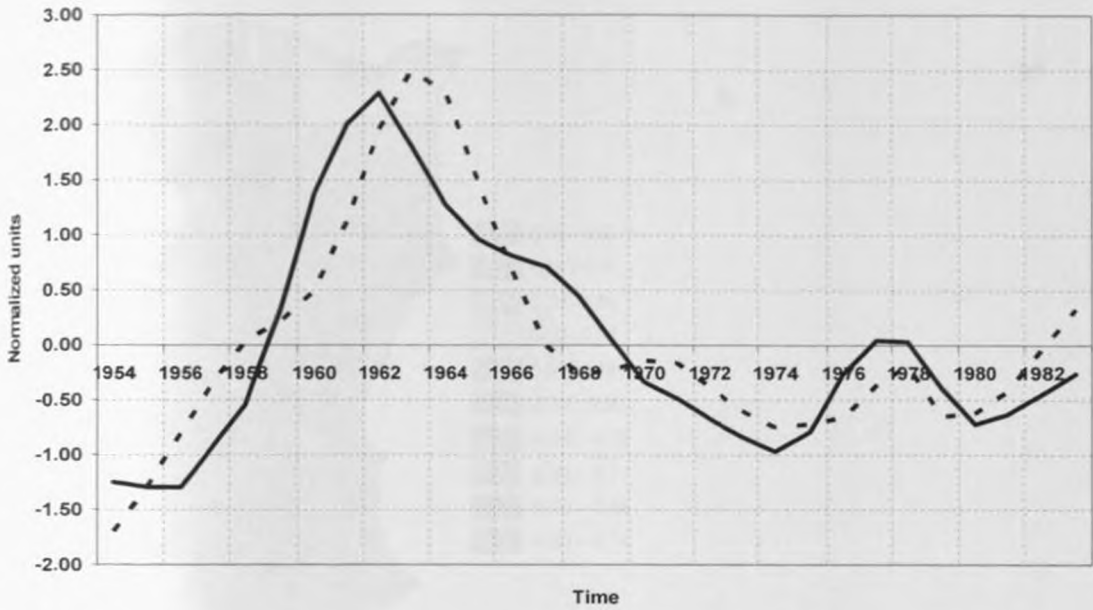
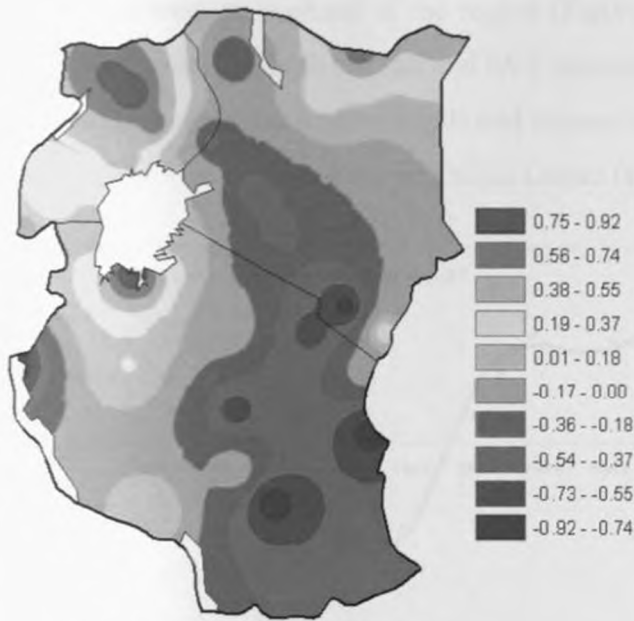


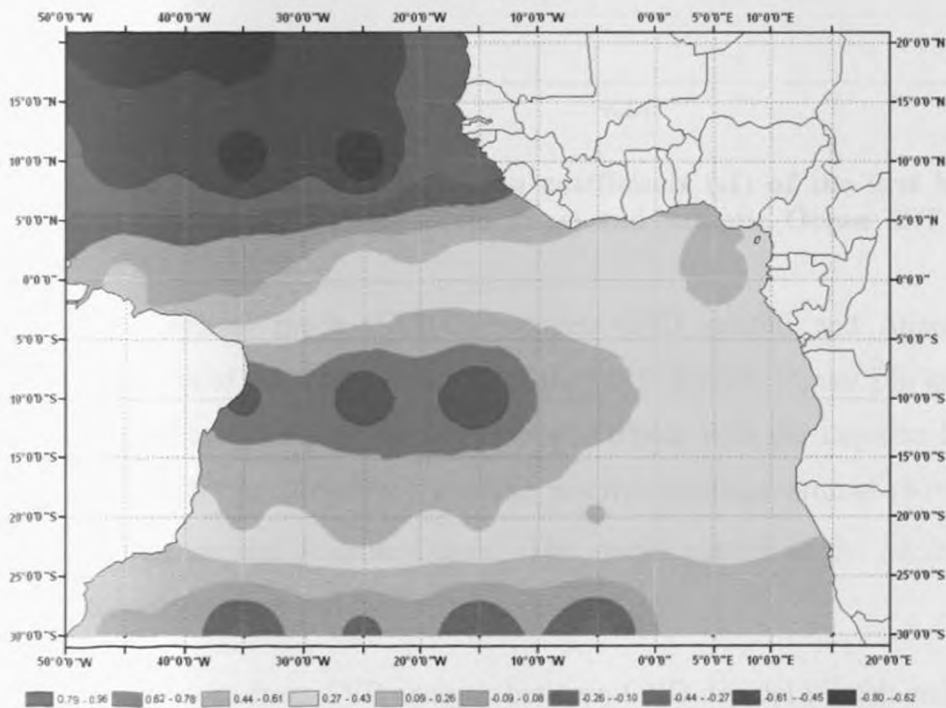
Figure 24c: Time series of expansion coefficients (s_2) of the second SVD mode for October - December rainfall and Indian Ocean SST anomalies.

The time series of expansion coefficients of mode 2 is presented in Figure 24c. The correlation between the expansion coefficients of the second SVD mode (SVD-2) for OND rainfall and Indian Ocean SST anomalies is 0.98. The time series also indicates stronger decadal variability signals during 1960s; while depressed negative phases between 1970s and early 1980s.

Table 8 together with figures 25 and 26 provide summary of the results from Singular Value Decomposition (SVD) analysis for East Africa OND rainfall season and the Atlantic Ocean SSTs. Note that the Atlantic Ocean is to the west of the region of study. Moisture influx from the ocean is associated with enhanced westerly circulation that also favours the incursions of moisture from the always wet tropical forests of Congo, Zaire and other central African countries. The SST variability in the Atlantic Ocean reaches its maximum in the period January to May (Wu et al. 2007). The first three SVD modes for Atlantic Ocean SST and October-December seasonal rainfall accounted for about 84 % of the total square covariance. The first SVD mode (SVD-1) between OND rainfall and SST fields (47.8%) is characterized by a meridional dipole like pattern with negative loadings over the northern equatorial Atlantic Ocean and positive loadings over the southern equatorial Atlantic basin (Figure 25b).



(a) OND rainfall Mode 1



(b) SST Mode 1

Figure 25: Spatial patterns (S1) of the first SVD mode for (a) October-December rainfall (b) Atlantic SST presented as homogeneous correlation maps

The OND rainfall component of this mode is characterised by SE – NW dipole pattern with negative loadings over the south-eastern sub-sector while positive loading

over north-western segment of the region (Figure 25a). The time series of expansion of SVD coefficients of both rainfall and SST anomalies has a correlation coefficient of 0.97 (Figure 25c) also shows some trends and enhancement of the decadal amplitudes in some years just as was observed for the Indian Ocean (Figure 24c).

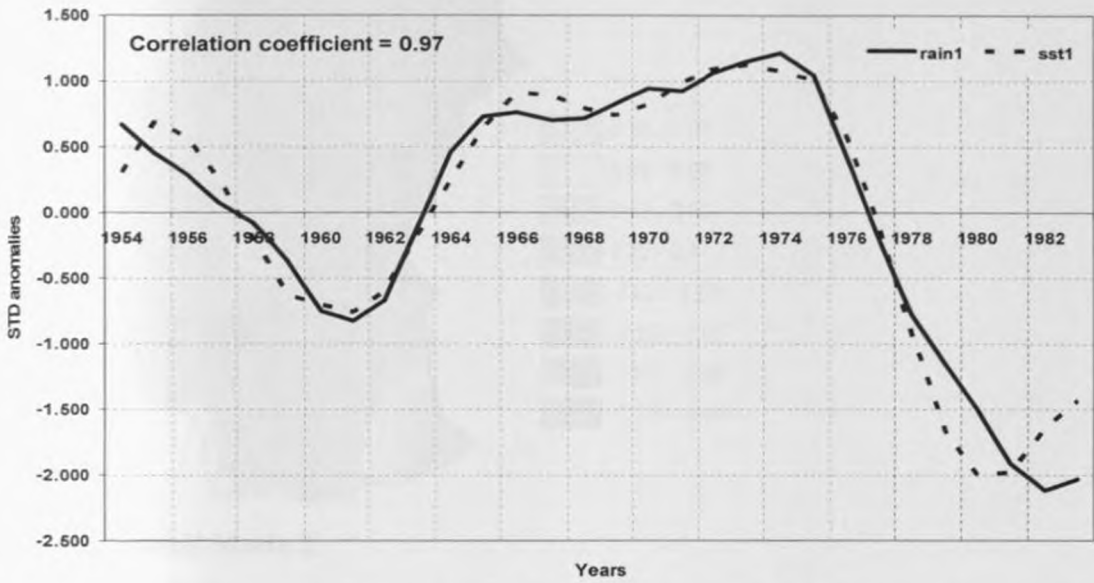
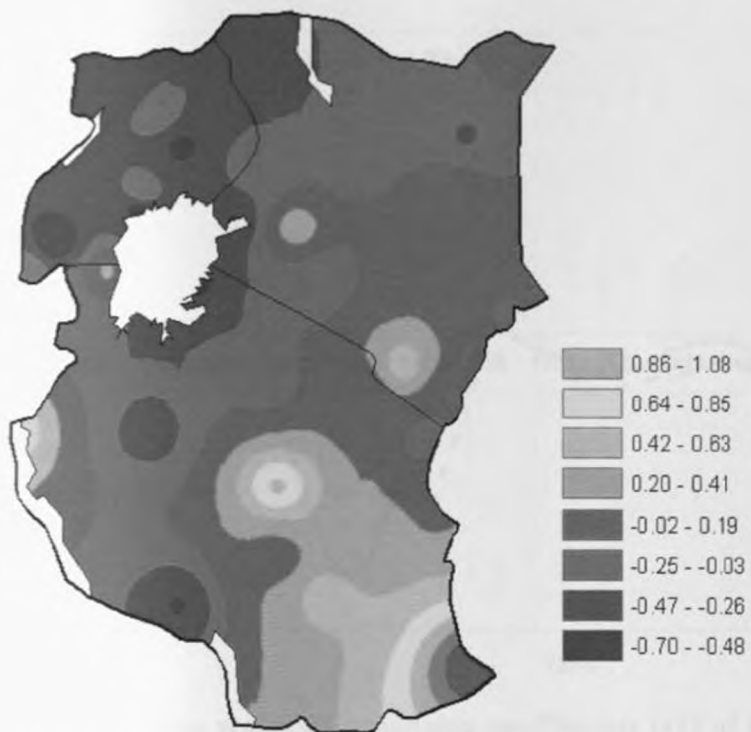


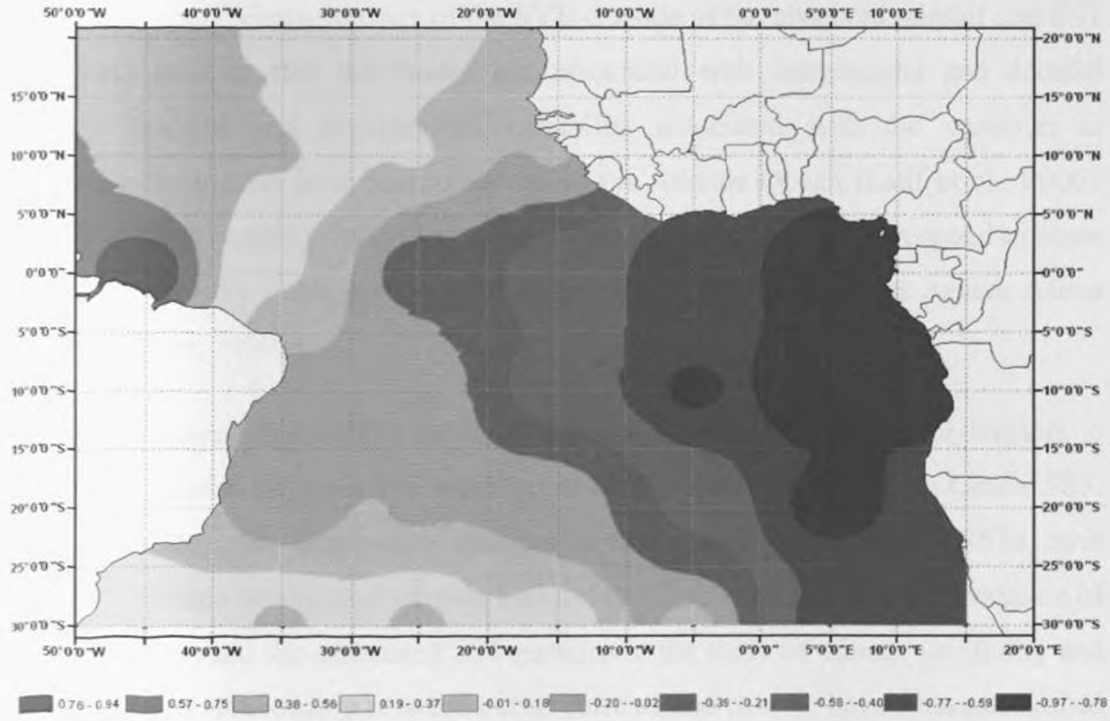
Figure 25c: Time series of expansion coefficients (s1) of the first SVD mode for October - December rainfall (bold lines) and Atlantic Ocean SST (dotted lines) anomalies.

The second mode (SVD-2) between OND rainfall and Atlantic SST fields explains 23.1% of the total covariance of the OND rainfall. Figure 26b indicates that the SVD-2 mode represents an inter-hemispheric dipole with the negative loading centred around (5°W-15°E, 20°S-5°N,) and the positive loadings around (50°W-40°W, 2°S-10°N) of the tropical Atlantic Ocean. The spatial pattern of the rainfall seems to be opposite to those observed for SVD-1mode.

The results from SVD analysis between OND decadal rainfall and Atlantic SSTs has shown that a flip in the interhemispheric loading patterns in the Ocean causes corresponding flip in the spatial and temporal regional rainfall loading patterns. When the loading pattern in the Atlantic Ocean is positive in the north and negative in the south, the regional rainfall pattern is associated with negative loading in the northern sector and positive loading in the southern sector and vice versa. Similar change takes place in the time series expansion coefficients of the two fields.



(a) OND rainfall Mode 2



(b) SST Mode 2

Figure 26: Spatial patterns (S2) of the second SVD mode for (a) October-December rainfall (b) Atlantic SST presented as homogeneous correlation maps

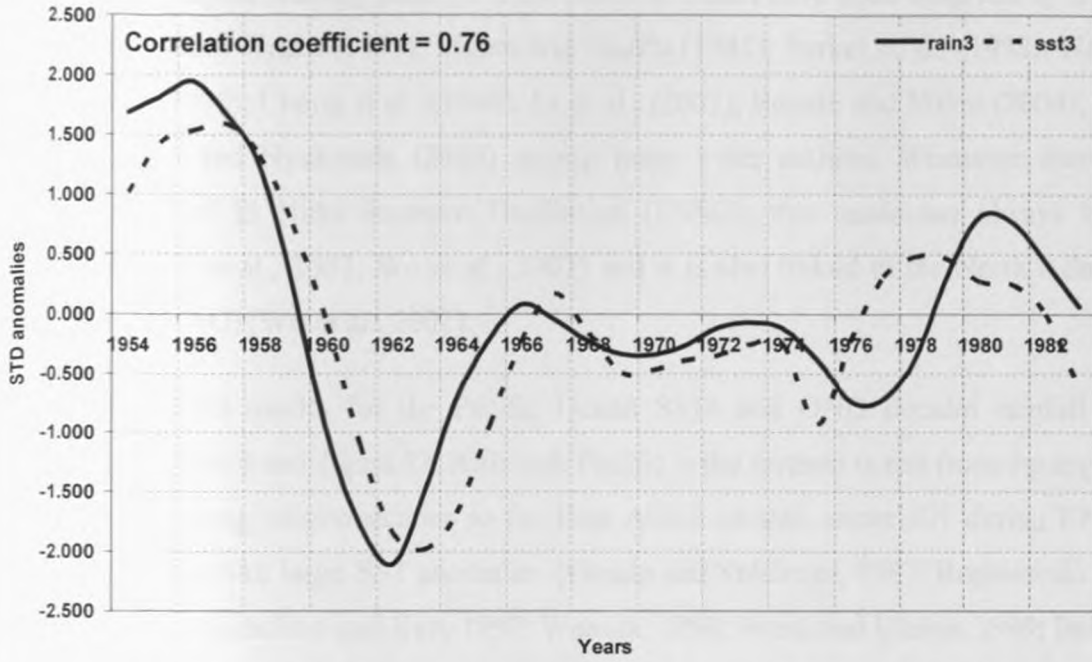


Figure 26c: Time series of expansion coefficients (s2) of the second SVD mode for October - December rainfall (bold lines) and Atlantic Ocean SST (dotted lines)

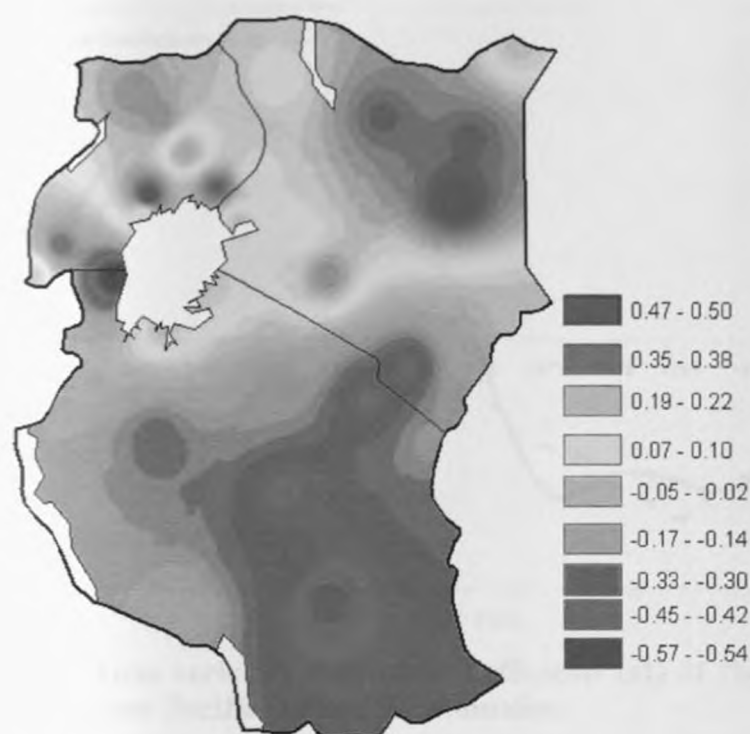
The temporal characteristics of the SVD-2 mode of the observed rainfall and SST (Figure 26c) indicate that the modes are associated with interdecadal and decadal variability. Decadal and multidecadal variability associated with the variation of thermohaline circulation have been observed in the Atlantic Ocean (Latif et al., 2006). The years of large positive / negative values of the time coefficients correspond to some of the major wet / dry years over parts of central and eastern parts of the eastern Africa region (Nicholson, 2000b).

It is observed that SVD-1 mode of Atlantic Ocean SST has similar impacts to OND decadal rainfall (Figures 23a and 25a) as SVD-1 mode of the Indian Ocean SST. This suggests that the large scale changes in the global ocean basins SSTs have significant influence on regional climate variability. This emphasizes the importance of the ocean currents and the associated SST patterns in the study of climate variability and prediction. Strong relationship between ocean currents and climate have been established to be the major influence of regional climates (Valsala and Ikeda, 2007; Cai and Cowan, 2007; Keller et al., 2007).

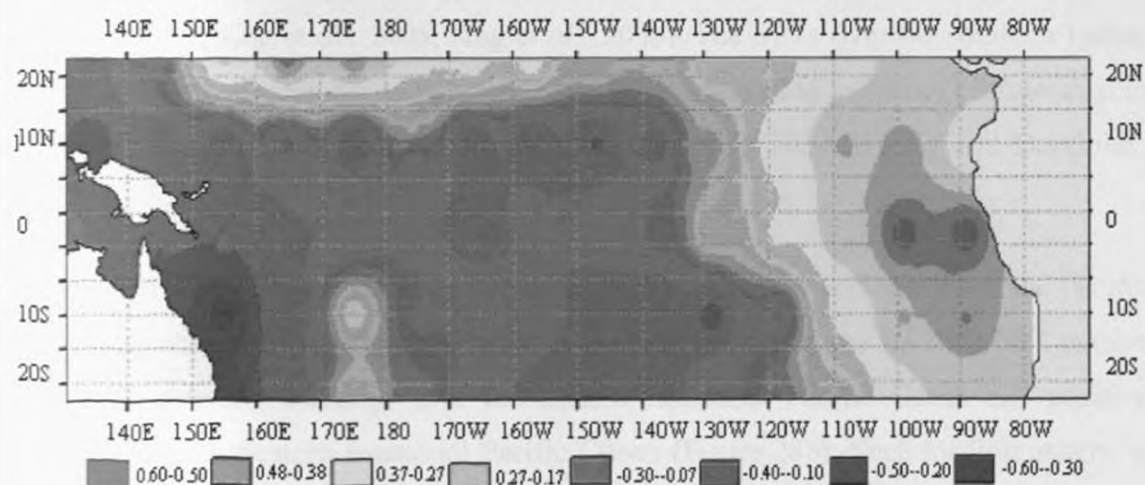
Such Dipole loading patterns in the Atlantic Ocean have been observed by many authors including Weare (1977); Moura and Shukla (1981); Parker et al., (1988); Nobre and Shukla (1996); Chang et al., (1998); Li et al., (2007); Repelli and Nobre (2004); Wu et al., (2007) and Nyakwada (2009) among many other authors. Whenever there is enhancement of El Niño Southern Oscillation (ENSO), this mode has always been manifested (Li et al., 2007; Wu et al., 2007) and it is also linked to the North Atlantic Oscillation (NAO) (Wu et al., 2007).

The SVD results for the Pacific Ocean SSTs and OND decadal rainfall are presented in table 8 and figure 27. Although Pacific is the furthest ocean from the region, it has some strong teleconnections to the East Africa climate, especially during ENSO and other years with large SST anomalies (Ogallo and Suleiman, 1987; Ropelewski and Halpert, 1987; Nicholson and Kim, 1997; Wassila, 1999; Wang and Eltahir, 1999; Indeje, 2000; Indeje et al., 2000; Schreck and Semmazzi, 2004; Korecha and Barnston, 2007). Past studies have shown that the influence of Pacific Ocean on East Africa rainfall will depend on the circulation anomalies over and above Indian and Atlantic Oceans and the surrounding land areas (Wolter, 1987). Many studies have also shown that strong circulation anomalies in Pacific Ocean have significant impacts on both Indian and Atlantic oceans (Wolter, 1987; Terray and Dominiak, 2005).

Table 8 shows results obtained when SVD technique was used to analyze coupling between global ocean SSTs and OND rainfall season for East Africa region. The first three Pacific and OND modes contribute to about 80% of the decadal rainfall covariance. The SVD-1 mode for the Pacific SST contributes about 39% of the total covariance and is characterized by the El Niño SST pattern (Figure 27b). The value of correlation observed with this SVD-1 mode was 0.99 indicating that it accounted for about 39% of OND rainfall covariance (Figure 27c). The impact of this SVD-1 on East Africa rainfall seems to bear some similarity to those observed for SVD-1 mode of the Indian Ocean (Figure 23a). This may be due to close responses of the circulation amongst the three oceans (Burroughs 1999).



(a) OND rainfall Mode 1



(b) SST Mode 1

Figure 27: Spatial patterns (S1) of the first SVD mode for (a) October – December rainfall (b) Pacific SST presented as homogeneous correlation maps.

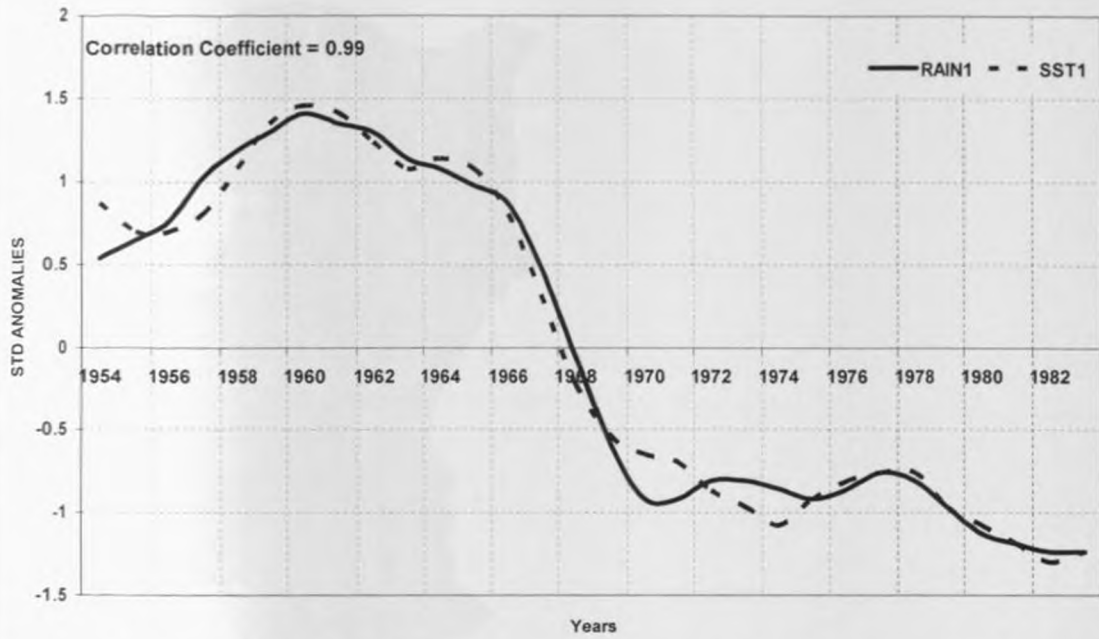


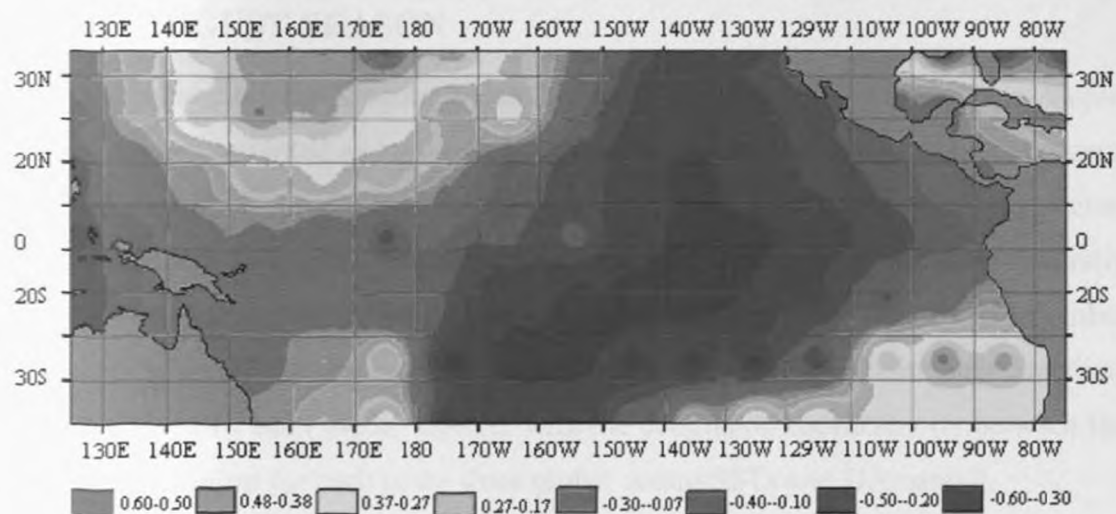
Figure 27c: Time series of expansion coefficients (s1) of the first SVD mode for OND rainfall and Pacific Ocean SST anomalies.

Various studies have shown that ENSO is linked to the Indian Ocean variability through the modulation of walker circulation (Xie et al., 2002; Krishnamurty and Kirtman, 2003; Kug et al., 2005; Kug *et al.*, 2006). The SSTs over the southern Indian Ocean during the December to February have been observed to influence climate shift in the Indian and Pacific Oceans and thus predictors of El Niño (Terray and Dominiak, 2005).

The SVD-2 mode (SVD-2) between OND rainfall and SST fields for the Pacific contributes about 28% of the covariance. It is characterized by the La Niña SST pattern with large negative loadings over the eastern equatorial Pacific Ocean and positive loading over the western equatorial Pacific Ocean (Figure 28b). Such loading pattern is associated with negative loading over the region and therefore depressed rainfall (Figure 28a). Past studies have shown close teleconnection within various Pacific Ocean modes. These include the recent studies that have examined teleconnection between ENSO (first Pacific mode) and the so called “El Niño Modoki” that often appears as a different mode of ENSO. More on El Niño Modoki and associated impacts on regional and global climates is discussed in section 4.4.2.



(a) OND rainfall Mode 2



(b) SST Mode 1

Figure 28: Spatial patterns (S2) of the second SVD mode for (a) October – December rainfall (b) Pacific SST presented as homogeneous correlation maps.

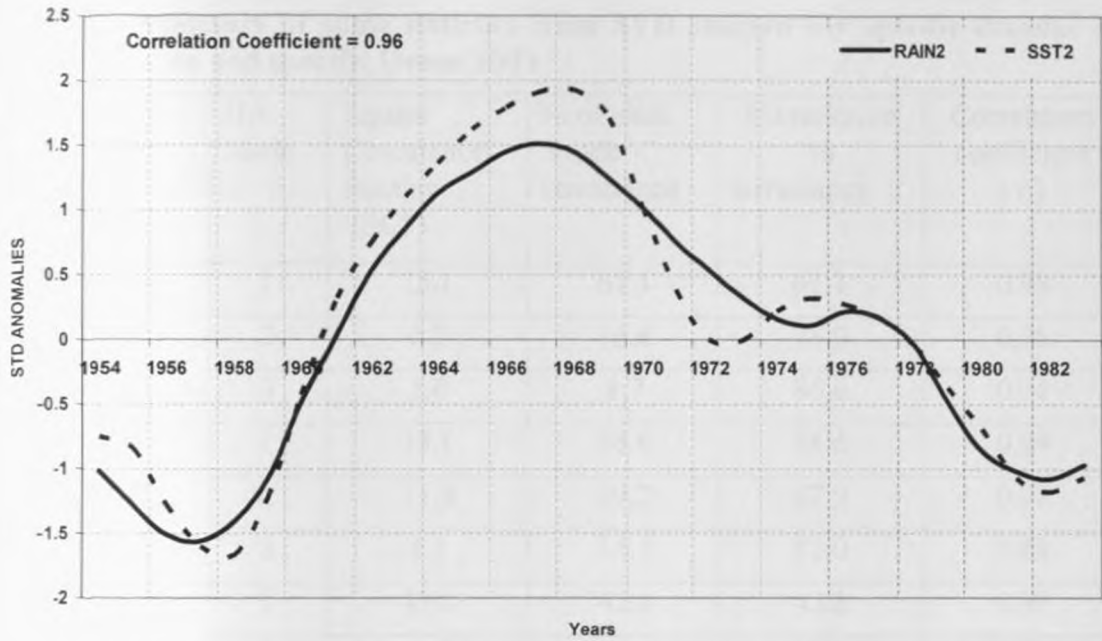


Figure 28c: Time series of expansion coefficients (s2) of the second SVD mode for OND rainfall and Pacific Ocean SST anomalies.

4.4.2 SINGULAR VALUE DECOMPOSITION (SVD) FOR THE JUNE TO AUGUST SEASON

In this section, the Singular Value Decomposition (SVD) results for June-August (JJA) season are presented and discussed. During the JJA season, the western and coastal parts of the region receive substantial amount of rainfall. Parts of the equatorial sector, covering northern Tanzania, western parts of East Africa and the coastal areas generally exhibit a trimodal rainfall regime centred around March-May, June –August, and October –December months. The results are presented based on the Square Covariance Fractions (SCF) explained by each mode, together with the correlation coefficient (r) between the expansion coefficient for each of the three global oceans SSTs and JJA rainfall.

The SVD analysis results for June-August seasonal rainfall and global SSTs are presented in table 9 and figure 29. Table 9 provides a summary of the results from SVD analysis for all the three basins and JJA rainfall season over East Africa. The leading modes in each case are discussed separately in this section.

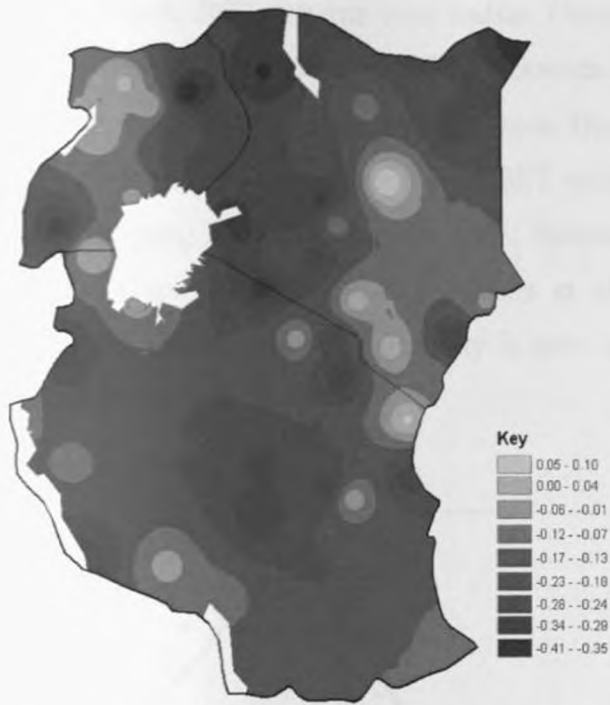
Table 9: Summary of some statistics from SVD analysis for specific decadal JJA rainfall season and specific Ocean SSTs

Oceans	JJA Mode	Square Covariance fraction (SCF)	% of total mode covariance	Cumulative % covariance	Correlation coefficient (r)
INDIAN	1	25.1	61.1	61.1	0.98
	2	6.9	16.8	78.0	0.96
	3	3.6	8.7	86.6	0.94
ATLANTIC	1	15.1	38.6	38.6	0.99
	2	11.4	29.2	67.9	0.97
	3	5.5	14.1	82.0	0.88
PACIFIC	1	43.0	42.1	42.1	0.99
	2	20.4	20.0	62.1	0.97
	3	15.6	15.3	77.4	0.85

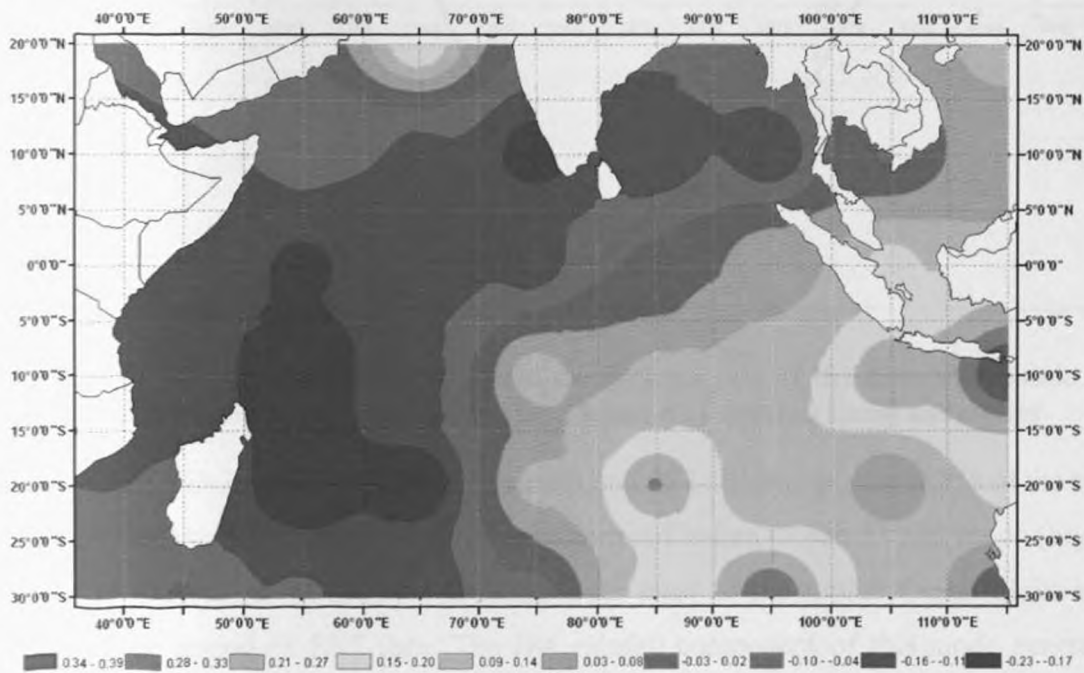
r is the correlation coefficient between the expansion coefficient of SSTs and JJA rainfall modes

For the Indian Ocean SSTs, table 9 shows that three dominant SVD modes, accounting for about 87% of the JJA rainfall season coupling with Indian Ocean SSTs are dominant. The SVD-1 mode between JJA rainfall and SST fields accounts for 61% of the covariance and is characterized by a dipole mode with pools of negative and positive loadings to the western and eastern parts of the equatorial Indian Ocean (Figure 29b), associated with depressed decadal rainfall over parts of the region with strong June-August rainfall seasonal mode. Time series of expansion of SVD coefficients of both rainfall and SST anomalies shown in Figure 29c demonstrates strong decadal variations in both time series with expansion coefficient of 0.98.

The spatial and temporal characteristics of this mode is similar to the one observed with the SVD-2 mode between the October-December rainfall and Indian Ocean SSTs (Figure 24a). The dominance of a single mode and dipole SST patterns such as the Indian ocean dipole have been a common feature in many past analyses.



(a) JJA Rainfall Mode 1



(b) SST Mode 1

Figure 29: Spatial patterns (S1) of the first SVD mode for (a) JJA rainfall season (b) Indian SST presented as homogeneous correlation maps

Dipole SST patterns over Indian Ocean have been observed by Harrison and Carson (2007); Ihara et al., (2008); Nyakwada (2009), among many others. The pattern also resembles the negative Indian Ocean Dipole (IOD), which has received a lot of attention with regard to the associated SST variability and regional rainfall patterns (Saji and Yamagata, 2003; Black et al., 2003; Behera et al., 2005; Owiti, 2005; Tozuka et al., 2007; Yu and Rienecker, 2000; Meyers et al., 2007; Huang and Shukla, 2007). An interesting dipole mode of variability is seen in the SVD-1 mode of the SSTs and JJA rainfall anomalies.

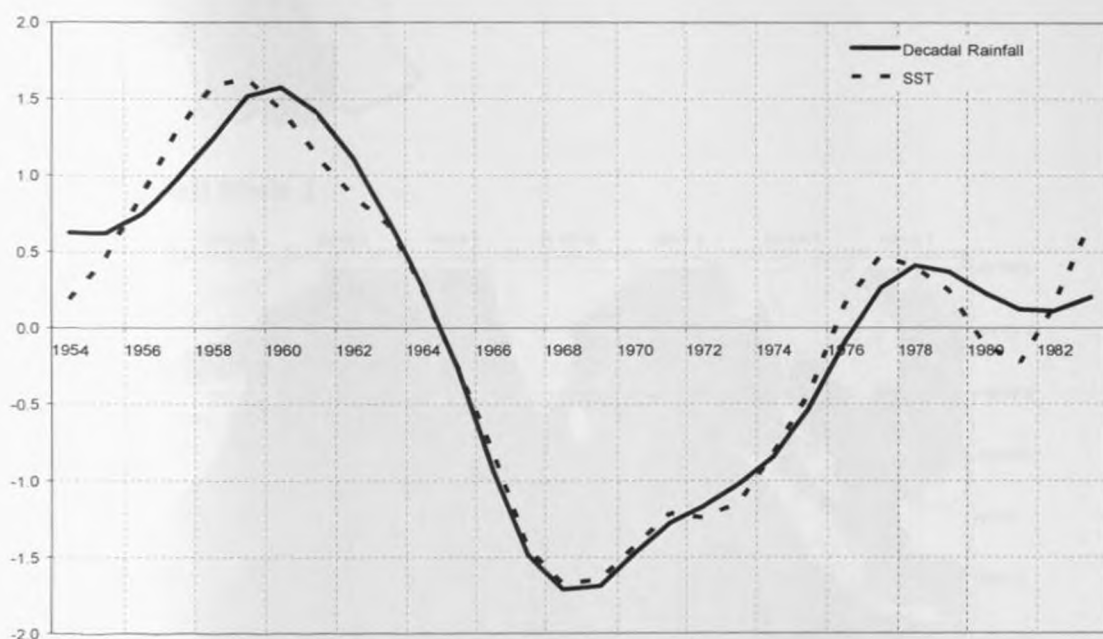
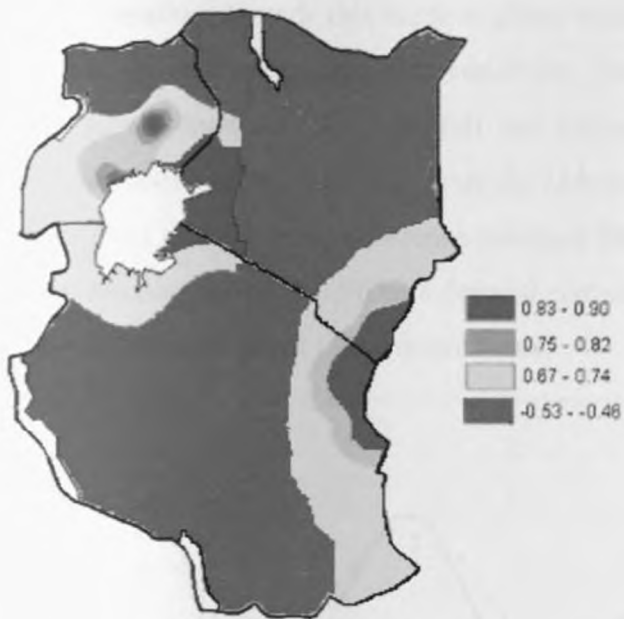
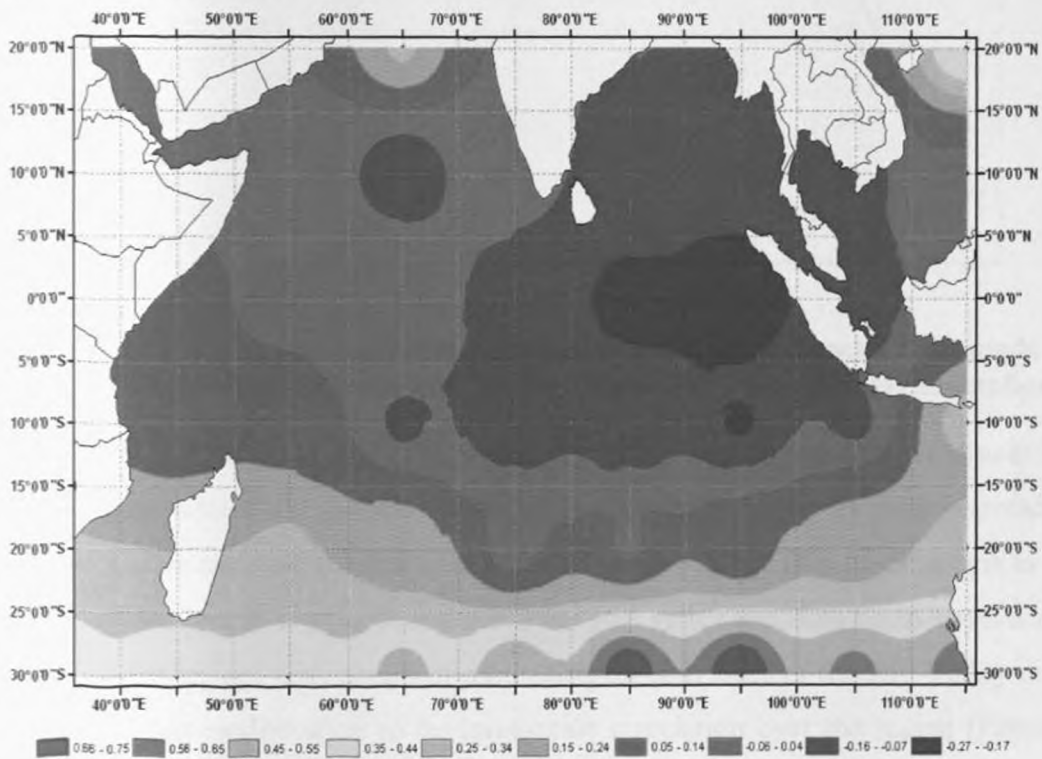


Figure 29c: (c) Time series of expansion coefficients (s1) of the first SVD mode for JJA rainfall (continuous lines) and Indian Ocean SST (dotted lines) anomalies

The SVD-2 mode between JJA rainfall and SST fields explains 16.8% of the total covariance of the JJA rainfall. The spatial patterns of Indian Ocean SVD-2 mode (Figure 30b) is characterized by negative loadings over most of the Indian Ocean basin with realistic long period of SST data. The JJA rainfall component of this mode generally depicts positive loadings over the coastal sector and western areas; and negative loading over the rest of the region that are often dry during June – August period (Figure 30a).



(a) JJA Rainfall Mode 2



(b) SST Mode 2

Figure 30: Spatial patterns (S2) of the second SVD mode for (a) JJA rainfall season (b) Indian SST presented as homogeneous correlation maps

Therefore, though this mode explains relatively low covariance, it seems to be a key mode for June –August rainfall variability. Similar pattern in ocean basin was evident in the second mode of OND rainfall and Indian Ocean (Figure 24b). Time series of expansion coefficients of SVD-2 mode for JJA rainfall and Indian Ocean SST anomalies (Figure 30c) shows strong coherence amongst the decadal rainfall and SST modes with correlation coefficient of 0.96 with decadal signals within this season. The dominance of negative phase is evident in the recent years.

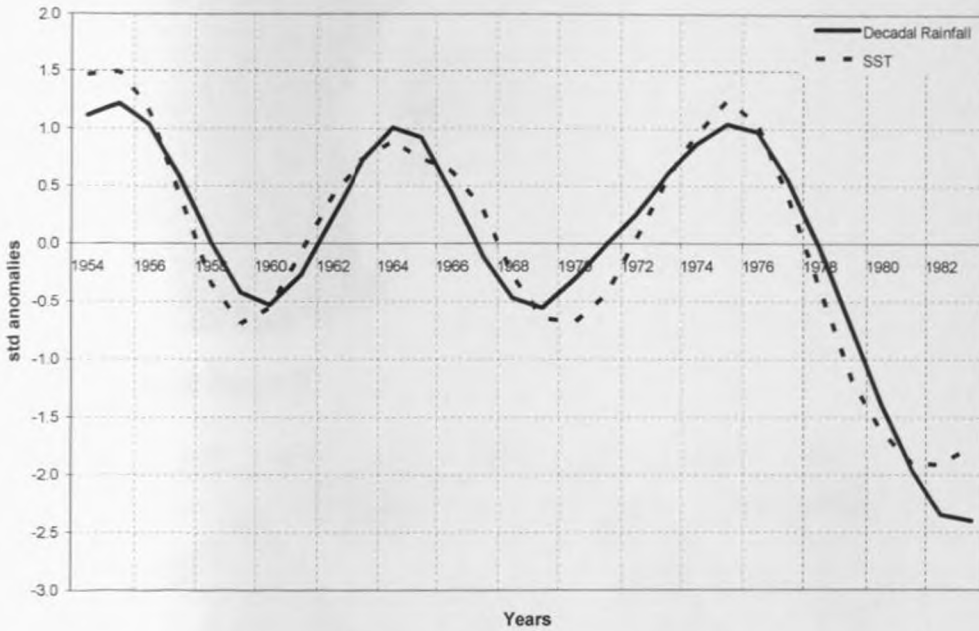
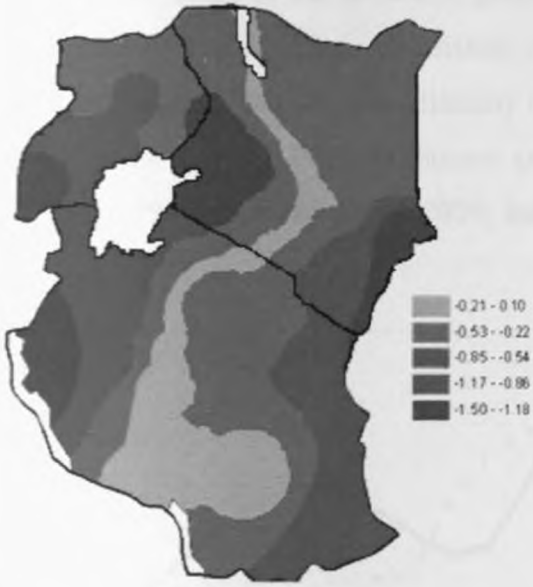


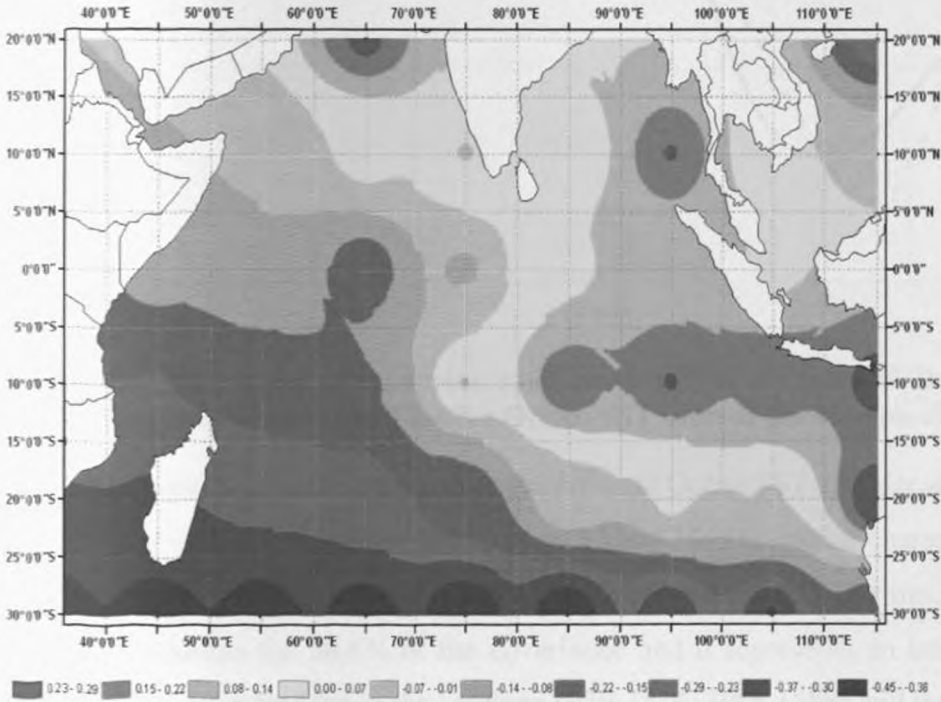
Figure 30c: Time series of expansion coefficients (s_2) of the second SVD mode for JJA rainfall (continuous lines) and Indian Ocean SST (dotted lines) anomalies

The SVD-3 mode that explained 8.7% of the total covariance had dipole loading patterns that were close to those observed for mode 1, except for wider spread of the positive modes over the tropical ocean basins (Figure 31b). This mode seems to signify the role of the central highlands and the Great Rift valley that runs north-south across the central of the region, with chains of mountains on both sides of the Rift Valley that have also significant modification to the large-scale circulation over the region (Figure 31a). The time series of expansion coefficients of this mode is characterised with some decreasing trend during the decades of 1970s and early 1980s (Figure 31c). Many parts of the region were under drought during these decades (Nicholson 2000b). Schreck and Semazzi (2004) isolated a decadal trend mode during these two decades influenced by

SST over the tropical South Atlantic Ocean. A similar and consistent trend was also found by Dai et al., (1997).



(a) JJA Rainfall Mode 3



(b) SST Mode 3

Figure 31: Spatial patterns (S3) of the third SVD mode for (a) JJA rainfall season (b) Indian SST presented as homogeneous correlation maps

Thus the study has delineated some coherence between June- August rainfall over East Africa with strong teleconnection to decadal SST variability over parts of the Indian Ocean basin. Some of the delineated patterns were consistent with those observed during OND season. The results are consistent with some of the past studies that have shown linkages between inter-annual variability of the regional climate and perturbations in the global SSTs (Ogallo, 1988; Nicholson and Kim, 1997; Saji et al., 1999; Goddard and Graham, 1999, Mutai and Ward, 2000; Indeje et al., 2000; and Nyakwada, 2009 amongst others).

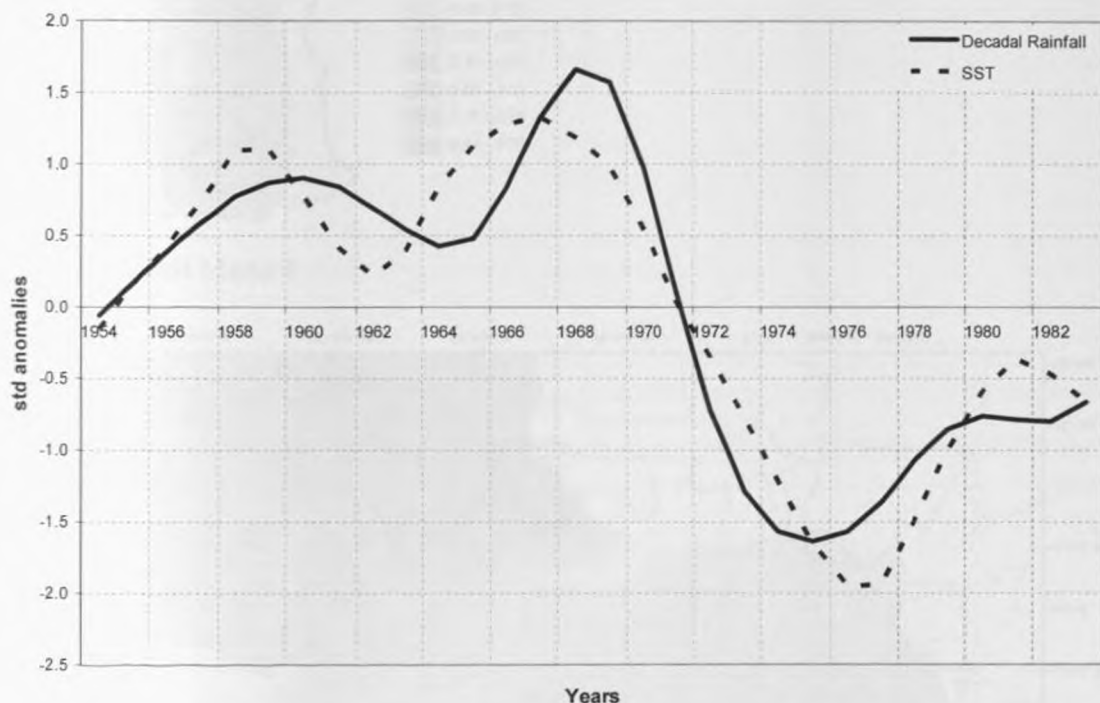
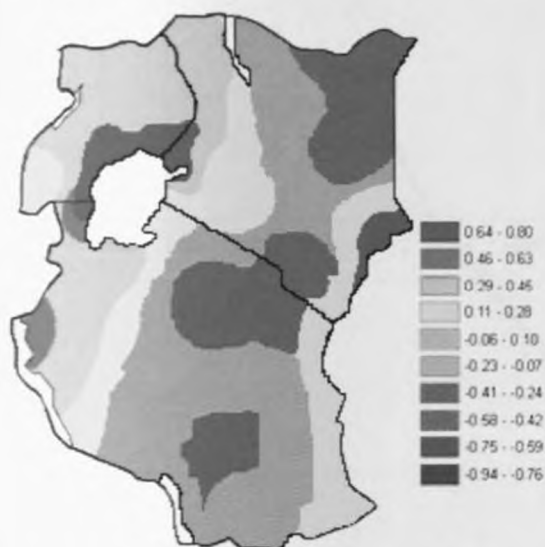


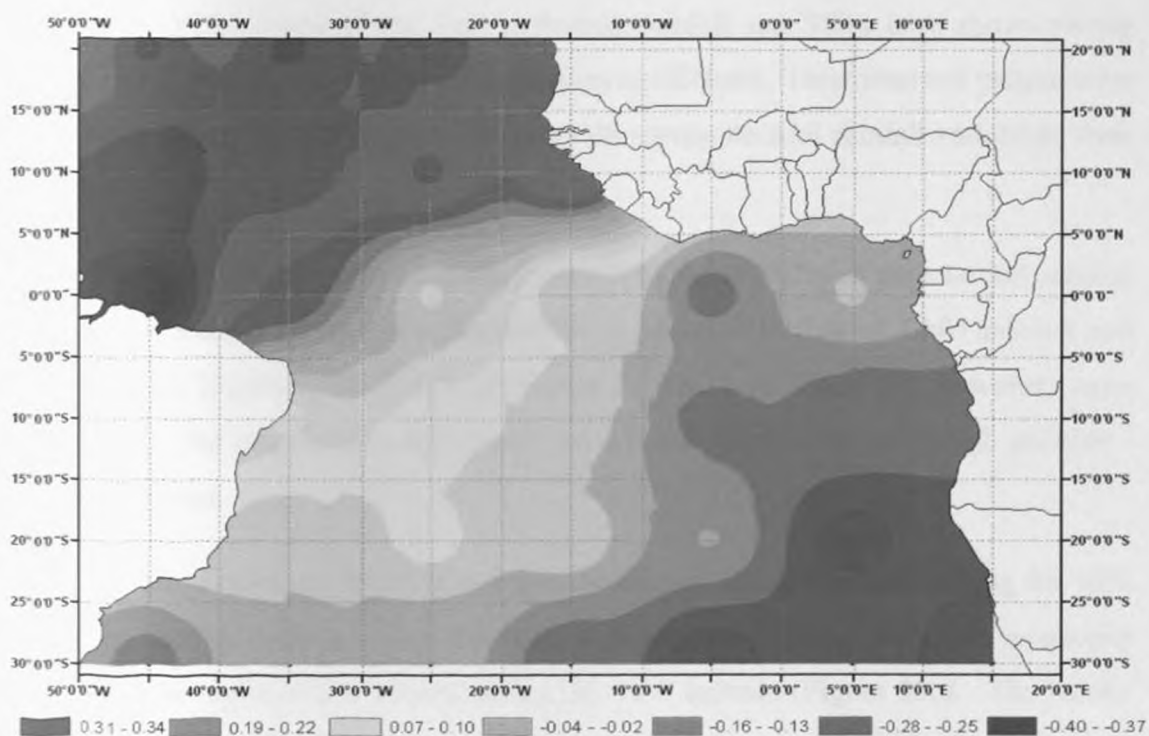
Figure 31c: Time series of expansion coefficients (s3) of the third SVD mode for JJA rainfall (continuous lines) and Indian Ocean SST (dotted lines) anomalies

The results of SVD analysis for the Atlantic Ocean SST and decadal JJA rainfall are presented in table 9 together with Figures 32 and 33. The spatial characteristics of the first two dominant modes explain 68% of the covariance. The SVD-1 mode between the two fields accounts for 38.6% of the covariance and it represents an inter-hemispheric dipole with positive loading in the southern (0°E-15°E, 30°S-15°S) and the negative pole in the northern part of the tropical Atlantic Ocean (50°W-35°W, 0°N-15°N). This mode is opposite to SVD-2 mode of OND rainfall and Atlantic Ocean (Figure 26b). These modes have been observed in some of the past SST variability studies over the Atlantic

Ocean (Nyakwada, 2009; Wu et al., 2007; Chang et al., 1997; Li et al., 2007; Bowden et al., 2004; Repelli and Nobre, 2004; Nobre and Shukla, 1996; among many other authors).



(a) JJA rainfall Mode 1



(b) SST Mode 1

Figure 32: Spatial patterns (S1) of the first SVD mode for (a) June - August rainfall (b) Atlantic SST presented as homogeneous correlation maps

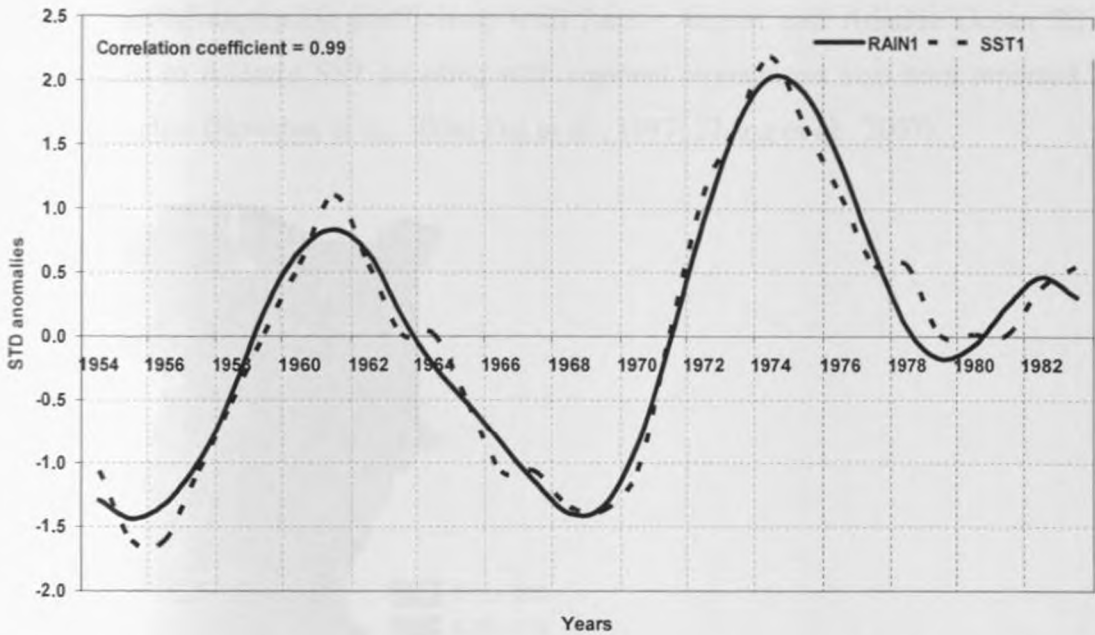


Figure 32c: Time series of expansion coefficients (s_1) of the first SVD mode for June - August rainfall and Atlantic Ocean SST anomalies.

The SVD-1 mode of the June – August rainfall and SSTs have shown strong decadal signal in their time series of expansion coefficients. This observed pattern over the Atlantic Ocean can possibly be linked to the strong decadal rainfall variability over the region.

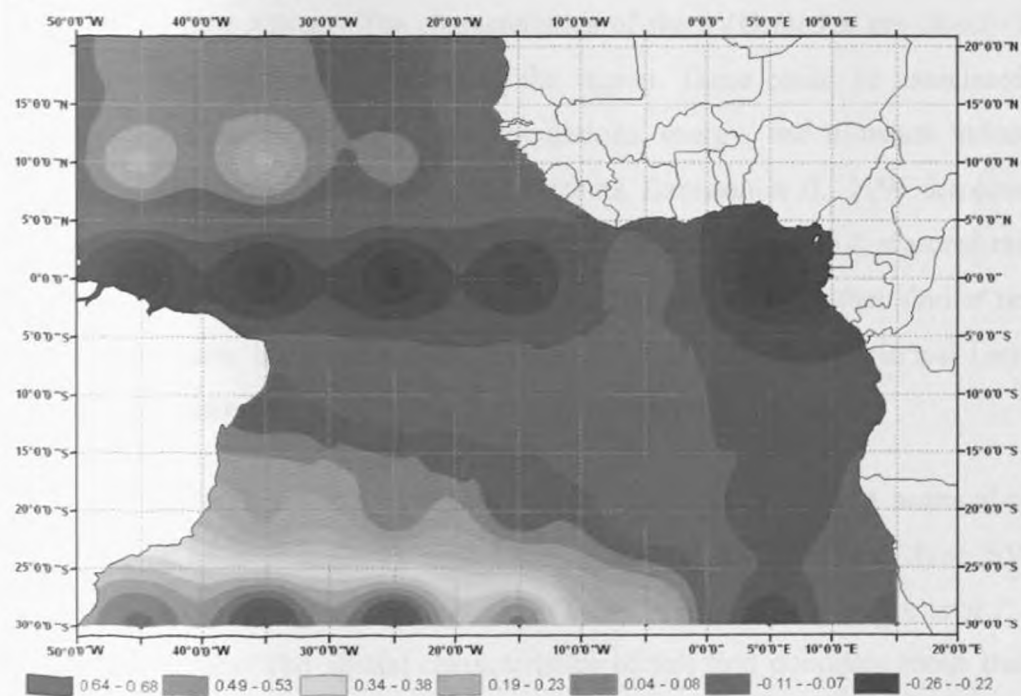
The second dominant SVD mode (SVD-2) explains 29.2% of the total JJA rainfall and SST covariance. Its spatial characteristic is opposite to that of OND rainfall and Atlantic Ocean (Figures 25b) hence not shown in this study. There are, however, some differences in the magnitudes and spatial spread over some areas with high positive / negative loadings.

The third (SVD-3) mode of Atlantic Ocean and JJA rainfall accounting for 14% covariance showed unique spatial patterns with negative loading along the equatorial Atlantic Ocean and positive loading along the 30°S latitude (Figure 33b). The results show that although the mode explains relatively low covariance, SST variability over these areas have homogenous impacts over East Africa. The corresponding regional rainfall patterns associated with this mode showed general negative loadings over the region (Figure 33a). The mode shows significant positive trend since 1960s (Figure 33c)

in time series of expansion coefficients with June - August and Atlantic Ocean SST. Positive trend in Atlantic SST coupling with regional climate has also been reported in some past studies (Bowden et al., 2004; Dai et al., 1997; Zhang et al., 2007).



(a) JJA Rainfall Mode 3



(b) SST Mode 3

Figure 33: Spatial patterns (S3) of the third SVD mode for (a) June - August rainfall (b) Atlantic SST presented as homogeneous correlation maps

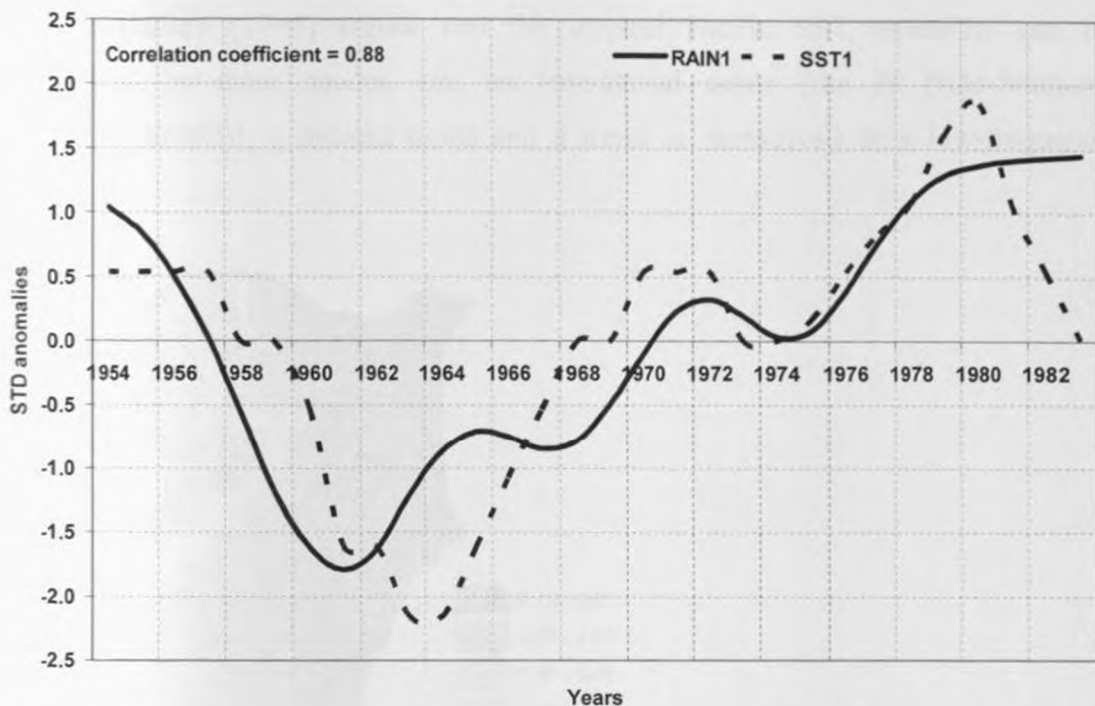
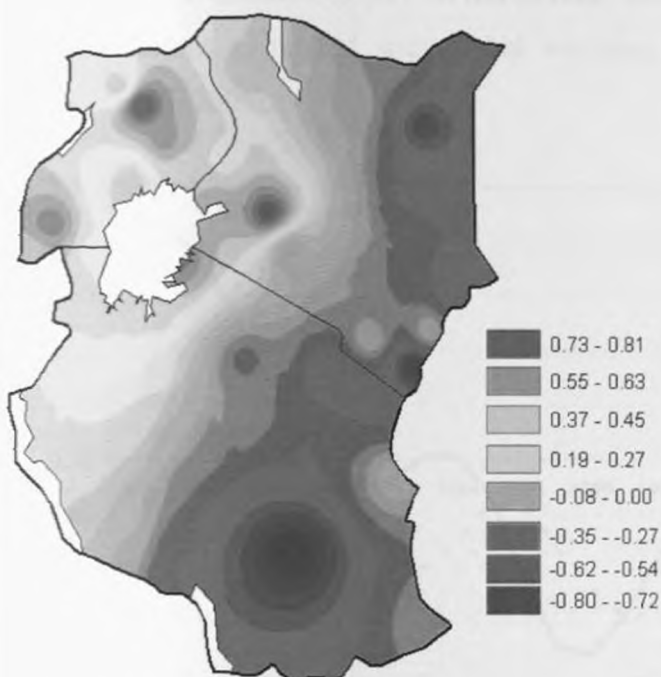


Figure 33c: Time series of expansion coefficients (s3) of the third SVD mode for June - August rainfall (full lines) and Atlantic Ocean SST anomalies (dotted lines).

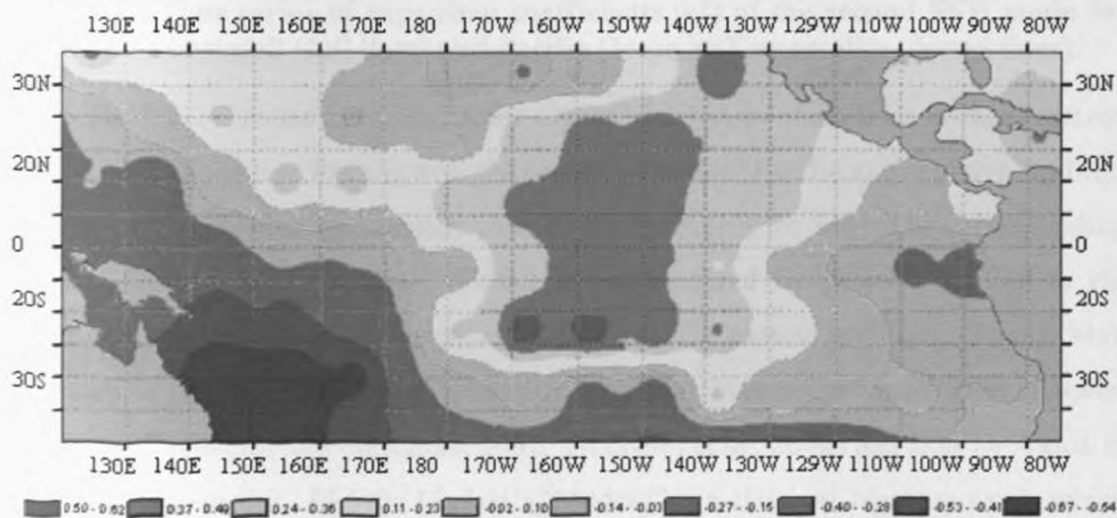
These results signify the importance of Atlantic Ocean SVD modes on decadal rainfall over East Africa. The characteristics of the SVD modes are closely associated with some climate extremes affecting the region. These could be associated with the implications of these modes on the circulations, energy, and moisture induced by the ocean, and other inland rain generating systems. Barnston et al., 1996 demonstrated that the time-space behaviour of the SST field alone influences the JJA seasonal rainfall over the region both on interannual and inter-decadal time-scales. Other similar results with JJAS season have been documented by Gissila et al., (2004); Segele and Lamb (2005); Korecha and Barnston (2007); Zewdu et al (2009) among others.

The results for SVD analysis for Pacific Ocean SSTs and JJA seasonal rainfall are presented in table 9 together with Figures 34 and 35. The first three SVD modes contributed to about 42%, 20% and 15% (Table 9) respectively of the total JJA decadal rainfall variability. The spatial characteristics of this first dominant mode that explains about 42% of the JJA covariance is characterised by El Niño-like variability pattern similar to one presented by mode 1 of the OND rainfall and Pacific Ocean in Figure 27b.

Latif and Barnett (1994) argued that the tropical Pacific SST variability can be characterized by three modes, i.e., an interannual mode [the El Niño-Southern Oscillation, (ENSO)], a decadal mode and a trend or unresolved ultra low-frequency variability.



(a) JJA rainfall Mode 2



(b) SST Mode 2

Figure 34: Spatial patterns (S2) of the second SVD mode for (a) JJA rainfall season (b) Pacific SST presented as homogeneous correlation maps

They argued that considerable SST variability can be attributed to a linear trend that might be related to greenhouse warming. Lau and Weng (1999) argued that a fast warming in the past few decades is mostly due to the advent of the warm phase of a decadal-interdecadal SST oscillation which is superimposed on linear trend. These results suggest that variabilities of SST on interannual, decadal to even longer timescales are all relevant factors associated with global warming signal (Shreck and Semazzi, 2004; Ramsay et al., 2008).

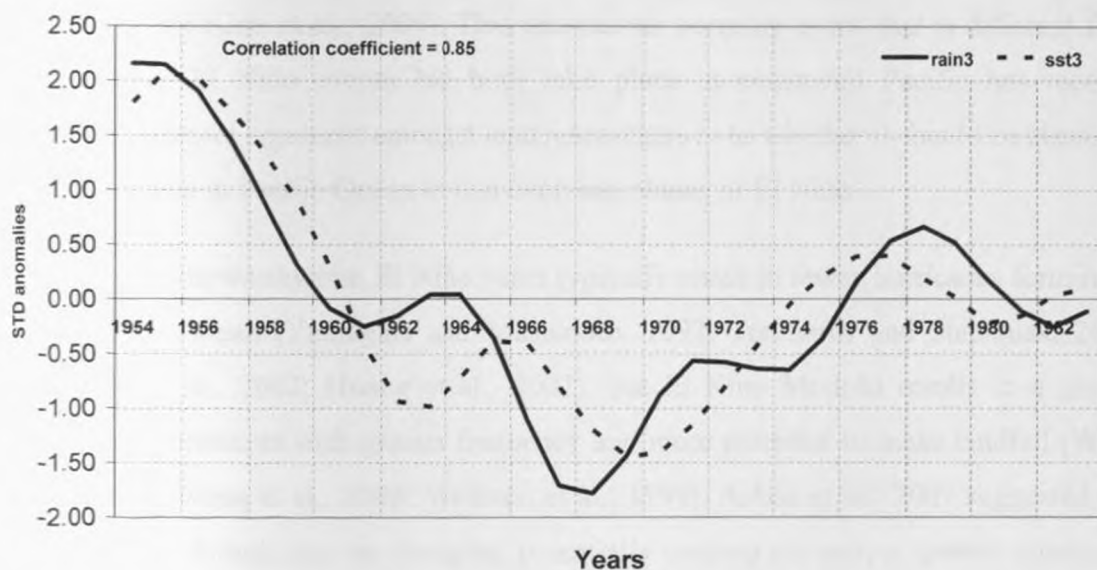


Figure 34c: Time series of expansion coefficients (s2) of the second SVD mode for June - August rainfall (full lines) and Pacific Ocean SST anomalies (dotted lines).

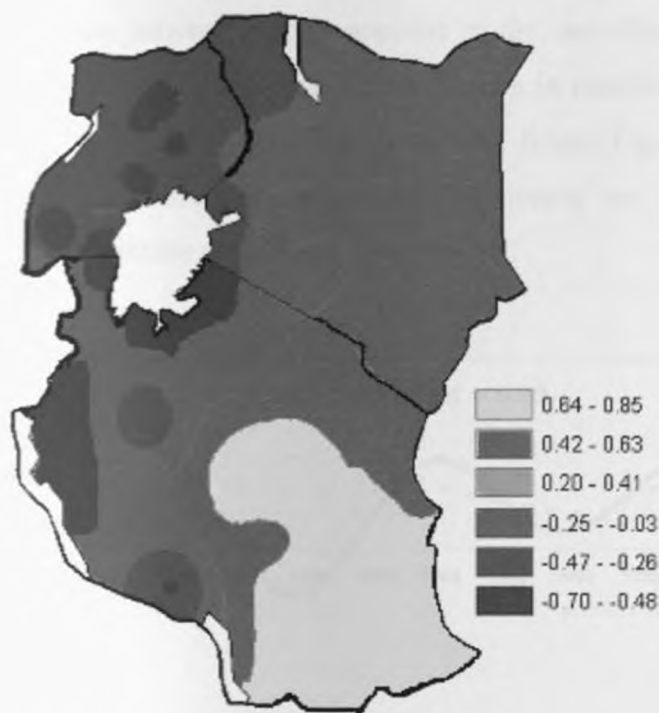
The SVD-2 mode between Pacific Ocean and JJA rainfall fields is characterized by large pool of positive loading over the central equatorial Pacific and negative loadings in the equatorial western and eastern parts of the basin (Figure 34b). The corresponding impact of this mode on regional rainfall is characterized by positive loading in the western parts of the region and negative loading over the eastern highlands (Figure 34a). This mode of tropical Pacific SST variability was first observed and referred to as trans-Niño index (Trenberth and Stepaniak, 2001; Trenberth et al., 2002) and later by Ashok et al., 2007 who named it '*El Niño Modoki*' ("Modoki" is a classical Japanese word, which means "a similar but different thing"). This mode that takes a horse-shoe pattern flanked by a colder sea surface temperature anomaly (SSTA) on both sides along the equator (Trenberth and Stepaniak, 2001; Trenberth et al., 2002, Ashok et al., 2007; Meyers et al.,

2007; Ashok et al., 2009; Hye-Mi Kim, et al., 2009) is characterized by enhanced and depressed rainfall respectively over western and eastern sectors of East Africa region.

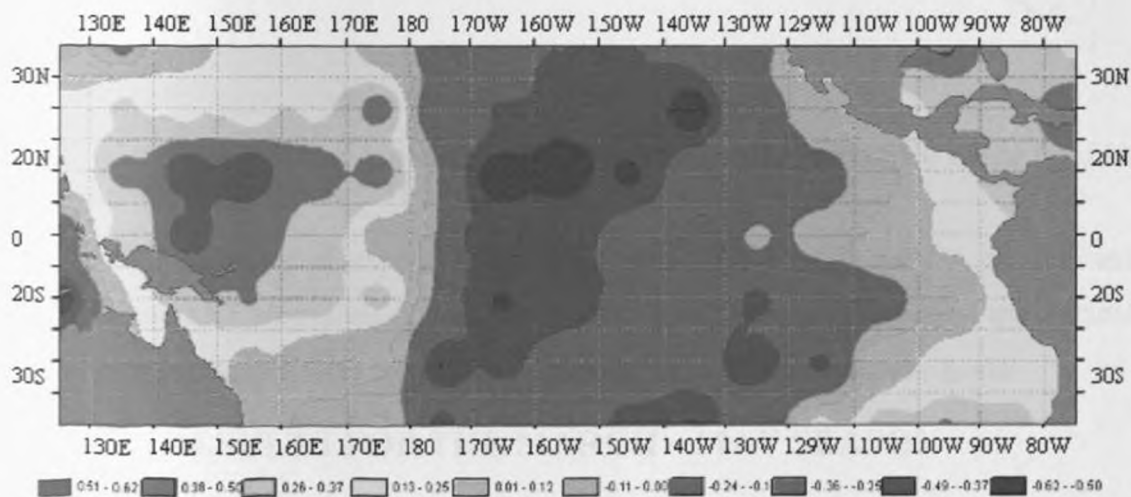
Since majority of such events forms in the Central Pacific, rather than the Eastern Pacific as the typical El Niño evolution does, the phenomenon is referred to as El Niño Modoki. El Niño Modoki involves ocean-atmosphere coupling processes which include a unique tripolar sea level pressure pattern during the evolution, analogous to the Southern Oscillation in case of El Niño (Ashok et al., 2007; Meyers et al., 2007; Ashok et al., 2009; Hye-Mi Kim, et al., 2009). This anomalous warming event that is different from conventional El Niño events but both take place in equatorial Pacific has recently generated counter argument amongst lead researchers as to whether it should be classified as a new mode in Pacific Ocean or just evolving phases of El Niño.

It is noteworthy that El Niño years typically result in fewer hurricanes forming in the Atlantic Ocean (Yamagata and Masumoto, 1992; Trenberth and Stepaniak, 2001; Trenberth et al., 2002; Huang et al., 2002), but El Niño Modoki results in a greater number of hurricanes with greater frequency and more potential to make landfall (Weng et al., 2007; Weng et al., 2008; Webster, et al., 1999). Ashok et al., 2007 suggested that the El Niño Modoki may be changing potentially causing not only a greater number of hurricanes than in average years, but also a greater chance of hurricanes making landfall along the Gulf coast and the coast of Central America. Studies show that ENSO influences the tropical Atlantic SST primarily through the Troposphere Temperature (TT) mechanism, which predicts a uniform warming in the tropical Atlantic following the mature phase of El Niño (Huang et al., 2002 and Yue 2005). As to whether it is El Niño that is changing to El Niño Modoki is not clear yet but several authors postulate that it could be part of different phases of evolving El Niño, or El Niño's response to a warming atmosphere. There are hints that the trade winds of the Pacific have become weaker with time and this may lead to the warming occurring further to the west (Weng et al., 2007; Weng et al., 2008).

UNIVERSITY OF NAIROBI
LIBRARY



(a) JJA Rainfall Mode 3



(b) SST Mode 3

Figure 35: Spatial patterns (S3) of the third SVD mode for (a) June - August rainfall (b) Pacific Ocean SST presented as homogeneous correlation maps

The SVD-3 mode between Pacific Ocean and JJA rainfall fields (15%) is characterized by positive loading over the western and eastern equatorial Pacific and negative loading in the central equatorial parts of the basin (Figure 35b). The impact of this mode on East Africa rainfall is associated with positive loading in the eastern highlands and negative loading over the western parts of the region (Figure 35a). This

mode has patterns exactly opposite to the one observed for SVD-2 mode for JJA and Pacific SST fields. A near similar pattern in rainfall was also observed in SVD-2 mode between OND rainfall and Atlantic SST fields (Figure 26a). This seems to confirm that robust teleconnection between global oceans are also manifested in their effects on regional climate as well.

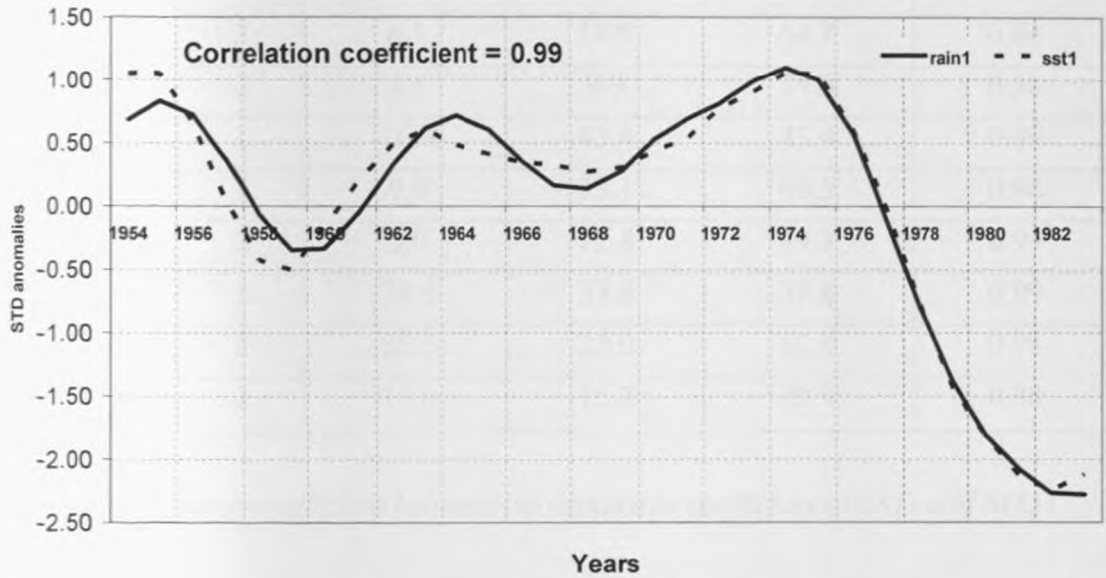


Figure 35c: Time series of expansion coefficients (s3) of the third SVD mode for JJA rainfall and Pacific Ocean SST anomalies.

The time series of expansion coefficients of SVD-3 mode for JJA rainfall and Pacific Ocean SST anomalies (Figure 35c) shows strong coherence amongst the decadal rainfall and SST modes with correlation coefficient of 0.99 with decadal signals.

4.4.3 SVD RESULTS FOR THE MARCH – MAY SEASON

In this section, modes of decadal variability for the individual global ocean SSTs and March-May (MAM) rainfall anomalies are analyzed and compared based on SVD analysis technique. The SVD results for the three ocean basins and MAM rainfall are presented in table 10 and figures 36-42.

The SVD results for the MAM rainfall season and Indian Ocean SST are presented in table 10 and figures 36 and 37. Table 10 provides a summary of the results from SVD analysis for all the three basins and MAM rainfall season over East Africa.

Table 10: Summary of some statistics from SVD analysis for decadal MAM rainfall seasons for the specific Ocean SSTs

Oceans	MAM Mode	Square Covariance fraction (SCF)	% of total mode covariance	Cumulative % covariance	Correlation coefficient (r)
INDIAN	1	20.5	49.9	49.9	0.73
	2	6.1	14.8	64.7	0.64
	3	4.1	9.9	74.6	0.38
ATLANTIC	1	16.9	43.4	43.4	0.99
	2	9.0	23.1	66.5	0.98
	3	5.0	12.8	79.3	0.97
PACIFIC	1	38.6	37.8	37.8	0.99
	2	25.5	25.0	62.8	0.98
	3	17.0	16.7	79.4	0.88

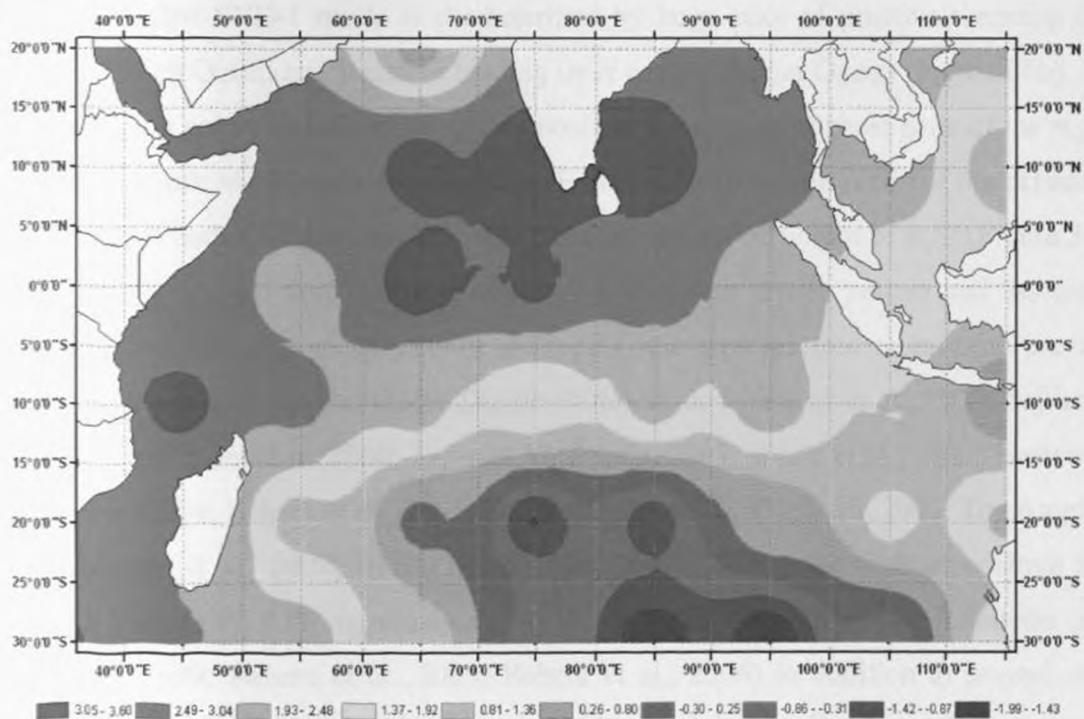
r is the correlation coefficient between the expansion coefficient of SSTs and MAM rainfall modes

MAM is the major rainfall season for the region that contributes about 80% of the total annual rainfall at some locations in East Africa (Hastenrath et al., 1993). Although it is the main and most important season for the region, the skill of its predictability with SST based predictors is still very low compared to the second main season of OND (Black et al., 2003; Clark et al., 2003; Hastenrath, 1995; Hastenrath et al., 1993; Mutemi, 2003; Omondi, 2005; Owiti, 2005; Nyakwada, 2009; Ogallo, 1989). Some skill for this season with empirical methods, however, has been reported by Njau (2006), Indeje and Semazi (2000), Owiti (2005), Omeny (2006), Nyakwada (2009) among others.

Indian Ocean SST and MAM seasonal rainfall SVD modes accounted for 74.6% of the total square covariance. The first, second and third SVD modes accounted for 49.9, 14.8 and 9.9 % respectively of the total square covariance of MAM rainfall season and Indian Ocean SST.



(a) MAM Rainfall Mode 1



(b) SST Mode 1

Figure 36: Spatial patterns of the first SVD mode for (a) MAM rainfall and (b) Indian Ocean SST presented as homogeneous correlation maps

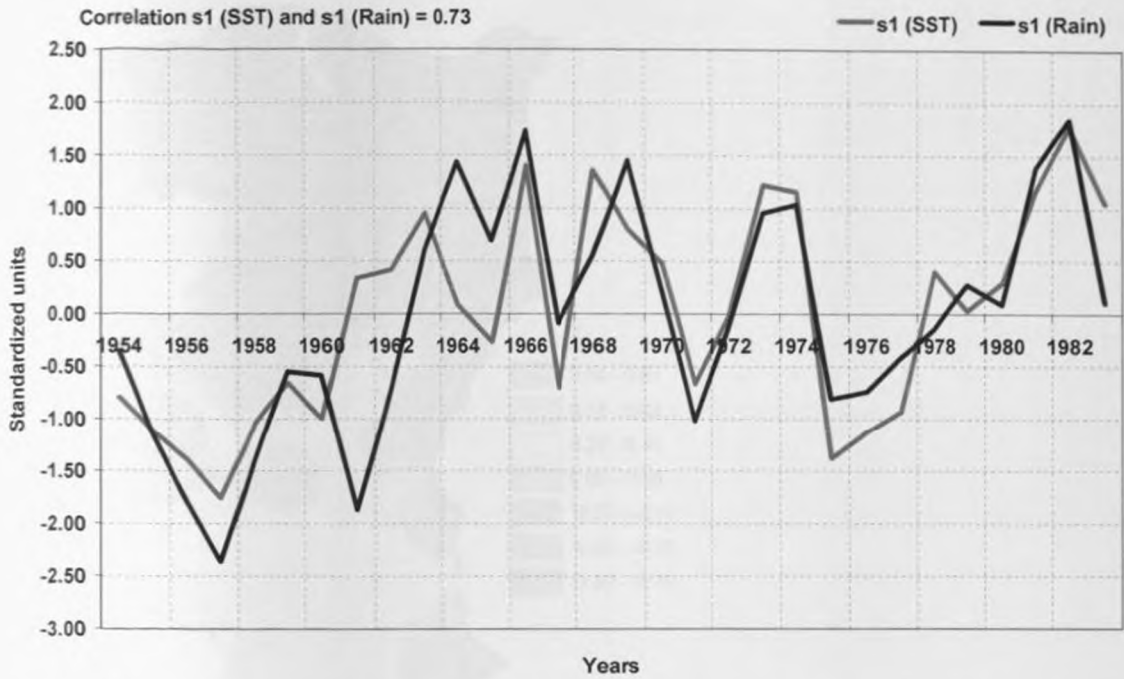
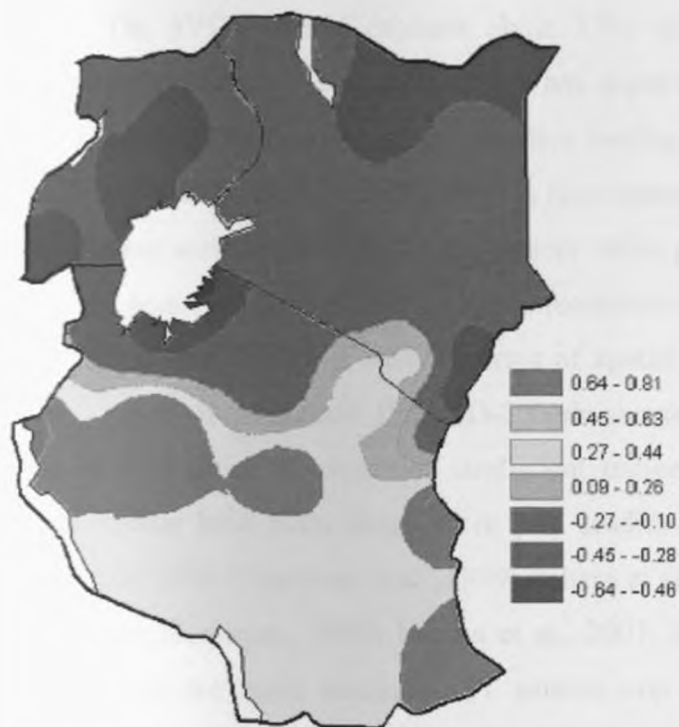
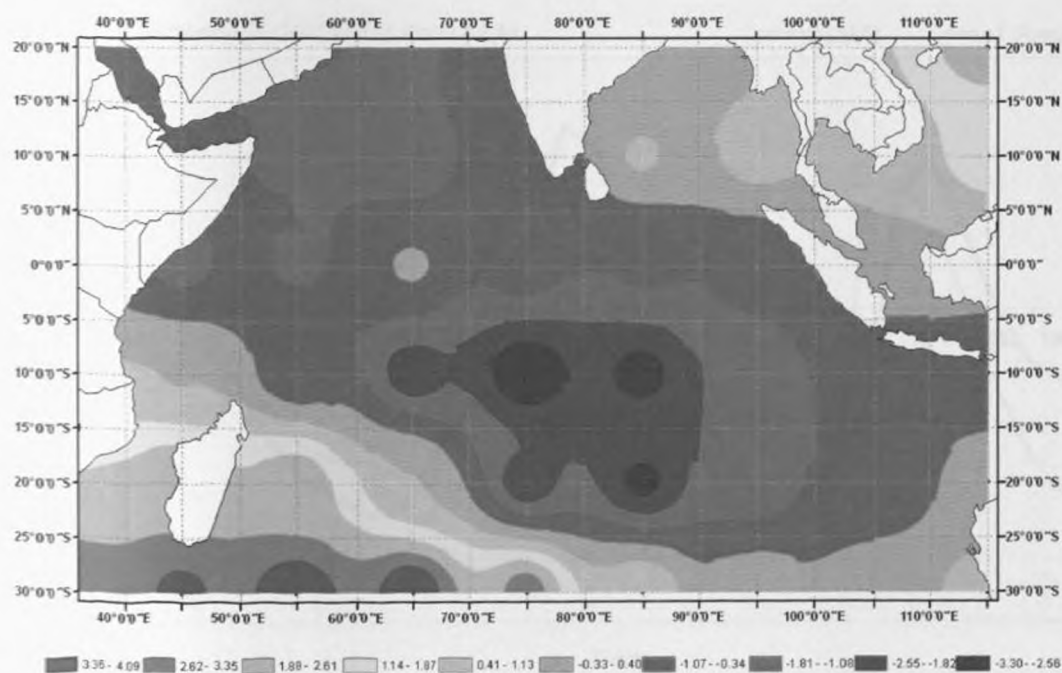


Figure 36c: Time series of expansion coefficients (s_1) of the first SVD mode for March - May rainfall and Indian Ocean SST anomalies

The first SVD-1 mode is characterized by large pool of positive warming over western Indian Ocean and negative loading over eastern Indian Ocean (Figure 36b). The corresponding precipitation pattern shows positive loadings over most parts of the region especially where MAM rains are dominant (Figure 36a). The time series of the expansion coefficient of both SST and rainfall fields has correlation coefficient of 0.73 (Figure 36c). This first SVD mode that is characterised with east-west dipole pattern and associated with much rainfall over most parts of the region has been referred to in some previous studies as the positive Indian Ocean Dipole (IOD) Mode (Webster et al., 1999; Saji et al., 1999; Yu and Rienecker, 2000; Saji and Yamagata, 2003; Black et al., 2003; Hastenrath and Polzin, 2004; Behera et al., 2005; Singhrattna et al., 2005; Owiti, 2005; Tozuka et al., 2007; Meyers et al., 2007; Huang and Shukla, 2007). During the peak of positive IOD phase in boreal fall, IOD rigorously affects rainfall over East Africa and Indonesia (e.g., Saji et al., 1999; Behera et al., 2005; Behera et al., 2006) in addition to several other regions of the globe (Saji and Yamagata, 2003). Negative loading spread over western and positive loading over eastern (i.e opposite pattern) Indian Ocean was evident in first mode for JJA and Indian Ocean SST that results in depressed rainfall over the region (Figure 29).



(a) MAM Rainfall Mode 2



(b) SST Mode 2

Figure 37: Spatial patterns of the second SVD mode for (a) MAM rainfall and (b) Indian Ocean SST presented as homogeneous correlation maps.

The SVD-2 mode explains about 15% of the total MAM seasonal rainfall covariance (Table 10). The spatial pattern has negative coherence loadings centred on the central equatorial Indian Ocean and positive loading over the south-western parts of the Ocean basin (Figure 37b). This pattern is also characterized with negative loadings over the northern sector as well as coastal sectors while positive loading is confined over the southern sector of the region. This Mode (correlation coefficient, $r = 0.64$) seems to be opposite to that of SVD-1 mode in terms of spatial spread in rainfall and also in time series expansion coefficient. But SVD-2 mode showed strong decadal trend mode (Figure 37c) in time series of expansion coefficient unlike in SVD-1 mode. Such patterns in Indian Ocean have been observed in past studies (Ward and Folland, 1991; Yu and Rienecker, 1999; Chambers et al., 1999; Behera et al., 2005; Schreck and Semazzi, 2004; Terray and Dominiak, 2005; Tozuka et al., 2007; Nyakwada, 2009) where it has been attributed to the mean seasonal SST pattern over the ocean when the overhead sun crosses the equator. Similar modes of variability were evident for other seasons (Figure 30) such as the JJA rainfall season and Indian Ocean basin SVD-2 mode.

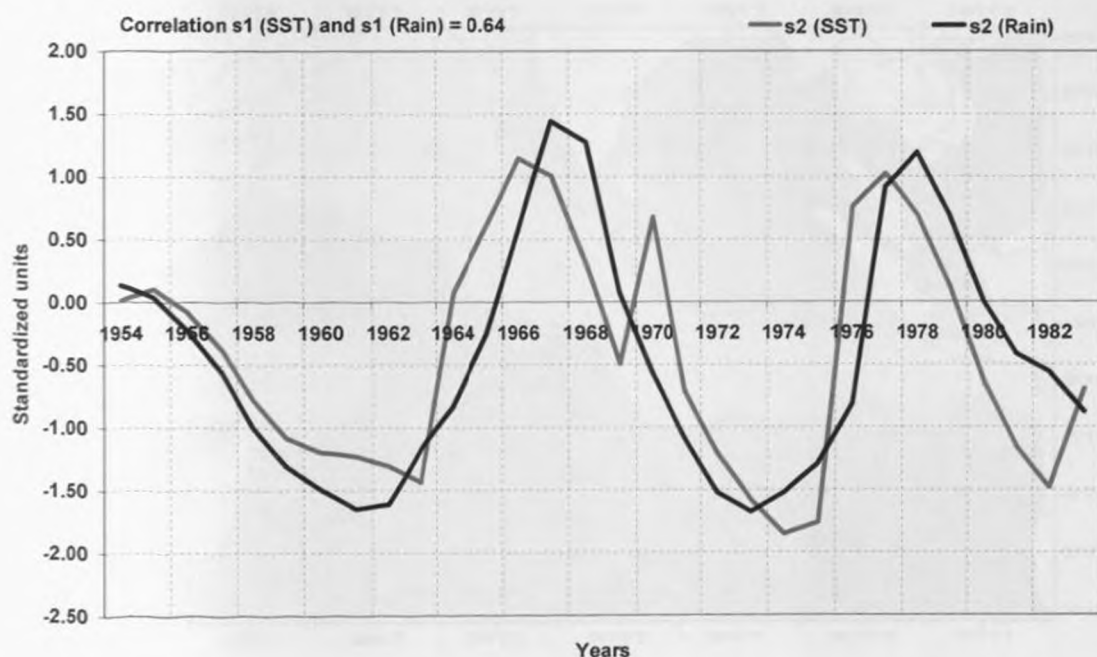
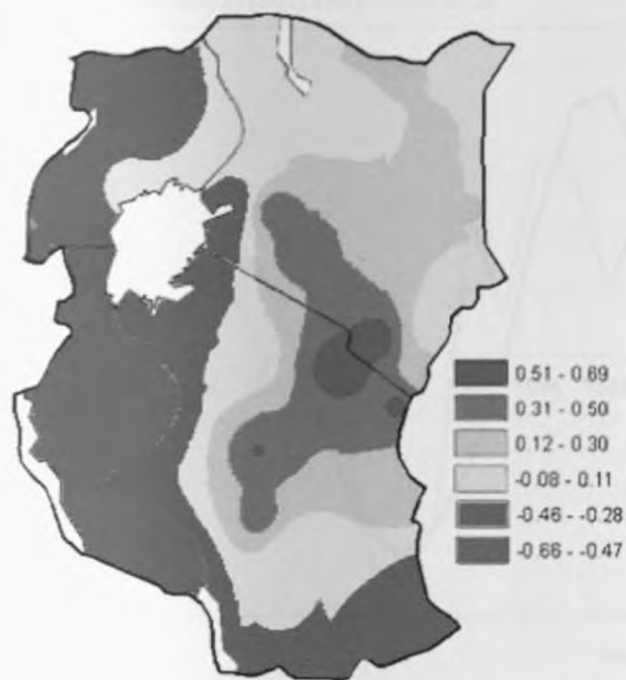
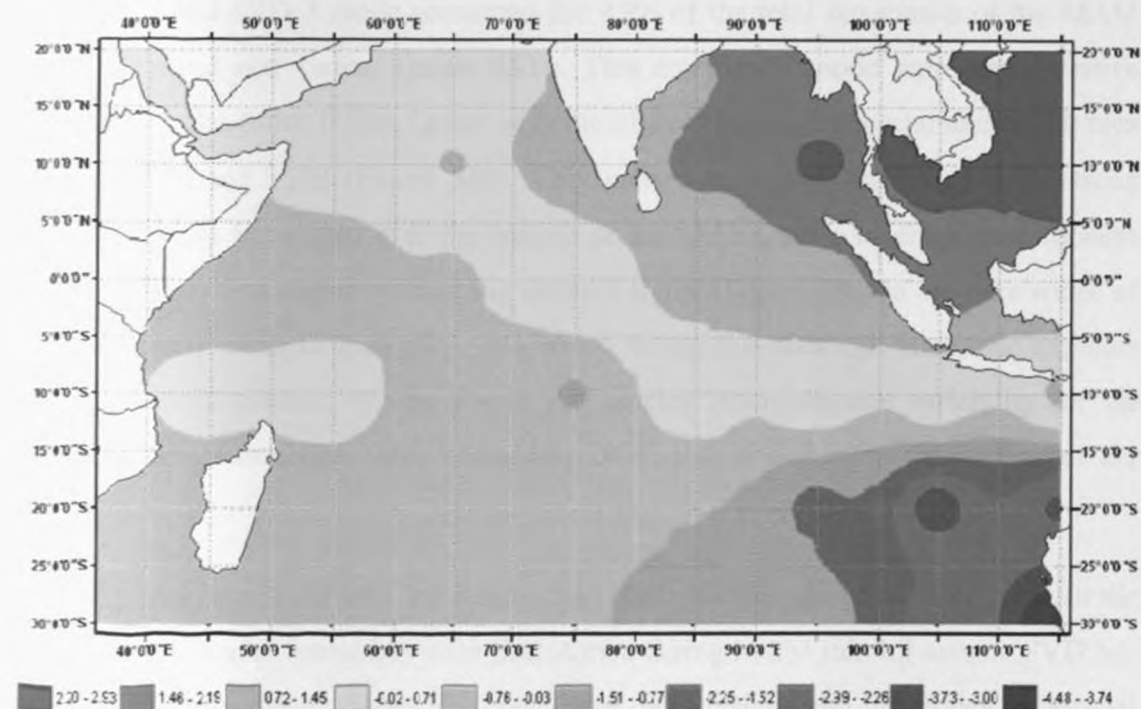


Figure 37c: Time series of expansion coefficients (s_2) of the second SVD mode for March - May rainfall and Indian Ocean SST anomalies



(a) MAM Rainfall Mode 3



(b) SST Mode 3

Figure 38: Spatial patterns of the third SVD mode for (a) MAM rainfall and (b) Indian Ocean SST presented as homogeneous correlation maps.

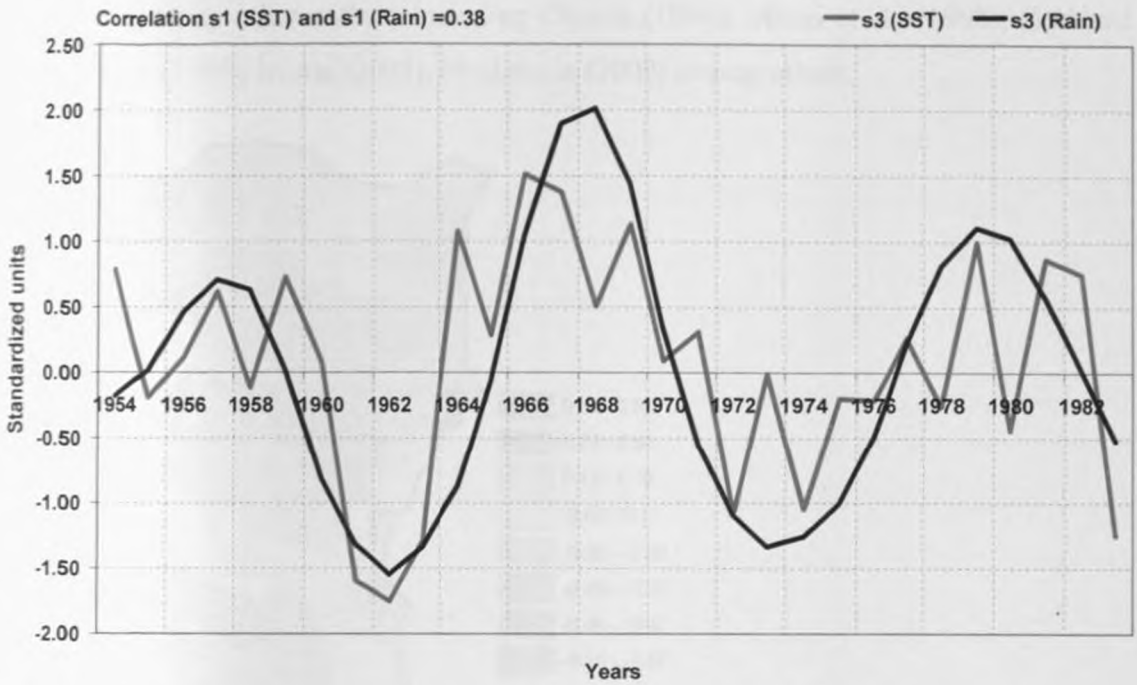
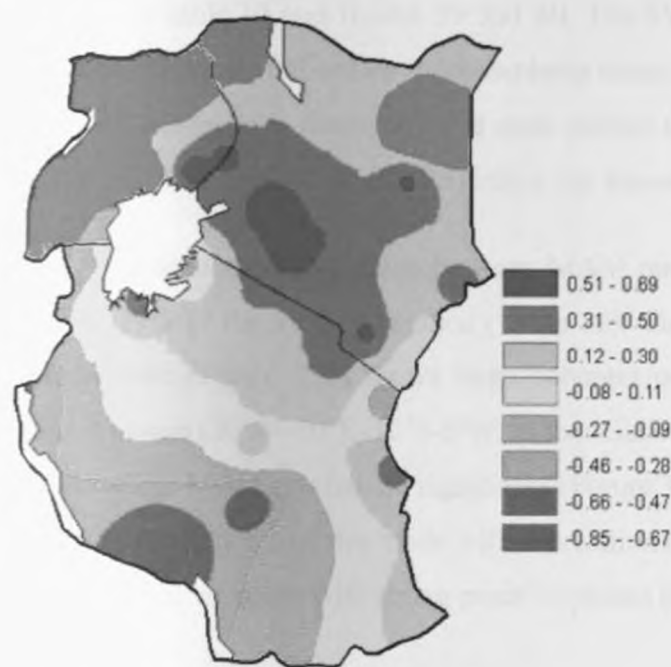


Figure 38c: Time series of expansion coefficients (s_3) of the third SVD mode for March - May rainfall and Indian Ocean SST anomalies

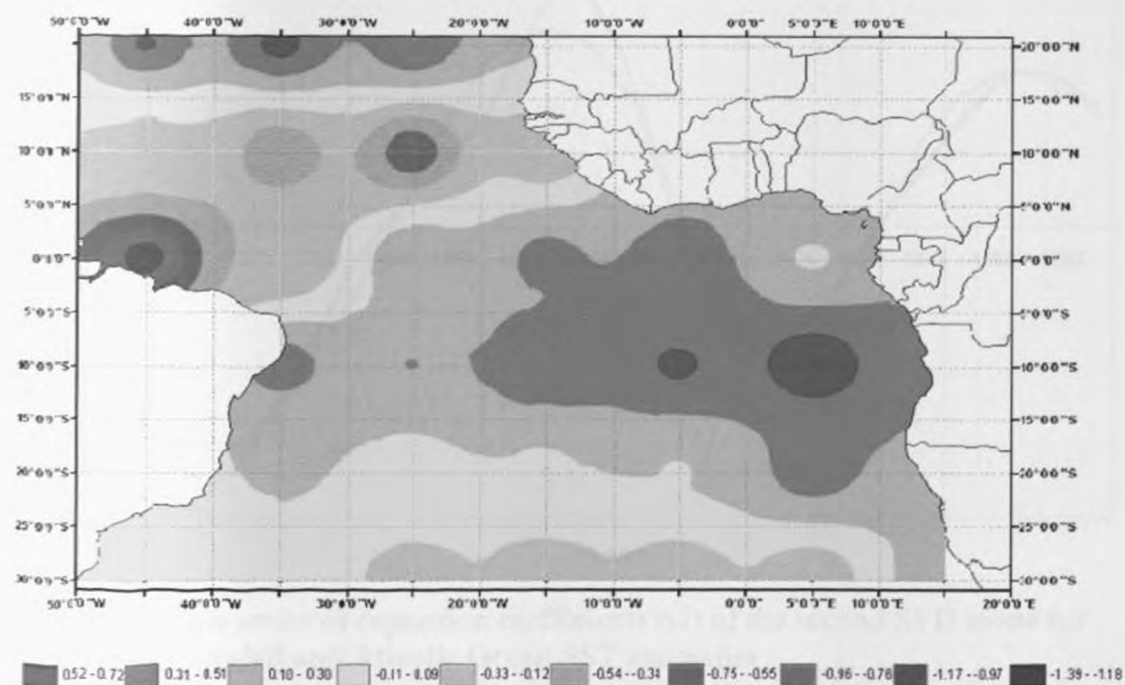
The third SVD-3 mode accounted for 9.9% of the total covariance of the MAM seasonal rainfall and Indian Ocean SSTs. This covariance mode represents positive loadings over the entire Indian Ocean with the highest loadings concentrated in the area between 20°N and 15°S (Figure 38b). This pattern is further associated with strong positive loadings in rainfall over the eastern sector and negative loadings over western sector of East Africa region with strong decadal signal (Figure 38c) in the time series of expansion coefficients (Figure 38c). It is worth noting that although this mode explains relatively low covariance, it was able to still display strong decadal variability for the MAM rainfall season (Rao and Yamagata, 2004; Rao and Behera, 2005; Rao et al., 2007).

By and large, evidently the results from SVD analysis discussed here confirm the complexity of rainfall variability over East Africa during MAM rainfall season. SVD has however delineated three modes that could give more insight into the modes of decadal rainfall variability in East Africa. The dominance of the modes representing zonal SST variability in the Indian Ocean which may be associated with the strong influence of this ocean on the climate of the region has been indicated and consistent with observation

analyses by many other authors including Okoola (1996); Mutai et al., (1998); Goddard and Graham (1999); Mutai (2003); Nyakwada (2009) among others.



(a) MAM rainfall Mode 2



(b) SST Mode 2

Figure 39: Spatial patterns of the second SVD mode (S2) for (a) MAM rainfall and (b) Atlantic Ocean SST presented as homogeneous correlation maps

The SVD results for the MAM rainfall season and Atlantic Ocean SSTs are presented in table 10 and figures 39 and 40. The SVD-1 mode between Atlantic Ocean SSTs and MAM rainfall season fields explains about 43% of total covariance. The spatial pattern of this mode is observed to be quite similar to that of the SVD-1 mode for OND rainfall and Atlantic SST (Figure 23) hence not shown in this section.

The second SVD-2 mode between MAM rainfall and Atlantic Ocean SST fields explains 23% of the total covariance (Table 10). The spatial patterns of Atlantic Ocean SVD-2 mode (Figure 39b) shows large coherent positive loadings over the equatorial Atlantic Ocean (20°W-10°E, 15°S-5°N) in association with large positive loading in most regions where MAM rainfall are significant (Figure 39a). Figure 39c shows time series of expansion coefficients of this mode with correlation of 0.98. The time series further show strong decadal variation with strong positive phases in the 1960s and 1980s.

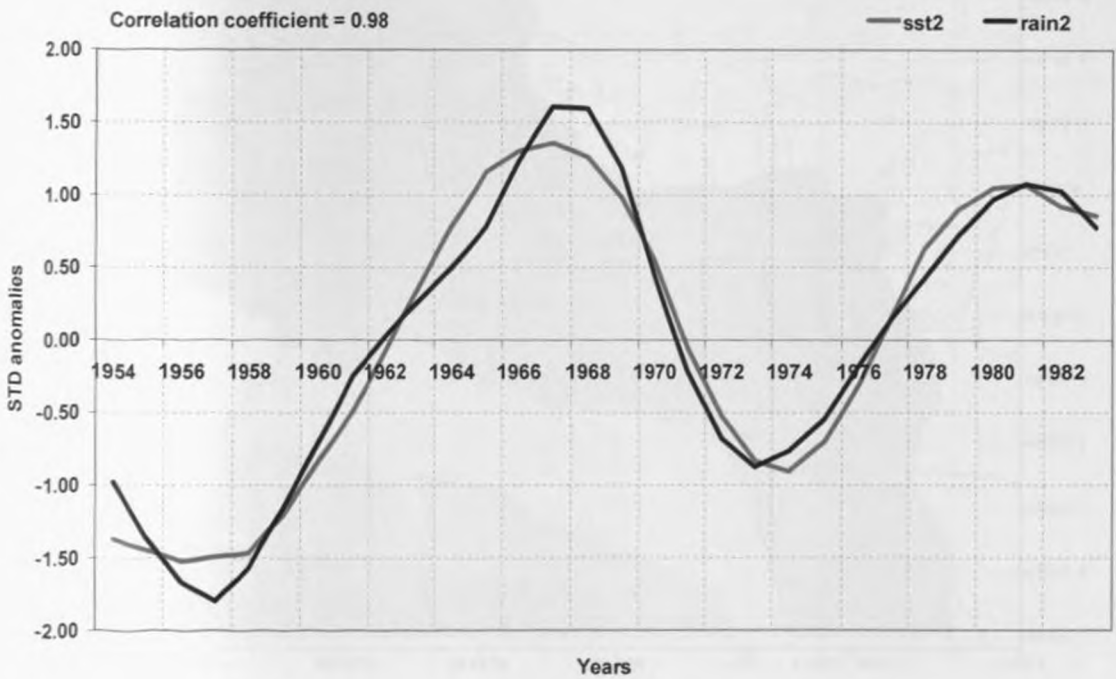
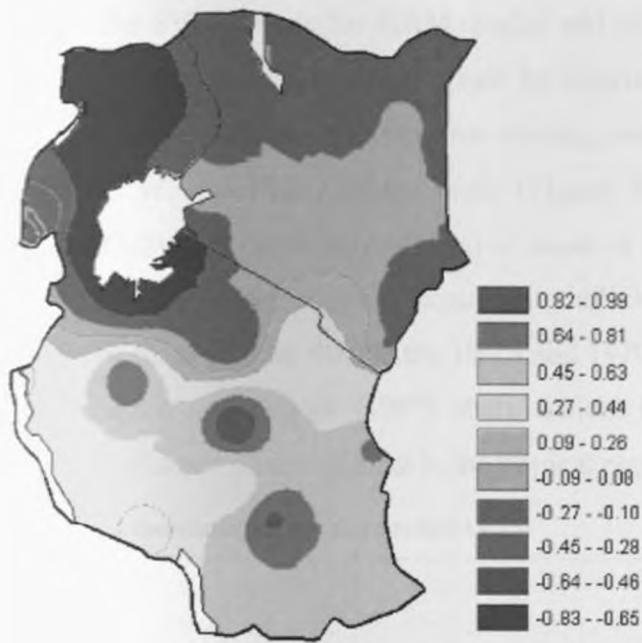
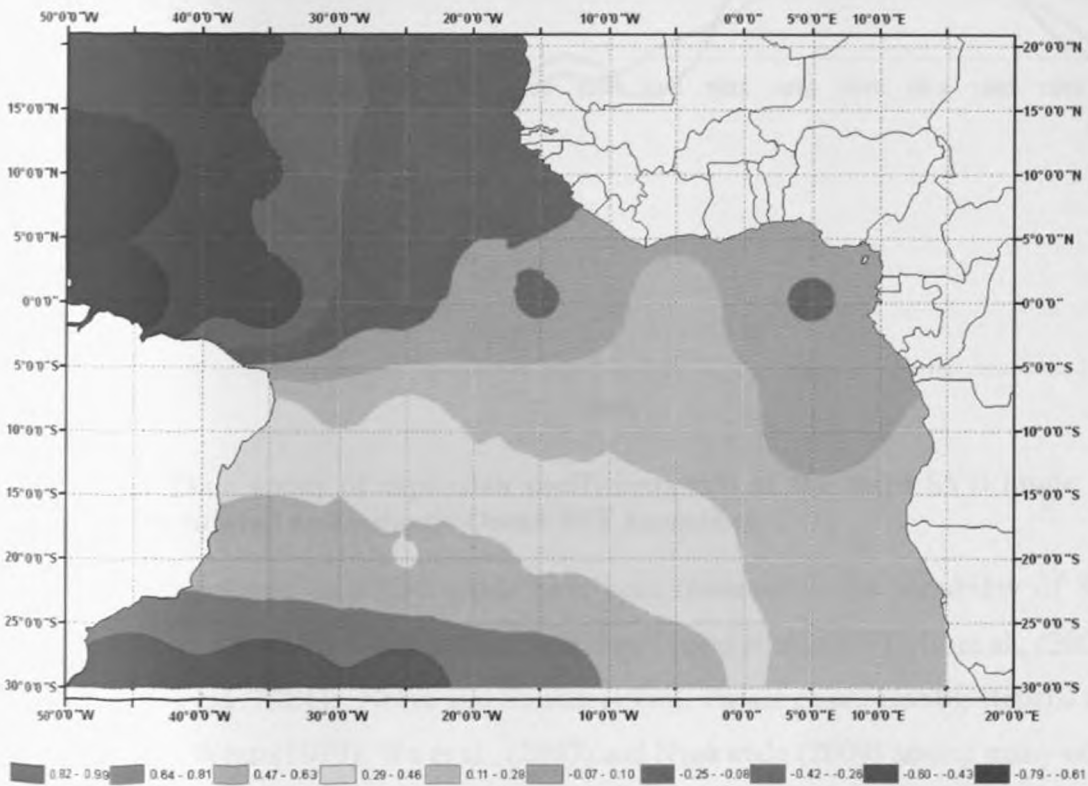


Figure 39c: Time series of expansion coefficients (s2) of the second SVD mode for March - May rainfall and Atlantic Ocean SST anomalies



(a) MAM rainfall Mode 3



(b) SST Mode 3

Figure 40: Spatial patterns of the third SVD mode (S3) for (a) MAM rainfall and (b) Atlantic Ocean SST presented as homogeneous correlation maps

The SVD-3 mode for MAM rainfall and Atlantic Ocean SST that explains 12.8% of the total covariance is characterised by inter-hemispheric positive loading over the southern Atlantic Ocean and negative loading over northern hemisphere with centre at (50°W-35°W, 4°S-15°N) of the basin (Figure 40b). The regional rainfall variability associated by this mode (Figure 40a) is more or less opposite to that of SVD-2 mode (Figure 39a). The time series of expansion coefficients of this mode is characterised with increasing trend (Figure 40c) in the 1960s and 1970s decades. This seems to be consistent with Lindzen and Nigam (1987) study which indicated that such gradients have a stronger influence on the climate in the tropical regions.

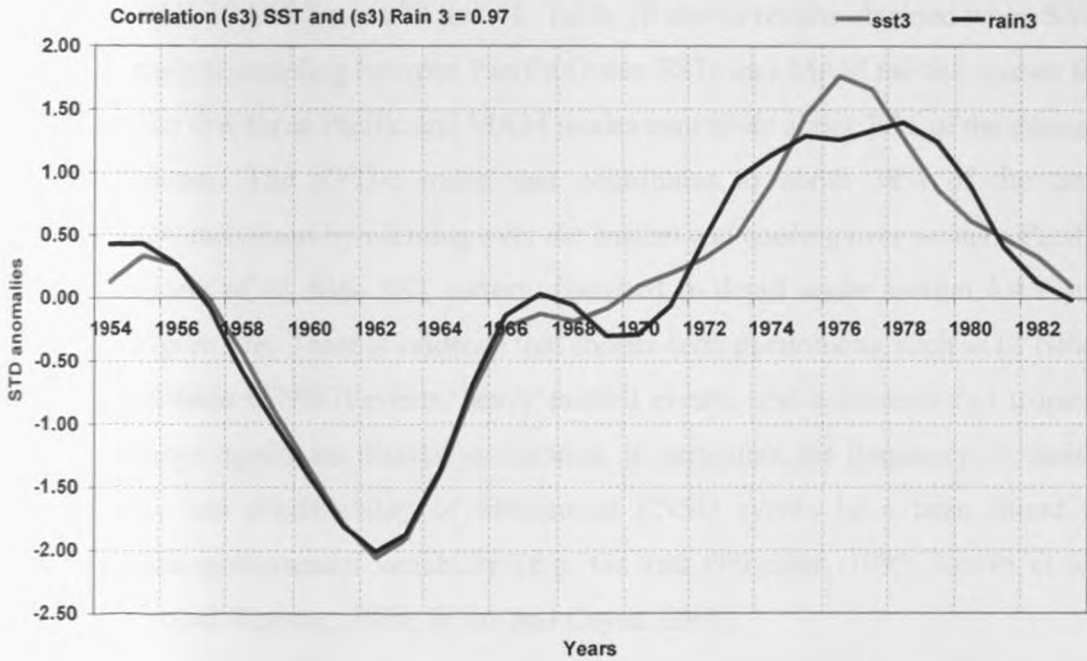


Figure 40c: Time series of expansion coefficients (s3) of the third SVD mode for March - May rainfall and Atlantic Ocean SST anomalies

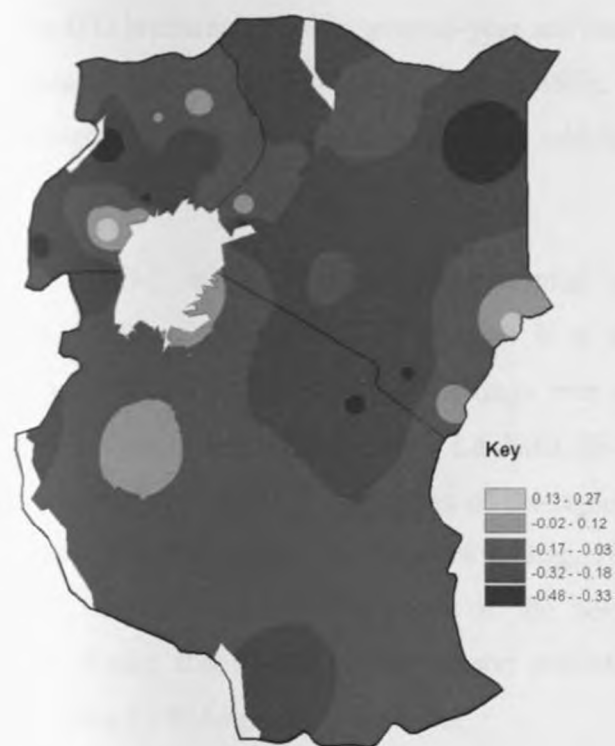
Similar patterns to SVD-3 mode have been observed in the variability of SST over the Atlantic Ocean by many authors including Chang et al., (1997); Li et al., (2007); Moura and Shukla (1981); Nobre and Shukla (1996); Parker et al., (1988); Repelli and Nobre (2004); Weare(1977); Wu et al., (2007) and Nyakwada (2009) among many other authors. Such SST mode has been associated with the development of ENSO (Li et al., 2007; Wu et al., 2007) and has linkage with the North Atlantic Oscillation (NAO) (Wu et al., 2007). It has a strong influence on the climate of the regions neighbouring the

Atlantic Ocean and beyond (Chang et al., 1997; Hastenrath and Heller, 1977; Hu and Huang, 2006; Moura and Shukla, 1981; Parker et al., 1988; Sutton and Hodson, 2007).

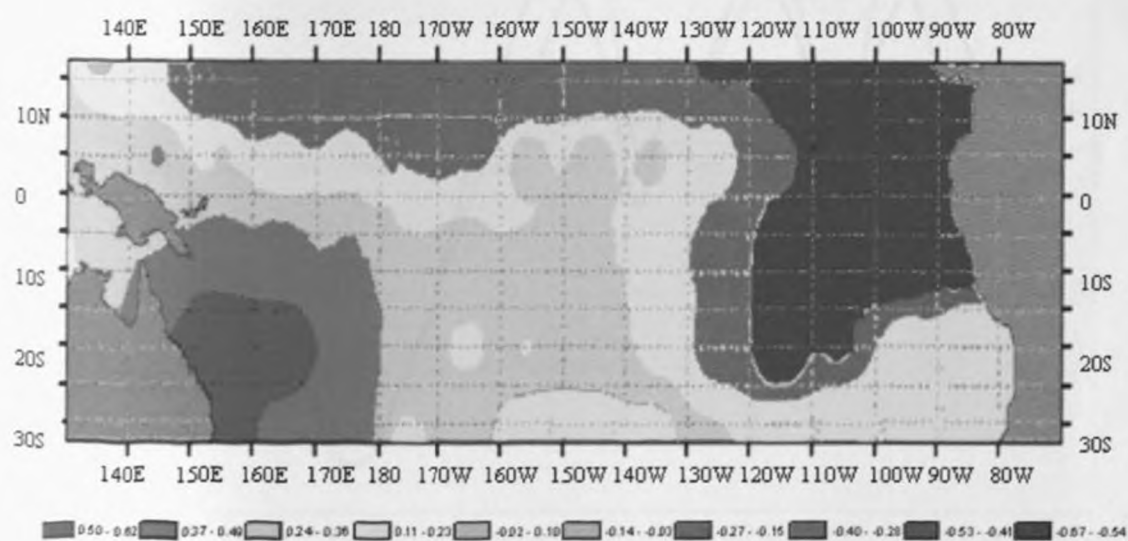
This SVD-3 mode displayed both zonal and meridional SST variability that has been observed to have significant influence on the rainfall over western Africa (Wasilla, 2007). The SSTs patterns over the area represented by the negative pole along the coast of West Africa are negatively correlated to rainfall over parts of the region (Nicholson and Entekhabi, 1987; Okoola, 1996).

The SVD results for the MAM rainfall season and Pacific Ocean SSTs are presented in table 10 and figures 39 and 41. Table 10 shows results obtained when SVD was used to analyze coupling between Pacific Ocean SSTs and MAM rainfall season for East Africa. The first three Pacific and MAM modes contribute about 79% of the decadal rainfall covariance. The SVD-1 mode that contributes to about 38% of the total covariance is characterized by warming over the eastern and cooling over western Pacific Ocean reminiscent of El Niño SST pattern discussed in detail under section 4.4.1 and presented in Figure 27b. There is evidence that shorter-term phenomena, such as El Niño-Southern Oscillation (ENSO) events, heavy rainfall events, and occurrences of tropical cyclones, undergo significant decadal modulation. In particular, the frequency, intensity, spatial pattern, and predictability of interannual ENSO events have been found to undergo decadal-multidecadal variability (e.g. Gu and Philander, 1995; Kestin et al., 1998; Torrence and Webster, 1999; White and Cayan, 2000).

A number of researchers found that the dominant pattern of SST variability in the extratropical North Pacific varied at time scales of one or more decades and that this SST pattern is associated with the North Pacific Oscillation (NPO) (Walker, 1925; Walker Bliss, 1932) in the atmosphere. This dominant SST pattern is known as the Pacific Decadal Oscillation (PDO; Mantua et al., 1997). The Interdecadal Pacific Oscillation (Power et al., 1999) is a Pacific-wide SST pattern covering both hemispheres, showing a similar pattern of variability to the PDO in the North Pacific (Folland et al., 2002).



(a) MAM rainfall Mode 2



(b) SST Mode 2

Figure 41: Spatial patterns (S2) of the second SVD mode for (a) March - May rainfall (b) Pacific SST presented as homogeneous correlation maps.

The IPO is characterized by year-to-year and longer-term, predominantly decadal-to-multidecadal, variability of the Pacific Ocean SSTs, with opposite phases between the tropical-subtropical Pacific Ocean and the mid-latitude Pacific Ocean in both hemispheres (Parker et al., 2007).

The SVD-2 mode between MAM rainfall and SST fields for the Pacific contributes to about 25% of the covariance. It is characterized by strong negative loadings over the eastern and positive loadings over western equatorial Pacific Ocean (Figure 41b). This is the cold phase of La Niña SST pattern that is associated with deficient seasonal rainfall over most parts of the region (Tourre and Rasmusson, 1984; Enfield, 1989; Ropelewski and Halpert, 1989; Bigg, 1990; Indeje 2000; Mutemi, 2003). Njau (1987, 2005) observed that most of the severe droughts over Kenya were experienced during the MAM rainfall season preceding El-Niño event and rarely in MAM following El-Niño peak in December.

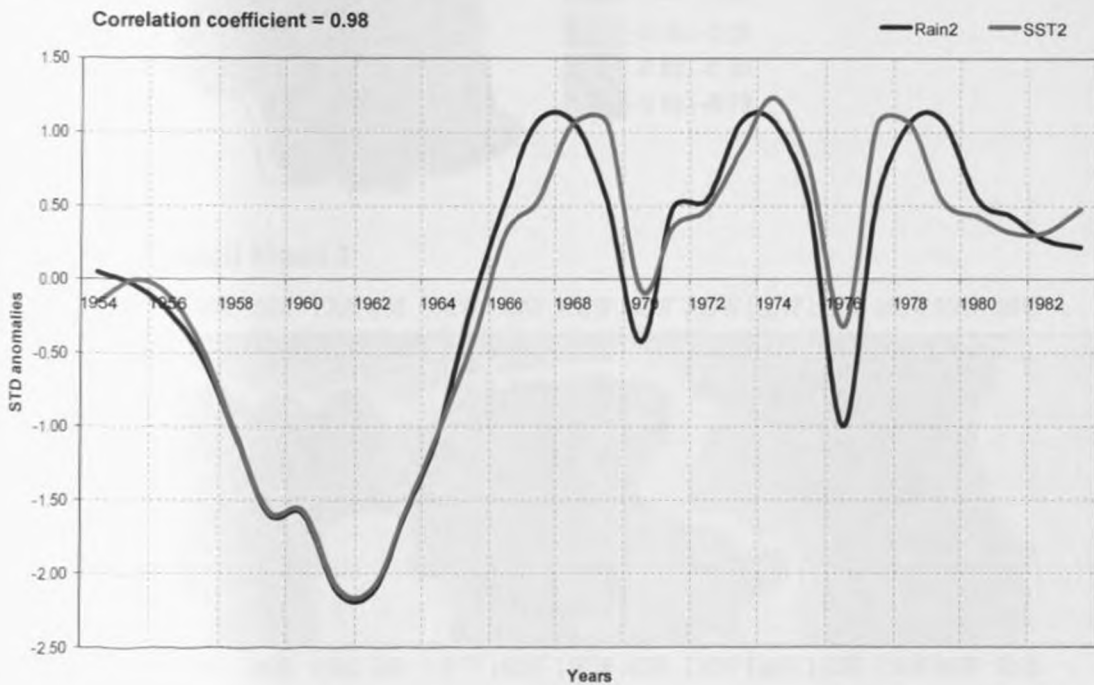
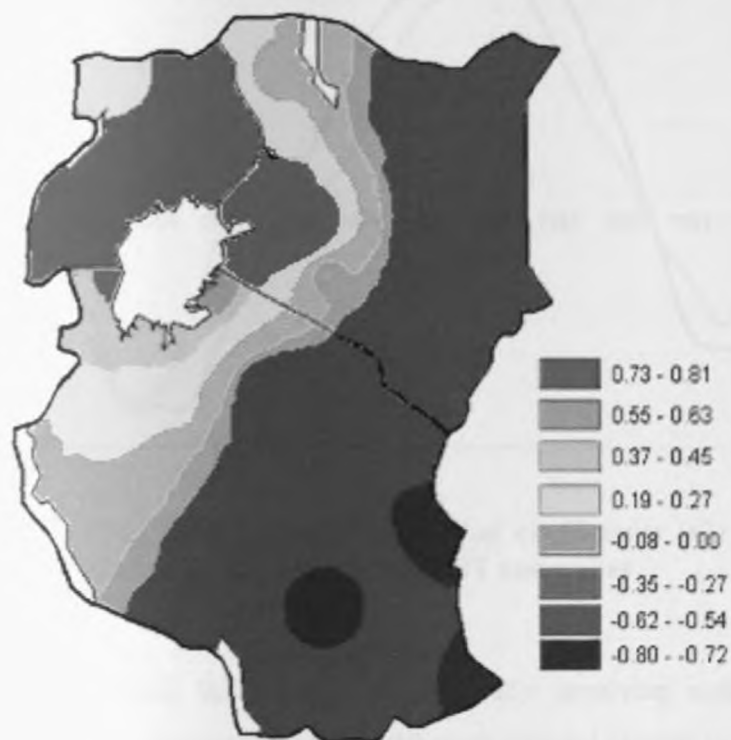


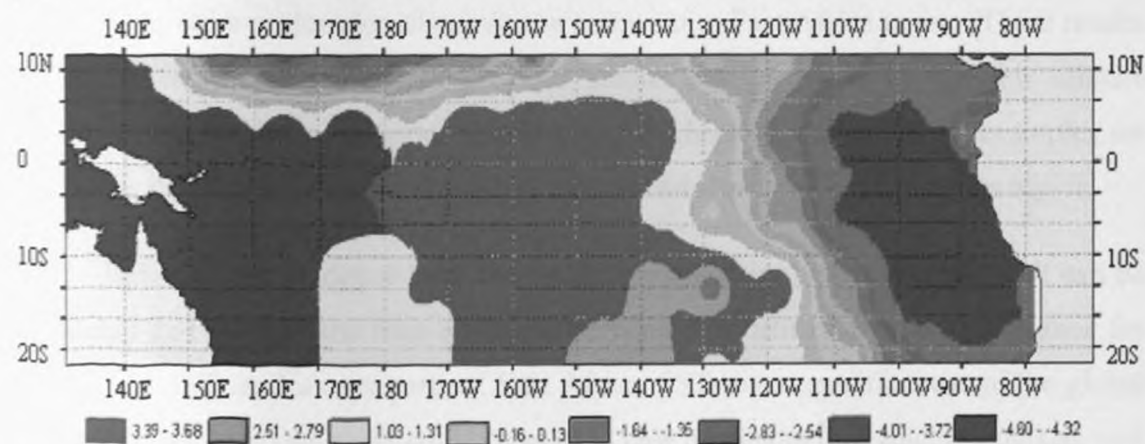
Figure 41c: Time series of expansion coefficients (s_2) of the second SVD mode for MAM rainfall and Pacific Ocean SST anomalies.

The SVD-3 for MAM rainfall and SST fields for the Pacific Ocean contributes overall 17% of the total covariance. It is characterized by unique negative loadings over

the eastern and western with positive loadings over the central equatorial Pacific Ocean (Figure 42b). This 'Modoki' El Niño like pattern discussed in details in section 4.4.2, causes similar decadal climate patterns over the region.



(a) MAM rainfall Mode 3



(b) SST Mode 3

Figure 42: Spatial patterns (S3) of the third SVD mode for (a) March - May rainfall (b) Pacific SST presented as homogeneous correlation maps.

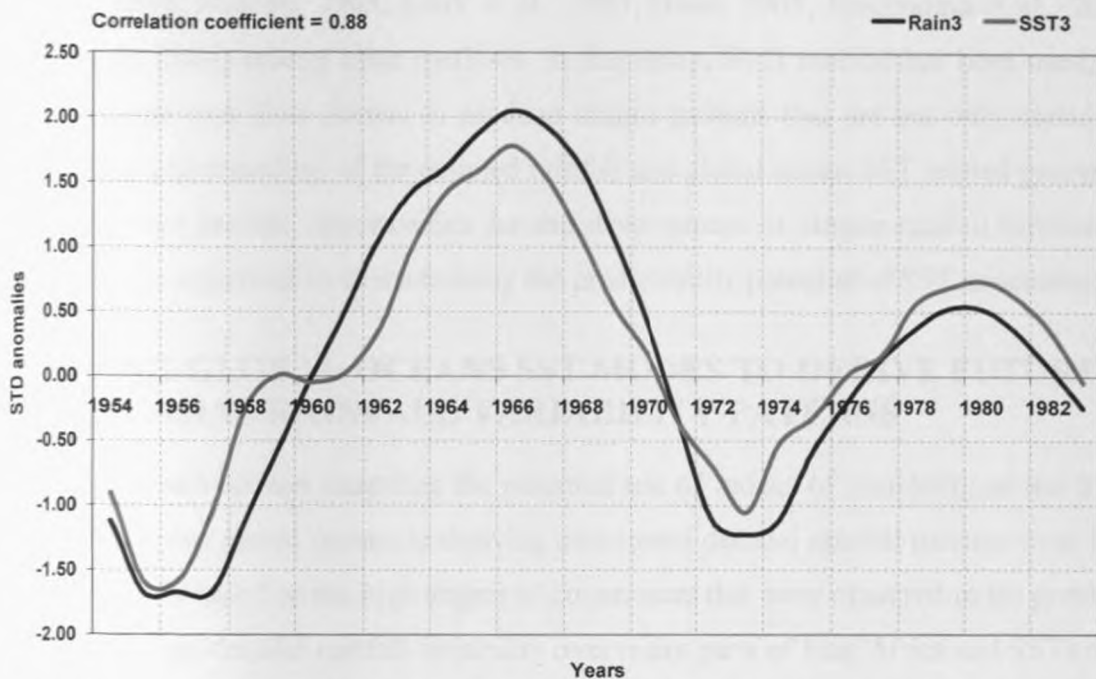


Figure 42c: Time series of expansion coefficients (s3) of the third SVD mode for MAM rainfall and Pacific Ocean SST anomalies

Overall, this section of the study involving comprehensive empirical (SVD) analyses has demonstrated that although decadal rainfall variability modes were generally common at all locations, some strong signals were only restricted to specific areas. But these signals were evident for all seasons over the entire East Africa region. These results are consistent with a number of previous studies that have shown that few climate extremes such floods and droughts spread over the whole of eastern Africa, examples are the floods of the early 1960s, and 1997/98 that extended over most parts of the region.

Based on the evidence from the results presented in this section so far, it can be concluded that for the first time SVD has been used to delineate strong covariance for rainfall and SST modes over parts of East Africa. SSTs over specific areas of the global oceans delineated in this study could be used as new predictors in prediction tools as well as for general improvement of numerical model skill, prediction and early warning of decadal rainfall variability. The use of simple correlation analysis and CCA provided some lead to such linkages but such linkages have been spread over many areas of the same basin often leading to the use of many dependent SST predictors (Ogallo, 1988);

(Indeje, 2000; Mutemi, 2003; Clark et al., 2003; Owiti, 2005; Singhrattna et al., 2005; Nyakwada, 2009) among other methods. In this study, SVD method has been used, for the first time over East Africa, to produce unique patterns that are not only useful for improving understanding of the coupled rainfall and global ocean SST related processes but SVD also provide opportunities for the development of simple rainfall forecasting tools. This is important in characterizing the predictability potential of SST anomalies.

4.5 USING GLOBAL OCEANS SST MODES TO DERIVE FUTURE DECADAL RAINFALL VARIABILITY PATTERNS

This sub-section examines the potential use of modes of variability of the SSTs over the various global oceans in deriving anticipated decadal rainfall patterns over East Africa. This is based on the high degree of covariances that were observed in the previous sections among decadal rainfall variability over many parts of East Africa and SSTs over various parts of the global oceans. The results for the specific seasons are presented and discussed in the following sections. The SVD modes of SST from the various oceans were used to extrapolate decadal rainfall variability patterns for specific regions of East Africa using multiple regression technique. The details of the method can be found in Camberlin and Philippon, (2001), and Hsieh (2004) as highlighted in section 3.5.1. The thirty year period 1954-1983 was used for fitting and training the regression models, while the data for the period 1984-2008 was used to test the skill of regression models, before the model was used to extrapolate decadal rainfall estimates beyond 2009. It should be noted that when the data is smoothed by a nine-point binomial coefficient filter, four years are smoothed out in the beginning and end of the training period and hence use of the period 1954-1983 rather than the 1951-1930.

4.5.1 RESULTS FROM DECADAL RAINFALL NOW CAST FOR SEPTEMBER – DECEMBER SEASON

Figure 43a and 43b gives the time series of the results obtained for two representative zones 1 and 3 during September – December (SOND) period that is a primary rainfall season (short rains) over the region. It is evident from Table 11 that, although there were significant variations of the skill of the models from region to region, as represented by the values of Heidke Skill Score (HSS), the HSS values were ≥ 0.30 at

all locations indicating the models could provide forecasts with useful skills. The results further indicate substantial variation of the model skill within various regions with decadal rainfall variance explained by SST modes ranging from 39% to 78%. The skill scores of the Multiple Linear Regression (MLR) models are also verified using contingency table for observations versus forecasts in each zone for 1984-2004 testing period. The percentage correct forecast in all categories was found to be between 38% and 64%. In post agreement scores, the models were found to be unbiased towards forecasting enhanced (wet decades) or depressed (dry decades) rainfall. The highest correct Percentage for forecasting dry was 70% (Zones 12), normal was 80 % (zones 12) and 85 % (zone 5 and 9) for wet. The nowcast prediction was however able to clearly delineate the wet and dry decades as is evident Figures 43a and 43b. This can provide very useful planning tool for mainstreaming rainfall risks in planning and management of all rainfall sensitive socio-economic sectors of East Africa.

Table 11: Assessment of the skill of the September -December regression models

Zone	Pearson's correlation	RMSE	Hit Score	Bias	HSS	Mean Absolute Error
Zone1	0.67	20.3	65.0	3.40	0.47	17.0
Zone2	0.62	10.0	63.0	0.03	0.44	8.4
Zone3	0.32	14.5	57.5	0.06	0.36	11.2
Zone4	0.53	14.1	57.5	0.06	0.35	12.3
Zone5	-0.66	11.9	12.5	1.15	0.63	9.4
Zone6	0.54	13.1	50.0	-0.20	0.35	11.2
Zone7	0.41	11.4	60.0	1.60	0.41	0.93
Zone8	0.46	18.0	48.0	-0.29	0.32	15.4
Zone9	0.46	16.2	62.5	0.72	0.44	12.6

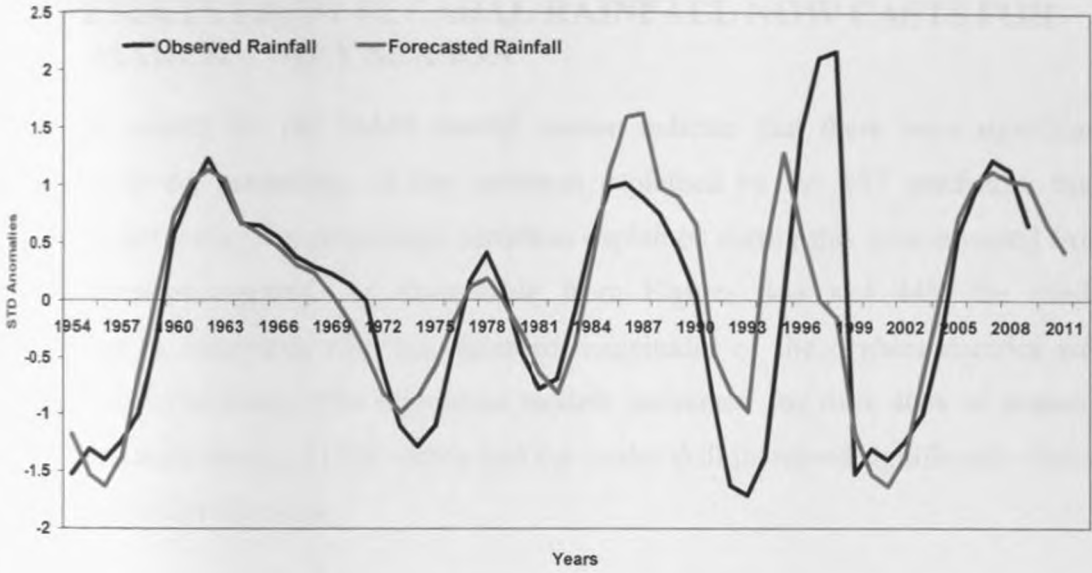


Figure 43a: Time series plot of the observed and model estimates of the September – December decadal rainfall for zone 1 as represented by Mbeya

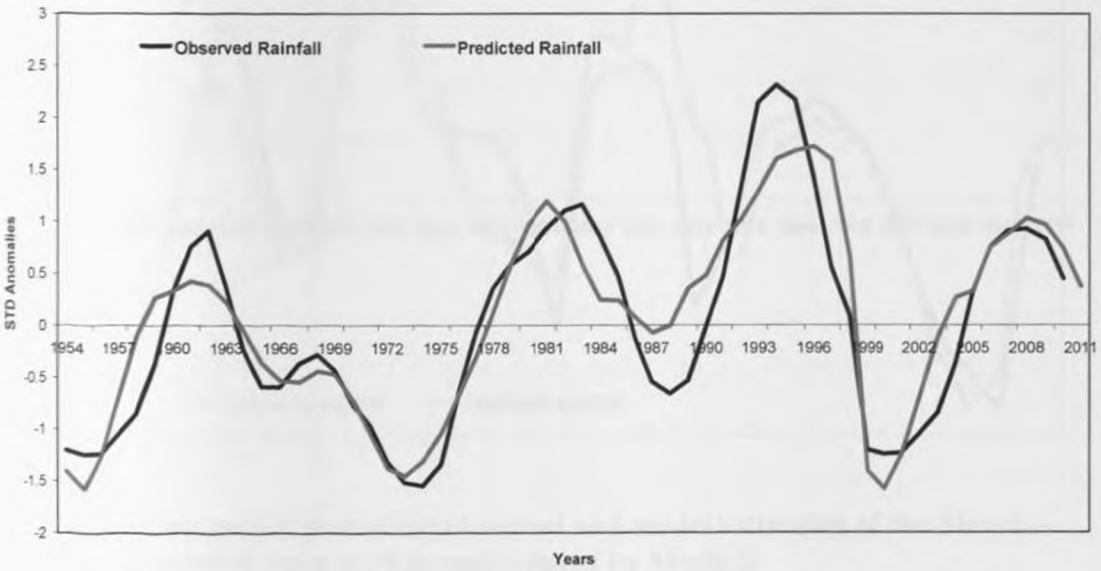


Figure 43b: Time series plot of the observed and model estimates of the October – December decadal rainfall for zone 3 as represented by Dodoma

In section 4.5.2, results for March – May (MAM) decadal rainfall prediction using multiple regression analysis is discussed.

4.5.2 RESULTS FROM DECADAL RAINFALL NOW CASTS FOR MARCH – MAY SEASON

The results for the MAM rainfall season indicate that there were significant differences in the percentage of the variances explained by the SST predictors from location to locations. The percentage variances explained during this season varied from 40-70% between regions. As discernable from Figures 44a and 44b, the model performance is consistent with the observed magnitudes of the dry/wet decades well estimated in most zones. The regression models accounted for over 40% of season's rainfall variability during MAM season and the model skill increased significantly during the strong ENSO/IOD years.

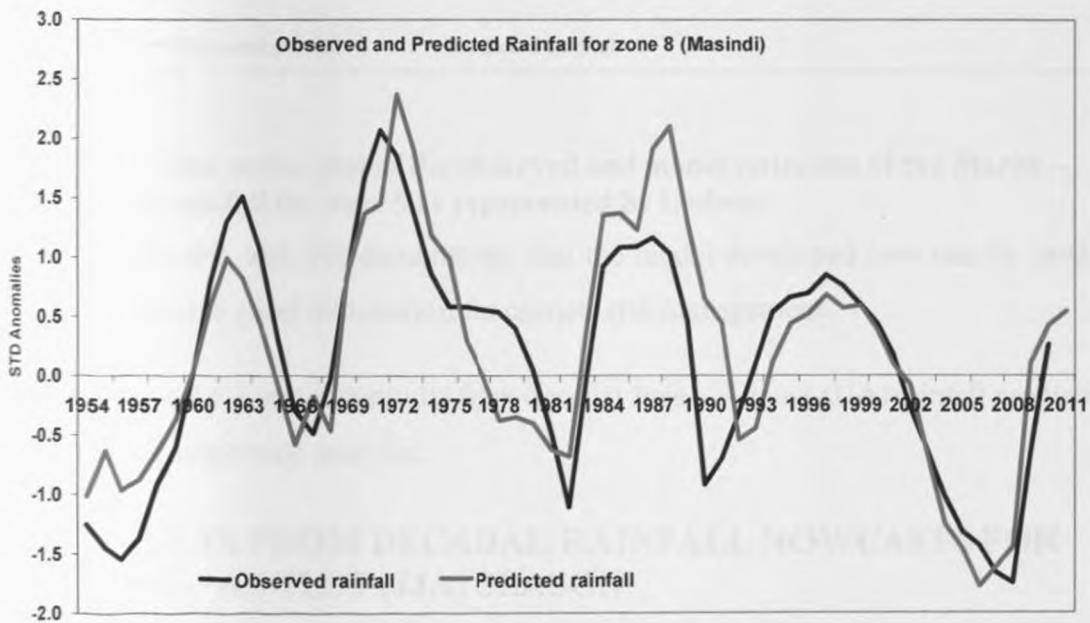


Figure 44a: Time series plot of the observed and model estimates of the March – May decadal rainfall for zone 8 as represented by Masindi

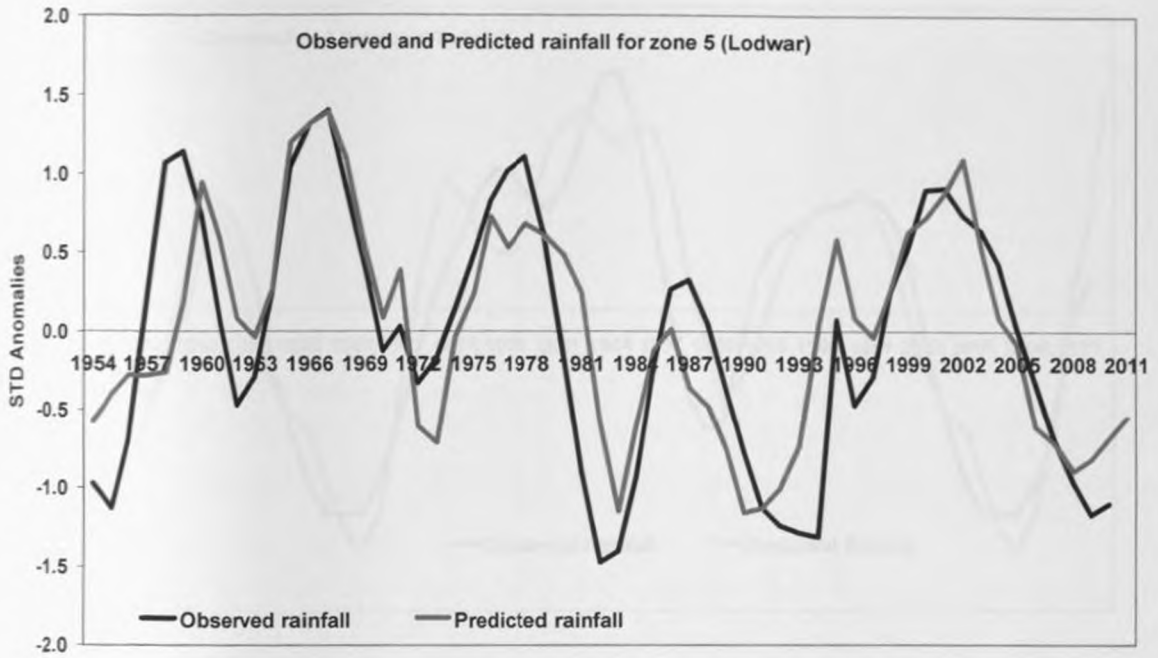


Figure 44b: Time series plot of the observed and model estimates of the March – May decadal rainfall for zone 5 as represented by Lodwar

Figures 44a and 44b demonstrate that the model developed here can be used to provide reasonable good information for climate risk management.

Section 4.5.3 presents results from decadal June – August (JJA) rainfall prediction using multiple regression analysis.

4.5.3 RESULTS FROM DECADAL RAINFALL NOWCASTS FOR JUNE – AUGUST (JJA) SEASON

Figures 45a and 45b show some examples of observed and predicted decadal rainfall for some locations in East Africa. Both models capture the decadal peaks fairly well in most locations. There was also significant region to region variability in the percentage of the rainfall variance accounted for by modes of SST variability. The results from the decadal rainfall nowcast for JJA season had Hielde Skill Score of 0.60 over zone 2 and hence reasonable skill.

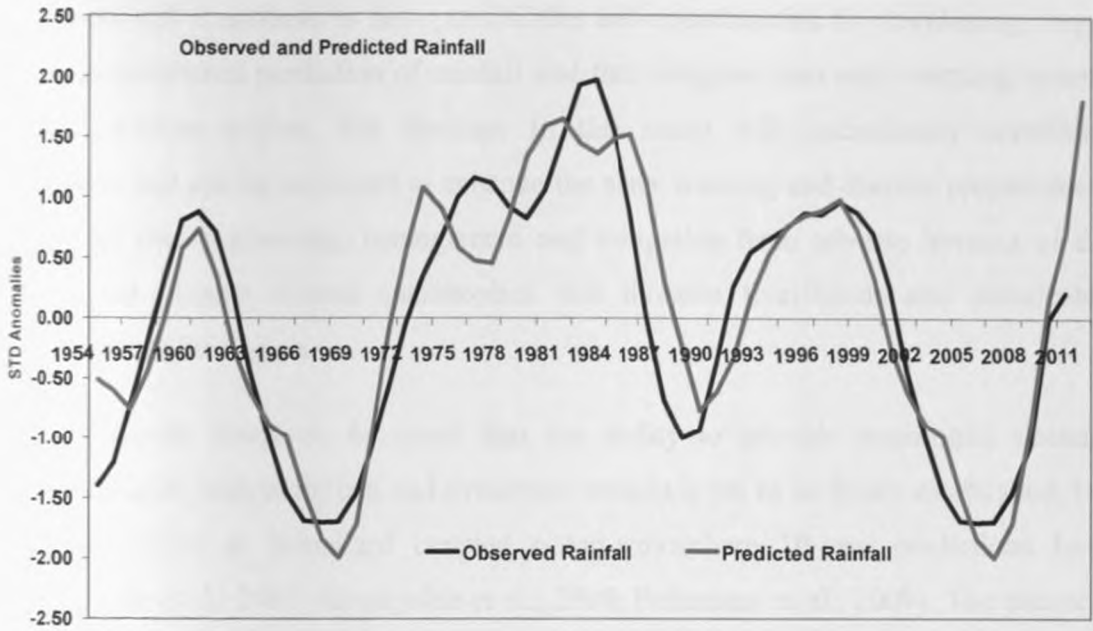


Figure 45a: Time series plot of the observed and model estimates of the June – August decadal rainfall for Kisumu

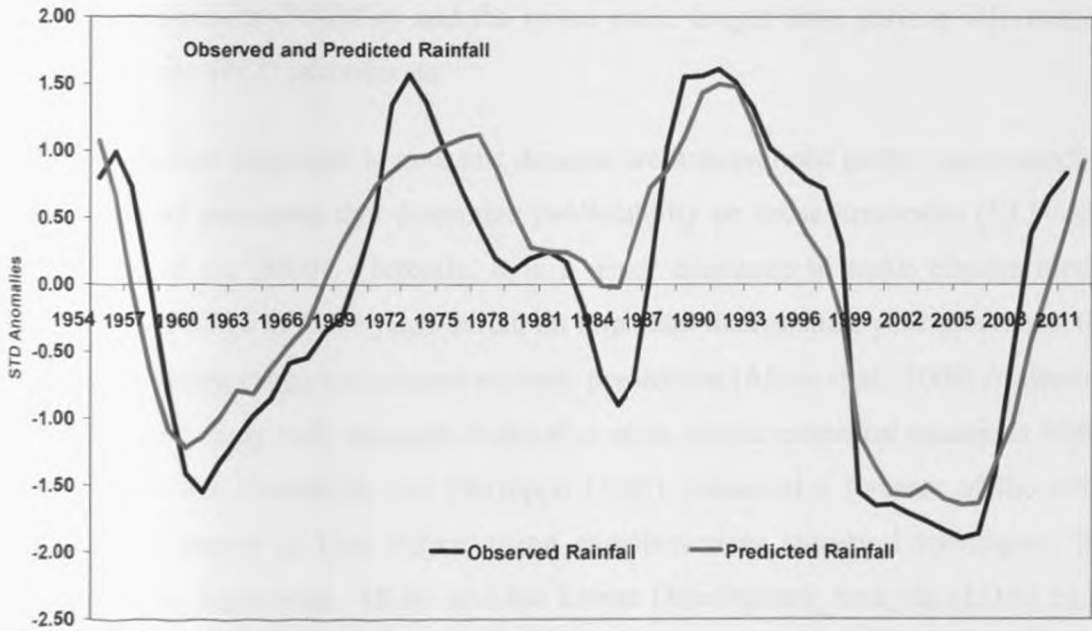


Figure 45b: Time series plot of the observed and model estimates of the June – August decadal rainfall for Mbarara

The results of section 4.5 have therefore indicated that for the first time it is possible to provide some reliable attempts of decadal rainfall prediction over the region.

These tools will contribute to new possibilities and opportunities for developing longer lead time operational prediction of rainfall and thus integrate into early warning system for East African region. The findings in this study will undoubtedly contribute information that can be advanced to enhance the early warning and disaster preparedness systems for timely planning, management and mitigation from adverse impacts of the weather and climate related catastrophes that threaten livelihoods and sustainable development in the region.

It should, however, be noted that the ability to provide meaningful decadal predictions using both empirical and dynamical models is yet to be firmly established, but pioneering efforts at initialized coupled ocean-atmosphere 10-year predictions have begun (Smith et al., 2007; Keenlyside et al., 2008; Pohlmann et al., 2009). The prospect of decadal prediction and its recognized importance has led, in part, to the initiation, in several countries, of climate services intended to bridge the gap between the short-term, seasonal-to-interannual climate information provided by the National Meteorological and Hydrological Services (NMHSs) and the broad scale, longer time horizon information considered by the IPCC assessments.

It is further important to note that decadal predictions need proper understanding of the important processes that determine predictability on these timescales (CLIVAR, 2007; Haines et al., 2009). Currently, it is a major challenge to make climate model forecasts with a range of 1–10 years ahead, an important intermediate period between the seasonal forecasting range and climate scenario predictions (Alves et al., 2004; Anderson, 2008). Thus this study only attempts to develop some simple empirical equations based on SST predictors. Camberlin and Philippon (2001) presented a forecast of the 2001 MAM rainfall season in East Africa, using complementary statistical techniques, the Multiple Linear Regression (MLR) and the Linear Discriminant Analysis (LDA) as in Folland et al., (1991). Their prediction scheme involved the use of Sea Surface Temperatures (SST) indices and other atmospheric predictors.

This study, therefore, provides for the first time some break through in providing decadal scale rainfall estimates for East Africa with specific regional details. The results from the study indicated that SVD derived SST modes could provide realistic decadal

rainfall now-casts. Else where in the world, attempts to provide forecast for the first year of the decade referred to as a now-cast of the decadal state variations has been provided by Alves et al., 2004; Smith et al., 2007; Anderson., 2008; Haines et al., 2009; among others.

In the next section, the Regional Climate Model (RCM), PRECIS, simulations are evaluated to examine if the model produces realistic outputs as well as climate change scenarios in comparison with observed decadal climate variability for various parts of East Africa.

4.6 DECADAL PREDICTIONS AND REGIONAL CLIMATE SCENARIOS DERIVED FROM PRECIS SIMULATIONS

This section presents the results from regional simulations that were generated using the PRECIS model. PRECIS was used in this study to generate regional climate change scenarios which were compared to the predicted decadal rainfall for the period 2010-2020 that were presented in section 4.5. The model output were extracted at similar latitude and longitude with the various observed stations used as representative for the climatological zones, subjected to binomial filter before compared to predicted values.

In the time between the second (IPCC, 1996) and fourth (IPCC, 2007) assessment reports, there has been a marked increase in the number of RCM simulations. However, there have been very few RCM studies done over East Africa (Sun et al., 1999a, 1999b; Indeje et al., 2000; Anyah 2005; Anyah et al., 2006; Anyah and Semazzi, 2006a, 2006b; Sabiti, 2008). Sun et al., (1999a, 1999b) used a 60 km resolution RCM (RegCM2 from NCAR, USA) to investigate rainfall over eastern Africa. Neither of these studies addressed future climate changes beyond 2010. Furthermore, climate change studies of the region have mostly focused on the changes in mean values over some past decades. However, it is now being increasingly recognized that the manifestations of such changes in the occurrence of extreme weather and climatic events, particularly on the regional and local scales, are of paramount importance in assessing the socio-economic impacts of climate.

The PRECIS simulations are first compared with output of the driving GCM output in order to evaluate the impact of increase in resolution. First, a number of PRECIS test simulations were performed to examine general sensitivity to domain size (Denis et al., 2002). In the end, the domain which covered the main regional and large scale features i.e. East Africa and Ethiopian Highlands, western Indian Ocean, Tropical (Congo) rainforest, large inland lakes (Victoria, Tanganyika and Malawi) reproduced more realistic distribution of simulated precipitation and other meteorological fields.

Table 12: Mean 1.5 m surface air temperature statistics for RCM and GCM for land points only over the region.

	DJF	MAM	JJA	OND
Mean:				
OBS	24.5	21.7	17.3	23.5
GCM	22.8	20.2	16.3	22.1
RCM	23.2	21.0	16.9	22.4
Spatial standard deviation:				
OBS	2.2	2.6	3.7	2.7
GCM	1.7	2.8	2.9	3.1
RCM	1.3	2.4	2.3	2.4
RMS error:				
GCM	2.3	1.5	1.7	1.9
RCM	2.1	1.3	1.6	1.4
Spatial correlations:				
RCM-OBS LS	0.51	0.74	0.75	0.81
GCM-OBS LS	0.73	0.80	0.83	0.87
RCM-GCM LS	0.91	0.89	0.91	0.98
RCM-OBS MS	0.72	0.71	0.70	0.69
GCM-OBS MS	-0.76	-0.80	-0.77	-0.78
RCM-GCM MS	-0.69	-0.72	-0.74	-0.75

Key : LS – Large-scale

MS – Meso-scale

4.6.1 SURFACE AIR TEMPERATURE

Table 12 gives summary statistics of results obtained from the simulation of mean surface air temperature by the GCM and PRECIS models. The CRU climatological data available over land points at the $0.5^\circ \times 0.5^\circ$ resolution (New *et al.*, 1999) are also shown in the same table 12. For all the analysis in this study, the GCM and CRU data were interpolated to the RCM grid, and only land points are used in the discussion of the results.

It is important to note that the CRU data may suffer from errors in certain areas due to inadequate station coverage (New *et al.*, 1999). Results from control simulation of mean surface air temperatures over the land show that the PRECIS output are closer to the observed CRU values compared to the HadAM3P in all seasons. The differences range from 0.4°C in JJA to 1.3°C in DJF between PRECIS and CRU, but 1°C to 1.7°C between GCM (HadAM3P) and CRU. The results from root-mean-square error (RMSE) show that the largest errors (about 2°C) in both PRECIS and HadAM3P are found in DJF. In all seasons the HadAM3P had a higher spatial standard deviation in temperature than PRECIS. This may be attributed to the increased fine-scale detail associated with the land surface and topography that are resolvable in PRECIS and not HadAM3P.

Table 12 further shows results obtained from the spatial correlations between the various large-scale components, as well as the mesoscale components of the PRECIS and the CRU climatology. Note that the large-scale component is obtained through aggregation of the data to the scale of the HadAM3P, by averaging all land points lying within each HadAM3P grid box, and the mesoscale component is obtained by calculating the difference between the large-scale component and the original data. Both the PRECIS and HadAM3P capture the basic large-scale temperature patterns in all seasons, with correlations above 0.51. The large-scale patterns of the PRECIS and driving HadAM3P are highly correlated (maximum correlations about 0.98). The results further showed that PRECIS captured the spatial patterns of the observed mesoscale signal. These impacts of improved resolution in the PRECIS are clearly depicted in Figure 46c where the spatial difference between the PRECIS and HadAM3P fields during December-February (DJF) was computed.

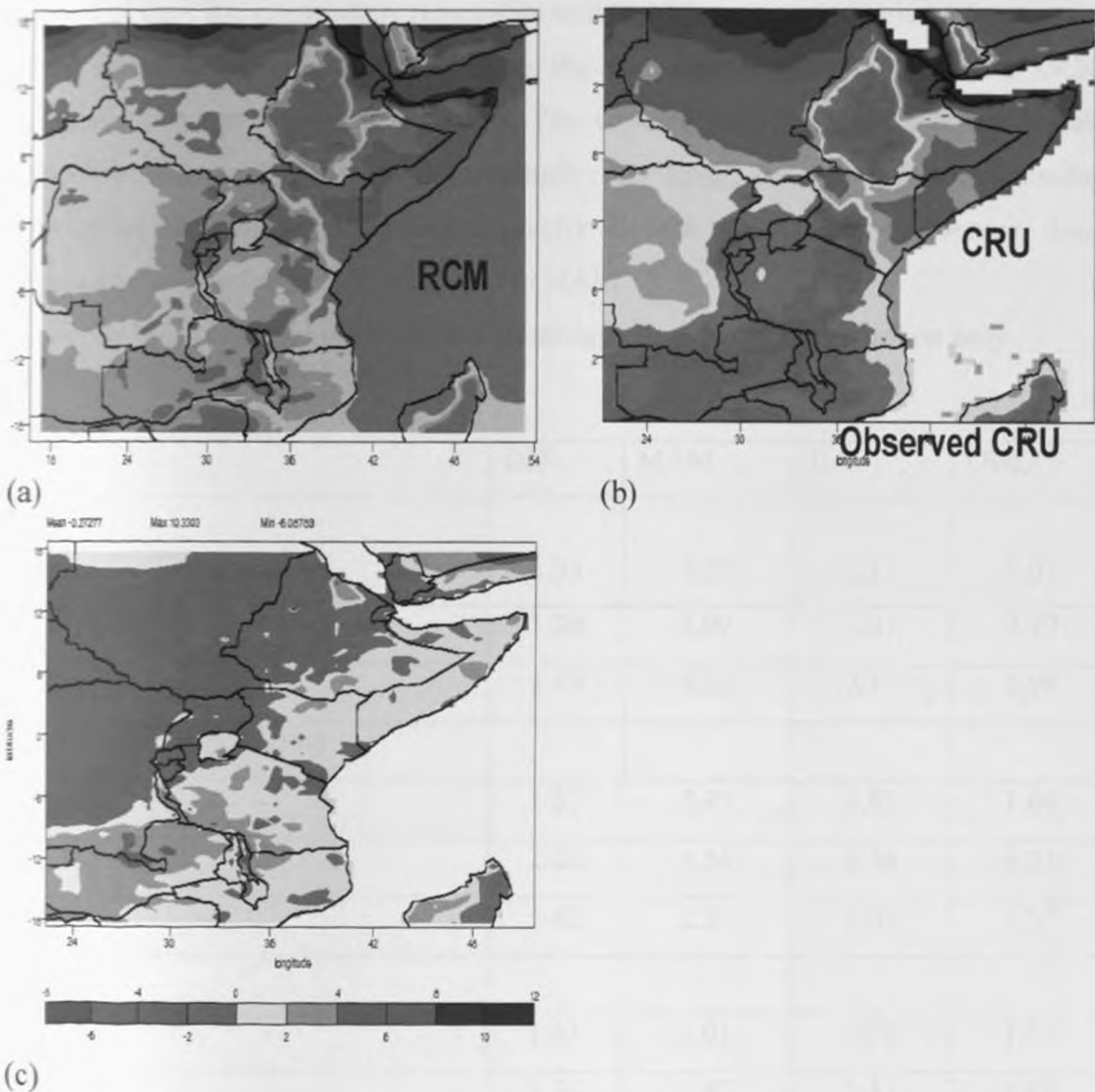


Figure 46: Mean surface temperature 1961-1990 (a) PRECIS (b) CRU (c) differences between CRU and PRECIS aggregated to the grid of the PRECIS

4.6.2 PRECIPITATION

Table 13 shows the results of spatial correlations between the various large-scale components, as well as the mesoscale components of the PRECIS and the CRU climatology. The PRECIS simulated precipitation amount is greater than the HadAM3P over the land in all seasons with largest absolute differences in DJF and MAM (i.e. 0.1 and 0.4 mm/day respectively). The root-mean-square error results show that the largest errors in precipitation are in MAM for both the GCM and RCM (1.87 mm/day for the RCM and 3.01 mm/day for the GCM). The GCM and RCM capture the large-scale

patterns of the CRU climatology reasonably well (the lowest correlation is +0.64), but the RCM shows better skill in reproducing the mesoscale component than the GCM (correlations range from 0.35 to 0.48). The correlations of the observed mesoscale component of precipitation with orography are small, as are the corresponding correlations between the RCM and orography. In both the model and observed, these correlations are larger in OND compared to MAM.

Table 13: Seasonal land precipitation (mm/day) statistics for land points only aggregated to the RCM domain

	DJF	MAM	JJA	OND
Mean:				
OBS	1.33	4.52	2.11	3.01
GCM	1.29	3.99	2.01	2.79
RCM	1.43	4.12	2.19	2.98
Spatial standard deviation:				
OBS	1.57	2.45	0.82	1.64
GCM	2.02	3.54	0.54	2.21
RCM	1.42	2.37	0.67	1.57
RMS error:				
GCM	1.53	3.01	0.57	1.77
RCM	1.36	1.87	0.33	1.01
Spatial correlations:				
RCM-OBS LS	0.67	0.81	0.78	0.87
GCM-OBS LS	0.64	0.70	0.72	0.82
RCM-GCM LS	0.69	0.87	0.92	0.93
RCM-OBS MS	0.35	0.40	0.45	0.48
GCM-OBS MS	0.26	0.35	0.24	0.40
RCM-GCM MS	0.27	0.33	-0.21	0.36

The results further showed that correlations during December-February season (mainly for southern Tanzania) were lower compared to all other seasons. It is noteworthy that

during this season, most parts of the region are dry except southern sector (mainly southern Tanzania) and thus with such small rainfall totals it is difficult to achieve meaningful correlations. If, however, just the southern Tanzania is considered, then the correlation between the mesoscale components of the model and CRU climatology increases to 0.76 (Table 14)

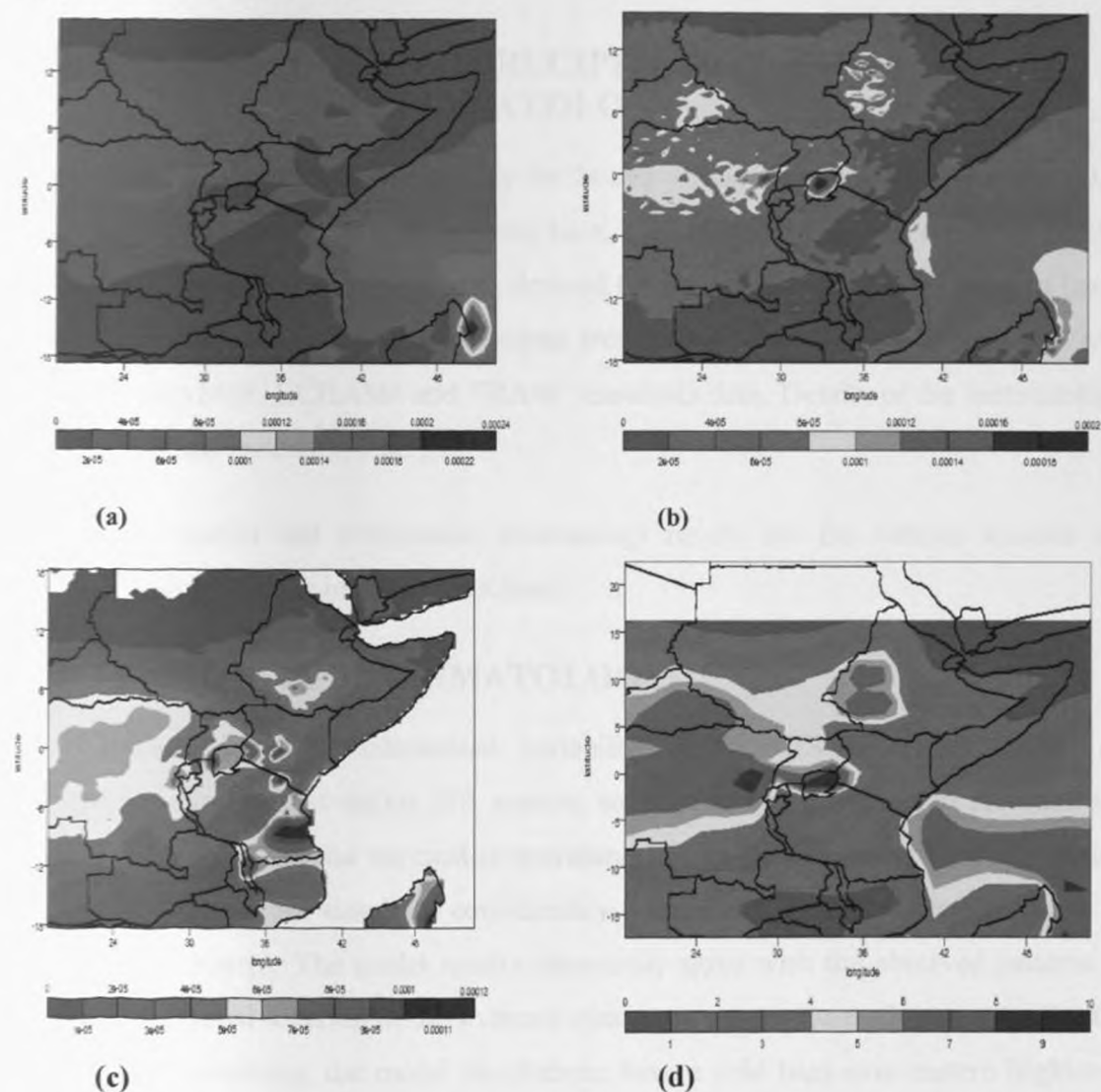


Figure 47: March-May (1961-1990) Mean Rainfall climatology for (a) GCM (b) RCM and (c) Observed CRU Rainfall aggregated to RCM grid

In summary, this section was focused on evaluating how the PRECIS model simulated both large-scale and meso-scale features of East Africa climate in comparison with the output of HadAM3 GCM that was used to provide initial and boundary conditions. The large-scale patterns simulated by PRECIS and those of the HadAM3P

GCM are highly correlated and also consistent with observations (CRU). However, only PRECIS captured the detailed spatial patterns of the observed mesoscale features. At the same time the PRECIS model tend to overestimate rainfall amount compared to the GCM over land points during all seasons. But, overall, the PRECIS model simulates the climatological features of regional climate fairly well compared to the GCM.

4.6.3 PRECIS SIMULATED PRECIPITATION AND TEMPERATURE CLIMATOLOGY

The PRECIS model climatology for March – May (MAM), June –August (JJA) and October – December (OND) seasons have been evaluated against observed (CRU) climatology. Rainfall climatology were derived for the base period 1961-1990 and based on PRECIS simulations forced with output from two Global Climate Models (GCMs) namely: HadAM3P, ECHAM4 and ERA40 reanalysis data. Details of the methodology were highlighted in section 3.6.3.

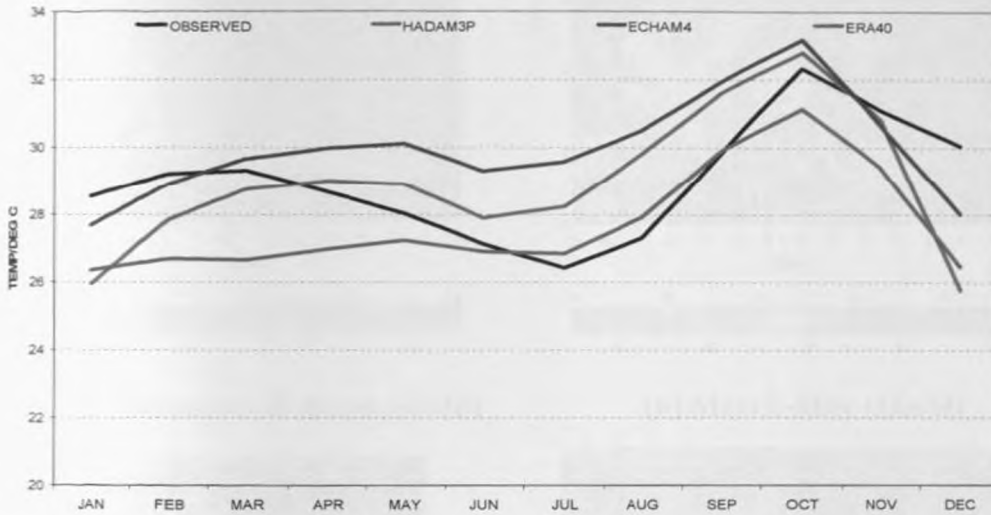
The rainfall and temperature climatology results for the various seasons are presented independently in the next sections.

4.6.4 TEMPERATURE CLIMATOLOGY

Results from the interannual variability of PRECIS simulated surface air temperature showed that during JJA season, some sections of the region recorded the lowest temperature and the warmest temperatures during the December-February period (Figure 48). The model simulated considerably warmer temperatures over most parts of North-eastern Kenya. The model results reasonably agree with the observed patterns in terms of the spatial location of the extreme maximum temperatures (Figure 49). For the minimum temperatures, the model simulations have a cold bias over eastern highlands during JJA season, but the spatial patterns were quite similar to observed patterns. The warm bias in PRECIS RCM simulations may be because of the deficiencies of the GCM simulations (McGregor, 1997). However, the cold bias observed over mountain regions was a common feature of regional climate simulations over different regions of the world (Giorgi et al., 2004; Solman et al., 2008). This might be due to the fact that the model

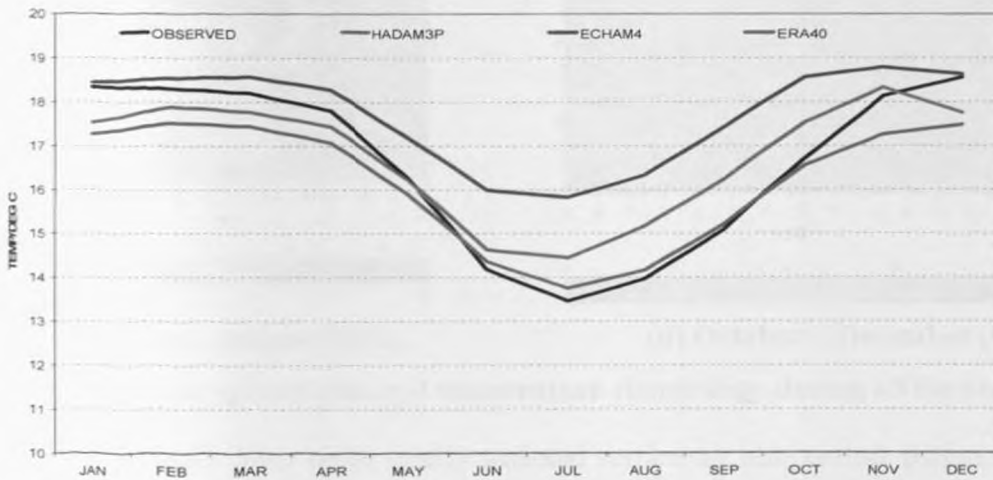
overestimates precipitation over the mountain areas, implying more convection and cloud cover and hence less radiation reaching the mountain top and thus colder temperatures.

ANNUAL CYCLE FOR SIMULATED AND OBSERVED MAXIMUM TEMPERATURE



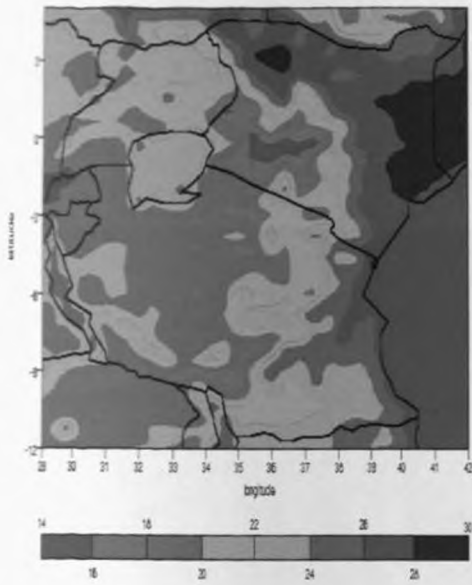
(a) Maximum temperature

ANNUAL CYCLE FOR SIMULATED AND OBSERVED MINIMUM TEMPERATURE

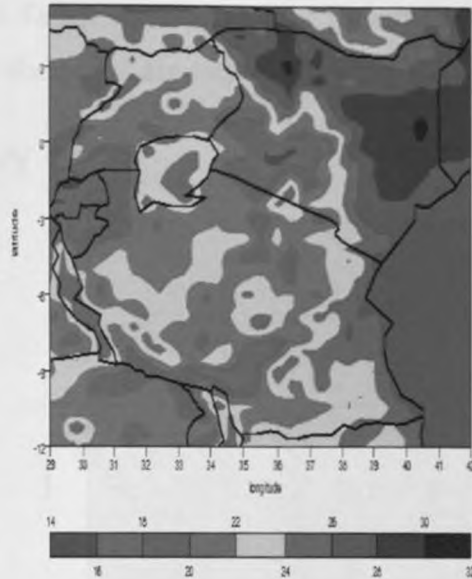


(b) Minimum temperature

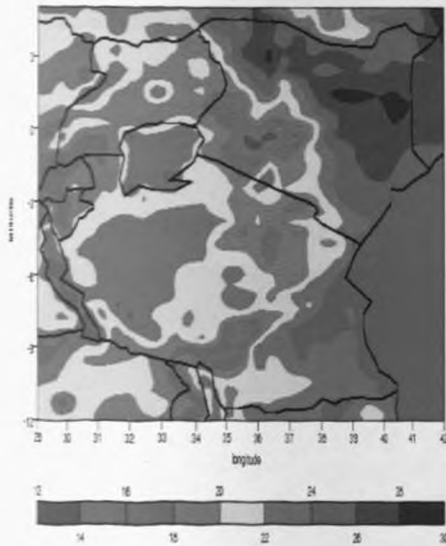
Figure 48: Observed and simulated annual cycle of RCM mean (a) maximum (b) minimum temperature patterns using CRU, HadAM3P, ECHAM4 and ERA 40 forcing data



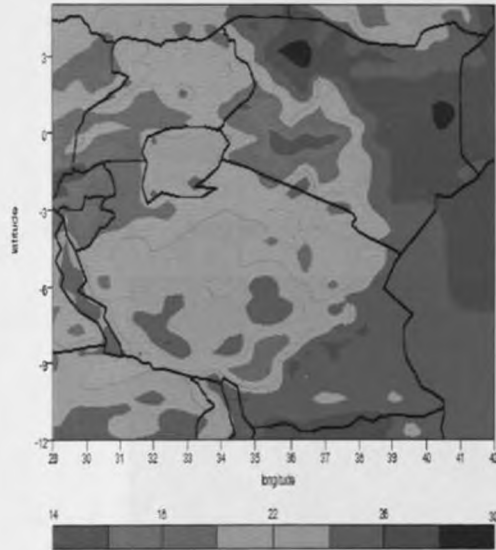
(a) December-February (DJF)



(b) March-May (MAM)



(c) June – August (JJA)



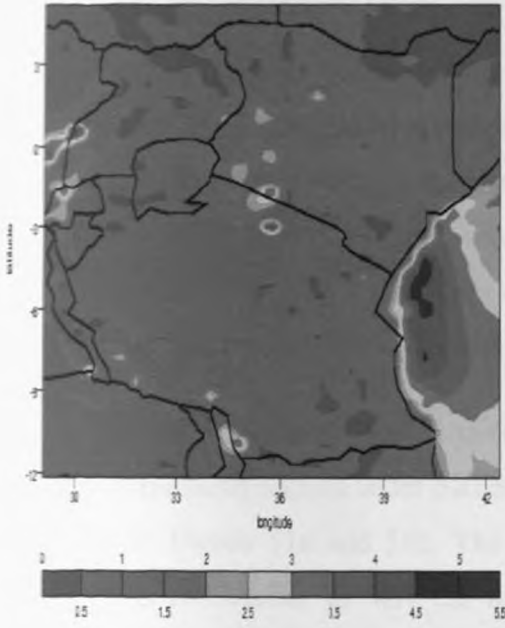
(d) October – December (OND)

Figure 49: Mean spatial seasonal temperature climatology during all the seasons

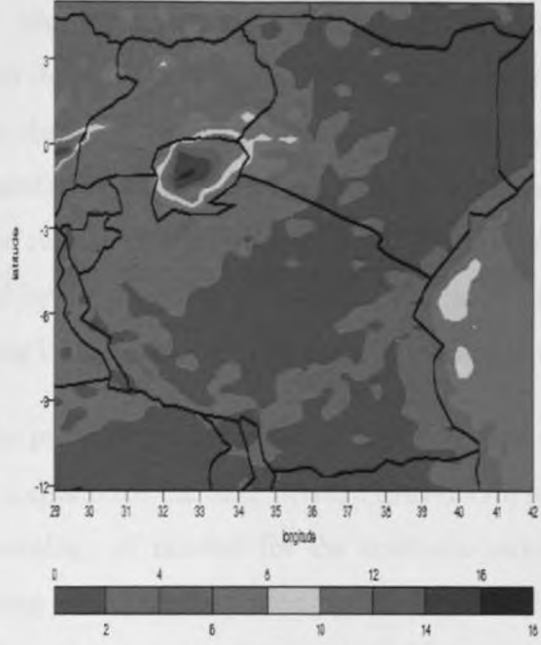
The results from mean spatial seasonal surface air temperature patterns over the region when compared with the observed fields also showed a general agreement of gross features. The differences between simulated and observed mean surface temperature was computed by interpolating the observed temperature to the PRECIS grids. Results showed no significant differences between the two data sets except for the southern sector that had significant differences compared to the northern segment (Figure 49). Average temperature differences of 1°C and 2°C exist over the arid and semi-arid sub

sectors of North-eastern Kenya and central Tanzania, respectively. The observed warmer temperatures in the North-eastern sector of the region are well captured by the model.

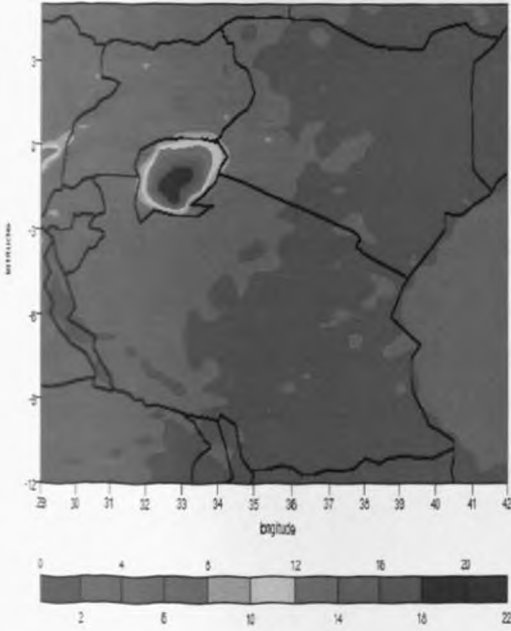
4.6.5 RAINFALL CLIMATOLOGY



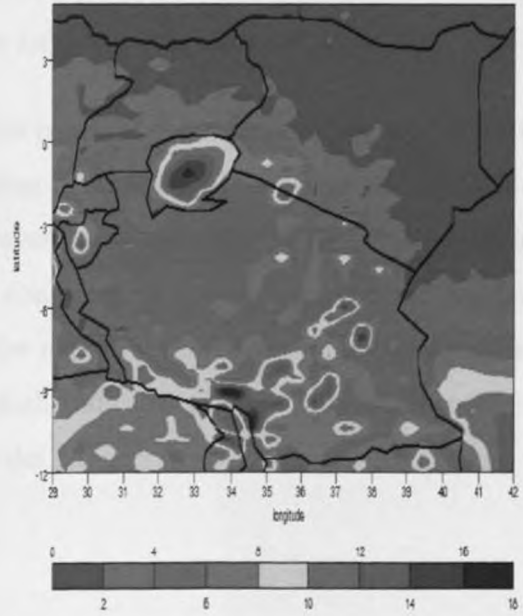
(a) March - May



(b) June - August



(c) October - December



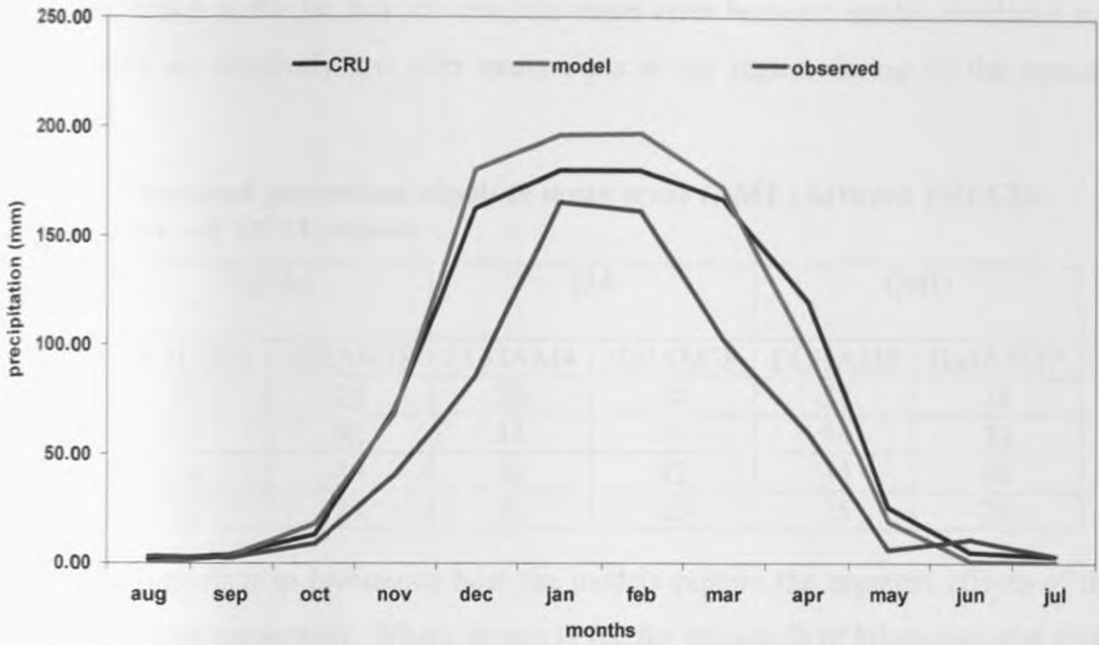
(d) December - February

Figure 50: Mean spatial seasonal rainfall climatology aggregated to RCM grid for all seasons

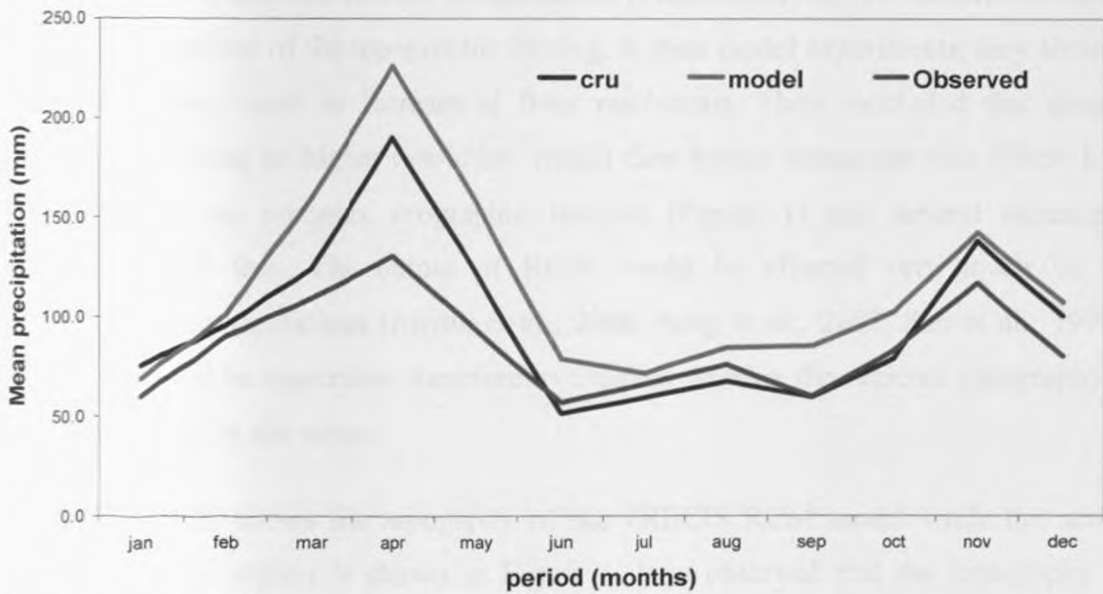
The PRECIS simulated spatial patterns of seasonal rainfall for the baseline period (1961-1990) of the four seasons, in comparison with the observed (gridded data based on the CRU data set aggregated to the RCM grid) are shown in Figure 50. The results show that, compared to observations (CRU) the model underestimates rainfall over most parts of eastern highlands during OND (Figure 50c) while over the central sector (Lake Victoria area) the model overestimates rainfall during DJF (Figure 50b). On the contrary, over northern sector, the model produces the observed rainfall reasonably well. It is thus evident that the PRECIS model simulated rainfall is fairly consistent with the observed values over most parts of the study area. The rainfall maximum over Lake Victoria and western sectors in general, are well simulated by the model in all seasons. Similar results were obtained by Sabiti 2008 in his study using PRECIS model over Lake Victoria basin.

The results of mean annual cycles for precipitation over the southern, central or Lake Victoria basin sectors under SRES A2 scenario for the base period (1961-1990) are presented in Figure 51a and 51b. The climatology of rainfall for the southern sector, which starts in October to May the following year, was captured by the model with seasonal peak in January/February (Figure 51a). Although the direction is well simulated, the model was observed to overestimate rainfall compared to the observed data. Similar results were obtained for simulated rainfall over Lake Victoria basin (Figure 51b).

The seasonal precipitation patterns in the baseline simulation are quite similar to those observed, indicating that the baseline simulations provide an adequate representation of present-day conditions. However, some quantitative biases do exist in the spatial patterns. A conspicuous bias is the considerably lower than observed rainfall over eastern highlands and coastal sectors of the region in the baseline simulation. This bias also exists in the GCM (HadAM3P), which indicates that the regional model is influenced by biases from the driving global model.



(a) Southern sector



(b) Lake Victoria basin

Figure 51: Simulated and observed mean annual rainfall cycles for stations in the region

The results also show that although the annual cycles were well captured the biases in precipitation of PRECIS RCM simulations were evident during all the three seasons examined here. The magnitude of biases in HadAM3P GCM is somewhat less compared to PRECIS simulations forced with ECHAM4 and ERA40 initial and boundary

conditions, which indicates that the absolute mean error between model-simulated and CRU rainfall are relatively low over many parts of the region during all the seasons (Table 14).

Table 14: Computed percentage absolute mean error (AME) between PRECIS RCM outputs and GCM outputs

Sector/ season	MAM		JJA		OND	
	ECHAM4	HadAM3P	ECHAM4	HadAM3P	ECHAM4	HadAM3P
Northern	28	25	28	34	37	28
Western	34	42	31	39	34	33
Eastern	48	49	40	42	44	46
Southern	32	27	35	25	35	29

It is important to investigate how the models capture the apparent effects of the complex regional topography. Where terrain is flat for thousands of kilometres and away from coastal features, the coarse resolution of a GCM may not matter. Giorgi and Marinucci (1996) showed that the simulation of precipitation may be sensitive to model resolution regardless of the topographic forcing. In their model experiments, they showed that precipitation tends to increase at finer resolutions. They concluded that greater topographic forcing at higher resolution would then further strengthen this effect. East Africa region has complex orographic features (Figure 1) and several mountains exceeding 4000 feet. The output of RCM would be affected very much by its topographical configurations (Anyah et al., 2006; Song et al., 2002; Sun et al., 1999a, 1999b). It would be imperative therefore to examine whether the regional topography is well represented by the model.

Figure 52 shows the topography of the PRECIS RCM model while the actual elevation for the region is shown in Figure 1. It is observed that the topography of PRECIS RCM is generally similar to the actual topography of the region; however, some major features that influence convection over the region like the Rift Valley and some important highlands are not well represented (Figure 52). This could have contributed to the model bias in simulating rainfall over the eastern highlands.

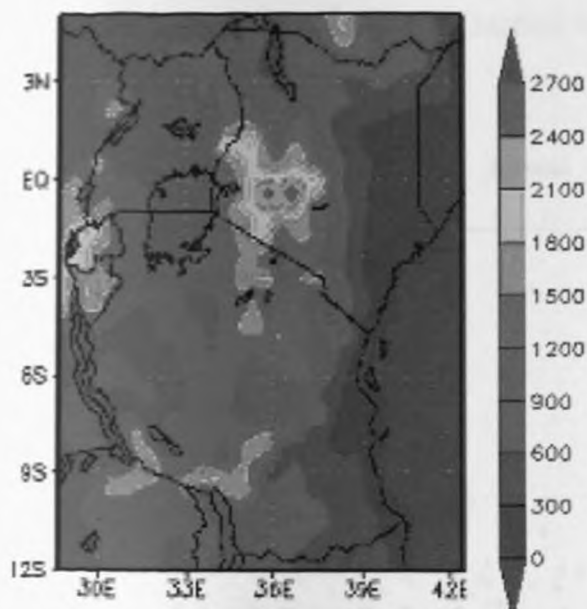


Figure 52: East Africa topography showing values of altitude in meters (m) as is represented in PRECIS RCM model.

In summary, the interannual variability of observed temperature over the East Africa region is captured fairly well by the model. This could be attributed to the general homogeneity in temperature over the region. The annual cycle of rainfall is also well captured in both GCM output and PRECIS simulations, although some biases in PRECIS simulated rainfall are evident during all the three seasons.

4.6.6 FURTHER PRECIS MODEL VALIDATION

In an attempt to project the future climate of the region, it was critical to validate the PRECIS model. Validation of rainfall and temperature simulated by PRECIS was performed for the region using Climate Research Unit (CRU) data for the period 1961–1990. The results for the period 1961–1990 were used as reference to examine variation of PRECIS-projected rainfall and temperature. The statistical summary results of the validation are shown in Table 15 while Figure 53 shows scatter plots of CRU data plotted against simulated data for each driving data i.e. ECHAM4, HadAM3P, ERA 40 and ensemble mean of the GCMs used as input forcing to PRECIS. ECHAM4 and HadAM3P are very similar but slightly underestimated rainfall amounts with $R^2=53\%$ and $R^2=51\%$ (Figures 53a and 53b) respectively. ERA40 ($R^2=54\%$) estimates rainfall fairly well in all the sub-sectors (Figure 53c and Table 15). The scatter plot of the ensemble mean of all

the models (Figures 53d) showed the highest model regression coefficient ($R^2=70\%$) with observed CRU data.

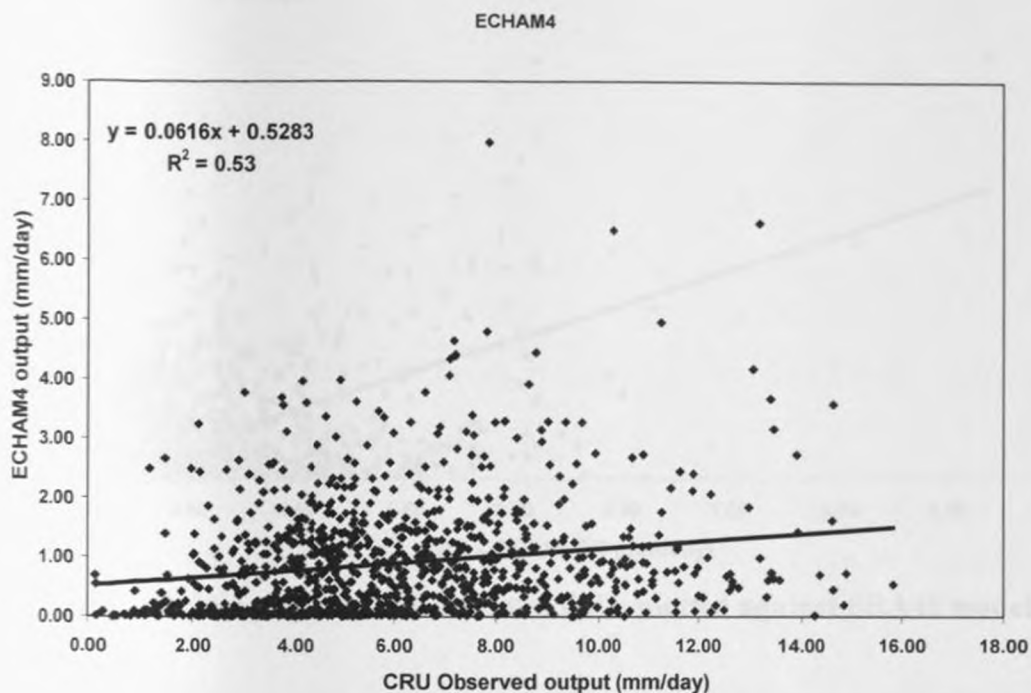


Figure 53a: Scatter plot for semi-observed CRU plotted against ECHAM4 model output

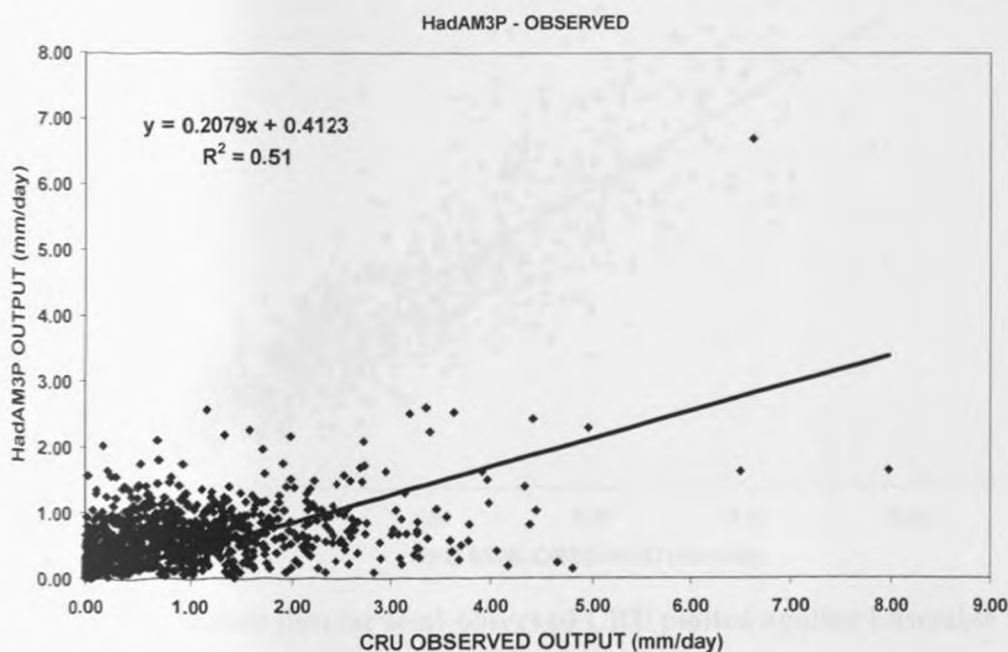


Figure 53b: Scatter plot for semi-observed CRU plotted against HadAM3P model output

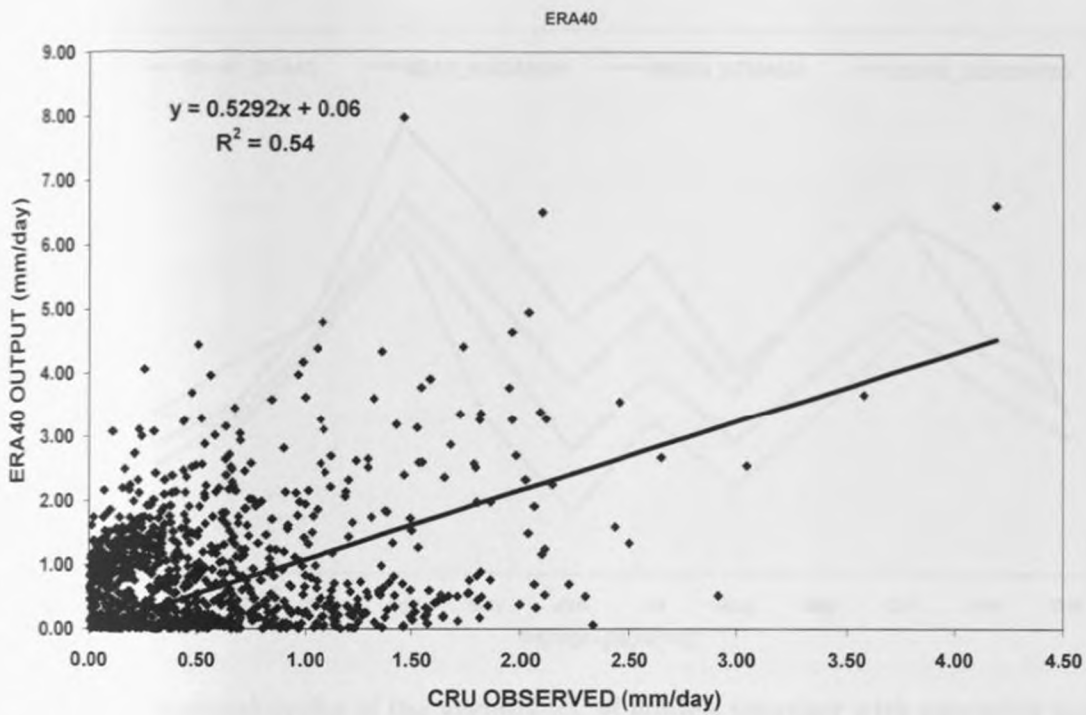


Figure 53c: Scatter plot for semi-observed CRU plotted against ERA40 model output

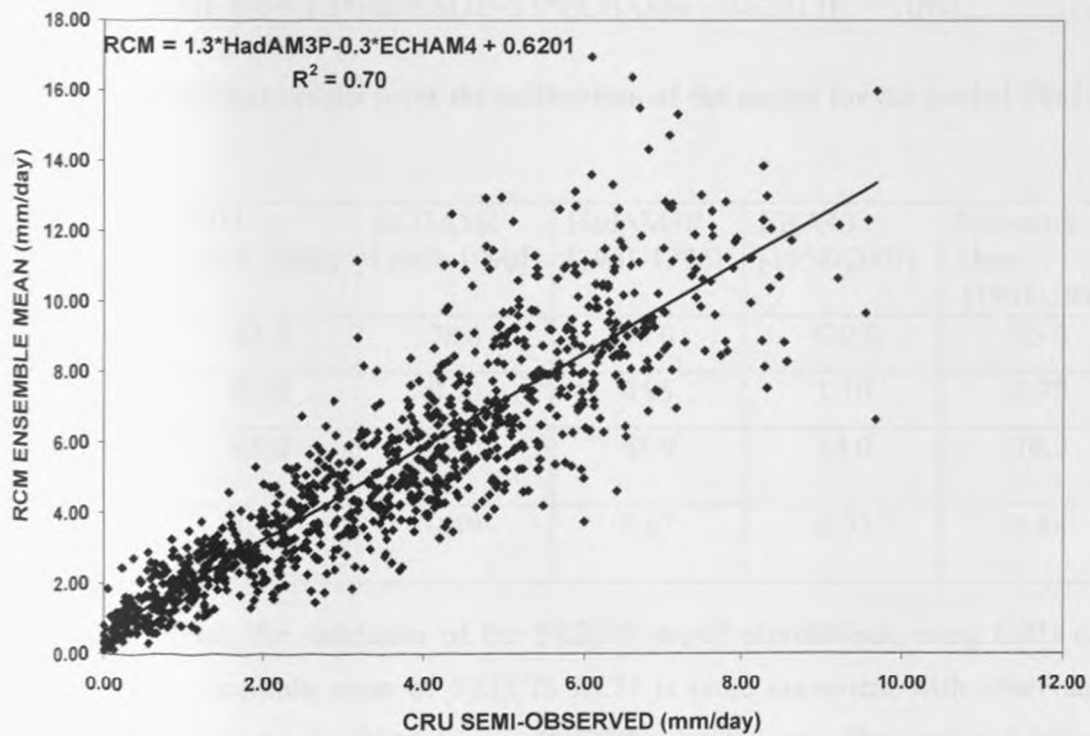


Figure 53d: Scatter plot for semi-observed CRU plotted against Ensemble Mean PRECIS output

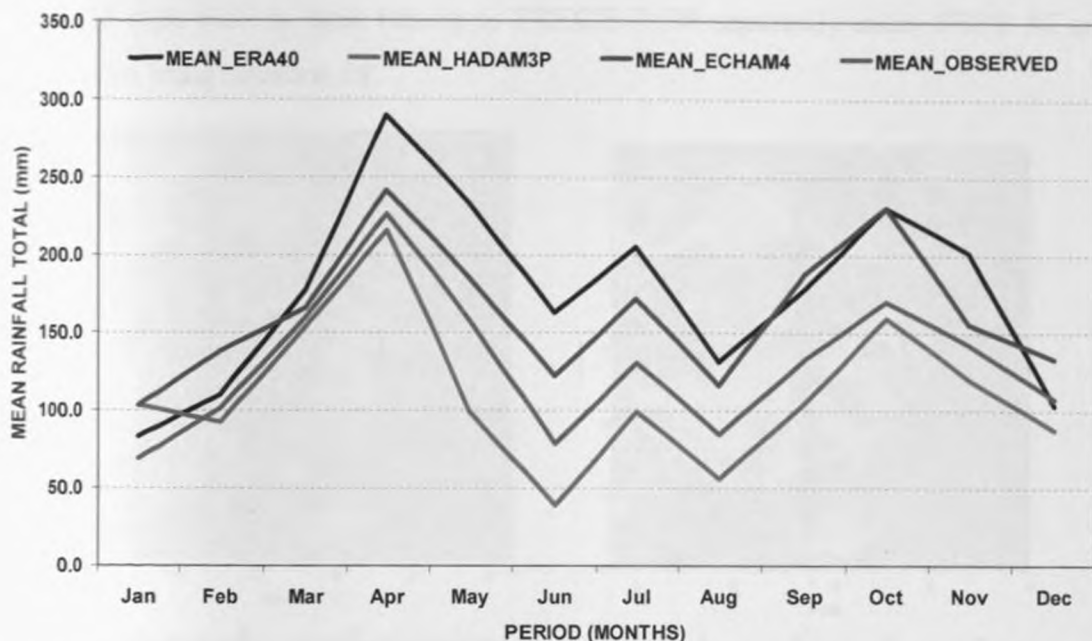


Figure 54: Seasonal cycles of the various RCM models together with ensemble mean output after calibration.

$$\text{ENSEMBLE MEAN} = 1.3 * \text{HadAM3P} - 0.3 * \text{ECHAM4} + 0.6201 \quad (R^2 = 70\%) \dots (18)$$

Table 15: Statistical results from the calibration of the model for the period 1961-1990

	CRU [1961-1990]	ECHAM4 [1961-1990]	HadAM3P [1961-1990]	ERA40 [1958-2001]	Ensemble Mean [1961-1990]
Mean	93.0	78.0	93.0	120.0	95.0
SD	0.87	0.70	0.95	1.10	0.78
RMS (%)	65.0	43.0	48.0	54.0	70.0
Correlation coefficient	1.00	0.49	0.67	0.53	0.84

In general, the validation of the PRECIS model simulations, using CRU data, show that the ensemble mean of PRECIS RCM is more consistent with observation, compared to individual GCM-driven PRECIS simulations. The regional climate projections was obtained from weighting when ensemble members of the ECHAM4 and

HadAM3P were used as input forcing to PRECIS RCM separately under SRES A2 and B2 scenarios using equation 18.

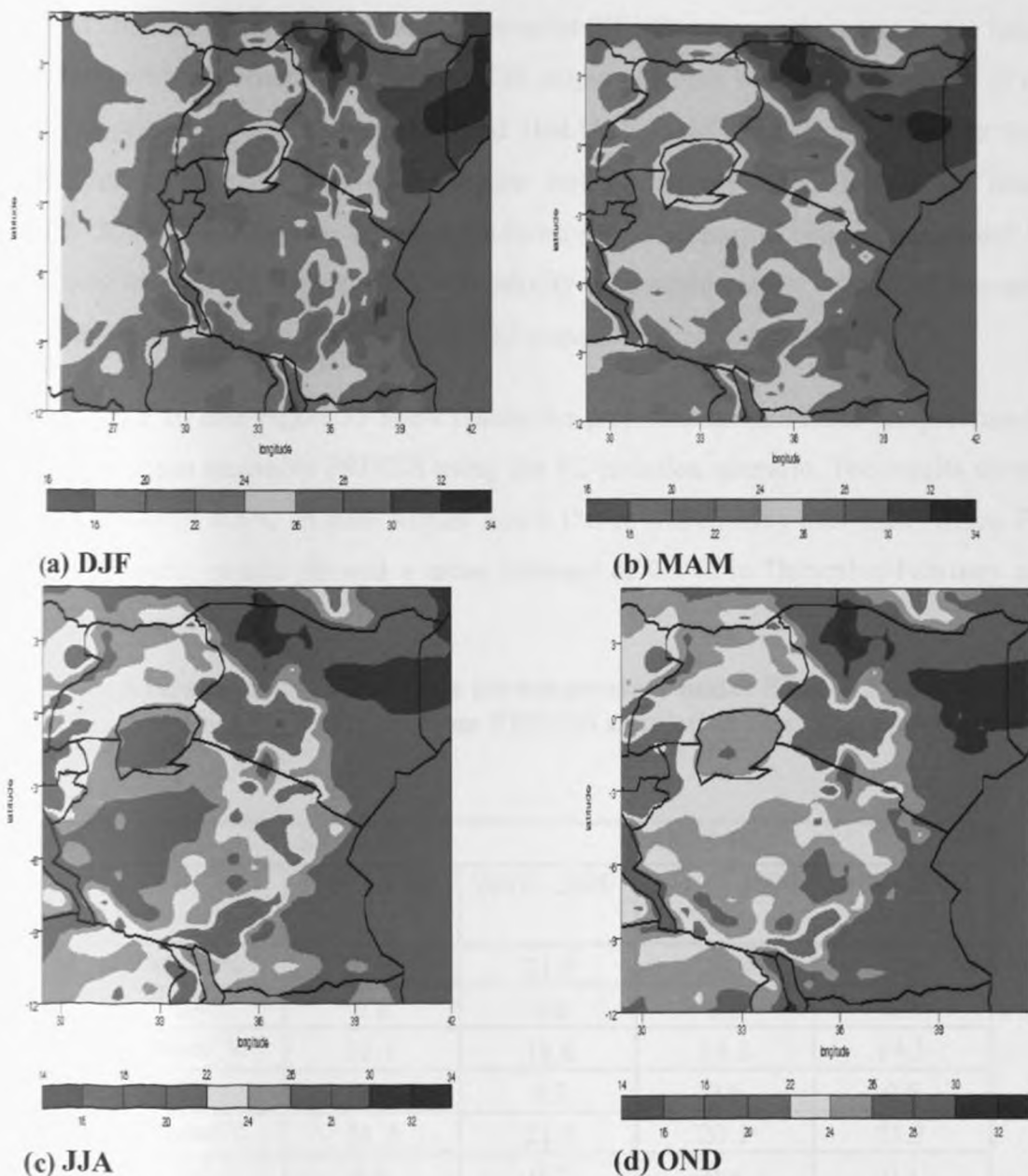


Figure 55: Future temperature for 2020 using Mean Ensemble projection SRES A2

Results of the PRECIS RCM regional climate projections of climate are presented in the next section.

4.6.7 PROJECTION OF CLIMATE FOR THE REGION

As discussed in section 3.6.4, two emission scenarios A2 and B2 developed for the IPCC Special Report on Emissions Scenarios (SRES) were used separately for future projection with the ensemble mean PRECIS output obtained by weighting output of the ensemble members of the ECHAM4 and HadAM3P used as forcings. Results from simulations of future climate of the region using mean ensemble PRECIS for future periods 2010–2100 for two different socio-economic scenarios both characterized by regionally focused development but with priority to economic issues in one (A2 scenario) and to environmental issues in the other (B2 scenario) are presented.

Table 16 and Figure 55 show results for projected mean surface temperature by 2020 from mean ensemble PRECIS using the A2 emission scenario. The results show a mean increase of 0.5°C in June-August and 0.1°C in March-May over East Africa. For the B2 scenario, results showed a mean increase of 0.3°C in December-February and 0.2°C for June-August.

Table 16: Average changes of surface air temperature under SRES A2 and B2 scenarios over East Africa region from PRECIS simulation relative to baseline (1961-1990)

HADAM3P		SRES A2		SRES B2	
		1961 - 1990	2010 - 2020	1961 - 1990	2010 - 2020
MAM	Mean/°c	21.4	21.5	20.8	22
	Sd	0.8	0.6	0.8	0.7
JJA	Mean/ °c	18.1	18.6	19.1	19.3
	Sd	0.9	0.7	0.6	0.5
SOND	Mean/ °c	21.2	21.9	20.1	21.3
	Sd	0.9	0.7	0.4	0.4
DJF	Mean/ °c	22.5	22.7	21.7	22
	Sd	0.7	0.5	0.8	0.8

The PRECIS projections for 2071–2100 indicate increasing trend in warming over the region associated with increasing greenhouse gas concentrations (Figure 56 and Figure 57). The annual mean surface air temperature rise by the end of the century ranges

from 2.2 to 3.1°C in A2 scenario, whereas the rise lies between 2.3 and 3.4°C in the B2 scenario with more pronounced warming over the northern sector. The northern sector (for example Turkana area) is projected to warm up by 0.3 °C more than the rest of the sectors by the end of 2010 decade. The southern sector, in particular the semi-arid central Tanzania, showed less warming than the surrounding region by about 0.1 °C to 0.2 °C during December – February season under A2 scenario.

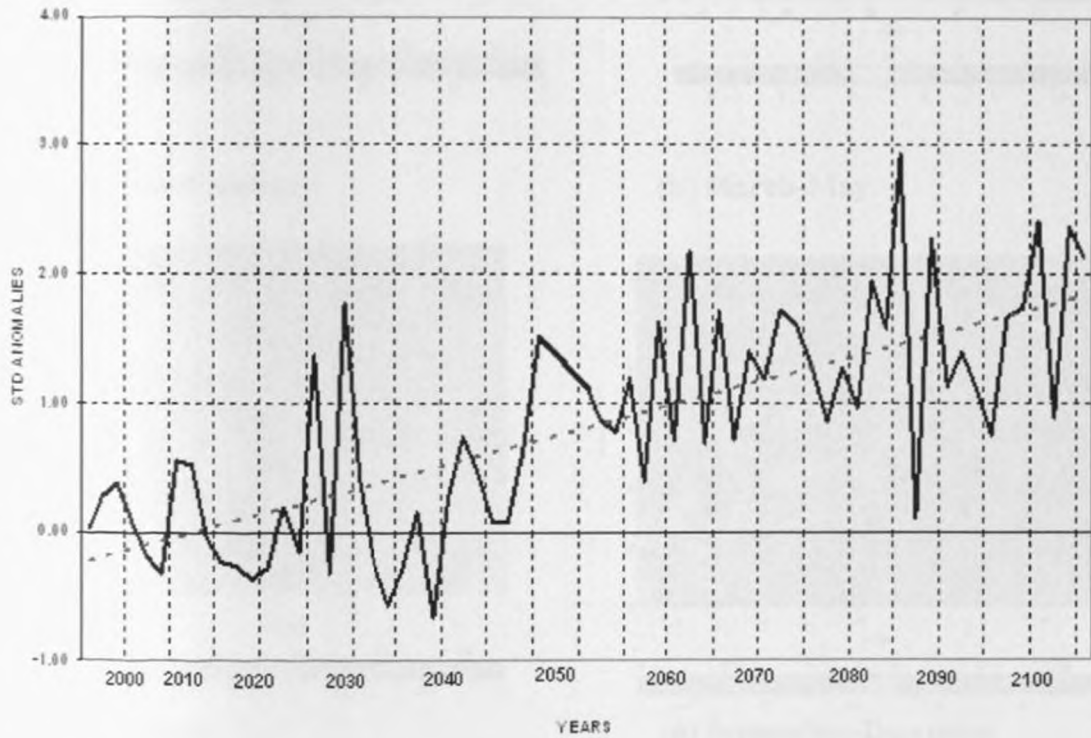
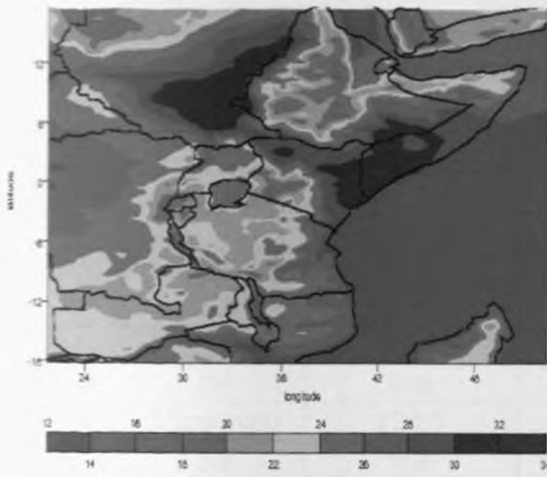
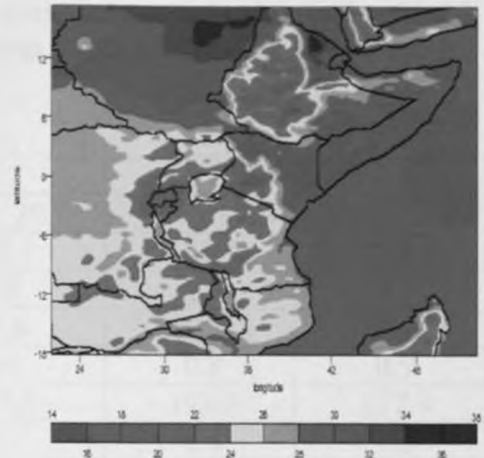


Figure 56: Projection of future mean surface temperature (°C) for the period 2100 with reference to the baseline of 1961-1990 for the mean ensemble RCM under A2 scenario for December-February season

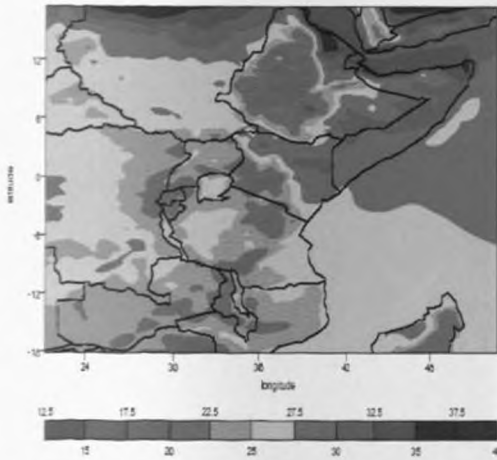
The PRECIS projections of the rainfall show that all the sub-regions (sectors) depicted fairly well the north-south rainfall pattern that follows the migration of the ITCZ with associated locations of maximum rainfall. The difference in resolution between CRU and model data was resolved by regriding the CRU to the PRECIS RCM grid. Table 17 shows the average changes of Ensemble mean PRECIS RCM simulated precipitation under SRES A2 and B2 scenarios over East Africa for 2 time slices i.e the baseline 1961-1990 and the projected decade of 2010-2020.



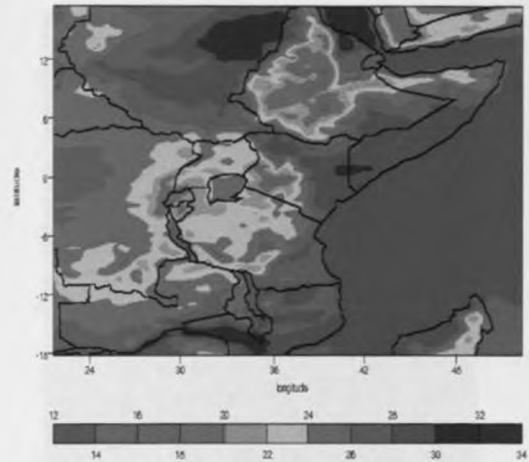
(a) December-February



(b) March-May



(c) June-August



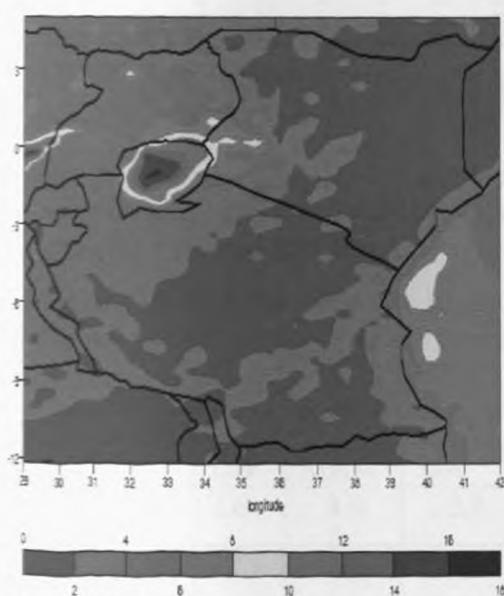
(d) September-December

Figure 57: Spatial patterns of the changes in seasonal mean surface air temperature ($^{\circ}\text{C}$) for the period 2071-2100 with reference to the baseline of 1961-1990 under the Mean Ensemble A2 scenario for (a) December-February (b) March-May (c) June-August and (d) September-December.

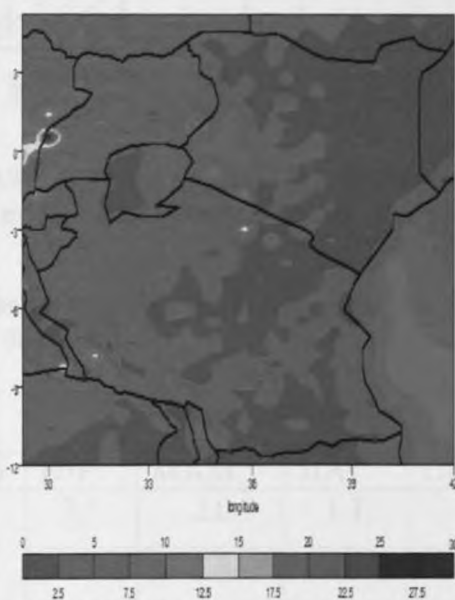
The spatial patterns of rainfall change indicate that most parts of the East Africa would have insignificant change in rainfall by the end of the century (Figure 58). The graphical projection (Figure 59) also shows decrease in the MAM seasonal rainfall over south-eastern sector during the decade 2010-2020. This compares fairly well to the predicted value in Figure 44b as represented by Lodwar. Rainfall was also observed to increase in the north-eastern and south-western sectors in all the seasons. Spatial patterns of rainfall change indicate maximum increase over the western sector for both A2 and B2 scenarios (Figure 58).

Table 17: Average changes of 2010-2020 mean seasonal precipitation under SRES A2 and B2 scenarios over East Africa region from PRECIS simulation relative to baseline (1961-1990)

Ensemble Mean		SRES A2		SRES B2	
		1961 - 1990	2010 - 2020	1961 - 1990	2010 - 2020
MAM	Mean/mm	155.1	192.3	197.7	229.5
	Sd	1.7	1.9	1.7	1.7
JJA	Mean/mm	49.8	50.4	42.2	64.4
	Sd	0.6	0.4	0.8	0.9
SOND	Mean/mm	120.3	157.2	193.2	237.9
	Sd	0.8	0.5	1.4	1.5
DJF	Mean/mm	118.2	146.4	122.7	129.6
	Sd	0.9	1.3	1.3	0.9



(a) SRES A2



(b) SRES B2

Figure 58: The future change in March to May (MAM) seasonal precipitation for the period 2010-2020 in mm/day and also as a percentage of the present day with reference to the baseline of 1961-1990.

Results for the projection of both rainfall and temperature for the period 2071-2100 under A2 scenario is shown in Table 18. The future changes are expressed as percentages relative to the baseline period 1961-1990. PRECIS projections for 2071-2100 indicate an all-round warming over the region associated with increasing greenhouse gas concentrations (Figure 56).

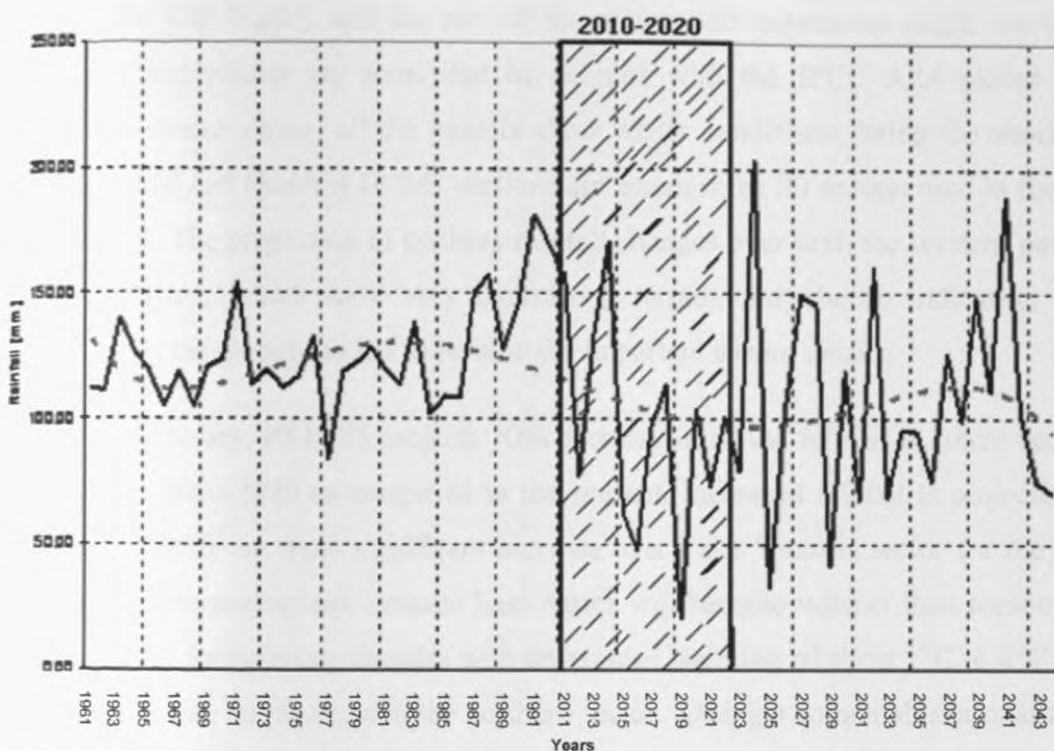


Figure 59: Graphical plot for projected MAM seasonal rainfall for North-eastern sub-region as represented by Lodwar using smoothed (dotted lines) and unsmoothed (completed lines)

Table 18: 2071-2100 changes of mean seasonal rainfall and temperature under SRES A2 scenario from PRECIS relative to 1961-1990

Sector	Rainfall change/%				Temperature change/%			
	DJF	MAM	JJA	OND	DJF	MAM	JJA	OND
North-western	2.6	3.8	2.9	3.5	2.1	2.0	1.1	1.1
North-Eastern	-2.1	4.2	-3.0	3.7	1.9	1.8	1.9	1.9
Western	2.7	4.7#	3.1	3.9	2.0	0.9	2.1	1.4
Eastern	2.0	2.9	2.4	2.8	2.2	2.1	1.2	1.2
South-western	2.8	3.0	3.1	2.9	2.2	1.9	1.0	2.2
South-eastern	1.9	3.1	2.6	3.1	1.8	1.5	1.8	2.1

significant change

Again during the long rains of MAM season, most parts of the region are projected to have increase in rainfall by 2100 under both A2 and B2 scenarios. However; the largest increase occurs over the areas neighbouring Lake Victoria. During the short rains of September-December, the increase in rainfall would be confined to the western

parts of the Rift Valley and the rest of the region will experience slight decrease in rainfall. These results are somewhat in contrast with the IPCC AR4 global model projections where almost all the models show wetter conditions during the short rains. Both ECHAM and HadAM GCMs versions are amongst the 20 models used in the IPCC AR4 (2007). The projection of positive rainfall changes over both the western parts and the Rift Valley, which have very contrasting terrain, may be an indication of the deficiency of the global models to resolve the important terrain details.

In summary, PRECIS projects 10% decrease in MAM rainfall in future scenarios for the year 2010-2020 as compared to the present. Increased rainfall is projected over most zones, with the most significant increase over Lake Victoria sector for the period 2010-2020. The projections indicate East Africa will become warmer than present in all seasons in the forthcoming decades with an average warming of about 1°C to 4°C across the whole region, but more so in the northern sector. Changes in rainfall seasonality over forthcoming decades are unlikely but trend towards more extremely wet seasons is likely for the September-December rains, particularly in northern sector, in the forthcoming decades. PRECIS regional model simulations show wetter conditions in the Long Rains although in the Short rains the changes are confined to western sector. Droughts are likely to continue particularly in northern sector, with more frequent drought events than present.

The unique results of this thesis research are provided in the next chapter on the summary and conclusions. Recommendations arising from research performed under this study are also presented.

CHAPTER FIVE: SUMMARY, CONCLUSIONS AND RECOMMENDATIONS

This chapter provides the major conclusions that were drawn from the various results from the study. Some recommendations and suggestions are also given for future research.

5.1 SUMMARY

This thesis was organized into five chapters. The Introduction, Chapter One, highlights the objectives and motivation of this research. Among other things, the chapter highlighted the occurrences of extreme climatic events that often lead to devastation of most economic, social and environmental systems in the region. It emphasized that most socio-economic developments in the region are rain dependent yet very little efforts have been made in the region to mainstream climate risks in the planning and development of all climate sensitive sectors. The knowledge of decadal rainfall variability patterns both in time and space is therefore very essential for sustainable socio-economic planning of all rainfall dependent activities. Mainstreaming climate risks in the planning and development requires good knowledge of the past climate variability and change together with long term future predictions and projections. Many of the past studies in the region have concentrated in climate studies within the temporal range running from sub-diurnal, seasonal to interannual time scales. This study was therefore devoted to improving our understanding of climate variability over East Africa at decadal (ten-year) time scale that is critical for development of medium to long term climate risk management strategies.

The overall objective of this study is to investigate the dominant spatial and temporal decadal rainfall variability modes over East Africa region and their teleconnection with decadal variability modes of the specific global oceans. The study recognises that knowledge of extreme climate variations at decadal timescale is extremely useful for planning and decision making of long term climate risk management strategies for sustainable socioeconomic development. In order to adequately address the overall objective the study, several specific objectives were formulated.

The first specific objective involved use of Principal Component Analysis (PCA) and simple correlation analysis approaches to delineate the region into zones with similar modes of decadal rainfall variability. This analysis was mainly to group together stations with common decadal rainfall characteristics into homogeneous zones. The stations highly correlated with each other were identified as representative stations for every zone used for the analyses in the study. The second specific objective involved subsection of the representative station in each zone to spectral and trend analyses. The third specific objective involved the use of Singular Value Decomposition (SVD) analysis in order to delineate existence of covariance amongst regional rainfall and the individual global basins Sea Surface Temperatures (SSTs). The results from analyses performed to address the first to third specific objectives were then used to demonstrate the possibility of providing some reliable information about decadal rainfall predictability and prediction and thus early warning tools for the region. Besides delineation and prediction of regional decadal rainfall pattern, an attempt was further made to generate regional climate change scenarios using high resolution Regional Climate Model (RCM), PRECIS, and results compared to the predicted decadal rainfall during the period 2010-2020 using empirical model derived from this study.

The data sets used in the study included monthly observed rainfall over East Africa and global SSTs covering the period 1950 to 2008. Other data sets used include gridded data base from University of East Anglia, Climatic Research Unit (CRU) for the period 1961 to 1990 and the European Centre for Medium-range Weather Forecasts (ECMWF-) 40 years Re-Analysis (ERA40) products. The data used in the study were smoothed using a nine point binomial coefficient filter to remove all fluctuations equal to and less than 9 years.

The specific objectives were investigated using various methods. The methods for assessing the quality of data used in the study included standard parametric and non parametric methods such as Man-Kendall rank statistics; while both trend analysis and spectral analysis were used to investigate the patterns of the existing decadal rainfall variability. Principle Component Analysis (PCA) and Singular Value Decomposition (SVD) techniques were on the other hand used to delineate the East Africa into

homogenous zones with similar modes of decadal variability using empirical model derived from this study, and also to investigate linkages amongst the observed regional decadal rainfall variability modes with decadal modes of variability over various parts of the global SSTs. The predictability potentials of the regional decadal rainfall variability patterns were assessed using correlation and Multiple Linear Regression (MLR) methods. Modelling systems using high resolution PRECIS RCM was employed to generate regional climate change scenarios that their results were compared with the predicted decadal rainfall modes for the period 2011-2020. The results obtained from the various methods are presented in chapter four.

Results from quality control analyses indicated that most of the records used were of good quality, and this formed the foundation of the analyses that were undertaken in this study. Results from trend analysis showed discernible trends in some of the smoothed and unsmoothed time series. The inter annual patterns showed that although wet and dry decades were recurrent, and sometimes extend over large areas, there were very few decades when floods or drought covered the whole of East Africa region except for the wet decade of 1961-1970 during October-December season.

Results from spectral density analysis showed dominance of significant spectral peaks within decadal period for the data where fluctuations less than or equal to nine years had been removed. The observed spectral peaks were significant at 95% confidence level when both white and red noise hypotheses were used. The results showed that although decadal spectral peaks were dominant at all locations in all the seasons, there were however significant differences in the amplitudes and spectral bands of the spectral peaks from various parts of East Africa. This could be a reflection of the complex nature of the regional climate systems that include complex topography and large water bodies that include Lake Victoria (the second largest fresh water lakes in the world). Therefore, the results from this study show that although decadal rainfall variability modes were generally common at all locations, some decadal variability modes were restricted to some specific areas and seasons over East Africa region. The Principal Component Analysis results from decadal rainfall records yielded seven to nine homogeneous decadal rainfall zones for the seasons that were used in the study (i.e. OND and MAM)

respectively. Over 27 homogenous regions have been observed with interannual rainfall records in previous studies. Thus for the first time the study has provided detailed decadal rainfall modes for East Africa, and further categorize them into homogenous zones that can be of great use in the planning and management of all rainfall dependent activities in the region.

The results obtained from the teleconnections of the regional decadal rainfall variability patterns to the global SSTs using Singular Value Decomposition (SVD) analysis showed that decadal variability of the SSTs in the Pacific, Atlantic and Indian Oceans all have significant influence on regional decadal rainfall variability over East Africa. Significant coupling of the SSTs and rainfall fields were observed with high values of Square Covariance Fractions (SCF) explained by the first three modes for each of the three oceans. In general, the study revealed that even when decadal variability of one of the oceans contributed most of the variance of decadal rainfall variability, the roles of the other two oceans were still very significant. This signifies the close interaction among the global oceans (SSTs) and the complex regional scale climate processes. The first three SVD modes of the basin SSTs and decadal rainfall accounted for over 75% of the total square covariance for all the seasons, with statistically significant expansion coefficients of time series of the SVD mode of the two fields' anomalies.

As an example, the results for Singular Value Decomposition analysis for March-May (MAM) rainfall season with Indian, Atlantic and Pacific Oceans SST modes showed the first modes accounted for 49.9%, 43.4% and 37.9 % respectively of the total square covariance. The results indicated that decadal rainfall over the region during the major rainfall season of March – May (MAM) was influenced mainly by the east/west zonal mode over the Indian Ocean. The dipole-like pattern with negative / positive loading centred on western/eastern Indian Ocean basin was characterized by negative/positive loading patterns of rainfall over the southern/northern sector of the region. The SVD results for MAM rainfall and SST fields over the Atlantic Ocean was characterized by a meridional dipole like pattern with negative loadings over the northern equatorial Atlantic Ocean and positive loadings over the southern equatorial Atlantic basin coupled with southeast – northwest dipole pattern in decadal rainfall with negative loadings over the south-eastern highlands while positive loading over north-western highlands of the

region. The time series of expansion of SVD coefficients of both rainfall and SST anomalies showed decadal trend modes with enhanced amplitudes in some years. SVD analysis results for MAM rainfall season and Pacific Ocean SST modes showed that the regional decadal rainfall patterns were affected by decadal variability modes of the ENSO phenomenon.

Results for SVD analysis for October-December (OND) rainfall season with Indian, Atlantic and Pacific Oceans SST modes showed the first modes accounted for 65.2%, 47.8% and 39.2 % respectively of the total square covariance. Decadal rainfall variability for this season was dominantly characterized by decadal variability modes of the ENSO phenomenon over the equatorial Pacific Ocean. The SVD mode results for OND rainfall and Indian Ocean SST fields showed dipole-like pattern with positive loading centred on eastern Indian Ocean Indian Ocean basin and negative loadings over the western Indian Ocean. The first SVD mode between OND rainfall and Atlantic Ocean SST fields displayed meridional dipole like pattern with negative loadings over the northern equatorial Atlantic Ocean and positive loadings over the southern equatorial Atlantic basin with OND rainfall component of this mode characterised by SE – NW dipole pattern with negative loadings over the south-eastern highlands while positive loading over north-western highlands of the region

Results for SVD analysis for the third rainfall season of June – August (JJA) with Indian, Atlantic and Pacific Oceans SST modes showed the first modes accounting for 61.1%, 38.6% and 42.1% respectively of the total square covariance. The key modes of variability that seemed to drive the June –August rainfall significantly was the interhemispheric tropical Atlantic variability with meridional dipole pattern in the Atlantic Ocean. A unique tripolar mode of variability observed during this season was characterized by large pool of positive loading over the central equatorial Pacific and negative loadings in the equatorial western and eastern parts of the basin. This mode is associated with regional rainfall variability characterized by positive loading in the western parts of the region and negative loading over the eastern highlands. The third SVD mode that explained 8.7% of the total covariance had dipole loading patterns that were close to those observed for mode one, except for wider spread of the positive modes

over the tropical ocean basin. This mode seems to signify the role of the central highlands and the Great Rift valley that runs north-south across the central of the region, with chains of mountains on both sides of the Rift that have significant modification to the large-scale circulation over the region

In conclusion the results for Singular Value Decomposition (SDV) analysis have been able to delineate unique covariances among decadal rainfall variability modes in East Africa and SSTs decadal variability modes over parts of the global oceans. Teleconnection between global SSTs and regional rainfall extremes have been documented in many previous studies at seasonal to interannual time scales, especially those linked to ENSO and IOD modes and the results of this study are consistent with some of these early studies.

Results from the regression analyses showed significant relationship between specific seasons / basin SST modes and decadal rainfall indices over the region. The results showed substantial variation of the SSTs based rainfall estimates model skill within various zones with decadal rainfall variance explained by SST modes ranging from 39% to 78%. The results further indicated that although there were significant variations in the skill of the models there were significant differences not only from season to season but also from one decadal homogenous rainfall zone to another. The Heidke Skill Score (HSS) values were ≥ 0.30 at all locations indicating that the models could provide forecasts with useful skills. This component of the study has for the first time indicated that simple statistical models can be used to translate decadal variability signals over various parts of the global oceans to decadal rainfall variability implications over East Africa region. These tools offer new opportunities for interpreting the potential impacts of global climate changes such as rising global SSTs at regional levels. This would help in the development of realistic local, regional and global climate change mitigation and adaptation strategies.

Results from PRECIS Regional Climate Model (RCM) simulated rainfall and temperature climatology over the land points showed that the model outputs were closer to the observed CRU values compared to the GCM (HadAM3P and ECHAM4) output for all seasons. The simulated temperatures indicated the largest root-mean-square error of

about 2°C in both PRECIS and the two GCMs during the dry season of December - February. In all seasons the PRECIS simulations generally showed better skills in reproducing the mesoscale climate components when compared to the GCMs. The differences were, however, not very significant during the years with large global SSTs anomalies like during strong ENSO events. This may be due to the fact that both models are driven by SSTs and because the PRECIS was driven by GCM output.

The results from the generated regional climate change scenarios using high resolution Regional Climate Model (RCM) showed that ensemble mean PRECIS was much superior compared to single model driving PRECIS outputs. The temperature projections were however more consistent compared to regional rainfall changes. For example, the PRECIS regional projections showed a mean increase of 0.5°C in June-August and 0.1°C in March-May over the region by 2020 under A2 scenario. For the B2 scenario, results showed a mean increase of 0.3°C in December-February and 0.2°C for June-August. The results however showed an all-round warming for 2071–2100 over the region. The annual mean surface air temperature rise by the end of the century ranged from 2.2 to 3.1°C in A2 scenario, whereas the rise ranged between 2.3 and 3.4°C in the B2 scenario, and with more pronounced warming over the northern sector.

PRECIS projects 10% decrease in MAM rainfall in future scenarios for the year 2010-2020 as compared to the present. Increased rainfall is projected over most zones, with the most significant increase over Lake Victoria sector for the period 2010-2020. The spatial patterns of projected rainfall change indicated inconsistency in the rainfall change patterns like have been observed by IPCC and many projections of rainfall scenarios in previous studies. The results however showed that most parts of the region would have insignificant change in rainfall. Spatial patterns of rainfall change indicated maximum increase over the western sector for both A2 and B2 scenarios. A decrease was observed in March – May rainfall during the 2010-2020 decade over south-eastern sector. Rainfall was however observed to increase in the north-eastern and south-western sectors in all the seasons. Some of these results compared well with the projections from Multiple Linear Regression analysis for the 2011-2020 decade. The study therefore produced regional climate change scenarios credible enough to inform climate impacts, vulnerability and mitigation assessments and adaptation strategies for the region.

The next section presents the major conclusions from the study.

5.2 CONCLUSIONS

This study has delineated and further categorized significant decadal rainfall modes into homogenous zones over East Africa region. It has further found strong covariances of these rainfall variability and specific global SST modes. The strong linkages provided useful skills in predicting decadal rainfall variability that compared closely with projected values from regional climate model, for the near-term period (2010-2020). The results of this study could therefore potentially contribute and add value in the planning and management strategies of all rainfall dependent activities/sectors in the region. These results further provides useful isight and potential input for the improvement of tools developed for early warnings of extreme rainfall events and disaster risk reduction necessary for sustainable socio-economic development in the region. Results obtained from statistical analysis of present day climate variability and those derived from numerical model simulations of the present and future climate can contribute to and provide new climate risk management capability for coping and adaptation to climate change challenges already prevalent in East Africa region.

The next section provide some specific recommendations for future studies together with some specific application areas

5.3 RECOMMENDATIONS

The recommendations of this study have been geared towards climate research scientists, policy makers, National Meteorological and Hydrological Services (NMHSs), regional climate centers (e.g ICPAC) and various professional stakeholders in all sectors that are directly and indirectly affected by rainfall. Such sectors include meteorology, hydrology, agriculture, industries, energy and researchers among many others.

5.3.1 RECOMMENDATIONS FOR FURTHER RESEARCH WORK

A lot of research on decadal atmospheric variability in relation to changes in the nearby oceans as well as near-global SST have been undertaken. However, knowledge on

changes in the patterns of decadal rainfall variability in relation to land surface characteristics, sea level pressure field and other atmospheric circulation patterns at decadal time scales needs to be further strengthened based on findings of this groundbreaking study since they are major components of low-frequency rainfall variability from both regional to global-scale climate processes contributing to decadal climate variability (CLIVAR, 1995). It is important to know the extent of decadal variability of the regional climate in observations and model simulations, as a background to understanding seasonal to interannual predictability. Further research study is needed to link the observed cycles in the decadal rainfall variability to modes of variability of some of the local, regional or global scale climate controlling systems other than the Sea Surface Temperatures. Particularly the modulation of the modes of decadal variability by interactions between large scale and local scale climate forcings is very critical and need to be pursued in future research in this area.

Research studies have shown that ocean temperatures in the Northern Pacific Ocean oscillate between warm and cool conditions over twenty to thirty year time periods (Jones and Moberg, 2003). These oscillations are termed the Pacific Decadal Oscillation (PDO), and they have their counterpart in the North Atlantic Ocean which is named the North Atlantic Oscillation (NAO). Rainfall patterns along the Pacific Coast correlate with the PDO, in that coastal areas from central California northward receive more precipitation during the cool cycles and south California and Arizona receive more rainfall during the warm cycles. There is therefore need to explore if there is any relationship between these indices to East Africa rainfall patterns especially at longer timescale or similar decadal oscillations over the Indian Ocean.

In this study, the global Ocean basins are considered to be linked to regional rainfall as separate entities yet in this study situations whereby they interact simultaneously to impact the regional climate were apparent. Therefore, there is need to carry out further research to investigate rainfall variability when all the global basins are considered to be acting together as single entity in influencing the regional climate.

This study employed Multiple Linear Regression analysis method to develop models to predict decadal rainfall modes. It was observed that the method had varying

capabilities both in the fitting of the models and skill. Dynamical approach should be employed to simulate and predict decadal climate variability and also to establish the physical and dynamical factors associated with the linkages between SST, other predictors and decadal rainfall variability.

Further research is also needed to strengthen assessments and reduce uncertainty in prediction models. There has been relatively little regional climate modelling carried out in the region and there is much uncertainty in the climate modelling carried out in this study even though the best available models, data and scenarios have been used. The uncertainties in the future projections apply more to rainfall than temperature. To address this challenge it would need multiple regional models and emission scenarios. Researchers also need to provide a wide range of possible future climates projections corresponding to a number of the most distant time period needed (2071-2100) and for a high emissions scenario (for example, SRES A1FI). This will give a clear signal of climate change against the noise of natural variability and thus providing robust patterns of change.

It would also be important that future research extend some of the findings and recommendations in this study to look at regional impacts, vulnerability and adaptation issues based on the generated scenarios.

5.3.2 RECOMMENDATIONS TO POLICY MAKERS

The policy makers and planners of the respective governments are challenged to mainstream climate in their development plan and also improve on their long term planning by using the products of this study as a stepping stone to invest in and improve understanding, characterization and predictability of decadal climate variability and changes for the East Africa. This information will help put in place mitigation and/or adaptation measures in place and build the required infrastructure to advocate for changes in policy due to the potential impacts of climate anomalies, including climate change.

The results of this study has offered unique opportunity and foundational information that the governments of the three countries, donors and strategic partners can incorporate in building regional climate change adaptation capacity.

5.3.3 RECOMMENDATIONS TO USERS OF CLIMATE INFORMATION AND PREDICTION PRODUCTS

Informed decisions could be made if information about the regional climate, delineated into zones with similar decadal rainfall variability characteristics is available. Use of the products from this study should enable the climate information user communities in these zones take advantage of the positive aspects of climate extreme and minimize the related negative risks. Users of climate information should take joint responsibility with the climate experts in development of detailed climate information relevant to their applications. This can be achieved through the surveys of the user needs, for example, the climate event(s) to which the productivity of a given sector is vulnerable, the forecast quality required by specific sector, and the cost and losses involved in the application of climate information.

5.3.4 RECOMMENDATIONS TO NATIONAL METEOROLOGICAL AND HYDROLOGICAL SERVICES

The National Meteorological and Hydrological Services (NMHSs) over the region are responsible for data collection, data processing, data archiving, and data dissemination and exchange. The existing rainfall observation network is not adequate to give a complete coverage of the study region. Some remote and inaccessible areas do not have any representative stations. Some of the existing stations over the region are sparse with some stations having incomplete and/or short period data. It is therefore necessary to maintain an optimal, efficient and continuously operational network of ground stations for rainfall observations. There is need to set aside adequate financial resources for maintaining of personnel and instruments for observations, recording and archiving the recorded observations.

There is need to strengthen climate data acquisition, analysis and communication, to enhance seasonal forecasting, early warning of extreme events and near long-term projections, in particular, improving the capability of East Africa's meteorological and climate forecasting services, building/enhancing on the incipient regional climate information capability.

6. REFERENCES

- Agumba, F. O., 1985: Fluctuations of long rains in Kenya in relation too large scale circulation, IMTR Res. Report No. 1/85, 27 pp.
- Alves, O., Balmaseda, M. A., Anderson, D. L. T. & Stockdale, T. N. 2004: Sensitivity of dynamical seasonal forecasts to ocean initial conditions. *Quart. J. R. Meteorol. Soc.* 130, 647–667.
- Anderson, D. L. T. 2008: Overview of seasonal forecasting. In *Seasonal climate: forecasting and managing risk* (eds A. Troccoli, M. Harrison, D. L. T. Anderson & S. J. Mason). NATO Science Series, pp. 47–68. Dordrecht, The Netherlands: Springer Academic Publishers. (doi:10.1007/978-1-020-6992-5_3)
- Annamalai, H., K. Hamilton, and K. R. Sperber, 2007: The South Asian Summer Monsoon and Its Relationship with ENSO in the IPCC AR4 Simulations. *J. Climate*, 20, No.6, 1071–1092.
- Anyah, R. O., 2005: Modelling the variability of the climate system over Lake Victoria basin: PhD. thesis, Department of Marine, Earth and Atmospheric Sciences, North Carolina University, USA.
- Anyah, R. O., F.H.M. Semazzi, and L. Xie, 2006: Simulated physical mechanisms associated with climate variability over Lake Victoria Basin in East Africa. *Mon. Wea. Rev.*, 134, 3588-3609
- Anyah, R. O., and F. H. M. Semazzi, 2006: NCAR-AGCM ensemble simulations of the variability of the Greater Horn of Africa climate, Special Issue, *Theoretical and Applied Climatology*, 86, 39-62
- Anyah, R.O. and F.H.M. Semazzi, 2007: Variability of East African rainfall based on multiyear RegCM3 simulations. *Int. J. Climatol.*; DOI: 10.1002/joc1401.
- Anyamba, E.K., 1983: On the monthly mean tropospheric circulation and the anomalous circulation during the 1961/62 floods in East Africa: *MSc. thesis, Department of Meteorology, University of Nairobi.*
- Anyamba, E K, 1984: Some aspects of the origin of rainfall deficiency in East Africa. *Proceeding of the WMO regional scientific conference; On GATE, WAMEX and Tropical Meteorology, Dakar, Senegal*, pp 110-112
- Anyamba, E.K. and L.J. Ogallo, 1985: Anomalies in the wind field over Africa during the East African rainy season of 1983/84. *WMO/TD No. 67 – 72.*
- Anyamba E.K., 1990: A diagnostic Study of Low Frequency in Tropical Outgoing Long Wave Radiation. *PhD thesis, Department of Meteorology, University of Nairobi*
- Anyamba, E.K., 1993: On the dynamics of weather systems in Eastern Africa; *Proceedings third technical conference on the meteorological research in Eastern and*

- Arakawa, A., and V. R. Lamb, 1977: Computational design of the basic dynamical processes of the UCLA general circulation model. In: *Methods in Computational Physics*, 17 [J. Chang (ed.)]. Academic Press, New York, 173-265.
- Ashok, K., S. K. Behera, S. A. Rao, H. Weng, and T. Yamagata (2007), El Niño Modoki and its possible teleconnection, *J. Geophys. Res.*, 112, C11007, doi: 10.1029/2006JC003798.
- Ashok, K., S. Iizuka, S. A. Rao, N. H. Saji, and W.J. Lee, 2009: Processes and boreal summer impacts of the 2004 El Niño Modoki: An AGCM study, *Geophys. Res. Lett.*, 36, L04703, doi: 10.1029/2008GL036313.
- Asnani, G. C. and J. H. Kinuthia, 1979: Diurnal variation of precipitation in East Africa. Research Report No 8/79, 1-58.
- Asnani, G. C., 1993: *Tropical meteorology*, Published by Pashan, Pune : Indian Institute of Tropical Meteorology , 1993.
- Bader, J., and M. Latif, 2003: The impact of decadal-scale Indian Ocean sea surface temperature anomalies on Sahelian rainfall and the North Atlantic Oscillation. *Geophys. Res. Lett.*, 30, doi: 10.1029/2003GL018426.
- Barnett, T.P and R. Preisendorfer, 1987: Origins and levels of monthly and seasonal forecasts skill for United States surface air temperatures determined by Canonical Correlation Analysis. *Mon. Wea. Rev.*, 115, 1825 – 1850
- Barnston A. G., Thiao W. and Kumar, V., 1996: Long-lead forecasts of seasonal precipitation in Africa using CCA. *Weather and Forecasting* 11: 506-520.
- Barring, L., 1987: Spatial patterns of daily rainfall in Central Kenya: Applications of Principal Component Analysis, Common Factor Analysis. *J. Clim.*, 7, 7-287
- Bark, D.L., 1978: History of American Droughts. *North American Droughts. A Selected Symposia Series*. Westview Press, Boulder Colorado, N.J. Rosenberg, Ed., pp 9-23.
- Basalirwa, C.P.K (1991): Raingauge network designs for Uganda, *Ph.D Thesis, University of Nairobi, Kenya*.
- Basalirwa, C.P.K (1979): Estimation of areal rainfall in some catchments of the Upper Tana River. *Msc. Thesis, University of Nairobi, Kenya*.
- Bazira, E., 1997: Predictive potential of East African seasonal rainfall derived from SST modes. *MSc. thesis, Department of Meteorology, University of Nairobi, Kenya*

- Behera, S. K., J. J. Luo, S. Masson, P. Delecluse, S. Gualdi and A. Navarra, 2005: Paramount Impact of the Indian Ocean Dipole on the East African short Rains: ACGCM study. *J. Climate*, 18, 41-54
- Behera, S. K., J. J. Luo, S. Masson, S. A. Rao and H. Sakuma, 2006: A CGCM Study on the Interaction between IOD and ENSO, *Journal of Climate*, Volume 19, 1688-1705
- Beltrando, G., 1990: Space-time variability of rainfall in April–November over East Africa during the period 1932–1983. *Int. J. Climatol.*, 10, 691–702.
- Beltrando, G., and D L Cadet, 1990: Relationship between the short rain season in Africa and the atmospheric circulation over Africa and Indian Ocean. Proc. 2nd Techn. Conf on weather forecasting in East and southern Africa, Nairobi, Kenya 3-7 September 1990. pp 64-66.
- Beltrando, G and P. Camberlin, 1993: Interannual variability of rainfall in eastern horn of Africa and indicators of atmospheric circulation. *Int. J. Climatol.* 13, 533-524.
- Beraki A.F., 2005: Climate change scenario simulations over Eritrea by using a fine resolution limited area climate model: temperature and sensitivity, Masters Thesis, University of Pretoria, Department of Geography, Geoinformatics and Meteorology, Eritrea, Niger.
- Beresford, A. K. V. 1982: Recent Climatic change in East Africa: Lake levels, rainfall and upper air flow. Phd thesis, University of East Anglia, UK., 283 pp.
- Black, E, J. Slingo and K. R. Sperber, 2003: An observational study of the relationship between excessively strong short rains in the coastal East Africa and Indian Ocean SST., *Mon Wea. Rev.* 131, 74-94.
- Black, E., 2004: The relationship between Indian Ocean sea-surface temperature and East African rainfall, *Phil. Trans. R. Soc. A* 2005 363, 43-47, DOI: 10.1098/rsta.2004.1474
- Bloomfield, P., 1976, *Fourier analysis of time series: An introduction*: John Wiley and sons, p.256-.799 [Smoothed periodogram method of spectral analysis]
- Boer, G. J., and S. J. Lambert, 2008: Multi-model decadal potential predictability of precipitation and temperature. *Geophys. Res. Lett.*, 35, doi: 10.1029/2008GL033234.
- Bowden, J., Semazzi, F. H. M., R. Anyah and C. Schreck., 2004: Intraseasonal to Decadal Variability of the Greater Horn of Africa, North Carolina State University, Raleigh, North Carolina
- Bowden, J. and F. H. M. Semazzi, 2007: Empirical analysis of intraseasonal climate variability over the Greater Horn of Africa. *J. Climate* 20 (23) 5715-5731

- Bretherton, C. S., Smith, C., and Wallace, J. M., 1992: An intercomparison of methods for finding coupled patterns in climate data. *J. Clim.*, 5:541-560
- Bromwich, D. H., and R. L. Fogt, 2004: Strong trends in the skill of the ERA-40 and NCEP-NCAR reanalyses in the high and middle latitudes of the Southern Hemisphere, 1958-2001. *J. Climate*, 17, 4603-4619.
- Bunting, A.H., Dennett, M.D., Elston, J and Milford, J.R (1975) Rainfall trends in the West African Sahel. *Q.J.R. Meteorol. Soc.*, 102, pp. 59-64
- Burroughs, W. J., 1999: The climate revealed., *Mitchell Beazley, An Imprint of Octopus Publishing Group Ltd, 2-4 Heron Quays, London; 129pp.*
- Burt, C., (1952): Tests of significance in factor analysis. *Br. J. Psycho.*, 5, pp.109-133.
- Castell, R.B. (1966): 'The scree test for the number of factors', *Multivar. Behav. Res.*, 1, 245-276.
- Cadet, D. and P. Olory-Togbe 1977: The propagation of Tropical Disturbances over Indian Ocean during the summer monsoon. *Mon. Wea. Rev.* 105, 700-708.
- Cadet, D. 1978: The importance of moving tropical disturbances over the Indian Ocean during the summer monsoon. *Indian J. Met. Hydrol. Geophys.*, 29, 138-148.
- Cadet, D. L. and B. C. Diehl, 1984: Interannual variability of surface fields over the over Indian Ocean during recent decades. *Mon. Wea. Rev.* 112, 1921-1935.
- Cadet, D. L. 1985: The Southern Oscillation over the Indian Ocean. *J. Climatol.*, 5, 189 - 212.
- Cadet, D. L. and G. Beltrando, 1987: Relationship between surface fields over Indian Ocean and rainfall over East Africa. Report of the Third Session of the SCOR-IOC/CCCO Indian Ocean Climate Studies Panel, UNESCO / ICSU, 13-17.
- Cai, W., and T. Cowan, 2007: Trends in the southern Hemisphere circulation in IPCC AR4 models over 1950-99: Ozone depletion versus greenhouse forcing. *J. Climate*, 20, No.4, 681-693.
- Camberlin, P. and N. Philippon, 2001: The east African March-May rainy season associated atmosphere dynamics and predictability over the 1968-97 period. *Am. Meteorol. Soc.* 15: 1002-1019.
- Camberlin, P., F. Chauvin, H. Douville, and Y. Zhao, 2004: Simulated ENSO-tropical rainfall teleconnections in present-day and under enhanced greenhouse gases conditions. *Clim. Dyn.*, 23, 641-40 657.
- Chatfield, C., 1975, the analysis of time series: Theory and practice, Chapman and Hall, London, p. 263 pp.
- Camberlin and R. E. Okoola, 2003: The onset and cessation of the "long rains" in eastern Africa and their inter-annual variability. *J. Theor. Appl. Climatol.*, 75, 43-54

- Cattel, R. B., 1966: The Scree test for the number of factors. *Multivar. Behav. Res.*, 1, 245-259.
- Chang, P., L. Ji, and H. Li, 1997: A decadal climate variation in the tropical Atlantic Ocean from thermodynamic air-sea interactions. *Nature* 385, 516-518.
- Chang, P., 1998: The Unusual tropical Atlantic Ocean temperatures Cause climate swings in Brazil and West Africa. *Quarterdeck*, 2, No.2, summer, 1998, <http://www-ocean.tamu.edu/Quarterdeck/QD6.2/chang.html#model>
- Charnock, H., 1955: Wind stress on a water surface. *Q. J. R. Meteorol. Soc.*, 81, 639-640.
- Chervin, R. M., and M. Druyan, 1984: The influence of ocean surface temperature gradient and continentality on the Walker circulation. Part I: Prescribed tropic changes. *Mon Wea Rev*, 112, 1510-1523.
- Cherry, S., 1997: Singular value decomposition analysis and canonical correlation analysis. *J. Climate*, 9, 2003-2009
- Clark, C. O., P. J. Webster and J. E. Cole, 2003: Interdecadal variability of the relationship between the Indian Ocean Zonal Mode and East African coastal rainfall anomalies. *J. Climate*, 16, 548-554.
- Claud, C, and P. Terry, 2007: Revisiting the possible links between Quasi-biennial oscillation and Indian summer monsoon using NCEP R-2 and CMAP. *J. climate*, 20 No. 5, 773-78
- CLIVAR VACS, 2007: Decadal variability issues in Africa.
- Cohen, S.J. (1983): Classification for 500 mb Height Anomalies using obliquely rotated principal components. *J. of Applied Meteor.* vol.22, No.12, 1975-1988.
- Colberg, F., and C.J.C. Reason, 2004: South Atlantic response to El-Nino-Southern Oscillation induced climate variability in an ocean general circulation model. *J. Geophys. Res.*, 109, C12015, 14pp.
- Colberg, F., and C.J.C. Reason, 2004: South Atlantic response to El-Nino-Southern Oscillation induced climate variability in an ocean general circulation model. *J. Geophys. Res.*, 109, C12015, 14pp
- Collins, W. J., D. S. Stevenson, C. E. Johnson and R. G. Derwent, 1997: Tropospheric ozone in a global scale three-dimensional Lagrangian model and its response to NOx emission controls. *J. Atmos. Chem.*, 26, 223-274.
- Collins M, and co-authors, 2006: Interannual to decadal climate predictability in the North Atlantic: A Multi-model ensemble study. *J. Climate*, 19, 1195-1203.

- Collimore, C., D.W. Martin, M.H. Hitchman, A. Huesmann, and D.E. Waliser, 2003: On the relationship between the QBO and Tropical Deep Convection. *J. Climate*, 16, 2552-2558.
- Cox, P. M., R. A. Betts, C. B. Bunton, R. L. H. Essery, P. R. Rowntree and J. Smith, 1999: The impact of new land surface physics on the GCM simulation of climate and climate sensitivity. *Clim. Dyn.*, 15:183-203.
- Craddock, J.M., 1968: A simple statistical test for use in the study of climatic change. *Weather*, volume, 12, No. 8, pp. 252-258
- Craddock, J.M., (1973): Problems and prospects for eigenvector analysis in Meteorology. *Statist.*, 22, pp. 133-145.
- Craddock, J.M. and S. Flintoff, (1970): Eigenvector representation of Northern Hemispheric fields. *Quart. J. Royal Met. Soc.*
- Crawford, W., Martinez, R. and Suga, T., 2006: List of possible applications for decadal prediction. CLIVAR Pacific Panel Document.
- CRED EM-DAT (2007): www.emdat.be.
- Cullen, M. J. P., 1993: The unified forecast/climate model. *Meteorol. Mag.*, 122, 81-94.
- Curry, R. and C. Mauritzen, 2005. Dilution of the northern North Atlantic in recent decades. *Science*, 308, 1772-1774.
- Dai A, I.Y. Fung and A.D.D.Genio, 1997: Surface observed global land precipitation variations during 1900-1988. *J. Climate*, 10, 2943-2962.
- Diaz, H.F. (1981): Eigenvector analysis of seasonal temperature, precipitation and synoptic scale system frequency over the contiguous United States. Part II: spring, summer, fall and annual. *Mon. Wea. Rev.*, 109, 1285-1404.
- Diaz, H.F. and Fulbright, D.C. (1981): Eigenvector analysis of seasonal temperature, precipitation and synoptic scale system frequency over the contiguous United States. Part I: winter. *Mon. Wea. Rev.*, 109, 1267-1284.
- Denis B, R Laprise and J Côté, 2002: Downscaling ability of one-way nested regional climate models: *The big-brother experiment*
- Deser, C., A.S. Phillips, and J.W. Hurrell, 2004: Pacific interdecadal climate variability: Linkages between the tropics and the north Pacific during boreal winter since 1900. *J. Climate*, 17, 3109-3124.
- Durman, C. F., Gregory, J. M., Hassell, D. C., Jones, R. G., and Murphy, J. M., 2001: A comparison of extreme European daily precipitation simulated by a global and a

- regional climate model for present and future climates, *Q. J. Roy. Meteor. Soc.*, 127, 1005–1015.
- Eckmann, J.-P., and D. Ruelle (1985): Ergodic theory of chaos and strange attractors, *Rev. Mod. Phys.*, 57, 617–656. Correction, *Rev. Mod. Phys.*, 57, 1115.
- Ehrendorfer, M., 1987: A regionalization of Australia's precipitation climate using principal component analysis. *J. Climat.*, 7, 71–89.
- Enfield, D.B., A.M. Mestas-Núñez, and P.J Trimble, 2001: The Atlantic Multidecadal Oscillation and its relation to rainfall and river flows in the continental US. *Geophys. Res. Lett.*, 28, 2077–2080.
- England, M. H., and F. Huang, 2005: On the interannual variability of the Indonesian through flow and its linkage with ENSO., *J Climate*, **18**, 1435-1444.
- ENSEMBLES, 2007. <http://www.ensembles-eu.org/>
- ERA-40 re-analysis: *Quart. J. R. Meteorol. Soc.*, 131, 2961-3012. doi:10.1256/qj.04.176
- Farmer, S., 1971: An investigation into the results of principal component analysis of data derived from random numbers. *Statistician.*, 1971; **20**: 63–72.
- Findlater, J., 1971: Mean monthly airflow at low levels over the western Indian Ocean. *Geophys. Mem.*, No. 115, HMSO London, UK
- Folland, C. K., T. N. Palmer, and D. E. Parker, 1986: Sahel rainfall and worldwide sea temperatures, 1901-85. *Nature*, **320**, 602-607.
- Folland, C. K., J. A. Owen, N. M. Ward, and A. W. Coleman, 1991: Prediction of seasonal rainfall in the Sahel region using empirical and dynamical methods, *J. Forecasting*, **10**, 21-56
- Folland, C.K., J.A. Renwick, M.J. Salinger and A.B. Mullan, 2002: Relative influences of the Interdecadal Pacific Oscillation and ENSO on the South Pacific Convergence Zone. *Geophys. Res. Lett.*, 29 (13), 1643, doi: 10.1029/2001GL014201.
- Fowler, H. J. and Kilsby, C. G., 2007: Using regional climate model data to simulate historical and future river flows in northwest England, *Climatic Change*, 80, 337–367.
- Frederiksen, C. S., H Zhang, R C. Balgovind, N. Nicholls, W Drosdowsky, and L Chambers, 2001: Dynamical Seasonal Forecasts during the 1997/98 ENSO Using Persisted SST Anomalies. *J Climate*, 14, 2675-2695
- Fremming, D. 1970: Notes on easterly disturbances affecting East Africa. 5-7 September 1967 E.A.M.D. Tech. Memo. No. 13

- Funk, J. P. and Garnham, G. J., 1962: Australian Ozone observations and a suggested 24-months cycle. *Tellus*, 14, 378-382.
- Giannini, A., R. Saravanan, and P. Chang, 2003: Oceanic forcing of Sahel rainfall on interannual to interdecadal time scales. *Science*, 302, 1027-1030.
- Giorgi, F. and Marinucci, M. R., 1996: An investigation of the sensitivity of simulated precipitation to model resolution and its implications of climate studies, *Month. Weather Rev.*, 124, 148-166.
- Giorgi, F., and L. Mearns 1999: Introduction to special section. Regional climate modelling revisited. *J. Geophys. Res.*, 104, 6335-6352
- Giorgi F, Marinucci M. R., Bates G. T., 1993a: Development of a second-generation regional climate model (RegCM2), Part I: Boundary layer and radiative transfer processes. *Mon Wea. Rev.*, 121, 2794-2813
- Giorgi, F. Marinucci, M. R., Bates, G. T., 1993b: Development of a second generation regional climate model (RegCM2), Part II: Convective processes and assimilation of boundary conditions. *Mon. Wea Rev.*, 121, 2814-2832
- Giorgi, F., Bi, X., and Pal, J. S., 2004: Mean, interannual variability and trends in a regional climate change experiment over Europe, I. Present-day climate (1961-1990), *Clim. Dynam.*, 22, 733-756.
- Gissila T. Black E. Grimes D. I. F. Slingo J. M., 2004: Seasonal forecasting of Ethiopian summer rains. *International Journal of Climatology*, 24, 1345-1358.
- Gitau, W. K., 2005: Characteristics of the Wet and Dry Spells during the Wet Seasons over Kenya: MSc. Thesis, Department of Meteorology, University of Nairobi, Kenya.
- Ghil, M., and S. Childress, 1987: *Topics in Geophysical Fluid Dynamics: Atmospheric Dynamics, Dynamo Theory and Climate Dynamics*, 485 pp., Springer-Verlag, New York.
- Ghil, M., and N. Jiang, 1998: Recent forecast skill for the El Niño-Southern Oscillation, *Geophys. Res. Lett.*, 25, 171-174.
- Ghil, M., and C. Taricco, 1997: Advanced spectral analysis methods, in *Past and Present Variability of the Solar-Terrestrial System: Measurement, Data Analysis and Theoretical Models*, edited by G. C. Castagnoli and A. Provenzale, pp. 137-159, Soc. Ital. di Fis., Bologna, Italy.
- Ghil, M., and R. Vautard, 1991: Interdecadal oscillations and the warming trend in global temperature time series, *Nature*, 350, 324-327.

- Ghil, M., M. R. Allen, M. D. Dettinger, K. Ide, D. Kondrashov, M. E. Mann, A. W. Robertson, A. Saunders, Y. Tian, F. Varadi, and P. Yiou, 2002: Advanced Spectral Methods for Climatic Time Series. *Reviews of the Geophysics*, 40, pp 1-44.
- Ghil, M., and P. Yiou, 1996: Spectral methods: What they can and cannot do for climatic time series, in *Decadal Climate Variability: Dynamics and Predictability*, edited by D. Anderson and J. Willebrand, pp. 445-481, Springer-Verlag, New York.
- Goddard, L., and N.E. Graham, 1999: Importance of the Indian Ocean for simulating rainfall anomalies over eastern and southern Africa. *J. Geophysical Research*, 104, No. D16, 19099 - 19116.
- Goldenberg, S.B., C.W. Landsea, A.M. Mestas-Nuñez, and W.M. Gray, 2001: The recent increase in Atlantic hurricane activity: Causes and implications. *Science*, 293, 474-479.
- Gordon, C., C. Cooper, C. A. Senior, H. Banks, J. M. Gregory, T. C. Johns, J. F. B. Mitchell and R. A. Wood, 2000: The simulation of SST, sea ice extents and ocean heat transports in a version of the Hadley Centre coupled model without flux adjustments. *Clim. Dyn.*, 16:147-168
- Gregory, S. (1963): *Statistical methods and the Geographer*. Longman Group Ltd. The Chancer Press, Bungay, Suffolk, 1963, 240pp.
- Gregory, S. (1975): On the delimitation of Regional patterns of recent climatic fluctuations. *Mon. Wea. Rev.*, 30,276-287.
- Gregory, S. (1979): The definition of wet and dry periods for discrete regional units. *Weather, in press*.
- Gregory, D., and P. R. Rowntree, 1990: A mass-flux convection scheme with representation of cloud ensemble characteristics and stability dependent closure. *Mon. Wea. Rev.*, 118:1483-1506.
- Gregory, D., and S. Allen, 1991: The effect of convective downdraughts upon NWP and climate simulations. In: *Ninth conference on numerical weather prediction*, Denver, Colorado, pages 122-123.
- Gregory, D., R. Kershaw and P. M. Inness, 1997: Parametrization of momentum transport by convection II: Tests in single column and general circulation models. *Q. J. R. Meteorol. Soc* 123:1153-1183.
- Gross, M.G., 1972: *Oceanography-A view of the Earth*, Prentice-Hall, Inc., Eaglewood Cliffs, New Jersey, 581pp
- Gu, D.F., and S.G.H. Philander, 1995: Secular changes of annual and interannual variability in the tropics during the past century. *J. Clim.*, 8, 864-876.

- Haines K, L. Hermanson, C. Liu, D. Putt, R. Sutton, A. Iwi and D. Smith, 2008: Decadal climate prediction (project GCEP), *Phil. Trans. R. Soc. A* (2009) 367, 925–937 doi:10.1098/rsta.2008.0178
- Hakkinen, S., and P. B. Rhines, 2004: Decline of subpolar North Atlantic circulation during the 1990s. *Science*, 304, 555–559.
- Hannan, E. J., 1960: *Time Series Analysis*, 152 pp., Methuen, New York.
- Harrison, D. E., and M. Carson, 2007: Is the world ocean warming? Upper ocean temperature trends: 1950-2000. *J. Phys. Oceanogr.*, 37, No. 2, 174-187.
- Hasebe, F., 1980: A global analysis of the fluctuations of total ozone-II; Non-stationary annual oscillation, quasi-biennial oscillation and long-term variations in total ozone. *J. Met. Soc. Japan*, 58, 104-117.
- Hashizume, H., S-R Xie, N. Fujwana, M. Shiotani, T. Watanabe, Y. Tanimoto, W.T. Liu, and K. Takeuchi, 2003: Direct Observations of Atmospheric Boundary layer response to SST variations associated with tropical Instability waves over the eastern Equatorial Pacific. *J. Climate*, 15, 3379 – 3393
- Hastenrath, S., and L. Heller, 1977: Dynamics of Climate Hazards in the Northeast Brazil. *Quart. J. Roy. Meteor. Soc.*, 103, 77-92
- Hastenrath, S., M., C. Wu, and P. S. Chu, 1984: Towards the monitoring and prediction of north-east Brazil droughts. *Quart. J. Roy. Meteor. Soc.*, 110, 411-425
- Hastenrath, S., 1990: Decadal – scale changes of the circulation in the tropical Atlantic sector associated with Sahel drought. *Int. J. Climatol.* , 10, 459-472.
- Hastenrath, S., A. Nicklis and L. Greishar, 1993: Atmospheric-hydrospheric mechanisms of climate anomalies over the western equatorial Indian Ocean. *J. Geophys. Res*, 98, 20 219-20 235
- Hastenrath, S. 1995: Recent advances in tropical climate prediction. *J. Climate*, 8, .1519-1532
- Hastenrath, S, 2000: Zonal circulations over the equatorial Indian Ocean. *J. Climate*, 13, 2746-2756.
- Hastenrath, S., 2002: Dipoles, temperature gradients, and tropical climate anomalies. *Bull. Amer. Meteor. Soc.*, 83, 735-738.
- Hastenrath, S. and Polzin. D, 2003: Circulation mechanisms of climate anomalies in the equatorial Indian Ocean. *Meteorol. Z.*, 12, 81-93.
- Hasternrath, S. and D. Polzin, 2004: Dynamics of the surface wind field over the equatorial Indian Ocean, *Q.J.R. Meteor. Soc.*, 130, 503-517

- Hendon, H.H., M. C. Wheeler and C. Zhang, 2007: Seasonal dependence of the MJO-ENSO relationships. *J. Climate*, 20, NO.3, 531-543
- Herman, H.H. (1976): Modern factor analysis. The University of Chicago press. *Chicago and London, 1976, 487pp.*
- Hoerling, M. P., J. W. Hurrell, J. Eischeid, and A. Phillips, 2006: Detection and Attribution of 20th Century Northern and Southern African Rainfall Change. *J. Climate*, 19, 3989-4008.
- Holton, J. R. and R. S. Lindzen, 1972: An updated theory for quasi-biennial oscillation, *Journal of Atmospheric Science* 20: 1070-1080.
- Houghton JT, Meira Filho LG, Callander BA, Harris N, Kattenberg A, Maskell K (eds). 1995. *Climate Change 1995, Intergovernmental Panel on Climate Change (IPCC)*. Cambridge University Press: Cambridge.
- Houghton JT, Ding Y, Griggs DJ, Noguer M, van der Linden PJ, Xiaosu D (eds). 2001. *Climate Change 2001: The Scientific Basis, Contribution of Working Group I to the Third Assessment Report of the Intergovernmental Panel on Climate Change*. Cambridge University Press: Cambridge.
- Hsieh, W. W., 2004: Nonlinear multivariate and time series analysis by neural network methods. *Rev. Geophysics*, 42, RG1003/2004, 25pp
- Huang, B., P. S. Schopf, and Z. Pan, 2002: The ENSO effect on the tropical Atlantic variability: A regionally coupled model study. *Geophys. Res. Lett.*, 29, 2039, doi: 10.1029/2002GL014872.
- Huang, B., and J. Shukla, 2007: Mechanisms for the Interannual Variability in the Tropical Indian Ocean. Part I: The Role of Remote Forcing from the Tropical Pacific, *J. Climate*, 20, 2917-2936
- Hudson, D. A. and Jones, R.G., 2002: Regional Climate model simulations of present-day and future climates over southern Africa, Technical Note 39, Hadley Centre for Climate Prediction and Research, Met Office, Bracknell, UK.
- Hulme M. 1992. Rainfall changes in Africa — 1931-1960 to 1961-1990. *International Journal of Climatology* 12: 685-699.
- Hu, Z.-Z., and B. Huang, 2006: Physical Processes Associated with the Tropical Atlantic SST Meridional Gradient. *J. Climate*, 19, 5500-5518
- Hye-Mi Kim, Peter J. Webster, Judith A. Curry, 2009: Impact of Shifting Patterns of Pacific Ocean Warming on North Atlantic Tropical, *Science* 3 July 2009: Vol. 325. no. 5936, pp. 77 - 80

ICPAC, 1999: Homogeneous Climatological Zoning *DMC Lecture Notes, chapter 3*, 29 – 43

ICPAC, 2006: Seasonal Prediction For September– December 2006 Rainfall Using Empirical Statistical Models, Capacity Building Training Workshop for The Great Horn Of Africa (GHA) Regions, IGAD Climate Prediction and Application Centre, Nairobi-Kenya 14 – 30 August 2006

Ihara, C., Yochanan Kushnir, and Mark A. Cane, 2008: Warming Trend of the Indian Ocean SST and Indian Ocean Dipole from 1880 to 2004, *J. Climate*, 21., 2035–2046

Indeje, M. and Semazzi, F.H.M, 2000: Relationships between QBO in the lower equatorial stratospheric zonal winds and East African seasonal rainfall, *Meteorol. Atmos. Phys.*, 73, 227-244

Indeje, M., Semazzi, F.H.M., Ogallo L. J., 2000: ENSO signals in East African rainfall seasons. *Int. J. Climatology*, 20, 19-46.

Indeje, M., 2000: Prediction and numerical simulation of regional climate of equatorial eastern Africa. PhD Thesis, North Carolina State University, U.S.A. pp 327

Ininda, J.M., 1994: Numerical Simulation of the Influence of SST Anomalies on the East African Seasonal Rainfall. *Ph.D Thesis, University of Nairobi*.

Ininda, J.M., 1995: Numerical simulation of the influence of sea surface temperature anomalies on the East African seasonal rainfall. PhD. thesis, Department of Meteorology, University of Nairobi, Kenya

IPCC (2007): Summary for Policymakers. In: *Climate Change 2007: The Physical Science Basis. Contribution of Working Group I to the Fourth Assessment Report (AR4) of the Intergovernmental Panel on Climate Change* [Solomon, S., D. Qin, M. Manning, Z. Chen, M. Marquis, K.B. Averyt, M.Tignor and H.L. Miller (eds.)]. Cambridge University Press, Cambridge, United Kingdom and New York, NY, USA

IPCC (2007): Forth Assessment Report, *Climate Change 2007 (AR4)*, Working Group II summary for policy makers.

ISDR, 2005: World Conference on Disaster Reduction, 18 to 22 January 2005, Kobe, Hyogo Prefecture, Japan.

Islam, N., M. Rafiuddin, A.U. Ahmed and R. K., Kolli, 2007: Callibration of PRECIS in employing future scenarios in Bangladesh. *Int. J. Climatol.* DOI: 10.1002

Jenkins, G.M. and Watts, D.G., 1968: *Spectral Analysis and Its Applications*. Holden-Day, California, U.S.A

Jochum, M., C. Deser, and A Phillips, 2007: Tropical Atmospheric Variability forced by ocean internal variability. *J. Climate*, 20, 765-771

- Johnson, D. H., 1962: Rain in East Africa. *Quart. J. Roy. Met. Soc.*, 88, 1-19.
- Jolliffe, I. T., 2002: *Principal Component Analysis*, 2nd Ed. Springer, 487pp.
- Jones P. D, Hulme M. 1996. Calculating regional climatic time series for temperature and precipitation: methods and illustrations *International Journal of Climatology* 16: 361-377
- Jones, A., D. L. Roberts and A. Slingo, 1994: A climate model study of indirect radiative forcing by anthropogenic sulphate aerosols. *Nature* 370:450-453.
- Jones R.G, J.M Murphy and M Noguera (1995): Simulation of climate over Europe using a nested regional climate model. Part 1: Assessment of control climate including sensitivity to location of lateral boundaries. *Quart J Royal Meteor. Soc.*, 121, 1413-1449
- Jury M. R., 1993: A preliminary study of Climatological Associations and characteristics of tropical cyclones in the SW Indian Ocean. *Meteorology and Atmospheric Physics* 51, 101 – 115.
- Jury, M.R., C.A. McQueen, and K.M. Levey, 1994: SOI and QBO signals in the African region. *Theoretical and Applied Climatology*, 50, 103 – 115.
- Jury, M.R., B.A. Parker, N. Raholijao and A. Nassor, 1995: Variability of summer rainfall over Madagascar: climatic determinants at interannual scales. *Int. J. Climatology*. 15, 1323 – 1332.
- Jury, M. R., B. Pathack and B. Parker, 1999: Climatic determinants and statistical prediction of tropical cyclone days in the Southwest Indian Ocean. *J Climate*, 12, 1738-1746.
- Kabanda, A.T and Jury M.R. 1999: Synoptic forcing and evolution of composite wet spells over northern Tanzania: descriptive analysis. *Geography Dept. Univ. Zululand*.
- Kaiser, H.F. (1958): The Varimax Criterion for Analytic Rotation in Factor Analysis. *Psych.*, 23, pp.187-200.
- Kaiser, H.F. (1959): 'Computer program for varimax rotation in factor analysis', *Educ. Psychol. Meas.*, 19, 1413-1420.
- Kanamitsu, M., W. Ebisuki, J. Wollen, S. K Yang, J. J. Hnilo, M. Fiorino and G. L. Potter ,2002: NCEP –DOE AMIP– II reanalysis ,R-2, *Bull. Amer. Meteor. Soc.*, 83, No. 11, 1631-1643

- Karoly, D. J., P. Hope, and P. D. Jones, 1996: Decadal variations of the Southern Hemisphere circulation. *Int. J. Climatol.*, 16, 723 – 738.
- Kendall, M. G., 1938: A new measure of rank correlation. *Biometeorology*. 33: 81-93.
- Kendall, M. G., 1945: The treatment of ties in ranking problems. *Biometeorology*. 33: 297-298
- Kendall, M. G., 1948: Rank correlation Methods. London: Charles Griffin.
- Kendall, M. G., and A. Stuart, 1961: Advanced theory of Statistics. Charles Griffins, London
- Keenlyside, N., M. Latif, J. Junclaus, L. Kornblueh and E. Roeckner, 2008: Advancing decadal climate scale prediction in the North Atlantic. *Nature*, **453**, 84-88.
- Keller, K., C. Deutssch; M. G. Hall; And D. F. Bradford, 2007: Early detection of changes in the north Atlantic meridional overturning circulation: Implications for the design of ocean observation systems. *J. Climate*, 20 No. 2, 145-157
- Kestin, T. S., D. J. Karoly and J. I. Yano, 1998: Time-frequency variability of ENSO and stochastic simulations. *J. Clim.*, 11, 2258-2272.
- Kiangi, P. M. R., M. M. Kavishe, and J. K. Patnaik, 1981: Some aspects of the mean tropospheric motion field in East Africa during the long rains season. *Kenya J. of Sci. and Tech. (A)*, 2, 91-103.
- Kida, H., T. Koide, H. Sasaki and M. Chiba, 1991: A new approach to coupling a limited area model with a GCM for regional climate simulation. *J. Meteor. Soc. of Japan* 69:723-728.
- Kinuthia, J. H. and G. C. Asnani, 1982: A newly found jet in North Kenya (Turkana Channel). *Mon. Wea. Rev.*, 110, 1722 – 1728
- Kirtman, B. P., J. Shukla, B. Huang, Z. Zhu, and E. K. Schneider, 1997: Multiseasonal Predictions with a Coupled Tropical Ocean–Global Atmosphere System. *Mon. Wea. Rev.*, 125, 789-808
- Kolli R. K., A.K Kumar, K.K. Kumar, S.K. Patwardhan, P.K. Mishra, J.V. Revadekar, K. Kamala, G. B. Pant, 2006: High-resolution Climate change scenarios for India for the 21st century. *Current science* 90(3): 334-345
- Komutunga, E. T, 2006: Optimum cropping calendars derived for rain-fed agriculture of Uganda. *PhD Thesis, Department of Meteor. University of Nairobi, Kenya*.93pp
- Korecha, D. and A. G. Barnston, 2007: Predictability of June to September rainfall in Ethiopia. *Monthly weather Review*, **135**, 628-650.

- Knight, J., and co-authors, 2005: A signature of persistent natural thermohaline circulation cycles in observed climate. *Geophys. Res. Lett.*, **32**, L20708, doi: 1029/2005GL024233
- Knutson, T. R. and Tuleya, R. E., 2004: Impact of CO₂-induced warming on simulated hurricane intensity and precipitation: Sensitivity to the choice of climate model and convective parameterization. *J. Clim.* **17**, 3477–3495).
- Krishnamurthy, V., and B. P. Kirtman, 2003: Variability of the Indian Ocean: Relation to monsoon and ENSO. *Quart. J. Roy. Meteor. Soc.*, **129**, 1623–1646.
- Kug, J. S. and I. S. Kang, 2006: Interactive feedback between the Indian Ocean and ENSO. *J. Climate*, **19**, 1784–1801.
- Kug, J-S., S.-I., An, F-F. Jin, and I-S. Kang, 2005: Preconditions for El Niño and La Niña onsets and their relation to the Indian Ocean. *Geophys. Res. Lett.*, **32**, L05706.
- Kug, J. S., B. P. Kirtman and I. S. Kang, 2006: Interactive Feedback between ENSO and the Indian Ocean in an Interactive Ensemble Coupled Model. *J. Climate*, **19**, 6371–6381
- Kumar, K. R., A. K. Sahai, K. Krishna Kumar, S. K. Patwardhan, P. K. Mishra, J. V. Revadekar, K. Kamala and G. B. Pant, 2006: High-resolution climate change scenarios for India for the 21st century, current science, vol. 90, no. 3, PP 334-345
- Lamb P. J. and Pepler R. A. 1992: Further case studies of tropical Atlantic surface atmospheric and oceanic patterns associated with sub-Saharan drought. *Journal of Climate* **5**: 476–488.
- Lamb, P. J., 1978: Case studies of tropical Atlantic surface circulation patterns during recent sub-Saharan weather anomalies: 1967 and 1968. *Mon. Wea. Rev.*, **106**, 282–291.
- Landman, W. A. and S. J. Mason, 1999: Change in the association between Indian Ocean sea-surface temperatures and summer rainfall over South Africa and Namibia. *Int. J. Climatol.*, **19**, 1477-1492.
- Landsberg, H. E., 1975: Sahel drought, change or part of climate. *Arch. Meteorol. Geophys. Bioclimatol. Ser. B23*: 193-200.
- Latif, M. and Barnett, T. P., 1994: Causes of decadal climate variability over the North Pacific and North America, *Science*, **266**, 634–637.
- Latif, M., M. Collins, H. Pohlmann, and N. Keenlyside, 2006: A Review of Predictability Studies of Atlantic Sector Climate on Decadal Time Scales. *J. Climate*, **19**, 5971–5987

- Lau, K. M., and H. Weng, 1999: Interannual, decadal-interdecadal, and Global warming signals in sea surface temperature during 1955-97.
- Lee, T. C. K., F. Zwiers, X. Zhang, and M. Tsao, 2006: Evidence of decadal climate prediction skill resulting from changes in anthropogenic forcing. *J. Climate*, 19, 5305-5318.
- Li, S., W.A. Robinson, M.P. Hoerling and K. M. Weickmann, 2007: Dynamics of the extratropical response to a tropical Atlantic SST anomaly. *J. Climate*, 20, No.3, 560-574.
- Lindzen, R. S. and S. Nigam, 1987: On the role of sea surface temperature gradients in forcing low-level winds and convergence in the tropics. *J. Atmos. Sci.*, 44, 2418-2436.
- L'Hôte Y, Mahé G, Somé B, Triboulet J. P. 2002. Analysis of a Sahelian annual rainfall index from 1896 to 2000; the drought continues. *Hydrological Sciences Journal—Journal Des Sciences Hydrologiques* 47: 563–572.
- Lozier, M.S., S. J. Leadbetter, R. G. Williams, V. Roussenov, M.S.C. Reed, and N.J. Moore, 2008: The spatial pattern and mechanisms of heat content change in the North Atlantic, *Science*, 319, 800-803.
- Lough, J. M., 1986: Tropical Atlantic sea surface temperature and rainfall variations in Sub-Saharan Africa. *Mon. Wea. Rev.*, 114, 561-570.
- Lu, J., and T. Delworth, 2005: Oceanic forcing of the late 20th century Sahel drought. *Geophys. Res. Lett.*, 32, L22706, doi: 10.1029/2005GL023316.
- Madden R. A. and P. R. Julian (1972): Description of global-scale circulation cells in the tropics with a 40-50 day period. *J. Atmos. Sci.*, 29, 1109-1123
- Madden R. A. and Julian P. R (1994): Observation of 40-50 days tropical Oscillation: *Mon. wea. Rev.*, 122, 814-837
- Mann E. M. and J. Park (1996): Joint Spatiotemporal Modes of surface Temperature and Sea Level Pressure Variability in the Northern during the Last Century. *Journal of Climate*, 9, 2137-2162.
- Mantua, N.J., S.R. Hare, Y. Zhang, J.M. Wallace, and R.C. Francis, 1997: A Pacific decadal climate oscillation with impacts on salmon. *Bull. Amer. Meteorol. Soc.*, 78, 1069-1079.
- Martin, G. M., D. W. Johnson and A. Spice, 1994: The measurement and parametrisation of effective radius of droplets in warm stratocumulus clouds. *J. Atmos. Sci.* 51:1823-1842

- Marmorino, G. O., G. P. Smith, and G. J. Lindemann, 2004: Infrared imaging of ocean internal waves. *Geophys. Res. Letters*, 111309, 4pp.
- Mason, S. J. and P. D. Tyson 1992: The modulation of sea surface temperature and rainfall associations over Southern Africa with solar activity and the Quasi-biennial Oscillation. *J. Geophys. Res.* 97, 5847 – 5856.
- Mason, S. J., L. Goddard, N. E. Graham, E. Yulaeva, L. Sun, and P. A. Arkin, 1999: The IRI seasonal climate prediction system and the 1997/98 El Niño event. *Bull. Amer. Meteor. Soc.*, 80, 1853–1874.
- Matthews, A. J., 2008: Primary and successive events in the Madden-Julian Oscillation, *Quart. J. Royal Meteorol. Society*, 134 No. 631, 439 – 453
- McGregor, J. L. 1997: Regional climate modelling, *Meteorol. Atmos. Phys.*, 63, 105–117.
- McPhaden, M. J., M. J., A. J. Busalacchi, R. Cheney, J-R. Donguy, K. S. Gage, D. Halpern, M. Ji, P. Julian, G. Meyers, G. T. Mitchum, P. P. Niiler, J.I Picaut, R. W. Reynolds, N. Smith, and K. Takeuchi 1998: The tropical ocean global atmosphere (TOGA) observing system: A decade of progress. *J. Geophys. Res.*, 103, 14169–14240.
- Meehl, G.A., and K.A. Hibbard, 2007: A strategy for climate change stabilization experiments with AOGCMs and ESMs. WCRP Informal Report No. 3/2007, ICPO Publication No. 112, IGBP Report No.57, World Climate Research Programme: Geneva, 35 pp.
- Meehl, G.A. L. Goddard, J. Murphy, R.J. Stouffer, G. Boer, G. Danabasoglu, K. Dixon, M.A. Giorgetta, A.Greene, E. Hawkins, G. Hegerl, D. Karoly, N. Keenlyside, M. Kimoto, B. Kirtman, A. Navarra, R.Pulwarty, D. Smith, D. Stammer, and T. Stockdale, 2009: Decadal prediction: Can it be skillful? *Bull. Amer. Meteorol. Soc.*, accepted.
- Mehta, V. M., and T. Delworth, 1995: Decadal variability of the tropical Atlantic Ocean surface temperature in shipboard measurements and in a global ocean-atmosphere model. *J. Climate* 8, 172-190.
- Mehta V.M., 1998b: Variability of the tropical SSTs at decadal time-scales. Part II: the Pacific and Indian Oceans. *J. Clim*, 11, 2467–2475
- Mehta, V. M., 1998a: Variability of the tropical ocean surface temperatures at decadal–multidecadal timescales. Part I: The Atlantic Ocean. *J. Climate*, 11, 2351–2375.
- Mehta, 1999: Inter-decadal modulation of the impact of ENSO on Australia. *Climate. Dyn.*, 15, 319-324.

- Mesinger, F., 1981: Horizontal Advection Schemes of a Staggered Grid - An Enstrophy and Energy-Conserving Model. *Mon. Wea. Rev.* 109 pp 467-478.
- Meyers, G., P. McIntosh, L. Pigot, and M Pook, 2007: The Years of El Niño, La Niña, and Interactions with the Tropical Indian Ocean. *Journal of Climate*, 20, 2872-2880
- Mistry, V. V. and D. Conway, 2003: Remote forcing of East African rainfall and relationships with fluctuations in levels of Lake Victoria. *Int. J. Climatol.*, 23, 67-89.
- Minja, W. S., 1984: A comparative Investigation of weather anomalies over East Africa during the 1972 drought and 1977/78 wet periods: *M.Sc. Thesis, University of Nairobi*.
- Mitchell, T.D., T.R. Carter, P.D. Jones, M. Hulme, M. New., 2005: An improved method of constructing a database of monthly climate observations and associated high resolution grids. *Int J. Climatol*, 25, 693-712
- Moura, A. D., and J. Shukla, 1981: On the dynamics of droughts in northeast Brasil: observations, theory, and numerical experiment with a general circulation model. *J Atmos. Sci*, 38, 2653-2375.
- Mukabana, J. R., 1992: Numerical Simulation of the influence of the large-scale monsoon flow on the weather patterns over Kenya using a three-dimensional limited area model: *Ph.D. Dissertation, Dept. of Met: University of Nairobi*.
- Mukabana, J.R., and R.A. Pielke, 1996: Investigating the influence of synoptic scale winds and meso-scale circulations and diurnal weather patterns over Kenya using a mesoscale numerical model. *Mon Wea Rev.*, 124: 224-243.
- Mukherjee, B. K., Indira, K., Reddy, R. S., Ramana Murty, BH. V., 1979: High-level warming, winds and Indian summer monsoon. *Mon. Wea. Rev.*, 107, 1581-1588.
- Murakami, T. and W. L. Sumathipala, 1989: Westerly Bursts during the 1982/83 ENSO. *J Climate* , 2. 71-85.
- Murtugudde, R.G., J.P McCreary, and A.J. Busalacchi, 2000: Oceanic processes associated with anomalous events in the Indian Ocean with relevance to 1997-199, *J Geophys Res.*, 105, 3295-3306.
- Mutai, C.C., and M.N. Ward, 2000: East African rainfall and the tropical circulation / convection on intraseasonal to interannual time scales. *J. Climate*, 13, 3915-3939.
- Mutai, C.C., 2003: The role of Indian Ocean SST on East African Short rains. Proc. The sixth Kenya Meteor. Soc. Workshop on Meteor. Research, Applications and Services, Mombasa, Kenya, 29 September to 3 October 2003. pp 55-59.
- Muthama, N. J., M. M. Manene and C. J. Ndetei, 2008: Simulation of Decadal Precipitation over Nairobi in Kenya. *Journal for Science*, 13 (2008) 43-54

- Mutua, F. M; Mutemi J. N and Oludhe, C., 1999: Homogeneous Climatological Zoning. DMC Lecture Notes, chapter 3, p29 – 43.
- Mutemi, J. N, 2003: Climate anomalies over eastern Africa associated with various ENSO evolution phases: Ph.D. Thesis, University of Nairobi, Kenya.
- Mwale, D., T. Y. Gan, and S. Shen, 2004: Wavelet analysis on variability, teleconnectivity and predictability of East Africa rainfall. 1st International CLIVAR Science Conference, June 21-25, 2004, Baltimore, MD USA
- Nagura, M, K. Ando, and K. Mizuno, 2008: Pausing of the ENSO Cycle: A Case Study from 1998 to 2002, *J. Climate*, **21**, No.2, 342–363
- Nagura, M. and M. Konda, 2007: The Seasonal Development of an SST Anomaly in the Indian Ocean and Its Relationship to ENSO. *Journal of Climate*, **20**, No.1, 38–52.
- Nakamura, K., 1968: Equatorial Westerlies over East Africa and their climatological significance. *Geographical reports of Tokyo Metropolitan University* No. 3, 43-61.
- New, M., Hulme M. and Jones, P. 1999. Representing twentieth-century space-time climate variability. Part I: Development of a 1961-90 mean monthly terrestrial climatology. *Journal of Climate*, 12: 829-856.
- Newell, R. E., 1979: *Climate and the Ocean: American Scientist*, vol. 67, pp. 405-416.
- Nicholson, S.E. and R. M. Chervin, 1983: Recent Rainfall Fluctuations in Africa interhemispheric teleconnections. *Variations in the Global Water Budget* (A. Street-Perrott, M. Beran, R. Ratcliffe, eds), Reidel, Dordrecht, pp 221-238.
- Nicholson, S.E. and Entekhabi, D. 1986: The quasi-periodic behavior of rainfall variability in Africa and its relationship to the Southern Oscillation, *Arch. Meteorol. Geophys. Bioclimatol. Ser. A*, 34, pp. 311-348
- Nicholson, S. E., and Entekhabi, D., 1987: Rainfall variability in Equatorial and Southern Africa: Relationships with sea surface temperature along the south-western coast of Africa. *J. Climate Applied Meteor.*, 26, 561-578
- Nicholson, S. E., Kim J., and Hoopingarner, J., 1988: *Atlas of African Rainfall and Its Interannual Variability*: Florida State University, pp, 252
- Nicholson, S. E. and J. Kim, 1997a: The relationship of the El Niño–Southern Oscillation to African rainfall. *Int. J. Climatol.*, 17, 117–135.
- Nicholson, S.E., and J. Kim, 1997b: An analysis of the ENSO signals in the Tropical Atlantic and Western Indian Ocean. *Int. Journal of Climatol.*, 17, 345-375.

- Nicholson, S. E. and X. Yin; 1998: Variations of African lakes during the last two centuries. In *Water resources variability in Africa during the 20th Century* (E. Servat, D. Hughes, J.-M; Fritsch and M. Hulme, eds.), IAHS Press, Wallingford, UK, 181-188
- Nicholson S. E., 2000a: Land surface processes and Sahel climate. *Reviews of Geophysics* 38: 117-139.
- Nicholson, S.E., 2000b: The nature of rainfall variability over Africa on time scales of decades to millennia. *Global Planet. Change*, 26, 137-158.
- Njau, L. N., 2006: Diagnostics and predictability of East Africa rainfall with tropospheric circulation parameters. *PhD Dissertation, Department of Meteorology University of Nairobi*, 170pp
- Nobre, P. and J. Shukla, 1996: Variations of sea surface temperature, wind stress, and rainfall over the Tropical Atlantic and South America. *J. Climate*, 9, 2464 – 2479.
- Noguer, M., Jones, R. and Murphy, J. 1998: Sources of systematic errors in the climatology of a regional climate model over Europe. *Climate Dynamics*, 14, 691-712.
- North, G.R., Bell, T.L. and Cohalan, R.F. (1982): Sampling errors in estimation of empirical orthogonal functions. *Mon. Wea. Rev.*, vol.110,699-706.
- Nyakwada, W., 2009: Predictability of East African Seasonal Rainfall with Sea Surface Temperature Gradient Modes: Ph.D. Dissertation, Dept. of Met: University of Nairobi.
- Nyenzi, B.S., 1992: An analysis of interannual variability of rainfall over East Africa. *J. Africa Meteo. Soci. (SMA)*, 1, 57-79.
- Ogalo, L. J., 1977: Periodicities and trends in the annual rainfall over Africa. MSc. thesis, Department of Meteorology, University of Nairobi, Kenya
- Ogalo, L. J., 1979: Rainfall variability in Africa. *Mon. Wea. Rev.*, 107, 1113 – 1139
- Ogalo, L.J., 1980a: Regional classification of East African rainfall stations into homogeneous groups using the method of principal component analysis. *Stat. climatology. Devel. in Atmos. Sci.* 13, p255-266.
- Ogalo, L. J., 1980b: Time series analysis of rainfall in East Africa. Ph.D: Thesis University of Nairobi.
- Ogalo, L.J., 1981a: The nature of homogeneity in rainfall records over East Africa. *Res. Report No. 4/81, Kenya Met. Dept. 1981, 18pp.*
- Ogalo, L. J., 1981b: Trend of rainfall in East Africa. *Kenya J. Sci. and Technol. (A)*, 2, 83-90.

- Ogallo, L.J., 1982: Quasi-Periodic patterns in the East Africa rainfall records. *Kenya Journal of Science and Technology* A3: pp 43-54.
- Ogallo, L.J., 1983: Temporal fluctuations of seasonal rainfall in East Africa. *Mausam*, 35, 175-180.
- Ogallo, L. J., 1987: Climate data processing. *WMO Regional Training Seminar for the National Instructors for Regions I and IV, 26-10 to 6-11 1987, Niamey, Niger*
- Ogallo, L. J., and K. A. Suleiman, 1987: Rainfall characteristics in East Africa during the El-Nino years. Proc First Techn Conf on Meteorological Res. in Eastern and Southern Africa, Nairobi, Kenya, 6-9 January 1987, pp 76-80.
- Ogallo, L. J., 1988: Relationships between seasonal rainfall in East Africa and the Southern Oscillation. *J. Climatol.*, 8, 31 – 43
- Ogallo, L.J., Janowiak J.E. and M. S. Halpert, 1988: Teleconnection between seasonal rainfall over East Africa and global seas surface temperature anomalies. *J. Meteor. Soc. Japan*, 66, 807 – 821.
- Ogallo, L.J., 1989: The spatial and temporal patterns of the East African seasonal rainfall derived from principal component analysis. *J. climat.*, 9, 145-167.
- Ogallo, L.A., R.E. Okoola and D.N. Wanjohi, 1994: Characteristics of quasi-biennial oscillation over Kenya and their predictability potential for the seasonal rainfall. *Mausam*, 45, No.1, 57 – 62.
- Okoola, R. E., 1989: Westwards moving disturbances in the south-west Indian Ocean. *Met. Atmos. Phys.*, 41, 33-44.
- Okoola, R E A., 1996: Space-time Characteristics of the ITCZ over equatorial Eastern Africa during anomalous rainfall years. *PhD Thesis Department of Meteorology, University of Nairobi, Kenya*
- Okoola, R. E., 1998: Spatial evolutions of the active patterns across the equatorial Eastern Africa region during northern hemisphere spring season using Outgoing Longwave Radiation records. *Meteorol. Atmos. Phy.* 66, 51-63
- Okoola, E.R 1999: A Diagnostic study of the Eastern African Monsoon circulation during the northern hemisphere spring season. *Int. J. Climatol.* 19, 143 - 168.
- Omeny, P.A., 2006: East African Rainfall Variability Associated With the Madden-Julian Oscillation. *MSc Thesis, Department of Meteorology, University of Nairobi, pp 70*
- Omondi P. A., 2005: Potential causes and predictability of the space - time patterns of the decadal rainfall variability modes over east Africa. *MSc Thesis, Department of Meteorology, University of Nairobi*

- Oort, A. and J. J. Yienger, 1996: Observed inter-annual variability in the Hadley circulation and its connection to ENSO, *J. Climate*, 9, No.11, 2751-2767.
- Owiti, O. Z., 2005: Use of the Indian Ocean Dipole indices as predictor east African rainfall anomalies. *MSc Thesis, Department Of Meteorology, University of Nairobi*,
- Palmer, T. N., G. J. Shutts and R. Swinbank, 1986: Alleviation of a systematic westerly bias in general circulation and numerical weather prediction models through an orographic gravity wave drag parameterization. *Q. J. R. Meteorol. Soc.* 112:1001-1039.
- Parker, D. C. Folland, A. Scaife, J. Knight, A. Colman, P. Baines and B. Dong, 2007: Decadal to multidecadal variability and the climate change background. *J. Geophys. Res.*, 112, D18115, doi: 10.1029/2007JD008411.
- Parker, D. E., C. K. Folland, and M. N. Ward., 1988: Sea surface temperature anomaly patterns and prediction of seasonal rainfall in the Sahel region of Africa, *Nature*, 324, 483-485.
- Paulhus, J.L.H., and M.A. Kohler, (1952): Interpolation of Missing Precipitation Records. *Mon. Weather Rev.*, vol.80, No.8, pp.129-133.
- Peixoto, J. P., and A. H. Oort, 1992: *Physics of Climate*. American Institute of Physics, NY. pp. 492-496.
- Pohl B. and P.Camberlin (2006): Influence of the Madden-Julian Oscillation on East African rainfall. Part I: Intraseasonal variability and regional dependency», *Quart. J. Roy. Meteorol. Soc.*, 132, 2521-2539
- Pohlmann, H., J.H. Jungclaus, A. Köhl, D. Stammer, and J. Marotzke , 2009: Initializing decadal climate predictions with the GECCO Oceanic Synthesis: Effects on the North Atlantic. *J. Climate*, in press, DOI: 10.1175/2009JCLI2535.1.
- Power, S., Folland, C., Colman, A. and V. Mehta, 1999: Inter-decadal modulation of the impact of ENSO on Australia. *Climate Dynamics*, 15, 319-324.
- PREDICATE, 2006: <http://ugamp.nerc.ac.uk/predicate/>
- Qiao, F., Y. Yuan, Y. Yang, Q. Zheng, C. Xia, and J. Ma, 2004: Wave-induced mixing in the upper ocean: Distribution and application to a global ocean circulation model. *Geophys. Res Letters*, 31, L11303, pp4
- Rajagopalan, B., Y. Kushnir, and Y. M. Tourre, 1998: Observed decadal midlatitude and tropical Atlantic climate variability. *Geophys. Res. Lett.*, 25 3967-3970.
- Ramsay, H. A., Leslie, M. L., P. J. Lamb, M. B., Richman, M. Leplastrier, 2008: Interannual Variability of Tropical Cyclones in the Australian region, Role of large-scale environment. *Journal of Climate* 21: 1083-1103.

- Rao, S. A., and T. Yamagata (2004): Abrupt termination of Indian Ocean dipole events in response to intraseasonal disturbances, *Geophys. Res. Lett.*, 31, L19306, doi:10.1029/2004GL020842.
- Rao, S. A., and S. K. Behera (2005): Subsurface influence on SST in the tropical Indian Ocean: Structure and interannual variability, *Dyn. Atmos. Ocean*, 39, 103–135.
- Rao, S. A., S. Masson, J. J., Luo, S. K. Behera, and T. Yamagata (2007), Termination of Indian Ocean dipole events in a general circulation model, *J. Clim.*, 20, 3018–3035, doi:10.1175/JCLI4164.1.
- Rasmusson, E. M., Akhrin, P. A., Chen, W. Y. and J. B. Jalickee, 1981: Biennial variations in the surface temperature over the United States as revealed by Singular Value Decomposition. *Mon. Wea. Rev.*, 109, pp. 587-598.
- Reason, C. J. C., Allan, R. J., Lindesay J. A. and Ansel T. A., 2000: ENSO and Climate signals across the Indian Ocean basin in global context. *Int. Jr. of Climatol.*, 20, 1285-1327.
- Reiter, E. R. 1961: *Jet Stream Meteorology*. University of Chicago Press, Chicago, U. S.A 515pp.
- Repelli, C. A. and P. Nobre, 2004: Statistical prediction of sea-surface temperature over the tropical Atlantic. *Int. J. Climatolog.*, 24, 45-55.
- Reynolds, R.W., and D.C. Marsico, 1993: An improved real-time global sea surface temperature analysis. *J. Climate*, 6, 114-119.
- Reynolds, R. W., and T. M. Smith, 1994: Improved global sea surface temperature analyses using optimum interpolation. *J. Climate*, 7, 929-948.
- Reynolds, R.W., N.A. Rayne, T.M. Smith, D.C. Stokes, and W. Wang, 2002: An Improved In Situ and Satellite SST Analysis for Climate, *J. Climate*, 15, 1609-1625.
- Richard, J., D. Hassell, D. Hudson, S. Wilson, G. Jenkins and J. Mitchell., 2003: Workbook on generating high resolution climate change scenarios using PRECIS, Hadley Centre for Climate Prediction and Research, Met Office, Bracknell, UK October, 2003
- Richman, M.B. (1986): Review Article: Rotation of principal components. *J. climat.*, 6, 293-335.
- Rinne, J. and V. Karhila, (1979): Empirical Orthogonal Functions of 500 mb Heights in Northern Hemisphere Determined from a large sample of Data. *Quart. J. Roy. Meteor. Soc. vol.105*, 873-884.
- Rinne, J. and J. Simmo, (1986): 'Truncation of Empirical Orthogonal Function (EOF) series representing 500mb heights'. *Q. J. R. Meteorol. Soc.*, 105, pp.885-897.

- Robertson, A. W., C. R. Mechoso, and Y. J. Kim, 2000: The influence of Atlantic sea surface temperature anomalies on the North Atlantic Oscillation. *J. Climate*, 13 122-138.
- Rocha, A. and I. Simmonds, 1996: Interannual variability of south-eastern Africa summer rainfall. Part I relationships with air-sea interaction processes. *Int. J. Climatology*, 17, 235 – 266.
- Rodhe, H., 1974. Year to year variations in some hydrological parameters in Kenya, Secretariat Inter. Ecology Sweden (SIES) 4: 1-7.
- Rodhe, H. and H. Virji, 1976: Trends and periodicities of East African rainfall data. *Monthly Weather Review*, 104: 307-315
- Ropelewski, C. F., and M. S. Halpert, 1987: Global and regional scale precipitation patterns associated with the El-Nino/Southern Oscillation. *Mon. Wea. Rev.*, 115, 1606-1626.
- Ropelewski, C. F., and M. S. Halpert, 1996: Quantifying Southern Oscillation-precipitation relationships. *J. Climate*, 9, 1043–1059.
- Rupa Kumar, K., Sahai, A.K., Krishna Kumar, K., Patwardhan, S.K., Mishra, P.K., Revadekar, J.V., Kamala, K., Pant, G.B., 2006: High-resolution climate change scenarios for India for the 21st century. *Current Science*, 90, 334-345.
- Sabiti, G., 2008: Simulation of Climate Scenarios over the Lake Victoria Basin using the PRECIS Regional Climate Model, *MSc Thesis, Department Of Meteorology, University of Nairobi*
- Sadler, J. C., M.A. Lander, A. M.Hori, and L. K. Oda, 1987: Tropical marine climatic atlas. Vol.1, Indian Ocean and Atlantic Ocean. UHMET, 87-01, Dept. Meteor. Univ. Hawaii, 51pp
- Saji, N. H., B. N. Goswami, P. N. Vinayachandran, and T. Yamagata, 1999: A dipole mode in the tropical Indian Ocean. *Nature*, 401, 360–363.
- Saji, N. H., and T. Yamagata 2003a: Possible impacts of Indian Ocean dipole events on global climate, *Clim. Res.*, 25, 151–169.
- Saji, N. H., and T. Yamagata, 2003b: Interference of teleconnection patterns generated from the tropical Indian and Pacific Oceans. *Climate Res.*, 25, 151–169.
- Saji, N. H., T. Ambrizzi, and S. E. T. Ferraz, 2005: Indian Ocean dipole mode events and austral surface air temperatures, *Dyn. Atmos. Ocean*, 39, 87–102.
- Schlesinger, M.E., and N. Ramankutty, 1994: An oscillation in the global climate system of period 65–70 years. *Nature*, 367, 723–726.

- Schreck, J. C and F. H. M. Semazzi, 2004: Variability of the recent climate of Eastern Africa. *Int. J. Climatol.* 24, 681 – 701.
- Schubert, S. D., M. J. Suarez, P. J. Pegion, R. D. Koster, and J. T. Bacmeister, 2004: Causes of long-term drought in the United States Great Plains. *J. Climate*, 17, 485–503.
- Sciremammano, F. 1979: Suggestion for the presentation of the correlation and their significance levels. *J. Phy. Oceanography.* , 9, 1273.
- Seager, R., Y. Kushnir, C. Herweijer, N. Naik and J. Velez (Nakamura), 2005: Modeling of tropical forcing of persistent droughts and pluvials over western North America: 1856-2000. *J. Climate*, 18(19), 4065-4088.
- Seager, R., 2007: The Turn of the Century drought across North America: global context, dynamics and past analogues. *J. Climate*, 20, 5527-5552.
- Seager, R., Y. Kushnir, M. Ting, M. Cane, N. Naik and J. Miller, 2008: Would advance knowledge of 1930s SSTs have allowed prediction of the dust bowl drought? *J. Climate.*, 21(13), 3261-3281.
- Segele, T. Z. and P. J. Lamb, 2005: Characterization and variability of Kiremt rainy season over Ethiopia. *Meteorology and Atmospheric Physics* 89: 153-180.
- Seth, A., and F. Giorgi (1998): The effects of domain choice on summer precipitation simulation and sensitivity in a regional climate. *J Clim*, 11, 2698-2712
- Schreck, J. C and F. H. M. Semazzi, 2004: Variability of the recent climate of Eastern Africa. *Int. J. Climatol.* 24, 681 – 701.
- Shukla, J., 1991: Short term climate variability and predictions, *Proceedings Second World Climate Conference*, 29 October-7 November 1990, Geneva, Switzerland, pp203-210
- Siegel, S., 1956: *Non-parametric statistics for Behavioral Sciences*. McGraw-Hill Kogakusha Ltd, Tokyo, 312.
- Simmons, A. J., and D. M. Burridge, 1981: An energy and angular-momentum conserving vertical finite difference scheme and hybrid vertical coordinates. *Mon. Wea. Rev.* 109:758-766.
- Simon, W., Hassell, D., Hein, D., Jones, R., Taylor, R., 2004: *Installing and Using the Hadley Centre Regional Climate Modelling System, PRECIS, Version 1.1*. Met Office Hadley Centre: Exeter.
- Singhrattna, N., B. Rajagopalan, M. Clark and K. K. Kumar, 2005: Seasonal forecasting of Thailand summer monsoon rainfall, *Int. J. Climatol.*, 25, 649-664.

- Smith, T. M., and R. W. Reynolds, 2002: Bias corrections for historic sea surface temperatures based on marine air temperatures. *J. Climate*, 15, 73–87.
- Smith, T. M. and R. W. Reynolds, 2004: Improved Extended Reconstruction of SST (1854–1997). *J. Climate*, 17, 2466–2477.
- Smith, R. N. B., 1990: A scheme for predicting layer clouds and their water content in a general circulation model. *Q. J. R. Meteorol. Soc.* 116:435–460.
- Smith, D. M., Cusack, S., Colman, A. W., Folland, C. K., Harris, G. R. & Murphy, J. M. 2007: Improved surface temperature prediction for the coming decade from a global climate model. *Science* 317, 796–799.
- Smith, T. M., R. W. Reynolds, T. C. Peterson, and J. Lawrimore, 2008: Improvements to NOAA's historical merged land-ocean surface temperature analysis (1880–2006). *J. Climate*, in press.
- Solman, S. A., Nunez, M. N., and Cabre, M. F. 2008: Regional climate change experiments over southern South America. I: present climate, *Clim. Dynam.*, 30, 533–552.
- Song Y, F.H.M Semazzi, L. Xie and L.J Ogallo (2004): A coupled regional climate model for Lake Victoria basin of East Africa. *Int. J. Climatol.* 24, 57-75
- Song, Q., G. A. Vecchi, and A. J. Rosati, 2007: Indian Ocean Variability in the GFDL Coupled Climate Model. *J. Climate*, 20, 2895–2916
- Sun L, Semazzi F.H.M., Giorgi, F, Ogallo L A., 1999a: Application of the NCAR Regional Climate model to Eastern Africa. Part 1: Simulation of the short rains of 1988. *J Geophys Res.*, 104, 6529-6548
- Sun L, Semazzi F.H.M., Giorgi, F and L.A. Ogallo, 1999b: Application of the NCAR Regional Climate model to Eastern Africa. Part II: Simulation of interannual variability of short rains. *J Geophys. Res.*, 104, 6549-6562
- Sutton, R. T., and D. L. R. Hodson, 2005: Atlantic Ocean forcing of North American and European summer climate. *Science*, 309, 115–118.
- Sutton, R. T., and D. L. R. Hodson, 2007: Climate Response to Basin-Scale Warming and Cooling of the North Atlantic Ocean. *J. Climate*, 20, No.5, 891–907
- Tanaka, K. L., N. Ishizaki and A. Kito, 2004: Trend and interannual variability of Walker, monsoon and Hadley circulations defined by the velocity potential in the upper troposphere. *Tellus*, 56A No.3, 250-269.
- Tanimoto, Y., and S. P. Xie, 1999: Ocean–atmosphere variability over the Pan–Atlantic basin. *J. Meteor. Soc. Japan*, 77, 31–46.

- Terray, P., and S. Dominiak, 2005: Indian Ocean Sea Surface Temperature and El Niño Southern Oscillation, *J Climate*, 18, 1351-1368
- Trauth, M.H. and Strecker, M.R., 1996: Late Pleistocene lake-level fluctuations in the Naivasha Basin, Kenya. In *The Limnology, Climatology and Pale climatology of the East African Lakes* (T.C. Johnson and E.O. Odada, eds.). Gordon and Breach Publ, Amsterdam, p. 549-558.
- Trenberth, K. E. and J. W. Hurrell, 1994: Decadal atmosphere-ocean variations in the Pacific: *Climate Dyn.* 9, 303-319.
- Trenberth, K. E., and D. P. Stepaniak, 2001: Indices of El Niño evolution, *J. Clim.*, 14, 1697-1701.
- Trenberth, K. E., J. M. Caron, D. P. Stepaniak and S. Worley, 2002: The evolution of ENSO and global atmospheric temperatures. *J. Geophys. Res.*, 107, 4065, doi: 10.1029/2000JD000298.
- Trenberth, and D.J. Shea, 2006: Atlantic hurricanes and natural variability in 2005, *Geophys. Res. Lett.*, 33, L12704, doi: 10.1029/2006GL026894.
- Trewartha, 1981: *The earth's problem climates*. 2nd Edition Univ. of Wisconsin Press, 371pp.
- Tomsett, J. E., 1969: Average monthly and annual rainfall maps of East Africa. Techn. Memo. No. 14, Kenya Meteorological Department, Nairobi
- Torrence, C., and P.J. Webster, 1999: Interdecadal changes in the ENSO-monsoon system. *J. Climate*, 12, 2679-2690.
- Tourre, Y. M., Y. Kushnir, and W. B. White, 1999: Evolution of interdecadal variability in sea level pressure, sea surface temperature, and upper ocean temperature over the Pacific Ocean. *J. Phys. Oceanogr.*, 9, 1528-1541.
- Tozuka, T., J.J. Luo, S. Masson, S. K. Behera, and T. Yamagata, 2005: Annual ENSO simulated in a coupled ocean atmosphere model. *Dyn. Atmos. Oceans*, 39, 41-60.
- Tozuka, T., J.J. Luo and T. Yamagata, 2006: Decadal Indian Ocean dipole simulated in an ocean-atmosphere coupled model. *J. Climate*, in press.
- Tozuka, T., J J. Luo, S. Mason, and T. Yamagata, 2007: Decadal Modulations of the Indian Ocean Dipole in the SINTEX-F1 Coupled GCM. *J. Climate*, 20, 2881-2894
- Taylor, K.E., R.J. Stouffer, and G.A. Meehl, 2008: A summary of the CMIP5 Experimental Design. <http://www-pcmdi.llnl.gov/>

- Tyson, P. D., T. G. J. Dyer and M. N. Mametse, 1975: Secular changes in South Africa rainfall. *Q. J. R. Met. Soc.*, 101: 817-833.
- Tyson, P.D., and R.A. Preston-Whyte, 2000: *The weather and climate of southern Africa*. Oxford University Press, southern Africa. pp 396.
- Tyson, P. D., G. R. J. Cooper, and T. S. McCarthy, 2002: Millennial to multi-decadal variability in the climate of southern Africa. *Int. J. Clim.*, 22 (9), 1105-1117.
- UNDP, 2002: *The factoring of weather and climate into disaster management*. ICPAC/KMD, 100pp
- Valsala, V. K. and M. Ikeda, 2007: Pathways and Effects of the Indonesian Throughflow Water in the Indian Ocean Using Particle Trajectory and Tracers in an OGCM., *J Climate*, 20, No.13, 2994–3017
- van Lieshout, M., Kovats, R.S., Livermore, M.T.J. and Martens, P., 2004: Climate change and malaria: analysis of the SRES climate and socio-economic scenarios. *Global Environmental Change* 14, 87-99.
- Venegas, S. A., L. A. Mysak, and D. N. Straub, 1996: Evidence for Interannual and Interdecadal Climate Variability in the South Atlantic, *Geophys. Res. Lett.*, 23(19), 2673–2676.
- Venegas, S. A., and L. A. Mysak, 2000: Is there a dominant timescale of natural climate variability in the Arctic? *J. Clim.*, 13, 3412-3434.
- Vera, C., M. Barange, O.P. Dube, L. Goddard, D. Griggs, N. Kobysheva, E. Odada, S. Parey, J. Polovina, G. Poveda, B. Seguin, and K. Trenberth, 2009: Needs assessment for climate information on decadal time scales and longer. White Paper, World Climate Conference 3 (WCC-3), Geneva, Switzerland, 31 August – 4 September, 2009
- Vidyunmala, V., R. S. Nanjundiah, and J. Srinivasan, 2007: The effect of variation in sea-surface temperature and its meridional gradient on the equatorial and off-equatorial ITCZ in an Aquaplanet General Circulation model. *Journal Meteorology and Atmospheric Physics*, 95, No. 3-4, 239-253.
- von Storch, H. and F. Zwiers, 1999: *Statistical analysis in climate research*; Cambridge University Press.
- von Storch, H. and Navarra, A., editors (1995). *Analyses of Climate variability – Applications of Statistical Techniques*. Springer.
- Wagner, A. J., 1971: Long period variations in seasonal sea level pressure over northern hemisphere. *Mon. Weather Rev.*, 99: 49-66.

- Wallace, J. M., Smith, C., and Bretherton, C. S. 1992: Singular value decomposition of wintertime sea surface temperature and 500-mb height anomalies. *J. Clim.*, 5:561-576
- Wallace, J. M., Rasmusson E. M., Mitchel T. P., Kousky V. E., Sarachick E. S., Von Storch H., 1998: On the structure and evolution of ENSO-related climate variability in the tropical pacific: lessons from TOGA. *Jr. of Geophys. Res.*, 103, 14241-14260.
- Walker G., 1931: On Periodicity in Series of Related Terms, *Proceedings of the Royal Society of London, Ser. A, Vol. 131*, pp 518-532.
- Walker, G.T., and E.W. Bliss, 1932: *World Weather V. Mem. Roy. Meteorol. Soc.*, 4, 53-84.
- Walsh, J.E. and Mostek, A., 1980: A quantitative analysis of Meteorological Anomaly patterns over the United States, (1900-1977). *Mon. Wea. Rev.* Vol.108, 615-629.
- Wang, B. and S. I., An, 2001: Why the properties of El-Nino changed during the late 1970s. *Geophys, Res. Lett.* 28, 3709-3712.
- Wang, G. and E. A. B. Eltahir, 1999: Use of ENSO Information in Medium- and Long-Range Forecasting of The Nile In Floods., *J. Climate*, 12, 1726-1737.
- Wang, C., 2001: Atlantic climate variability and its associated atmospheric circulation cells, *J. Climate*, 15, 1516-1536.
- Wang, C., 2002: Atlantic climate variability and its associated atmospheric circulation cells. *J. Climate*, 15, 1516-1536.
- Wang Y, L. R. Leung, J. L. McGregor, D. K Lee, W. C. Wang, Y. Ding and F. Kimura 2004: Regional climate modeling: Progress, Challenges and Prospects. *J. Meteorol. Soc. Japan* 112, 703-810.
- Wannacott, R.J., and T.H. Wannacott, 1985: *Introductory statistics*, 4th edition, 1985, John - Wiley and Sons, New York.
- Ward, M. N., and C. K. Folland, 1991: Prediction of seasonal rainfall in the north nordeste of Brazil using eigenvectors of sea surface temperature. *J climatol.*, 11, 711-743.
- Wassila, M.T., A.G. Barnston, and V. Kumar, 1999: Prediction of African rainfall on the seasonal timescale. *J. Geophysics. Res.*, 104, D24, 31589-31597
- WCRP, 2005: *The World Climate Research Programme Strategic Framework 2005-2015*, WRCF-123, WMO/TD-NO.1291, 59PP
- Weare, B.C, 1977: Empirical Orthogonal Analysis of Atlantic ocean surface temperatures, *Quart. J. R. Met. Soc.*, 103, 467-478.

- Webster, P. J., A. M. Moore, J. P. Loschnigg and R. R. Leben, 1999: Coupled Ocean-Atmosphere dynamics in the Indian ocean during 1997-98., *Nature*, 401,356-359.
- Webster, P.J., A. M. Moore, J. P. Loschnigg, 2005: Changes in tropical cyclone number, duration and intensity in a warming environment. *Science*, 309, 1844–1846.
- Weng, H., K. Ashok, S. K. Behera, S. A. Rao, and T. Yamagata, 2007: Impacts of recent El Niño on Modoki dry/wet conditions in the Pacific rim during boreal summer, *Clim. Dyn.*, 29, 113–129, doi:10.1007/s00382-007-0234-0.
- Weng H., Swadhin K. Behera and Toshio Yamagata, 2008: Anomalous winter climate conditions in the Pacific Rim during recent El Niño Modoki and El Niño events
- Wheeler M. C., and H. H. Hendon (2004): An All Season Real Time Multivariate MJO Index: Development of an Index for Monitoring and Prediction. *Mon. Wea. Review* 132, 1917-1932.
- White, W.B., and D.R. Cayan, 2000: A global ENSO wave in surface temperature and pressure and it's interdecadal modulation from 1900 to 1997. *J. Geophys. Res.*, 105, 11,223-11,242.
- Wilks, D. S., 1995: *Statistical methods in the atmospheric sciences*: Academic press, pp 45-50, 399-402.
- Wilks, D. S, 2006: *Statistical methods in atmospheric sciences*, Second Edition, vol. 91, International Geophysics Series, Academic Press, Elsevier, 627pp.
- Wilson, S., Hassell, D., Hein, D., Jones, R., and Taylor, R.: *Installing and using the Hadley Centre regional climate modelling system, PRECIS (version 1.4)*, Met Office Hadley Centre, 25 Exeter, UK, 2005.
- Wolter, K., 1987: The Southern Oscillation in Surface Circulation and Climate over the tropical Atlantic, Eastern Pacific and Indian Ocean as captured by cluster analysis. *J. Appl. Meteor*, 26, 540 – 558.
- Woodhouse, C. A. and J. T., Overpeck, 1998: 2000 years of drought variability in the central United States. *Bull.Amer.Meteor.Soc.*, 79, 2693-2714.
- Worster, D., 1979: *Dust Bowl: The Southern Great Plains in the 1930s*. Oxford University Press, New York, 277pp.
- WMO (1962): *The use of statistics in climatology. Guide to climatological practices. WMO supp.1. No.3, sept. 1962.*
- WMO (1966): *Climate change. WMO Tech. Note No.79, 79pp.*

- WMO (1970): Guide to Hydrometeorological practices. *WMO No. 168, p.82.*
- WMO (1979): Climatological series. *WMO Tech. Note No.79; WMO, 1979.*
- WMO (1986): Guidelines on the quality control of surface climatological data. *WCP-85, WMO/TD-No.111, 56pp.*
- Wu, L., F. He, Z. Liu, and C. Li, 2007: Atmospheric teleconnections of tropical Atlantic variability: Interhemispheric, tropical-extratropical, and cross-basin interactions. *J. Climate, 20, No.5, 856-870.*
- Wunsch, C. and P. Heimbach, 2006: Estimated Decadal Changes in the North Atlantic Meridional Overturning Circulation and Heat Flux 1993–2004. *J. Phys. Oceanography, 36, 2012–2024*
- Xie, S. and Y. Tanimoto, 1998: A pan-Atlantic decadal climate oscillation, *Geophys. Res. Lett., 25, 2185-2188.*
- Xie, S.-P., H. Annamalai, F. A. Schott, and J. P. McCreary Jr., 2002: Structure and mechanisms of South Indian Ocean climate variability. *J. Climate, 15, 864–878.*
- Xinhua C., and J. D., Timothy, 1995: Orthogonal Rotation of Spatial Patterns Derived from Singular Value Decomposition Analysis, *Journal of Climate, 8, pp 2631-2643*
- Xoplaki, E., J. Gonzalez-Rouco, D. Gyalistras, J. Luterbacher, R. Rickli, and H. Wanner, 2003: Interannual summer air temperature variability over Greece and its connection to the large-scale atmospheric circulation and Mediterranean SSTs 1950-1999. *Clim. Dyn. 20, 537-554.*
- Yamagata, T. and Y. Masumoto, 1992: Interdecadal natural climate variability in the western Pacific and its implication in global warming, *J. Meteorol. Soc. Jpn., 70, 167–175.*
- Yamagata, T., S. K. Behera, J. J., Luo, S. Masson, M. R. Jury, and S. A. Rao, 2004: The coupled ocean-atmosphere variability in the tropical Indian Ocean, in *Earth's Climate: The Ocean-Atmosphere Interaction, Geophys. Monogr. Ser., vol. 147, edited by C. Wang et al., pp. 189–211, AGU, Washington, D. C.*
- Yamaguchi, K., and A. Noda, 2005: Global warming patterns over the North Pacific: ENSO versus AO. *J. 48 Met. Soc. Japan.*
- Yinlong X, Xiaoying H, Yong Z, Wantao L, Erda L. 2006. Statistical analyses of climate change scenarios over China in the 21st Century. *Advances in Climate Change Research 2(Suppl. 1): 50–53.*
- Yu, L., and M. M. Rienecker, 2000: Indian Ocean warming of 1997-98., *J. Geophys. Res., 105, 16 923-16 939*

- Yule G., 1927: On a Method of Investigating Periodicities in Disturbed Series, with Special Reference to Wolfer's Sunspot Numbers, *Philosophical Transactions of the Royal Society of London, Ser. A, Vol. 226*, pp 267-298.
- Yue F., 2005: A coupled model study of the remote influence of ENSO on Tropical Atlantic SST Variability. PhD dissertation Department of Oceanography, Office of Graduate Studies of Texas A&M University
- Zebiak, S. E., 1993: Air-sea interaction in the equatorial Atlantic region. *J. Climate*, 6, 1567–1586.
- Zhang, Y., J. M. Wallace, and D. Battisti, 1997: ENSO-like interdecadal variability: 1990-1993, *J. Clim.*, 10, 1004-1020.
- Zang, C. and J. Gottschalk, 2002: SST anomalies of ENSO and the Madden-Julian Oscillation in the equatorial Pacific. *J. Climate*, 15 No. 17, 2429-2445.
- Zhang, R., and T. L. Delworth, 2006: Impact of Atlantic multidecadal oscillations on India/Sahel rainfall and Atlantic hurricanes. *Geophys. Res. Lett.*, 33, L17712, doi: 10.1029/2006GL026267.
- Zhang, R., T. L. Delworth, and I. M. Held, 2007: Can the Atlantic Ocean drive the observed multidecadal variability in Northern Hemisphere mean temperature? *Geophys. Res. Lett.*, 34, L02709, doi: 10.1029/2006GL028683.
- Zhang, Y., J. M. Wallace, and D. S. Battisti (1997), ENSO-like interdecadal variability: 1900–93, *J. Clim.*, 10, 1004–1020.
- Zhou, G., N. Minakawa, A.K. Githeko, and G. Yan. 2004: Association between climate variability and malaria epidemics in the East African highlands. *Proceedings of the National Academy of Sciences of the United States of America*. 101: 2375-2380
- Zewdu T. S., P. J. Lamb and L. M. Leslie, 2009: Large-scale atmospheric circulation and global sea surface temperature associations with Horn of Africa June – September rainfall, *Int. J. Climatol.*, **29**: 1075-1100
- Zveryaev, I. I., 2001: Interdecadal Changes in the Zonal wind and the intensity of decadal oscillations during boreal summer Asian monsoon, *Tellus 54A* (2002), 3, pp 288-298